

IntechOpen

# Recent Advances in Ionic Liquids

*Edited by Mohammed Muzibur Rahman*





---

# RECENT ADVANCES IN IONIC LIQUIDS

---

Edited by **Mohammed Muzibur Rahman**

## Recent Advances in Ionic Liquids

<http://dx.doi.org/10.5772/intechopen.74185>

Edited by Mohammed Muzibur Rahman

### Contributors

Syamsul Bahari Abdullah, Hanida Abdul Aziz, Zakaria Man, Yibo Wu, Sumit Kumar Panja, Raiza Hernandez, Alma Miranda, José Manuel Dominguez Esquivel, Magdalena Maciejewska, Anna Sowinska, Muhammad Saad Khan, Bhajan Lal, Bavoh Cornelius, Mohamad Azmi Bustam, Shouhei Kawada, Shinya Sasaki, Seiya Watanabe, Masaaki Miyatake, Michiaki Matsumoto, Pius Dore Ola, Sixberth Mlowe, Zikhona Tshemese, Siphamandla C. Masikane, Neerish Revaprasadu, Gloria VÍllora, Mercedes G. Montalbán, Guzmán Carissimi, A. Abel Lozano-Pérez, Jose L. Cenis, David L. Kaplan, Jeannine M. Coburn, Ahmet Karadağ, Hüseyin Akbaş, Chandrabhan Verma, Ronewa Phadagi, Indra Bahadur

### © The Editor(s) and the Author(s) 2018

The rights of the editor(s) and the author(s) have been asserted in accordance with the Copyright, Designs and Patents Act 1988. All rights to the book as a whole are reserved by INTECHOPEN LIMITED. The book as a whole (compilation) cannot be reproduced, distributed or used for commercial or non-commercial purposes without INTECHOPEN LIMITED's written permission. Enquiries concerning the use of the book should be directed to INTECHOPEN LIMITED rights and permissions department ([permissions@intechopen.com](mailto:permissions@intechopen.com)). Violations are liable to prosecution under the governing Copyright Law.



Individual chapters of this publication are distributed under the terms of the Creative Commons Attribution 3.0 Unported License which permits commercial use, distribution and reproduction of the individual chapters, provided the original author(s) and source publication are appropriately acknowledged. If so indicated, certain images may not be included under the Creative Commons license. In such cases users will need to obtain permission from the license holder to reproduce the material. More details and guidelines concerning content reuse and adaptation can be found at <http://www.intechopen.com/copyright-policy.html>.

### Notice

Statements and opinions expressed in the chapters are those of the individual contributors and not necessarily those of the editors or publisher. No responsibility is accepted for the accuracy of information contained in the published chapters. The publisher assumes no responsibility for any damage or injury to persons or property arising out of the use of any materials, instructions, methods or ideas contained in the book.

First published in London, United Kingdom, 2018 by IntechOpen

eBook (PDF) Published by IntechOpen, 2019

IntechOpen is the global imprint of INTECHOPEN LIMITED, registered in England and Wales, registration number:

11086078, The Shard, 25th floor, 32 London Bridge Street

London, SE19SG – United Kingdom

Printed in Croatia

British Library Cataloguing-in-Publication Data

A catalogue record for this book is available from the British Library

Additional hard and PDF copies can be obtained from [orders@intechopen.com](mailto:orders@intechopen.com)

Recent Advances in Ionic Liquids

Edited by Mohammed Muzibur Rahman

p. cm.

Print ISBN 978-1-78984-117-6

Online ISBN 978-1-78984-118-3

eBook (PDF) ISBN 978-1-83881-779-4

# We are IntechOpen, the world's leading publisher of Open Access books Built by scientists, for scientists

**3,700+**

Open access books available

**116,000+**

International authors and editors

**119M+**

Downloads

**151**

Countries delivered to

Our authors are among the  
**Top 1%**

most cited scientists

**12.2%**

Contributors from top 500 universities



**WEB OF SCIENCE™**

Selection of our books indexed in the Book Citation Index  
in Web of Science™ Core Collection (BKCI)

Interested in publishing with us?  
Contact [book.department@intechopen.com](mailto:book.department@intechopen.com)

Numbers displayed above are based on latest data collected.  
For more information visit [www.intechopen.com](http://www.intechopen.com)





# Meet the editor



Mohammed Muzibur Rahman received his B.Sc. and M.Sc. from Shahjalal University of Science and Technology, Sylhet, Bangladesh, in 1999 and 2001, respectively. He received his Ph.D. from the Chonbuk National University, South Korea, in 2007. After his Ph.D., he worked as a postdoctoral fellowship and assistant professor in pioneer research centers and universities located in South Korea, Japan, and Saudi Arabia (2007–2011). Since 2011 he has worked as Associate Professor in the Center of Excellence for Advanced Materials Research and Chemistry Department at King Abdulaziz University, Saudi Arabia. He has published more than 225 research articles and several proceedings in well-known high-impact ISI journals; attended more than 60 international and domestic conferences; and published several book chapters and 10 books as an editor. His research work has been largely in the area of carbon nanotubes, nanotechnology, sensors, ionic liquids, surface chemistry, electrochemistry, instrumental science, nanomaterials, self-assembled monolayers, photochemistry,  $\mu$ -chips and devices, etc.





---

# Contents

---

## **Preface XI**

### **Section 1 State of the Art Preparation 1**

Chapter 1 **Biopolymeric Nanoparticle Synthesis in Ionic Liquids 3**  
Mercedes G. Montalbán, Guzmán Carissimi, A. Abel Lozano-Pérez,  
José Luis Cenis, Jeannine M. Coburn, David L. Kaplan and Gloria  
Vílora

Chapter 2 **Phosphazene-Based Ionic Liquids 27**  
Ahmet Karadağ and Hüseyin Akbaş

Chapter 3 **Tribochemical Reactions of Halogen-Free Ionic Liquids on  
Nascent Steel Surface 47**  
Shouhei Kawada, Seiya Watanabe, Shinya Sasaki and Masaaki  
Miyatake

### **Section 2 State of the Art Characterization 67**

Chapter 4 **Progress in Green Solvents for the Stabilisation of  
Nanomaterials: Imidazolium Based Ionic Liquids 69**  
Zikhona Tshemese, Siphamandla C. Masikane, Sixberth Mlowe and  
Neerish Revaprasadu

### **Section 3 State of the Art Polymerization 91**

Chapter 5 **Ionic Polymerization in Ionic Liquids 93**  
Yibo Wu

Chapter 6 **Ionic Liquids for Desulphurization: A Review 107**  
Syamsul Bahari Abdullah, Hanida Abdul Aziz and Zakaria Man

**Section 4 State of the Art Applications 121**

Chapter 7 **Applications of Ionic Liquids in Elastomeric Composites:  
A Review 123**

Anna Sowinska and Magdalena Maciejewska

Chapter 8 **Metal Extraction with Ionic Liquids-Based Aqueous  
Two-Phase System 145**

Pius Dore Ola and Michiaki Matsumoto

Chapter 9 **Kinetic Assessment of Tetramethyl Ammonium Hydroxide  
(Ionic Liquid) for Carbon Dioxide, Methane and Binary Mix Gas  
Hydrates 159**

Muhammad Saad Khan, Bavoh B. Cornelius, Bhajan Lal and  
Mohamad Azmi Bustam

---

## Preface

---

It gives me immense pleasure to introduce this book, *Recent Advances in Ionic Liquids*, based on the state of the art of preparation, characterization, polymerization, as well as application of ionic liquids in various industrial settings. Discussion of these aspects develops through fundamental and applied experimental routes by various methods and comprises the interfacing of the scientific and technological worlds. Usually, ionic liquids have incontestably attained achievement of their conventional essence and have taken new directions from preparation and polymerization to potential applications in the research and development areas of science. The new routes and developing edges branch out from time to time around this advanced stage of stable ionic liquids. Advances in ionic liquids with instrumentation for evaluating the practical use of these materials now enables us to understand quite broadly almost all the events that take place for ionic liquids. Because of the exceptional and unique properties of ionic liquids, they can offer significant and great interest for developing green, efficient, and influential catalytic utilization and technologies. The latest advances in ionic liquid catalysis and applications are focused on different fields, *namely* preparation, properties, utilization, polymerization, applications of ionic liquids, and catalytic conversion or production of useful chemicals in ionic liquids. Particularly via selected samples preparation of ionic liquids, the advantages and potential applications of ionic liquids in exploring cleaner and efficient polymerization and catalytic technologies and processes can be described.

In this book, Prof. Villora et al. review the synthesis of biopolymeric nanoparticles using ionic liquids, such as trimethylsilyl cellulose or silk fibroin. They describe how high-power ultrasounds are capable of enhancing the dissolution process of silk proteins in ionic liquids and how silk fibroin nanoparticles can be directly obtained from the silk fibroin/ionic liquid solution by rapid desolvation in polar organic solvents.

Prof. Karadag et al. focus on the synthesis and possible application of cyclo- and polyphosphazene-based ionic liquids (PzILs). PzILs constitute an alternative class of phosphorous nitrogen compounds, and their derivatives have been widely used in biologically active materials, electrolytes, lubricants, catalysts, or nanomaterials. Considerable information is available on substitution reactions taking place in the phosphorous atoms of poly- and cyclophosphazenes, thus a wide variety of phosphazene derivatives have been obtained.

Prof. Kawada et al. describe the use of halogen-free anion-based ionic liquids as lubricants. In this approach, the study investigates the tribological performance and lubricating mechanisms of sulfur, phosphorus, and cyano-anion-based ionic liquids. Sulfur and phosphorous anion-based ionic liquids form reaction films on worn surfaces; the sulfur- and phosphorus-containing films exhibit low friction coefficients and specific wear rates, respectively. The steric hindrance of the ionic liquids affects their tribochemical reaction behaviors. Cyano-

anion-based ionic liquids also show low friction coefficients; however, their values are higher than those of halogen anion-based ionic liquids.

In this approach, Prof. Mlowe et al. describe how the physicochemical properties of ionic liquids differ significantly depending on the anionic/cationic species and alkyl chain length. Ionic liquids have found application in many scientific fields, the most recent being good solvents and stabilizing agents in nanomaterial synthesis. Their studies have shown that ionic liquids not only stabilize as synthesized nanomaterials but also provide environmentally green routes towards nanomaterial engineering.

Prof. Wu discusses the advantages and limitations of the application of ionic liquids as solvents for ionic polymerization processes. The most important types of cationic monomers, such as styrene and its derivatives, vinyl ethers, and isobutylene, have been polymerized in ionic liquids, and even undergo living polymerization. From his study, it is concluded that ionic liquids seem unsuitable solvents for anionic polymerization.

Prof. Abdullah et al. describe the interaction mechanism of ionic liquids with sulfur in a model oil system. The interaction is predicted using COSMO-RS where the strength of the hydrogen bond of anions should be reduced to increase thiophene extraction capacity. The absorption capacity of sulfur compounds in ionic liquids is strongly dependent on the chemical structures, physical properties, and compactness between the cation and the anion of the ionic liquids. Finally, the extractive desulfurization process using selective ionic liquids as the extractant is still in need of further research, starting from the screening of suitable ionic liquids for desulfurization, synthesis of ionic liquids, physical property analysis of ionic liquids, single batch extraction study encompassing process optimization up to actual diesel application, and the regeneration of spent ionic liquids.

In this approach, Prof. Maciejewska et al. reviews the advantages of ionic liquids as functional additives for elastomeric composites, with special emphasis on their use as dispersing agents for fillers, components of conducting rubber composites, crosslinkers, or components of crosslinking systems. An analysis of the recent literature reports indicates that ionic liquids are widely used in elastomeric composites as dispersing agents of fillers, conductive additives, crosslinkers or components of the crosslinking system (vulcanization accelerators or activators), catalysts for the silanization reaction, solvents for the depolymerization of natural rubber, or for the production of highly stretchable ionogels. Because the structure of ionic liquids can be designed for specific applications, it can be expected that the use of ionic liquids in elastomeric composites will continue to increase.

Prof. Matsumoto summarizes the use of an ionic liquids-based aqueous two-phase system (ATPS) for the separation of metals used in various areas of human life. An ATPS composed of ionic liquids and a salting-out agent is excellent for metal ion separation because of its efficiency, selectivity, and environmental friendliness. Due to the temperature dependence of a mixture comprised of ionic liquids with water, it has been manipulated for metal ion extraction known as homogeneous liquid/liquid extraction (HLL). HLL also showed high efficiency and selectivity in metal ion extraction. Metal ions can be extracted by both an ATPS and HLL, including transition metals, rare earth elements, and radioactive substances. Results reveal that tetramethylammonium hydroxide (TMAOH) tends to delay hydrate formation for all the studied hydrate systems at all concentrations. The presence of TMAOH also reduces the total gas consumed into hydrates and the initial rate of hydrate formation in most of the studied systems.

Lastly, Khan et al. highlight the impact of ammonium-based ionic liquid TMAOH on the formation kinetics of pure carbon dioxide ( $\text{CO}_2$ ), methane ( $\text{CH}_4$ ), and their binary mixed gas (50–50 mole%) hydrates. Hydrate formation induction time, the initial apparent rate of formation, and the total gas consumed into hydrate are the kinetic parameters used to evaluate the performance of TMAOH on hydrate formation.

This work aims to bridge the gap between undergraduate, graduate, and scientist in applied ionic liquids, to initiate researchers into ionic liquid study in as straightforward a way as possible, and to introduce researchers to the opportunities offered by applied science and technological fields. I have worked unswervingly to complete this work for the InTech open access publisher. I hope that this contribution would further enhance applied stable liquid materials in nano- and bioscience, biosynthesis, polymerization, desulfurization, stabilization, kinetic assessments, and metal extraction, especially in bringing new entrants into the applied and modified ionic liquids science and technology fields and helping scientists to develop their own field of specialization.

**Mohammed Muzibur Rahman**

Center of Excellence for Advanced Materials Research (CEAMR) and

Chemistry Department

Faculty of Science

King Abdulaziz University

Jeddah, Saudi Arabia



---

# State of the Art Preparation

---





---

# Biopolymeric Nanoparticle Synthesis in Ionic Liquids

---

Mercedes G. Montalbán, Guzmán Carissimi,  
A. Abel Lozano-Pérez, José Luis Cenis,  
Jeannine M. Coburn, David L. Kaplan and  
Gloria Víllora

Additional information is available at the end of the chapter

<http://dx.doi.org/10.5772/intechopen.78766>

---

## Abstract

Recently, much research has focused on the use of biopolymers, which are regarded as biodegradable, natural, and environmentally friendly materials. In this context, biopolymeric nanoparticles have attracted great attention in the last few years due to their multiple applications especially in the field of biomedicine. Ionic liquids have emerged as promising solvents for use in a wide variety of chemical and biochemical processes for their extraordinary properties, which include negligible vapor pressure, high thermal and chemical stability, lower toxicity than conventional organic solvents, and the possibility of tuning their physical–chemical properties by choosing the appropriate cation and anion. We here review the published works concerning the synthesis of biopolymeric nanoparticles using ionic liquids, such as trimethylsilyl cellulose or silk fibroin. We also mention our recent studies describing how high-power ultrasounds are capable of enhancing the dissolution process of silk proteins in ionic liquids and how silk fibroin nanoparticles can be directly obtained from the silk fibroin/ionic liquid solution by rapid desolvation in polar organic solvents. As an example, their potential biomedical application of curcumin-loaded silk fibroin nanoparticles for cancer therapy is also discussed.

**Keywords:** ionic liquid, biopolymer, nanoparticle, synthesis, silk fibroin

---

## 1. Introduction

### 1.1. Biopolymeric nanoparticles for biomedical applications

During the last 30 years, nanotechnology has attracted much attention in many engineering fields including electronic, mechanical, biomedical, and space engineering. Among these fields,

---

nanotechnology has led to significant progress being made in biomedicine through the development of efficient structures for controlled and targeted drug or gene delivery, tissue engineering, the imaging of specific sites, regenerative medicine, biosensing, and probing of the DNA structure [1]. More specifically, the role of nanoparticles in the progress made in this field is of particular note, and treatments involving nanoparticles have been widely applied in cancer therapy, diabetes, allergy, infection, and inflammation [2]. The main advantages of *nanoparticles* used as drug carriers for the treatment of these diseases are the following: (a) a size range similar to that of proteins, (b) a large surface area, which allows the presence of different functional groups acting as ligands, (c) fast absorption and release properties, and (d) particle sizes and surface features that can be specifically designed.

Nanoparticles for therapeutic application can be synthesized from (natural or synthetic) polymers, ceramics, and metals [3]. Polymeric nanoparticles have been widely studied as nanocarriers of active molecules such as drugs and genes [4–9]. The main drawbacks in the use of polymeric nanoparticles are the difficulty of scaling up, and their low drug loading capacity and wide size distribution [2]. However, as nanoplateforms, they show great potential because they allow the targeted release of drugs to specific cells or tissues [10]. Moreover, in contrast to ceramic or metal nanoparticles, polymeric nanoparticles can be synthesized in a wide range of sizes and forms and can sustain localized drug therapeutic agents for weeks [3]. While the above features are common to both natural and synthetic polymers, natural polymers, also known as biopolymers, have some extra advantages such as their inherent biocompatibility and biodegradability, non-antigenicity, a high nutritional value, the abundance of their renewable sources, and an extraordinary binding capacity with several drugs [11]. Biopolymers are natural macromolecules and can be polysaccharides, proteins, polyphenols, polyesters, or polyamides. The synthesis of biopolymer-based materials, such as nanoparticles, is still difficult due to the low solubility of biopolymers in conventional organic solvents as a result of their highly crystalline structure [1]. Therefore, the search for new solvents capable of dissolving biopolymers successfully is a continuous challenge in order to achieve the industrial fabrication of biomaterials.

## 1.2. Ionic liquids as media for the synthesis of nanoparticles

Ionic liquids (ILs) are organic salts that are liquid close to room temperature. They normally consist of an organic cation and a polyatomic inorganic anion. They have attracted great attention recently for use in a variety of chemical processes as “green” solvents. The most important advantage of ILs is their non-detectable vapor pressure, which makes them environmentally benign solvents compared with volatile organic solvents (VOSs). The growing awareness about the risk of using these solvents has led to a search for alternatives, and the discovery of ILs seemed to solve the problem [12]. They also show several advantages over classic organic solvents such as a good chemical and thermal stability, a high ionic conductivity, non-flammability, a large electrochemical window, solvation ability, and they can be used at high temperatures [13, 14]. Furthermore, the physical–chemical properties of ILs, such as their density, polarity, hydrophobicity, melting point, viscosity, and solvent properties, may be tuned by modifying the anion or the cation. Among other applications, ILs have been used as electrolytes, solvents, lubricants, matrices for mass spectrometry, for chromatography as

stationary phase, supports for the enzyme immobilization, as liquid crystals, in technologies of separation, for nanomaterials synthesis as templates, in the synthesis of catalytic membranes, and in the generation of high conductivity materials [13, 14].

ILs may be excellent candidates for dissolving biopolymers and developing biomaterials mainly because of the flexibility that can be achieved by combining different cations and anions, and green solvent properties such as non-volatility, non-flammability, and recyclability. During recent years, biopolymers such as cellulose, xylan, starch, chitin/chitosan, keratin, silk fibroin (SF), and heparin have been transformed from ILs into films, scaffolds, membranes, fibers, and micro- or nanoparticles. In addition, composites formed by biopolymer/biopolymer or biopolymer/synthetic polymer mixtures can also be synthesized by the co-dissolution of polymers in ILs [1]. The interesting properties of ILs make them excellent media for the synthesis and stabilization of nanoparticles [15]. Their most noteworthy features for the synthesis of nanoparticles are as follows:

- a. ILs can contribute to the synthesis of small particles due to their generally low surface tension, which leads to high nucleation rates.
- b. ILs enhance the electronic and steric stabilization of nanoparticles and reduce particle growth, since their constituents (anion and cation) form a protective electrostatic shell that prevents agglomeration processes. In addition, nanoparticles are stable in solution due to the coordination of anion or cation through ionic or covalent bonds.
- c. ILs have a significant effect on the shape of the synthesized nanoparticles because they are highly structured liquids which can form extended hydrogen-bonded networks.
- d. ILs can be designed using different cation/anion combinations to achieve the desired properties of density, viscosity, hydrophilicity, gas solubility, and so on.
- e. ILs can act as reactive agents, which may be of interest for the synthesis of nanoparticles by chemical reactions.
- f. The choice of IL used for the synthesis of nanoparticles determines, at least partially, their properties, including water solubility.
- g. ILs possess negligible vapor pressure and are non-flammable, which allows safer operation at high temperature and under vacuum than with conventional organic solvents.
- h. ILs can be tailored following the 12 principles of green chemistry developed by Anastas and Warner [16] which, besides non-volatility, low toxicity, non-corrosiveness, and non-flammability, do not include requiring auxiliary or separation solvents.

In short, the synthesis of nanoparticles using ILs can be carried out by the following procedures that are more environmentally friendly than those using conventional organic solvents.

In this chapter, the processes used to synthesize biopolymer (polysaccharide or protein) nanoparticles using ILs are reviewed. To the best of our knowledge, the biopolymers used to obtain nanoparticles in processes involving ILs are cellulose, xylan, starch, chitosan, keratin, and silk fibroin. A previous work of the authors based on the synthesis of silk fibroin nanoparticles by dissolving the protein in several ILs is discussed. An example of the biomedical application of curcumin-loaded silk fibroin nanoparticles obtained with this method is also shown.

### 1.3. Methods of synthesis

One method used to obtain nanoparticles in ILs is synthesis *via* physical vapor deposition (PVP) since, due to the negligible vapor pressure of most ILs, they can be manipulated under high vacuum conditions even at high temperatures [17]. This method has been used to obtain metal nanoparticles through vaporization of a metal, an intermetallic phase, or a metal salt in the presence of an IL, for example, copper nanoparticles in the IL butyl-3-methylimidazolium hexafluorophosphate, [bmim<sup>+</sup>][PF<sub>6</sub><sup>-</sup>]. By means of this technique, metal nanoparticles can be deposited not only on the IL but also onto materials dispersed in the IL, as occurs in the formation of Cu/ZnO nanocomposites in butyl-3-methylimidazolium bis((trifluoromethyl)sulfonyl)imide, [bmim<sup>+</sup>][NTf<sub>2</sub><sup>-</sup>]. Nevertheless, to our knowledge, the PVP method has never been applied to obtain nanoparticles from biopolymers in ILs.

Microwave synthesis may be used to profit from the presence of large ions with high polarizability and conductivity of the ILs, which makes them very good media for absorbing microwaves, leading to high heating rates that result in the rapid formation of nuclei (nanoparticles) [18, 19]. Control over the particle size range can be achieved by changing the process temperature and time, as well as reactant concentrations and the choice of the anion and cation constituents of the IL. If the heat spreads uniformly through the sample, a narrow nanoparticle size distribution may be obtained. As an example, silver and gold nanoparticles have been obtained by microwave synthesis in 2-hydroxyethyl-N,N,N-trimethylammonium bis((trifluoromethyl)sulfonyl)amide. Swatloski et al. [20] used microwave heating on a [bmim<sup>+</sup>][Cl<sup>-</sup>]/cellulose solution to dissolve cellulose, but they did not analyze cellulose degradation. Phillips et al. [21] tried to dissolve silk fibroin in [bmim<sup>+</sup>][Cl<sup>-</sup>] using a domestic microwave but were unsuccessful due to the thermal decomposition of the silk. However, our group has found that, by using a laboratory microwave with a strict control of the temperature and time, the integrity of the protein is preserved and nanoparticles can be obtained from silk fibroin-IL solutions by precipitation in polar organic solvents.

Ultrasound synthesis is another alternative that can be used as energy source for the preparation of many materials such as metal, oxide, sulfide, and carbide nanoparticles, and the use of ultrasound power has recently become popular in combination with ILs as the reaction medium [22]. We used high-power ultrasounds to enhance the dissolution process of silk proteins in ILs to obtain silk fibroin nanoparticles (SFNs) directly from the silk/ionic liquid solution (SIL) by rapid desolvation in polar organic solvents [23].

## 2. Synthesis of biopolymer nanoparticles using ILs

### 2.1. Cellulose

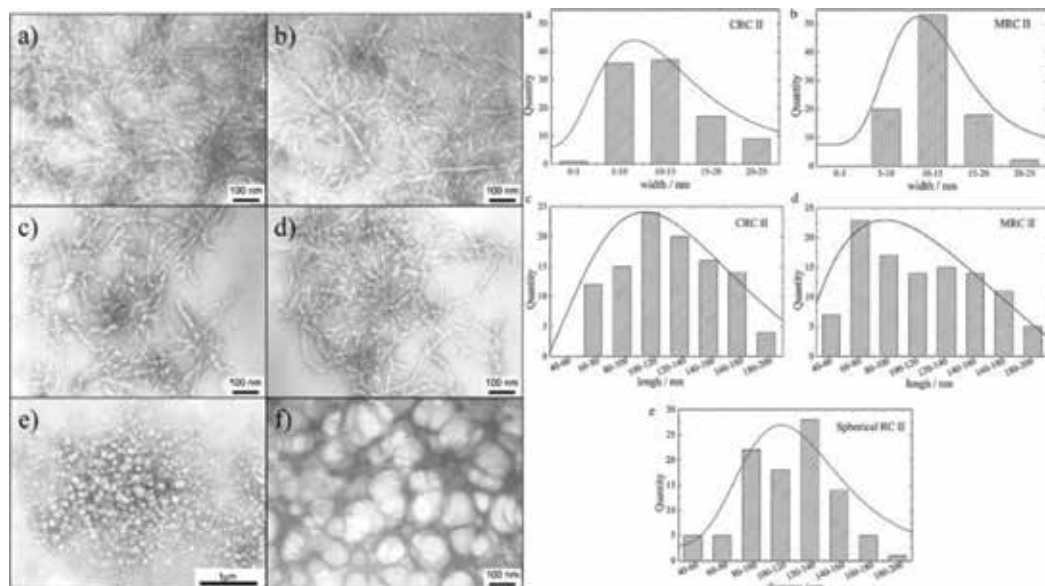
Cellulose is the main constituent of the vegetal kingdom and brown algae, making it the most abundant polysaccharide on earth. It plays a structural role in the cell wall and other surface structures of some amoebae, alveolates, chromists, and red and green algae. The molecular structure of this biopolymer is composed of D-glucopyranose units linked together by a  $\beta(1\rightarrow4)$

glycosidic bond to form a linear structure. The degree of polymerization (DP) varies from the source but can be as high as 23,000 units. Cellulose has a ribbon-like structure, with two units per turn of 1.03 nm, dictated by the allowed angles of C<sub>1</sub>-O and O-C<sub>4</sub> [24, 25]. In terms of density (1.5 Mg m<sup>-3</sup>), cellulose fibers are stiffer (Young's modulus 50–130 GPa) and stronger (1 GPa), when measured along the polymer length, than nylon, silk, chitin, collagen, tendon, or bone [26]. Cellulose is completely insoluble in water, mainly because its hydrogen-bonding capabilities are occupied by side chains, forming aggregates. Nevertheless, it has been demonstrated that the IL 1-butyl-3-methylimidazolium chloride ([bmim<sup>+</sup>][Cl<sup>-</sup>]) is able to solubilize cellulose even at high DP (6500 units), making it an appropriate reaction medium [24]. A review of the solubility of cellulose in ILs is provided by Lee et al. [1].

Swatloski et al. [20] carried out experiments using cellulose-dissolving pulps, fibrous cellulose, and Whatman cellulose filter papers. They prepared the cellulose solutions by the addition of the cellulose to the ionic liquids without pretreatment and heated on a heating plate or in a domestic microwave oven. These authors were able to dissolve 25 wt% cellulose in [bmim<sup>+</sup>][Cl<sup>-</sup>] using microwave heating. Nevertheless, ILs containing “non-coordinating” anions, including [BF<sub>4</sub>]<sup>-</sup> and [PF<sub>6</sub>]<sup>-</sup>, were nonsolvents, presumably because cellulose solubilizes through hydrogen bonding from hydroxyl functions to the anions of the solvent, [Cl<sup>-</sup>]. The authors did not analyze the peak temperature reached during the microwave dissolution step nor the extent of cellulose degradation.

Han et al. [27] synthesized cellulose nanoparticles by dissolving microcrystalline cellulose (MCC) or cotton cellulose (CC) in [bmim<sup>+</sup>][Cl<sup>-</sup>]. The preparation of cellulose nanoparticles involves four steps: dissolution, regeneration, homogenization, and freeze-drying. Before proceeding to the dissolution process, solid state [bmim<sup>+</sup>][Cl<sup>-</sup>], MCC, or CC have to be vacuum-dried to remove the remnants of water, whose presence can significantly impair cellulose solubility in IL by competing with the IL for hydrogen bonds to the cellulose microfibrils [20]. Then, the cellulose was dissolved in IL, using a magnetic hot plate stirrer with safety control, by stirring the 5% w/w disperse fibers for 5 h in a 125°C oil bath. When a clear phase was obtained, the solution was slowly poured into distilled water and a white dispersion of nanoparticles immediately appeared. In order to remove IL, the dispersion was filtered, centrifuged, washed three times, and, eventually, dialyzed. To further enhance the suspension, the sample was run through a high-pressure homogenization, and, finally, the suspensions were quickly frozen by mixing acetone and dry ice in an ice pot and transferred to a freeze-dryer. Particles regenerated from MCC yield rods of 112 ± 42 nm in length with an aspect ratio of 9.21 (**Figure 1c**) and spherical nanoparticles with a diameter of 118 ± 32 nm (**Figure 1e** and **f**). Particles regenerated from CC formed only nanorods of 123 ± 34 nm with an aspect ratio of 9.96 (**Figure 1d**).

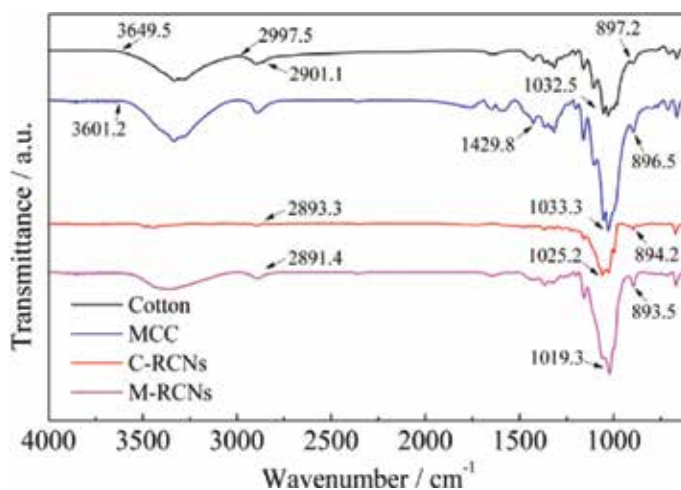
When infrared spectra were used to characterize the cellulose structure of samples, structural changes from a cellulose crystalline structure I to II were evident. For instance, after the regeneration of cotton cellulose, the -CH stretching vibration signals moved from 2901 to a lower 2893 cm<sup>-1</sup>, the CO stretching vibration at C-6 switched from 1033 to 1025 cm<sup>-1</sup>, and COC vibration from β-glycosidic linkage shifted from 897 to 894 cm<sup>-1</sup>, probably due to changes in glycosidic linkage torsion angles. For both the MCC and MCC-NP, spectra showed strong



**Figure 1.** (Left) TEM images of MCC-NP (a), CC-NP (b), homogenized MCC-NP (c), homogenized CC-NP (d), and spherical NP from MCC (e, f). (Right) The dimension distribution of homogenized CC-NP, MCC-NP, and spherical MCC-NP. (a) and (b) width distribution of C-RCNs and M-RCNs; (c) and (d) length distribution of C-RCNs and M-RCNs; (e) diameter distribution of spherical RCNs. From Ref. [27] with permission of Elsevier Limited.

hydrogen bonded OH stretching vibrations in the range of  $3000\text{--}3600\text{ cm}^{-1}$ . The signals at around  $1430$  and  $2900\text{ cm}^{-1}$  were awarded to  $\text{CH}_2$  (C6) bending vibration and CH stretching vibration, respectively. Adsorbed water was noticed by a peak at  $1644\text{ cm}^{-1}$  from O-H bending. Characteristic FTIR absorption bands related to the transition from cellulose I to cellulose II were also watched. A deeper analysis of the structural changes can be found in the author's publication [27] and references therein. The lack of absorption bands from  $[\text{bmim}^+][\text{Cl}^-]$  suggests that the ILs were successfully removed. The properties of regenerated cellulose nanoparticles produced from microcrystalline cellulose and cotton using a combined IL and high-pressure homogenization treatment point to the potential for application in the biomedicine field as drug delivery systems, biomarkers, tablet excipients, and more (**Figure 2**).

Cellulose is susceptible to modification due to its hydroxyl groups; for example, silylation is one possible route for the synthesis of water-soluble derivatives, thus broadening the spectrum of possibilities. Silylation can take place in heterogeneous media like pyridine, or in homogeneous media, like methyl sulfoxide/LiCl. Nevertheless, in heterogeneous media, the reaction is not even at whole cellulose molecule and the use of homogeneous media is not applicable on a large scale as it is impossible to regenerate the media. Heinz's research group [28] prepared trimethylsilyl cellulose (TMSC) nanoparticles by taking advantage of the solubilizing power of IL and the self-assembly capabilities of TMSC. In brief, cellulose is first solubilized in  $[\text{emim}^+][\text{Ac}^-]$  10% w/w, and hexamethyldisilane is added in a 3–1 excess molar ration with respect to the glucose units of cellulose. After a reaction time of 1 h at  $80^\circ\text{C}$ , a 2.65° of substitution (DS) was obtained. TMSC nanoparticles are dissolved in an organic solvent such as tetrahydrofuran



**Figure 2.** FTIR spectra of raw cotton, C-RCNs, untreated MCC and M-RCNs. From Ref. [27] with permission of Elsevier Limited.

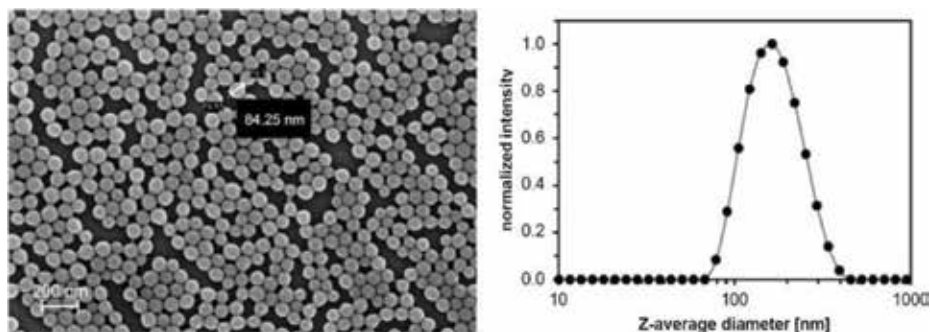
or dimethyl acetone and dialyzed against water. Nanoparticles of 170 nm are formed based on the slow exchange of an organic solvent against an anti-solvent (non-solvent).

Cellulose-magnetite composites have also been prepared by suspension and dispersion of particles of magnetite in a homogeneous solution of cellulose in IL followed by regeneration in water and the subsequent preparation of films, flocs, fibers, or beads. The materials prepared were ferromagnetic, with a small superparamagnetic response. Characterization by X-ray diffraction showed that the initial magnetite was chemically unaltered after encapsulation, with an average particle size of approximately 25 nm [29].

## 2.2. Xylan

Xylan is the second most abundant polysaccharide in the vegetal kingdom after cellulose. It is the major component of hemicellulose, constituting 25–35% of the biomass of woody tissues of dicots and lignified tissues of monocots and up to 50% of some tissues of cereal grains [30]. It has a linear backbone constituted by  $\beta$ -D-xylosa units bound together by a  $\beta(1\rightarrow4)$  glycosidic bond. Xylan normally presents side chain sugars such as 4-O-methyl-glucuronic acid, galacturonic acid, and arabinose.

Gerick et al. [31] synthesized nanoparticles with a hydrodynamic radius of ca. 160 nm (**Figure 3**) of modified xylan with phenyl carbonate groups (DS up to 2.0). For the synthesis of xylan nanoparticles, 2 g of xylan and 18 g [bmim<sup>+</sup>][Cl<sup>-</sup>] were stirred for 1 h at 80°C. Afterwards, 5 mL of pyridine was added and stirred for 18 h at 80°C. The solution was cooled to 25°C under nitrogen atmosphere; then 15 mL of pyridine followed by 3.82 mL of phenyl chloroformate (60.8 mmol) were added. After 3 h of reaction time at 25°C, the mixture was poured into 300 mL ice cold water. The precipitate was removed by filtration and washed twice with 150 mL of water and twice with 150 mL of ethanol. The crude product was dissolved in 40 mL of DMSO



**Figure 3.** (left) Scanning electron microscopy images of nanoparticles obtained by dialysis of xylan phenyl carbonate XPC 20. (right) Size distribution of XPC 20 nanoparticles obtained by dynamic light scattering. From Ref. [31] with permission of Elsevier Limited.

and then precipitated in 300 mL of ethanol. This functionalization allows the molecule to have a major electrophilic center for further functionalization with drugs, signaling molecules, recognition molecules, and so on. Many other xylan modifications/functionalizations are described in Petzold-Welcke's review [32]. For example, the modification of xylan with a methyl group can be used as polymeric tensides, and some esters showed good drug-carrying capabilities. Xylan sulfate may be applied as antiviral drugs and as blood coagulation inhibitor.

### 2.3. Starch

Starch is produced by green plants to store energy. Granules of starch accumulate at high concentrations in reproductive structures like cereal grains (e.g., wheat, rice, maize, barley, rye, oats, millet, and sorghum) and in vegetative structures such as tubers (potatoes) and roots (cassava and taro) [33]. The two major forms of starch are amylose and amylopectin. The first is the linear polymer of D-glucopyranose units bound by  $\alpha(1\rightarrow4)$  glycosidic bond. Its molecular weight varies from  $10^4$  to  $10^5$  with a DP of 250–1000 units. The second is a highly branched polymer of  $\alpha(1\rightarrow4)$  glycosidic bonds and lateral chains of  $\alpha(1\rightarrow6)$  with a molecular weight of  $10^6$ – $10^8$ , corresponding to a DP of 5000–50,000 units [34, 35].

Zhou et al. [36, 37] prepared starch nanoparticles with a controlled mean diameter of 64–255 nm with a water/ionic liquid emulsion (W/IL) cross-linked technique. To prepare the aqueous phase, 0.5 g of acid-treated granular starch was dissolved in 9.5 g of NaOH solution (20 M) and then added to 40 g of [bmim<sup>+</sup>][PF<sub>6</sub><sup>-</sup>] to form the water/IL microemulsion with 40 g of a mixture of TX-100 surfactant and 1-butanol cosurfactant (TX-100/1-butanol = 3:1, w/w). After several minutes of stirring, 1.84 g of epichlorohydrin was added to the above microemulsion as a cross-linker. At this point, the mixture was stirred at 50°C for 4 h. Next, this solution was allowed to reach room temperature and methanol was used as antisolvent to precipitate the starch nanoparticles. The precipitate was centrifuged and washed thoroughly with sufficient methanol and ethanol to eliminate unreacted epichlorohydrin, remaining [bmim<sup>+</sup>][PF<sub>6</sub><sup>-</sup>], TX-100, and 1-butanol. Finally, the solid was dried in a vacuum for 24 h at 45°C. More examples of starch nanoparticle synthesis in IL emulsions can be found in the



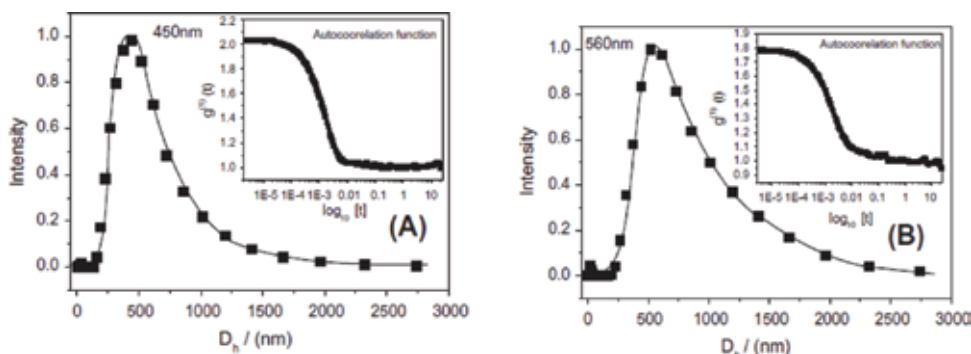
study [38–40]. The drug-loading and -releasing capabilities of the starch nanoparticles were tasted with mitoxantrone hydrochloride.

## 2.4. Chitosan

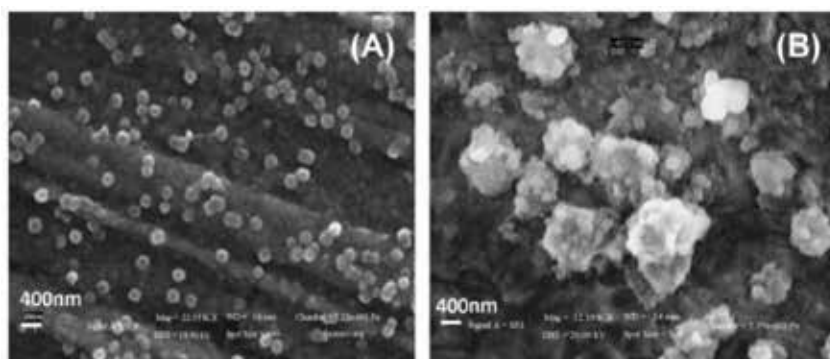
Chitosan is a lineal polysaccharide constituted by randomly distributed  $\beta$ -(1  $\rightarrow$  4)-linked D-glucosamine and N-acetyl-D-glucosamine. Chitosan is obtained from the deacetylation of chitin via basic hydrolysis. Chitin is mostly present in the exoskeleton of crustaceans, insect wings, and cell walls of fungi and algae, among others. Chitosan nanoparticles are widely used in food and bioengineering industries for the encapsulation of active food ingredients, enzyme immobilization, as a carrier for controlled drug delivery, and in agriculture as a plant antimicrobial agent and growth promoter [41]. For instance, Torzsas et al. showed that chitosan may have an important role in protecting against colon cancer [42] (**Figure 4**).

Bharmoria et al. [43] reported the synthesis of chitosan nanoparticles by ionic cross-linking with IL for the first time. The simple, self-assembling methods consist of adding [bmim<sup>+</sup>][C<sub>8</sub>OSO<sub>3</sub><sup>-</sup>] or [omim<sup>+</sup>][Cl<sup>-</sup>] above the critical micelle concentration to an aqueous solution of chitosan. The chitosan chains are attracted to IL micelles by charge interactions and aggregate in a gelled complex. Acetone is used as antisolvent to precipitate the nanoparticles, which have a mean hydrodynamic diameter in the range of 300–560 nm with Z potential above +58.5 mV, depending on the IL used. The authors assumed that the electrostatic and hydrophobic interaction produced between chitosan and IL directs the formation of chitosan nanoparticle, where IL aggregates act as templates. Scanning electron microscopy (SEM) revealed that the nanoparticles obtained from chitosan-[bmim<sup>+</sup>][C<sub>8</sub>OSO<sub>3</sub><sup>-</sup>] solutions have a greater sphericity and a lower tendency to agglomerate (**Figure 5**).

Chitosan nanoparticles have previously been tested for cellular uptake and trafficking to lymph nodes with very promising results [44]. Furthermore, chitosan-based nanoparticles are of special interest for the oral administration of insulin, as subcutaneous administration suffers disadvantages such as patient noncompliance and occasional hypoglycemia. Moreover, these last approaches do not mimic the normal physiological pattern of insulin release [45].



**Figure 4.** Hydrodynamic diameter (D<sub>h</sub>) plots of chitosan nanoparticles formed with (A) [bmim<sup>+</sup>][C<sub>8</sub>OSO<sub>3</sub><sup>-</sup>] and (B) [omim<sup>+</sup>][Cl<sup>-</sup>]. From Ref. [43] with permission of Elsevier Limited.



**Figure 5.** SEM images of nanoparticles formed with (A)  $[\text{bmim}^+][\text{C}_8\text{OSO}_3^-]$  and (B)  $[\text{omim}^+][\text{Cl}^-]$ . From Ref. [43] with permission of Elsevier Limited.

## 2.5. Silk fibroin

Due to its excellent biocompatibility and mechanical properties, silk fibroin (SF) obtained from *Bombyx mori* cocoons is an attractive biomaterial for use in biomedical and tissue engineering applications [46]. This biomaterial, formulated as particles, has potential applications in medicine for its capacity to adsorb, transport, and deliver a wide range of bioactive molecules [47]. Silks are insoluble in most solvents, including water, dilute acid, and alkali. There are two classical solvent systems to dissolve SF: *ionic hydro-alcoholic solutions*, such as a  $\text{CaCl}_2$ /ethanol/water mixture (Ajisawa's reagent) [48], or *ionic aqueous solutions*, traditionally 9.3 M LiBr or 50 wt%  $\text{CaCl}_2$  solution [49]. These solutions require to be dialyzed for 48 h against ultra-pure water using a cellulose semi-permeable membrane (cut-off 3.5 KD) to remove salts, pigments, small peptides, and other impurities of the silk solution. Both processes are time-consuming, and the solutions are unstable and aggregate to a gel state. For long-term storage, aqueous solutions of SF can be lyophilized and redissolved in organic solvents such as 1,1,1,3,3,3-hexafluoroisopropanol (HFIP). However, these solvents are toxic and extremely corrosive, requiring considerable care in handling [50].

The suitability of imidazolium-based ionic liquid solvents, such as 1-butyl-3-methylimidazolium chloride ( $[\text{bmim}^+][\text{Cl}^-]$ ), to form stable SF solutions was demonstrated [21]. Within an ionic liquid, the anion plays a larger role in dictating the ultimate solubility of the SF, attributed to the ability of the anion to disrupt the hydrogen bonding in the  $\beta$ -sheets of the silkworm SF to form solutions (mainly halogens or small carboxylates) [51]. The use of ILs as solvents has the advantage that the total number of steps required for the dissolution process is reduced and, furthermore, the cocoon can be dissolved directly because sericin was also dissolved in the selected ILs. However, complete dissolution of SF using the classic above-described methods takes several hours, even with intense heating at  $100^\circ\text{C}$  [21], resulting in the loss of protein integrity. Long treatments lead to breakage of the peptidic chains and poor mechanical properties of the resulting biomaterials. On the other hand, the process of silk dissolution may be improved by applying high-power ultrasounds to the SIL mixture to accelerate the process and by adding water to reduce the viscosity. High-power ultrasounds

have two important synergistic effects on the mixture: rapid heating and efficient disruption of the fibers at the same time. By applying the precipitation method commonly used for the coagulation of an aqueous SF solution in a water-miscible organic solvent, it is possible to obtain particles of regenerated SF [52].

The dissolution of *B. mori* SF using an oil bath as the heat source was investigated in the assembled state of the fibers. **Table 1** summarizes the results. Complete dissolution took over 1 h at 100°C, as described by Phillips et al. [21]. The saturated solubilities by weight for SF in 1-alkyl-3-methylimidazolium chlorides are dependent on the length of the alkyl substituent of the imidazolium ring.

It was checked that 1-alkyl-3-methyl imidazolium chlorides are able to disrupt the hydrogen bonding in silkworm SF and they are good solvents for silk dissolution when the length of the alkyl chain is lower than eight carbons [21]. The hydrophobicity of the organic cation increases with the cation alkyl chain length, so that long-aliphatic-chain ILs cannot dissolve SF. Likewise, ILs with highly hydrophobic anions cannot act as solvents of SF.

Silk proteins were successfully dissolved in the 1-alkyl-3-methylimidazolium chlorides (where 1-alkyl is: *methyl* [mim<sup>+</sup>][Cl<sup>-</sup>]; *ethyl* [emim<sup>+</sup>][Cl<sup>-</sup>]; *propyl* [pmim<sup>+</sup>][Cl<sup>-</sup>]; *butyl* [bmim<sup>+</sup>][Cl<sup>-</sup>] or *hexyl* [hmim<sup>+</sup>][Cl<sup>-</sup>]) using high-power ultrasounds and limiting the temperature at 100°C. The saturated solubility by weight and the time required for silk dissolution in selected ILs are listed in **Table 2**.

In an oil bath at 100°C, the thermal heating process of SF or SC dissolution in ILs takes hours, but instead, by using ultrasounds, a significant reduction is achieved in the time necessary to complete dissolution. The break of the β-sheet hydrogen bonds network of the proteins was enhanced by the use of the high-power ultrasounds.

Although the solubility of SF was highest in [emim<sup>+</sup>][Cl<sup>-</sup>], for particle formation, it is not necessary to reach a concentration higher than 10% (w/w), since an increased viscosity represents a handicap for handling.

IL	SF solubility (wt%)	IL	SF solubility (wt%)
[mim <sup>+</sup> ][Cl <sup>-</sup> ]	Soluble (>12%)	[eim <sup>+</sup> ][Cl <sup>-</sup> ]	Insoluble*
[emim <sup>+</sup> ][Cl <sup>-</sup> ]	Soluble (>23%)	[emim <sup>+</sup> ]EtSO <sub>4</sub> <sup>-</sup>	Insoluble*
[pmim <sup>+</sup> ][Cl <sup>-</sup> ]	Soluble (>15%)	[emim <sup>+</sup> ]TfO <sup>-</sup>	Insoluble*
[bmim <sup>+</sup> ][Cl <sup>-</sup> ]	Soluble (>12%)	[bmim <sup>+</sup> ]OctSO <sub>4</sub> <sup>-</sup>	Insoluble*
[hmim <sup>+</sup> ][Cl <sup>-</sup> ]	Soluble (>11%)	[bBmim <sup>+</sup> ]PF <sub>6</sub> <sup>-</sup>	Insoluble*
[omim <sup>+</sup> ][Cl <sup>-</sup> ]	Insoluble*	[3-MEP <sup>+</sup> ]EtSO <sub>4</sub> <sup>-</sup>	Insoluble*
[dmim <sup>+</sup> ][Cl <sup>-</sup> ]	Insoluble*	ETAN	Insoluble*

\*After 24 h at 90°C.

**Table 1.** Solubility (%wt) of SF in selected ILs at 90°C (heated in an oil bath). From Ref. [23] with permission of Wiley Online Library.

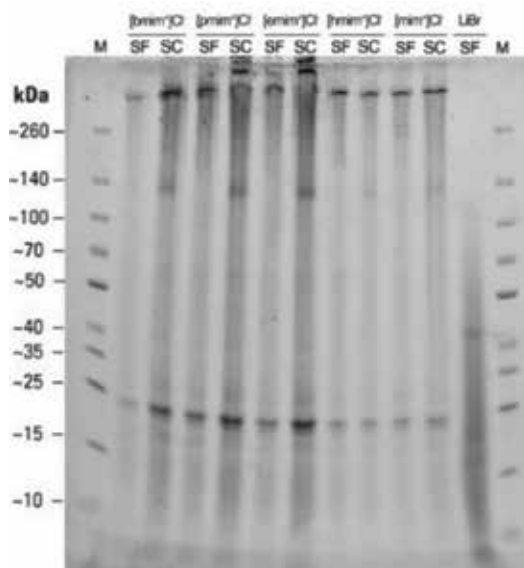
Solvent	Silk fibroin (SF)		Silk cocoon (SC)	
	Solubility (%wt)	Time (min.)	Solubility (%wt)	Time (min.)
[mim <sup>+</sup> ][Cl <sup>-</sup> ]	12.5 ± 0.1	4	12.5 ± 0.1	17
[emim <sup>+</sup> ][Cl <sup>-</sup> ]	23.0 ± 0.3	17	18.7 ± 0.6	67
[pmim <sup>+</sup> ][Cl <sup>-</sup> ]	15.2 ± 0.3	14	17.6 ± 0.1	27
[bmim <sup>+</sup> ][Cl <sup>-</sup> ]	12.7 ± 0.6	5	12.9 ± 0.4	24
[hmim <sup>+</sup> ][Cl <sup>-</sup> ]	10.9 ± 0.2	8	11.1 ± 0.3	20

Solubility is presented as the average value ± SD (standard deviation) (*n* = 3).

**Table 2.** Solubility and time required for dissolution of silk proteins, in selected ILs. From Ref. [23] with permission of Wiley Online Library.

Silk protein integrity in the SIL solutions was confirmed by sodium dodecyl sulfate-polyacrylamide gel electrophoresis (SDS-PAGE). It was found that the peptidic chain fragmentation that occurs when the classical dissolution methods are used is drastically reduced in the process with ILs and high-power ultrasound. In **Figure 6**, the molecular masses of the fragments of the SIL solutions may be observed, which are practically the same than that of the SF present in the silkworm gland [53].

The overall process of SFNs preparation from SIL solutions is summarized in **Figure 7**. The procedure is based on the method described previously by Zhang et al., with modifications [52].



**Figure 6.** Sodium dodecyl sulfate-polyacrylamide gel electrophoresis of the protein components of silk fibroin (SF) and white silk cocoons (SC) after the use of high-power ultrasounds in the solutions SC/IL or SF/IL with ILs: [bmim<sup>+</sup>][Cl<sup>-</sup>], [pmim<sup>+</sup>][Cl<sup>-</sup>], [emim<sup>+</sup>][Cl<sup>-</sup>], [hmim<sup>+</sup>][Cl<sup>-</sup>] and [mim<sup>+</sup>][Cl<sup>-</sup>]. From Ref. [23] with permission of Wiley Online Library.



**Figure 7.** Scheme of the overall process of SF dissolution, using ILs and ultrasonication, and consequent SFNs preparation from SIL solutions. From Ref. [23] with permission of Wiley Online Library.

In brief, to the freshly prepared SIL solution, ultrapure water was added to reduce its viscosity, and the SIL solution was slowly dripped into 100 mL of vigorously stirred cold methanol. After a few drops, a milky-white suspension appeared and the suspension was stirred for 2 h. The particle suspension was recovered by centrifugation at 18,000 g for 15 min, at 4°C. The supernatant (free of particles) was removed and reserved for subsequent recycling of the IL. The white precipitate was subjected to successive rinses with fresh methanol and ultrapure water. After lyophilizing the particles for 72 h at 0.5 mbar and −55°C (Edwards Modulyo 4 K Freeze Dryer), SFNs were obtained in the form of a dry powder. A rotary evaporator at 80 mbar and 80°C was used to recover the IL from the methanolic and water fractions.

The liquid silk fibroin can be regenerated as nanoparticles by pouring SIL solution into an excess of a polar organic solvent. In this case, methanol was used for SF regeneration. When the IL is dissolved in methanol from the SIL solution, the SF changes from random coil and  $\alpha$ -helix forms into anti-parallel  $\beta$ -sheet form by reconstitution of the hydrogen bonds network of the protein chains [52].

The particles were characterized by dynamic light scattering (DLS) and infrared spectroscopy (FTIR). The stability of the particles was tested in purified water at 25°C and in Dulbecco's Modified Eagle Medium (DMEM) (without Fetal Bovine Serum (FBS) supplementation) at 37°C. In MilliQ water at 25°C, the SFNs had an average size of 170–184 nm measured by DLS. The results indicate that the particles were slightly larger (183–341 nm) when dispersed in DMEM (see **Table 3**); these values are almost identical to those described previously in the corresponding study [52, 54].

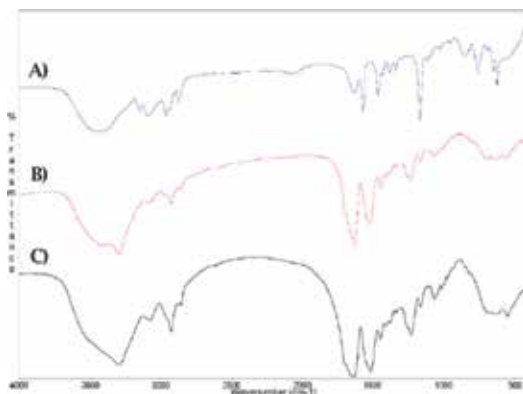
In **Figure 8**, a comparative FTIR spectrum of  $[\text{bmim}^+][\text{Cl}^-]$ , SFNs regenerated from SF/ $[\text{bmim}^+][\text{Cl}^-]$  solution and SFNs regenerated from classical  $\text{CaCl}_2/\text{EtOH}/\text{H}_2\text{O}$  solution, obtained using the classical Zhang's method [52] is presented. As can be observed,  $\beta$ -sheet is predominant in particles with peaks at 1230 (Amide III, C-H Stretching), 1516 (Amide II, N-H Bending), and 1626  $\text{cm}^{-1}$  (Amide I, C=O Stretching), which are typical of the  $\beta$ -sheet conformation [27]. The SFN profiles were similar to those of SFNs obtained by methanol immersion of SF dissolved

Solvent used	MilliQ water at 25°C			DMEM at 37°C		
	Diameter <sup>a</sup> (nm)	PdI <sup>b</sup>	Zpot <sup>a</sup> (mV)	Diameter <sup>a</sup> (nm)	PdI <sup>b</sup>	Zpot <sup>a</sup> (mV)
CaCl <sub>2</sub> /EtOH/H <sub>2</sub> O	174 ± 2	0.121	-26.23 ± 0.59	183 ± 3	0.140	-12.02 ± 0.42
[mim <sup>+</sup> ][Cl <sup>-</sup> ]	177 ± 4	0.153	-27.15 ± 0.74	208 ± 4	0.115	-12.08 ± 1.50
[emim <sup>+</sup> ][Cl <sup>-</sup> ]	181 ± 3	0.230	-25.65 ± 0.90	341 ± 9	0.393	-12.00 ± 2.12
[pmim <sup>+</sup> ][Cl <sup>-</sup> ]	175 ± 4	0.129	-27.53 ± 0.66	211 ± 4	0.076	-12.22 ± 1.09
[bmim <sup>+</sup> ][Cl <sup>-</sup> ]	184 ± 5	0.212	-24.53 ± 1.42	235 ± 4	0.245	-12.24 ± 1.66
[hmim <sup>+</sup> ][Cl <sup>-</sup> ]	176 ± 3	0.140	-27.90 ± 0.82	200 ± 3	0.133	-11.28 ± 0.55

<sup>a</sup>Z-average ± SD (n = 5) and accumulation times = 100.

<sup>b</sup>Average value.

**Table 3.** Comparative values for the particle size (diameter), polydispersity (PdI), and zeta potential of classical SFNs [52] obtained from CaCl<sub>2</sub>/EtOH/H<sub>2</sub>O solvent and SFNs produced from SIL solutions. From Ref. [23] with permission of Wiley Online Library.

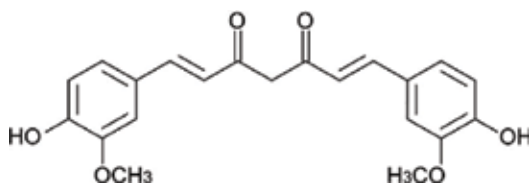


**Figure 8.** Comparative FTIR spectra of (A) only [bmim<sup>+</sup>][Cl<sup>-</sup>]; (B) SFNs regenerated from SF/[bmim<sup>+</sup>][Cl<sup>-</sup>] solution; (C) SFNs regenerated from classical CaCl<sub>2</sub>/EtOH/H<sub>2</sub>O solution [52]. From Ref. [23] with permission of Wiley Online Library.

in the Ajisawa solvent system [52, 55]. Characteristic signals of ILs (1572, 1465, and 1170 cm<sup>-1</sup>) were absent in the recorded spectrum of SFNs obtained from [bmim<sup>+</sup>][Cl<sup>-</sup>], indicating that the IL was efficiently washed out from the SFNs.

### 2.5.1. Synthesis of curcumin-loaded silk fibroin nanoparticles using ILs

Curcumin ((1E,6E)-1,7-bis(4-hydroxy-3-methoxyphenyl)hepta-1,6-diene-3,5-dione, **Figure 9**) is a hydrophobic polyphenol derived from turmeric: the rhizome of the herb *Curcuma longa* [56]. From the chemical point of view, curcumin is a bis- $\alpha,\beta$ -unsaturated  $\beta$ -diketone (also called diferuloylmethane) that shows keto-enol tautomerism, with a stable enol form in alkaline media and a predominant keto form in acidic and neutral solutions. Commercial curcumin is a mixture of curcuminoids (approximately, 77% diferuloylmethane, 18% demethoxycurcumin, and 5% bisdemethoxycurcumin) [57]. *C. longa* mainly grows in China and India although it can



**Figure 9.** Chemical structure of curcumin [5].

also be present in the rest of the Asian continent and has been widely employed in Ayurvedic medicine for centuries [58]. Its most relevant pharmacological effects are its anti-inflammatory [59], anticancer [57], antioxidant [60], and antimicrobial [60] activities.

Although curcumin is safe, nontoxic, and well tolerated in animal and human studies, it cannot be administered to patients directly due to its poor solubility in water [56] (estimated value: 3.12 mg/L at 25°C [61]). In an attempt to enhance the therapeutic efficiency of curcumin, improvements in its bioavailability have been tried. Several nanocarriers such as solid lipid nanoparticles [62], natural [63] or synthetic [64] polymer nanoparticles, and inorganic nanoparticles [65] can be found in the study as examples of nanoplatforms for the intracellular delivery of curcumin. Recently, research interests focus on the use of biopolymers such as SF to encapsulate curcumin and other similar drugs [66]. By virtue of their small size, SFNs can penetrate thin capillaries, fostering the uptake of drugs by cells. In addition, these SFNs are potential targeted delivery systems because, for instance, they can deliver antitumor drugs to tumor cells. Several research groups have studied curcumin encapsulation in SFNs by different techniques [67, 68].

The authors [5] studied the synthesis of curcumin-loaded SFNs (Curc-SFNs) to improve on current methods, using IL (1-ethyl-3-methylimidazolium acetate, [emim<sup>+</sup>][CH<sub>3</sub>COO<sup>-</sup>]) and high-power ultrasounds to dissolve the SF. The synthesis of Curc-SFNs developed in this chapter is a more scalable and continuous processing option than those already published in the study. The drug was loaded into the SFNs by physical adsorption, Curc-SFNs 1, and by coprecipitation, Curc-SFNs 2, in order to obtain Curc-SFNs.

For loading of curcumin by physical adsorption, 40 mL of a 1 mg/mL solution of curcumin in ethanol was used to resuspend 325 mg of SFNs obtained from an SF-IL solution. The suspension was ultrasonicated for 5 min and gently stirred at 30 rpm in a Tube Rotator for 24 h. Next, Curc-SFNs 1 were centrifuged for 15 min at 13,400 rpm. Finally, Curc-SFNs 1 were washed with water to eliminate the rest of ethanol. The drug loaded in the nanoparticles was indirectly determined by the measurement of the UV absorbance of curcumin at 421 nm in the centrifugation supernatants (ethanol and water) and in the initial curcumin solution.

To obtain Curc-SFNs 2 by coprecipitation, the drug was loaded in the nanoparticles throughout the synthesis step. In brief, an exact weighed amount of curcumin (25 mg) was dissolved in 3 mL of 0.1 M NaOH solution, and this solution was immediately dissolved in 5 g of a previously prepared SIL solution (10% wt.). The drug-SIL solution was heated to 60°C to reduce the viscosity of the mixture and sprayed with nitrogen onto 100 mL of gently stirred ethanol. The orange suspension was stirred for 2 h before being centrifuged at 13,400 rpm for

15 min, at 4°C. In this case, three washes with water were carried out to remove the IL. Lyophilization was carried out under the experimental conditions described earlier.

Drug loading content (DLC) and entrapment efficiency (EE) of Curc-SFNs 1 and Curc-SFNs 2 obtained were calculated according to the following expressions from the measurements of UV–Vis absorbance of curcumin:

$$DLC = \frac{\text{weight of the drug in nanoparticles}}{\text{weight of the nanoparticles}} \cdot 100 \quad (1)$$

$$EE = \frac{\text{weight of the drug in nanoparticles}}{\text{weight of the feeding drugs}} \cdot 100 \quad (2)$$

As can be seen in **Table 4**, DLC values in the physical adsorption assays were higher than in the coprecipitation experiments, probably due to the much higher initial curcumin/SF mass ratio in the physical adsorption experiments. Nevertheless, the EE values were about 50% for both types of nanoparticles. DLC and EE are in the same order or even higher than those found in the study [69, 70].

Furthermore, the mean hydrodynamic diameter (Z-average), the PdI, the zeta potential, and the electrophoretic mobility were measured by DLS. All measurements were performed in purified water at 25°C. The mean values of the measurements performed in triplicate are reported in **Table 5**. The results revealed that the Z-average of the SFNs was smaller than of the particles with curcumin, whereas the PdI values were similar and lower than 0.15 for all types of nanoparticles, resulting in size distributions practically monodisperse. The zeta potential of the nanoparticles with and without curcumin was highly negative and of the same order of magnitude, indicating their high colloidal stability and higher than the values found in

	Curc-SFNs 1 <sup>1</sup>	Curc-SFNs 2 <sup>1</sup>
DLC (%)	6.63 ± 0.09	2.47 ± 0.11
EE (%)	53.75 ± 0.81	48.84 ± 2.67

<sup>1</sup>Mean values ± SD (standard deviation) (n = 3).

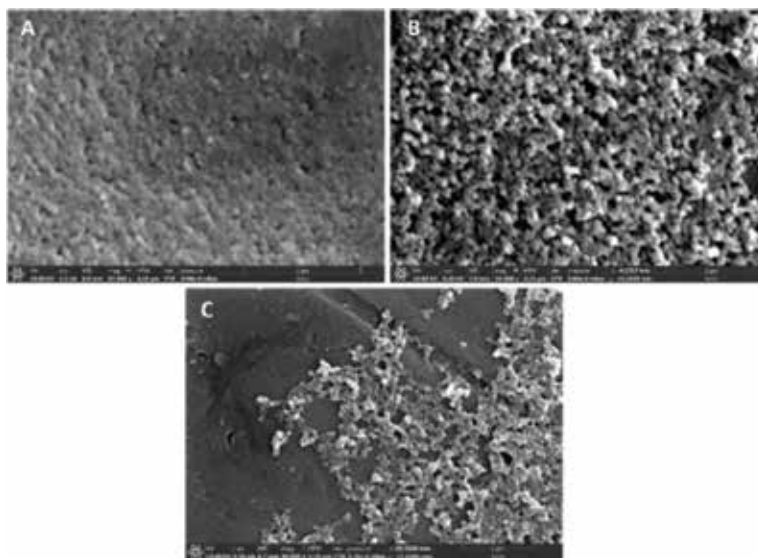
**Table 4.** Drug loading and encapsulation efficiency of the Cur-SFNs [5].

	Zeta potential (mV)	Z-average (nm)	Electrophoretic mobility (μmcm/Vs)	PdI
Curc-SFNs 1	−42.9 ± 2.8	166.0 ± 0.1	−3.362 ± 0.264	0.114 ± 0.003
Curc-SFNs 2	−45.9 ± 5.0	171.2 ± 2.6	−3.504 ± 0.348	0.106 ± 0.017
SFNs	−41.3 ± 0.6	157.9 ± 1.5	−3.396 ± 0.146	0.132 ± 0.011

Mean values ± SD (standard deviation).

**Table 5.** Physical characterization of the Curc-SFNs. From Ref. [5] with permission of MDPI.





**Figure 10.** FESEM pictures of (a) SFNs, (b) Curc-SFNs 1, and (c) Curc-SFNs 2 [5].

previous studies which synthesize SFNs by classical methods [52, 70], which reflects the improvement in stability of the SFNs and hence of the Curc-SFNs obtained with this new procedure.

The morphology of the nanoparticles was examined by field emission scanning electron microscopy (FESEM). As can be observed in **Figure 10**, SFNs and Curc-SFNs 1 present nanospherical morphology. However, Curc-SFNs 2 has elongated shape. FESEM micrographs showed smaller sizes than the DLS measurements. This could be due to the swelling of the nanoparticles in the water solution in DLS measurements. This difference has also been observed in previous works [52, 69].

The Curc-SFNs obtained in this work enhanced the antitumor activity of curcumin toward the two different tumor cell lines studied (hepatocellular carcinoma, Hep3B and human neuroblastoma, Kelly Cells), while the viability of the healthy cells (human bone marrow-derived mesenchymal stem cells, hBMSCs) did not decrease. This broadens the possibility of using these SFNs, which have been synthesized by an industrial process, as future systems for other drugs of hydrophilic or hydrophobic nature, such as curcumin.

### 3. Conclusions

ILs are excellent candidates to participate in the synthesis of biopolymeric nanoparticles mainly because they can dissolve biopolymers due to their design flexibility by combining different cation and anion and their green solvent properties such as non-volatility, non-flammability, and recyclability. Different biopolymers, such as cellulose, xylan, starch, chitosan, keratin, and

silk fibroin, were used to obtain nanoparticles in processes involving ILs. We synthesized SFNs by a new methodology using high-power ultrasounds to enhance the dissolution of the protein in the IL. From SIL solutions, SFNs were obtained by regeneration of the SF in an organic polar solvent, and SFNs showed a high degree of  $\beta$ -sheet, similar to that of the SF native fibers. In this way, large amounts of silk can be turned into biomaterials directly from the dissolved SIL solution, for use in a wide range of applications. Focusing on the biomedical application, Curc-SFNs were successfully synthesized by two environmentally friendly procedures using ILs and high-power ultrasound to dissolve the SF. High DLC and EE values were obtained in both cases compared with those in the study. The SFNs and the Curc-SFNs obtained showed a narrow size distribution, with a hydrodynamic diameter of <175 nm, and high zeta potential (in absolute terms), which make them excellent nanocarriers for use in therapeutic treatments.

## Acknowledgements

This work has been partially supported from the European Commission (FEDER/ERDF) and the Spanish MINECO (Ref. CTQ2014-57467-R and Ref. CTQ2017-87708-R) and the programme of support to the research of the Seneca Foundation of Science and Technology of Murcia, Spain (Ref. 19499/PI/14). The research contract of Dr. A. Abel Lozano-Pérez was partially supported (80%) by the ERDF/FEDER Operative Programme of the Region of Murcia (Project No. 14-20-01).

## Conflict of interest

The authors declare no conflict of interest.

## Author details

Mercedes G. Montalbán<sup>1</sup>, Guzmán Carissimi<sup>2</sup>, A. Abel Lozano-Pérez<sup>3</sup>, José Luis Cenis<sup>3</sup>, Jeannine M. Coburn<sup>4,5</sup>, David L. Kaplan<sup>4</sup> and Gloria Víllora<sup>2\*</sup>

\*Address all correspondence to: gvillora@um.es

1 Department of Chemical Engineering, University of Alicante, Alicante, Spain

2 Department of Chemical Engineering, Faculty of Chemistry, Regional Campus of International Excellence "Campus Mare Nostrum", University of Murcia, Murcia, Spain

3 Department of Biotechnology, Instituto Murciano de Investigación y Desarrollo Agrario y Alimentario (IMIDA), La Alberca (Murcia), Spain

4 Department of Biomedical Engineering, Tufts University, Medford, MA, USA

5 Department of Biomedical Engineering, Worcester Polytechnic Institute, Worcester, MA, USA

## References

- [1] Lee SH, Miyauchi M, Dordick JS, Linhardt RJ. Preparation of biopolymer-based materials using ionic liquids for the biomedical application. In: Malhotra SV, editor. *Ionic Liquid Applications: Pharmaceuticals, Therapeutics, and Biotechnology*. 1st ed. ACS Symposium Series, Washington D.C. (USA): ACS Publications; 2010. pp. 115-134. DOI: 10.1021/bk-2010-1038.ch010
- [2] Nitta SK, Numata K. Biopolymer-based nanoparticles for drug/gene delivery and tissue engineering. *International Journal of Molecular Sciences*. 2013;**14**:1629-1654. DOI: 10.3390/ijms14011629
- [3] Yih TC, Al-Fandi M. Engineered nanoparticles as precise drug delivery systems. *Journal of Cellular Biochemistry*. 2006;**97**:1184-1190. DOI: 10.1002/jcb.20796
- [4] Lozano-Pérez AA, Rivero HC, Pérez Hernández MC, Pagán A, Montalbán MG, Villora G, Cenis JL. Silk fibroin nanoparticles: Efficient vehicles for the natural antioxidant quercetin. *International Journal of Pharmaceutics*. 2017;**518**:11-19. DOI: 10.1016/j.ijpharm.2016.12.046
- [5] Montalbán MG, Coburn JM, Lozano-Pérez AA, Cenis JL, Villora G, Kaplan DL. Production of curcumin-loaded silk fibroin nanoparticles for cancer therapy. *Nanomaterials*. 2018;**8**:1-18. DOI: 10.3390/nano8020126
- [6] Gómez-Murcia V, Montalbán MG, Gómez-Fernández JC, Almela P. Development of poly (lactide-co-glicolide) nanoparticles incorporating morphine hydrochloride to prolong its circulation in blood. *Current Pharmaceutical Design*. 2017;**23**:2015-2025. DOI: 10.2174/1381612822666161201152604
- [7] Ahmed TA, El-Say KM. Development of alginate-reinforced chitosan nanoparticles utilizing W/O nanoemulsification/internal crosslinking technique for transdermal delivery of rabeprazole. *Life Sciences*. 2014;**110**:35-43. DOI: 10.1016/J.LFS.2014.06.019
- [8] Dangé C, Maincent P, Ubrich N. Oral delivery of insulin associated to polymeric nanoparticles in diabetic rats. *Journal of Controlled Release*. 2007;**117**:163-170. DOI: 10.1016/J.JCONREL.2006.10.023
- [9] Werfel T, Duvall C. Polymeric nanoparticles for gene delivery. In: Narain R, editor. *Polymers and Nanomaterials for Gene Therapy*. 1st ed. Amsterdam (Netherlands): Elsevier; 2016. pp. 147-188. DOI: 10.1016/B978-0-08-100520-0.00007-2
- [10] Yang Y-Y, Wang Y, Powell R, Chan P. Polymeric core-shell nanoparticles for therapeutics. *Clinical and Experimental Pharmacology & Physiology*. 2006;**33**:557-562. DOI: 10.1111/j.1440-1681.2006.04408.x
- [11] Elzoghby AO, Samy WM, Elgindy NA. Protein-based nanocarriers as promising drug and gene delivery systems. *Journal of Controlled Release*. 2012;**161**:38-49. DOI: 10.1016/J.JCONREL.2012.04.036

- [12] Mohammad Fauzi AH, Amin NAS. An overview of ionic liquids as solvents in biodiesel synthesis. *Renewable and Sustainable Energy Reviews*. 2012;**16**:5770-5786. DOI: 10.1016/j.rser.2012.06.022
- [13] Keskin S, Kayrak-Talay D, Akman U, Hortaçsu Ö. A review of ionic liquids towards supercritical fluid applications. *Journal of Supercritical Fluids*. 2007;**43**:150-180. DOI: 10.1016/j.supflu.2007.05.013
- [14] Montalbán MG, Hidalgo JM, Collado-González M, Díaz Baños FG, Villora G. Assessing chemical toxicity of ionic liquids on *Vibrio fischeri*: Correlation with structure and composition. *Chemosphere*. 2016;**155**:405-414. DOI: 10.1016/j.chemosphere.2016.04.042
- [15] Mudring A-V, Alammari T, Bäcker T, Richter K. Nanoparticle synthesis in ionic liquids. In: Plechkova NV, Rogers RD, Seddon KR, editors. *Ionic Liquids: From Knowledge to Application*. ACS Symposium Series, Washington D.C. (USA): ACS Publications; 2010. pp. 177-188. DOI: 10.1021/bk-2009-1030.ch012
- [16] Anastas PT, Warner JC. *Green Chemistry: Theory and Practice*. 1st ed. New York: Oxford University Press; 1998. 148 p
- [17] Torimoto T, Okazaki K, Kiyama T, Hirahara K, Tanaka N, Kuwabata S. Sputter deposition onto ionic liquids: Simple and clean synthesis of highly dispersed ultrafine metal nanoparticles. *Applied Physics Letters*. 2006;**89**:243117. DOI: 10.1063/1.2404975
- [18] Zhu Y-J, Wang W-W, Qi R-J, Hu X-L. Microwave-assisted synthesis of single-crystalline tellurium nanorods and nanowires in ionic liquids. *Angewandte Chemie International Edition*. 2004;**43**:1410-1414. DOI: 10.1002/anie.200353101
- [19] Bühler G, Feldmann C. Microwave-assisted synthesis of luminescent LaPO<sub>4</sub>:Ce,Tb nanocrystals in ionic liquids. *Angewandte Chemie International Edition*. 2006;**45**:4864-4867. DOI: 10.1002/anie.200600244
- [20] Swatloski RP, Spear SK, Holbrey JD, Rogers RD. Dissolution of cellulose with ionic liquids. *Journal of the American Chemical Society*. 2002;**124**:4974-4975. DOI: 10.1021/JA025790M
- [21] Phillips DM, Drummy LF, Conrady DG, Fox DM, Naik RR, Stone MO, Trulove PC, De Long HC, Mantz RA. Dissolution and regeneration of *Bombyx mori* silk fibroin using ionic liquids. *Journal of the American Chemical Society*. 2004;**126**:14350-14351. DOI: 10.1021/JA046079F
- [22] Flannigan DJ, Hopkins SD, Suslick KS. Sonochemistry and sonoluminescence in ionic liquids, molten salts, and concentrated electrolyte solutions. *Journal of Organometallic Chemistry*. 2005;**690**:3513-3517. DOI: 10.1016/J.JORGANICHEM.2005.04.024
- [23] Lozano-Pérez AA, Montalbán MG, Aznar-Cervantes SD, Cragolini F, Cenis JL, Villora G. Production of silk fibroin nanoparticles using ionic liquids and high-power ultrasounds. *Journal of Applied Polymer Science*. 2015;**132**:1-8. DOI: 10.1002/app.41702
- [24] Schluffer K, Schmauder HP, Dorn S, Heinze T. Efficient homogeneous chemical modification of bacterial cellulose in the ionic liquid 1-N-butyl-3-methylimidazolium chloride. *Macromolecular Rapid Communications*. 2006;**27**:1670-1676. DOI: 10.1002/marc.200600463

- [25] Gautam SP, Bundela PS, Pandey AK, Awasthi MK, Sarsaiya S. A review on systematic study of cellulose. *Journal of Applied and Natural Science*. 2010;**2**:330-343
- [26] Ashby MF, Gibson LJ, Wegst U, Olive R. The mechanical properties of natural materials. I. Material property charts. *Proceedings of the Royal Society A: Mathematical, Physical and Engineering Sciences*. 1995;**450**:123-140. DOI: 10.1098/rspa.1995.0075
- [27] Han J, Zhou C, French AD, Han G, Wu Q. Characterization of cellulose II nanoparticles regenerated from 1-butyl-3-methylimidazolium chloride. *Carbohydrate Polymers*. 2013; **94**:773-781. DOI: 10.1016/j.carbpol.2013.02.003
- [28] Köhler S, Liebert T, Heinze T. Interactions of ionic liquids with polysaccharides. VI. Pure cellulose nanoparticles from trimethylsilyl cellulose synthesized in ionic liquids. *Journal of Polymer Science Part A: Polymer Chemistry*. 2008;**46**:4070-4080. DOI: 10.1002/pola.22749
- [29] Swatloski R, Holbrey J, Weston JL, Rogers RD. Preparation of magnetic cellulose composites using ionic liquids. *Chimica Oggi*. 2006;**24**:31
- [30] Ebringerová A, Heinze T. Xylan and xylan derivatives—Biopolymers with valuable properties, 1: Naturally occurring xylans structures, isolation procedures and properties. *Macromolecular Rapid Communications*. 2000;**21**:542-556. DOI: 10.1002/1521-3927(20000601)21:9<542::AID-MARC542>3.0.CO;2-7
- [31] Gericke M, Gabriel L, Geitel K, Benndorf S, Trivedi P, Fardim P, Heinze T. Synthesis of xylan carbonates—An approach towards reactive polysaccharide derivatives showing self-assembling into nanoparticles. *Carbohydrate Polymers*. 2018;**193**:45-53. DOI: 10.1016/j.carbpol.2018.03.083
- [32] Petzold-Welcke K, Schwikal K, Daus S, Heinze T. Xylan derivatives and their application potential—Mini-review of own results. *Carbohydrate Polymers*. 2014;**100**:80-88. DOI: 10.1016/j.carbpol.2012.11.052
- [33] Ross AS. Starch in foods. In: *Food Carbohydrate. Chemistry*. 1st ed. New Jersey (USA): Wiley Online Library; 2013. pp. 107-133. DOI: 10.1002/9781118688496.ch7
- [34] Pérez S, Baldwin PM, Gallant DJ. *Structural Features of Starch Granules I*. 3rd ed. Amsterdam (Netherlands): Elsevier; 2009. DOI: 10.1016/B978-0-12-746275-2.00005-7
- [35] Ji J. *Structural Features of Starch Granules II*. 3rd ed. Amsterdam (Netherlands): Elsevier; 2009. DOI: 10.1016/B978-0-12-746275-2.00006-9
- [36] Zhou G, Luo Z, Fu X. Preparation and characterization of starch nanoparticles in ionic liquid-in-oil microemulsions system. *Industrial Crops and Products*. 2014;**52**:105-110. DOI: 10.1016/j.indcrop.2013.10.019
- [37] Zhou G, Luo Z, Fu X. Preparation of starch nanoparticles in a water-in-ionic liquid microemulsion system and their drug loading and releasing properties. *Journal of Agricultural and Food Chemistry*. 2014;**62**:8214-8220. DOI: 10.1021/jf5018725

- [38] Zhigang L, Linrong S, Meina Z. Preparation of starch nanoparticles in a new ionic liquid-in-oil micro-emulsion. *Journal of Formulation Science & Bioavailability*. 2017;**1**:1-8. DOI: 10.4172/2577-0543.1000116
- [39] Wang X, Cheng J, Ji G, Peng X, Luo Z. Starch nanoparticles prepared in a two ionic liquid based microemulsion system and their drug loading and release properties. *RSC Advances*. 2016;**6**:4751-4757. DOI: 10.1039/C5RA24495A
- [40] Ji G, Luo Z, Xiao Z, Peng X. Synthesis of starch nanoparticles in a novel microemulsion with two ILs substituting two phases. *Journal of Materials Science*. 2016;**51**:7085-7092. DOI: 10.1007/s10853-016-9952-1
- [41] Divya K, Jisha MS. Chitosan nanoparticles preparation and applications. *Environmental Chemistry Letters*. 2018;**16**:101-112. DOI: 10.1007/s10311-017-0670-y
- [42] Torzsas TL, Kendall CWC, Sugano M, Iwamoto Y, Rao AV. The influence of high and low molecular weight chitosan on colonic cell proliferation and aberrant crypt foci development in CF1 mice. *Food and Chemical Toxicology*. 1996;**34**:73-77. DOI: 10.1016/0278-6915(95)00083-6
- [43] Bharmoria P, Singh T, Kumar A. Complexation of chitosan with surfactant like ionic liquids: Molecular interactions and preparation of chitosan nanoparticles. *Journal of Colloid and Interface Science*. 2013;**407**:361-369. DOI: 10.1016/J.JCIS.2013.06.032
- [44] Al Kobiasi M, Chua BY, Tonkin D, Jackson DC, Mainwaring. Control of size dispersity of chitosan biopolymer microparticles and nanoparticles to influence vaccine trafficking and cell uptake. *Journal of Biomedical Materials Research Part A*. 2012;**100**:1859-1867. DOI: 10.1002/jbm.a.34153
- [45] Sonia TA, Sharma CP. An overview of natural polymers for oral insulin delivery. *Drug Discovery Today*. 2012;**17**:784-792. DOI: 10.1016/j.drudis.2012.03.019
- [46] Omenetto FG, Kaplan DL. New opportunities for an ancient material. *Science*. 2010;**329**:528-531. DOI: 10.1126/science.1188936
- [47] Hofmann S, Wong Po Foo CT, Rossetti F, Textor M, Vunjak-Novakovic G, Kaplan DL, Merkle HP, Meinel L. Silk fibroin as an organic polymer for controlled drug delivery. *Journal of Controlled Release*. 2006;**111**:219-227. DOI: 10.1016/j.jconrel.2005.12.009
- [48] Ajisawa A. Dissolution aqueous of silk fibroin with calcium chloride/ethanol solution. *The Journal of Sericultural Science of Japan*. 1997;**67**:91-94
- [49] Asakura T, Watanabe Y, Uchida A, Minagawa H. NMR of silk fibroin. Carbon-13 NMR study of the chain dynamics and solution structure of *Bombyx mori* silk fibroin. *Macromolecules*. 1984;**17**:1075-1081. DOI: 10.1021/ma00135a017
- [50] Rockwood DN, Preda RC, Yücel T, Wang X, Lovett ML, Kaplan DL. Materials fabrication from *Bombyx mori* silk fibroin. *Nature Protocols*. 2011;**6**:1612-1631. DOI: 10.1038/nprot.2011.379

- [51] Wang Q, Yang Y, Chen X, Shao Z. Investigation of rheological properties and conformation of silk fibroin in the solution of AmimCl. *Biomacromolecules*. 2012;**13**:1875-1881. DOI: 10.1021/bm300387z
- [52] Zhang Y-Q, Shen W-D, Xiang R-L, Zhuge L-J, Gao W-J, Wang W-B. Formation of silk fibroin nanoparticles in water-miscible organic solvent and their characterization. *Journal of Nanoparticle Research*. 2007;**9**:885-900. DOI: 10.1007/s11051-006-9162-x
- [53] Yamada H, Nakao H, Takasu Y, Tsubouchi K. Preparation of undegraded native molecular fibroin solution from silkworm cocoons. *Materials Science and Engineering: C*. 2001;**14**: 41-46. DOI: 10.1016/S0928-4931(01)00207-7
- [54] Kundu J, Chung Y-I, Kim YH, Tae G, Kundu SC. Silk fibroin nanoparticles for cellular uptake and control release. *International Journal of Pharmaceutics*. 2010;**388**:242-250. DOI: 10.1016/j.ijpharm.2009.12.052
- [55] Cao Z, Chen X, Yao J, Huang L, Shao Z. The preparation of regenerated silk fibroin microspheres. *Soft Matter*. 2007;**3**:910-915. DOI: 10.1039/b703139d
- [56] Bhawana BRK, Buttar HS, Jain VK, Jain N. Curcumin nanoparticles: Preparation, characterization, and antimicrobial study. *Journal of Agricultural and Food Chemistry*. 2011;**59**: 2056-2061. DOI: 10.1021/jf104402t
- [57] Anand P, Sundaram C, Jhurani S, Kunnumakkara AB, Aggarwal BB. Curcumin and cancer: An "old-age" disease with an "age-old" solution. *Cancer Letters*. 2008;**267**:133-164. DOI: 10.1016/j.canlet.2008.03.025
- [58] Wilken R, Veena MS, Wang MB, Srivatsan ES. Curcumin: A review of anti-cancer properties and therapeutic activity in head and neck squamous cell carcinoma. *Molecular Cancer*. 2011;**10**:1-19. DOI: 10.1186/1476-4598-10-12
- [59] Kohli K, Ali J, Ansari MJ, Raheman Z. Curcumin : A natural antiinflammatory agent. *Indian Journal of Pharmacology*. 2005;**37**:141-147. DOI: 10.4103/0253-7613.16209
- [60] Mahmood K, Zia KM, Zuber M, Salman M, Anjum MN. Recent developments in curcumin and curcumin based polymeric materials for biomedical applications: A review. *International Journal of Biological Macromolecules*. 2015;**81**:877-890. DOI: 10.1016/j.ijbiomac.2015.09.026
- [61] US EPA, Estimation Program Interface (EPI) Suite. Ver. 4.1. Nov. 2012
- [62] Hassan HA, Florentin M, Sandrine BNI, Pierrick D, Jordane J, Michel L. Shea butter solid nanoparticles for curcumin encapsulation: Influence of nanoparticles size on drug loading. *European Journal of Lipid Science and Technology*. 2015;**118**:1168-1178. DOI: 10.1002/ejlt.201500348
- [63] Anitha A, Maya S, Deepa N, Chennazhi KP, Nair SV, Tamura H, Jayakumar R. Efficient water soluble O-carboxymethyl chitosan nanocarrier for the delivery of curcumin to cancer cells. *Carbohydrate Polymers*. 2011;**83**:452-461. DOI: 10.1016/j.carbpol.2010.08.008

- [64] Akl MA, Kartal-Hodzic A, Oksanen T, Ismael HR, Afouna MM, Yliperttula M, Samy AM, Viitala T. Factorial design formulation optimization and in vitro characterization of curcumin-loaded PLGA nanoparticles for colon delivery. *Journal of Drug Delivery Science and Technology*. 2016;**32**:10-20. DOI: 10.1016/j.jddst.2016.01.007
- [65] Bhandari R, Gupta P, Dziubla T, Hilt JZ. Single step synthesis, characterization and applications of curcumin functionalized iron oxide magnetic nanoparticles. *Materials Science and Engineering: C*. 2016;**67**:59-64. DOI: 10.1016/j.msec.2016.04.093
- [66] Hu K, Huang X, Gao Y, Huang X, Xiao H, McClements DJ. Core-shell biopolymer nanoparticle delivery systems: Synthesis and characterization of curcumin fortified zein-pectin nanoparticles. *Food Chemistry*. 2015;**182**:275-281. DOI: 10.1016/j.foodchem.2015.03.009
- [67] Xie M-B, Li Y, Zhao Z, Chen A-Z, Li J-S, Hu J-Y, Li G, Li Z. Solubility enhancement of curcumin via supercritical CO<sub>2</sub> based silk fibroin carrier. *Journal of Supercritical Fluids*. 2015;**103**:1-9. DOI: 10.1016/j.supflu.2015.04.021
- [68] Song W, Muthana M, Mukherjee J, Falconer RJ, Biggs CA, Zhao X. Magnetic-silk core-shell nanoparticles as potential carriers for targeted delivery of curcumin into human breast cancer cells. *ACS Biomaterials Science & Engineering*. 2017;**3**:1027-1038. DOI: 10.1021/acsbomaterials.7b00153
- [69] Xiao L, Lu G, Lu Q, Kaplan DL. Direct formation of silk nanoparticles for drug delivery. *ACS Biomaterials Science & Engineering*. 2016;**2**:2050-2057. DOI: 10.1021/acsbomaterials.6b00457
- [70] Tian Y, Jiang X, Chen X, Shao Z, Yang W. Doxorubicin-loaded magnetic silk fibroin nanoparticles for targeted therapy of multidrug-resistant cancer. *Advanced Materials*. 2014;**26**:7393-7398. DOI: 10.1002/adma.201403562



---

# Phosphazene-Based Ionic Liquids

---

Ahmet Karadağ and Hüseyin Akbaş

Additional information is available at the end of the chapter

<http://dx.doi.org/10.5772/intechopen.76613>

---

## Abstract

This chapter presents the definition, synthesis, and possible application of cyclo and polyphosphazene-based ionic liquids (PzILs). PzILs constitute an alternative class of phosphorus nitrogen compounds and their derivatives have been widely used in biologically-active materials, electrolytes, lubricants, catalysts or nanomaterials. Considerable information is available on substitution reactions taking place at the phosphorus atoms of poly and cyclophosphazenes, thus, a wide variety of phosphazene derivatives have been obtained. However, quaternization of ring nitrogen atoms has received less attention. In addition, phosphazenes containing aliphatic and aromatic substituents with terminal tertiary amino groups are synthesized and subsequently quaternized with methyl iodide. The successive metathesis with salts such as  $\text{LiN}(\text{SO}_2\text{CF}_3)_2$  or  $\text{NaBF}_4$  gives the respective PzILs. In the compounds identified as protonic ionic liquids (PILs) or protic molten salts (PMOSs), the positively charged position is determined by X-ray diffraction study. PzILs are also soluble in water and in many polar organic solvents.

**Keywords:** phosphazene-based ionic liquid, biologically-active material, electrolyte, lubricant, catalyst

---

## 1. Introduction

Phosphazenes, which are cyclic or linear chain inorganic compounds formed by the bonding and repetition of phosphorus and nitrogen atoms with  $(\text{P}=\text{N})_n$  bonds, comprise an important class of inorganic compounds (**Figure 1**). There are many phosphazene compounds ranging from oligomers to polymers. Among the phosphazene compounds, the hexachlorocyclotriphosphazene ( $\text{N}_3\text{P}_3\text{Cl}_6$ , trimer) and octachlorocyclotetraphosphazene ( $\text{N}_4\text{P}_4\text{Cl}_8$ , tetramer) derivatives have attracted considerable attention (**Figure 1a,b**) [1]. The reaction of  $\text{PCl}_5$  with  $\text{NH}_4\text{Cl}$  in a chlorinated solvent gives a mixture of colorless solids of the formula  $(\text{NPCl}_2)_n$ . As the most popular compounds  $\text{N}_3\text{P}_3\text{Cl}_6$  and  $\text{N}_4\text{P}_4\text{Cl}_8$  are readily separated by

---

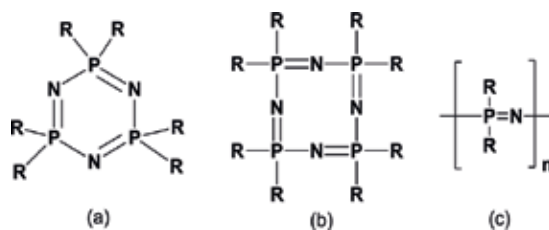


Figure 1. Phosphazene structures.

distillation under reduced pressure. Cyclic phosphazene compounds containing five, six, seven and higher  $-P=N$  units are also known, but these compounds are not very common [2]. Polyphosphazenes are inorganic–organic polymers containing alternate phosphorus and nitrogen atoms, each skeletal phosphorus atom having bonds with one or more organic or inorganic substituent (Figure 1c) [3].

Phosphazenes exhibit highly customizable physical and chemical characteristics which depend on the substituents bonded to the phosphorus atom. Thus, they have found wide application in a variety of fields involving their use in rechargeable batteries [4], membranes [5] and lubricants [6], liquid crystals [7], anticancer agents [8], antibacterial reagents [9], flame-retardants [10], biological materials [11], and synthetic bones [12].

This chapter deals with the structures and applications of PzILs which are formed by quaternization of the ring nitrogen or phosphorus in the phosphazene, or the nitrogen atom in the substituent bonded to the phosphorus atom.

## 2. Phosphazene-based ionic liquids

The PzIL consists of repeating phosphorus-nitrogen units having a pendant group bonded to the phosphorus atoms of the phosphazene. PzILs may have cyclic or linear structure (Figure 2). The positive charge is positioned in a substituent attached to the phosphorus atom, or in the skeleton nitrogen or phosphorus atom. The positive charge's position is reported to be effective on the stability, viscosity and other properties of PzIL [13].

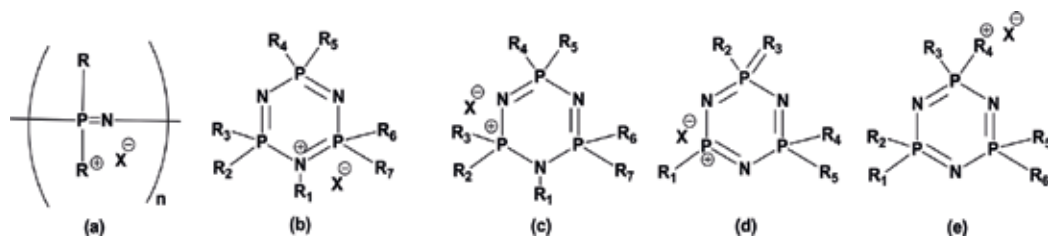


Figure 2. General chemical structure of PzILs.

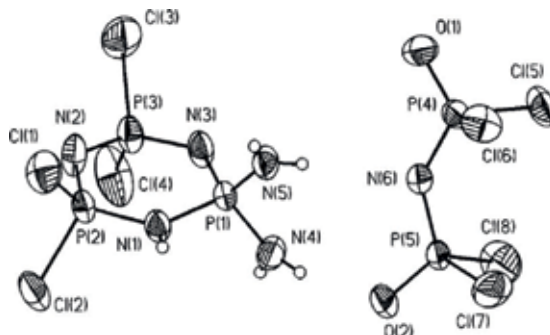
## 2.1. Phosphazene-based ionic liquids in which quaternization occurs on the nitrogen atom or phosphorus atom of phosphazene

Ring and the exocyclic nitrogens are two possible basic sites of cyclophosphazenes. The formation of the protonation and the pKa' values of cyclophosphazene derivatives were investigated in the literature [14–16]. The ring-nitrogen protonation of cyclophosphazene bases with HCl, HBr, HF, HClO<sub>4</sub>, and CH<sub>3</sub>COOH were supported by infrared and NMR data [17, 18]. The protonation of the ring was determined by the crystal structure of N<sub>3</sub>P<sub>3</sub>Cl<sub>2</sub>(NHPr<sup>i</sup>)<sub>4</sub>·HCl and [N<sub>3</sub>P<sub>3</sub>HCl<sub>4</sub>(NH<sub>2</sub>)<sub>2</sub>]<sup>+</sup> [N(POCl<sub>2</sub>)<sub>2</sub>]<sup>-</sup> (**Figure 3**) [19, 20].

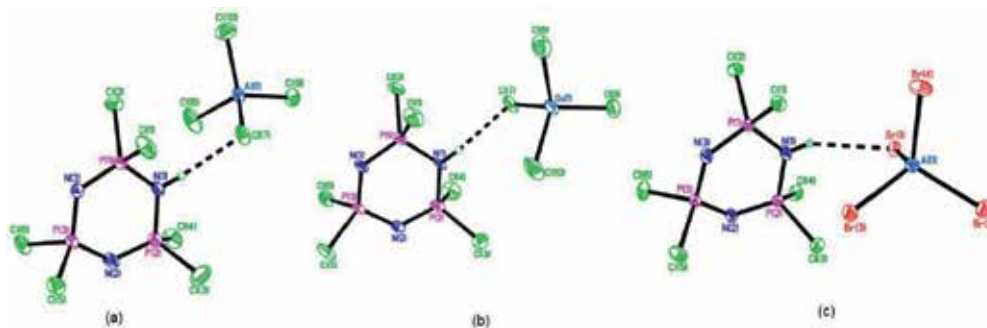
Reportedly, the reactions of N<sub>3</sub>P<sub>3</sub>Cl<sub>6</sub> with AlCl<sub>3</sub>, AlBr<sub>3</sub>, GaCl<sub>3</sub> under anaerobic conditions or in the presence of water or HX yielded protonated phosphazenes P<sub>3</sub>N<sub>3</sub>Cl<sub>6</sub>·HMX<sub>4</sub>. The protonated specie distorted the P<sub>3</sub>N<sub>3</sub> ring and weakened the two P – N bonds that flank the protonated nitrogen. The crystal structures of N<sub>3</sub>P<sub>3</sub>Cl<sub>6</sub>·HAlCl<sub>4</sub>, N<sub>3</sub>P<sub>3</sub>Cl<sub>6</sub>·HGaCl<sub>4</sub>, N<sub>3</sub>P<sub>3</sub>Cl<sub>6</sub>·HAlBr<sub>4</sub> are shown in **Figure 4** [21, 22].

Despite the low basicity and nucleophilicity, various phosphazanium compounds have been obtained using potent electrophilic reagents based on carborane anions. (**Figure 5**) [18].

N-alkyl phosphazanium cations are obtained by alkylation of the ring nitrogen atom of cyclotriphosphazenes containing organoamino substituents with alkyl halides (**Figure 6**). As



**Figure 3.** The crystal structure of [N<sub>3</sub>P<sub>3</sub>HCl<sub>4</sub>(NH<sub>2</sub>)<sub>2</sub>]<sup>+</sup> [N(POCl<sub>2</sub>)<sub>2</sub>]<sup>-</sup>.



**Figure 4.** The crystal structures of N<sub>3</sub>P<sub>3</sub>Cl<sub>6</sub>·HMX<sub>4</sub>, (a) N<sub>3</sub>P<sub>3</sub>Cl<sub>6</sub>·HAlCl<sub>4</sub>; (b) N<sub>3</sub>P<sub>3</sub>Cl<sub>6</sub>·HGaCl<sub>4</sub>; (c) N<sub>3</sub>P<sub>3</sub>Cl<sub>6</sub>·HAlBr<sub>4</sub>.

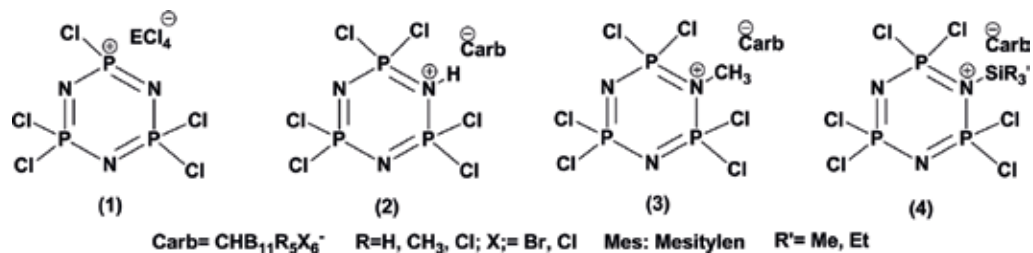


Figure 5. N-protonated, N-methylated, and N-silylated adducts of  $\text{N}_3\text{P}_3\text{Cl}_6$ .

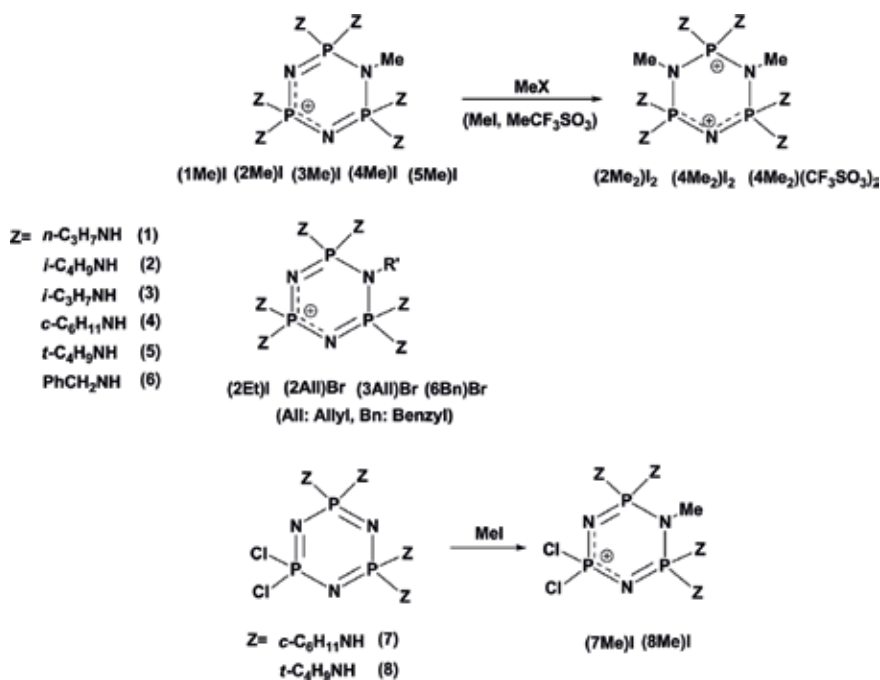


Figure 6. N-alkyl phosphazanium salts.

observed in the X-ray crystal structures, the associated P-N bonds of the alkylation of the ring N sites are significantly longer. Highly stable phosphazanium salts generate complex supra-molecular networks with  $\text{NH}\dots\text{X}$  interactions in the solid state (Figure 7). N-Alkyl phosphazanium salts react with silver nitrate to form complexes with silver ions. Depending on the steric requirement of the RNH substituents, one or both of the free ring nitrogen sites are coordinated with silver ions (Figure 8) [23].

Industrial application of High performance nonmetallic molecular phosphazene catalysts involves the synthesis of polypropylene glycols (PPGs). Phosphazanium salts (PZN) have giant cations that are 10–12 Å in diameter and they exhibit unique catalytic behavior in various anionic organic reactions that are highly demanded in chemical industry (Figure 9). Reportedly, a phosphazanium ion (a macrocations species), should considerably activate anionic active species [24, 25].

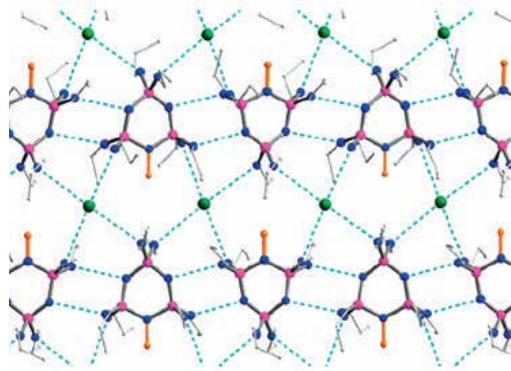


Figure 7. Supramolecular structure of (1Me)I. The dashed lines show hydrogen bonds.

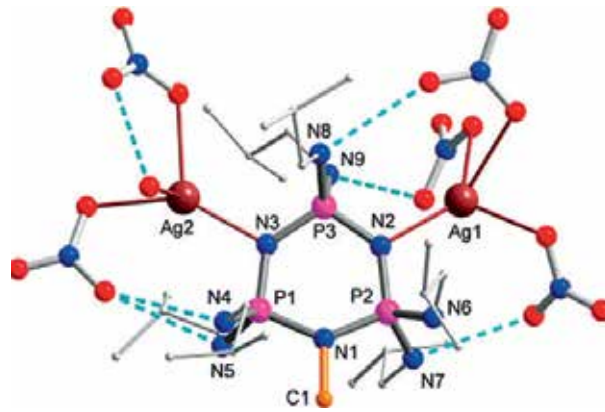


Figure 8. The crystal structure of  $\text{Ag}_2[2\text{Me}](\text{NO}_3)_3 \cdot \text{H}_2\text{O}$ .

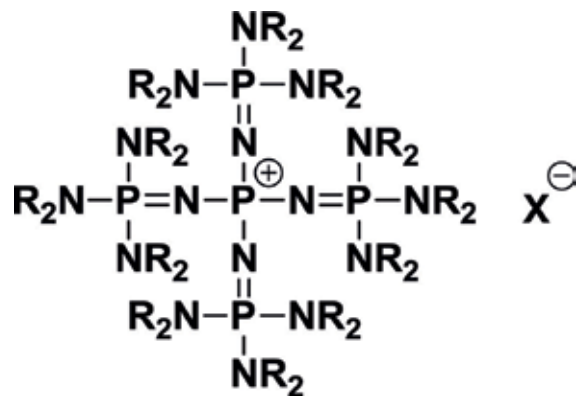


Figure 9. Chemical structure of phosphazanium salt (PZN).

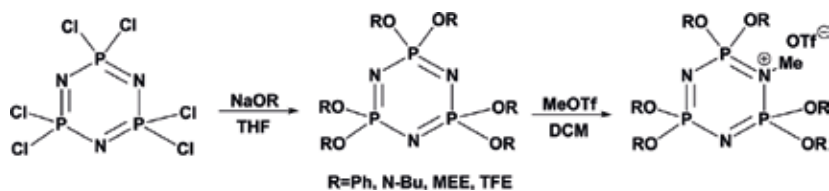


Figure 10. Quaternization of the cyclotriphosphazenes.

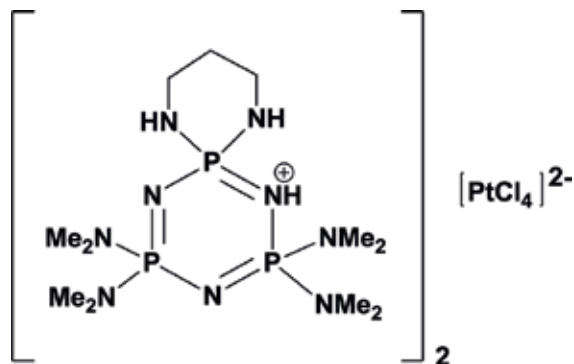


Figure 11. Mono protonated cyclotriphosphazene,  $[\text{HN}_3\text{P}_3(\text{NMe}_2)_4(\text{NHCH}_2\text{CH}_2\text{CH}_2\text{NH})_2]_2[\text{PtCl}_4]$ .

Organophosphazenes bearing -OR substituted groups are readily quaternized at the ring nitrogen atoms to form phosphazene cations with alkyl halides, methyl trifluoromethanesulfonate ( $\text{CF}_3\text{SO}_3\text{CH}_3$ ) or trimethyloxonium tetrafluoroborate  $[(\text{CH}_3)_3\text{O}(\text{BF}_4)]$  (Figure 10). Lower electron densities at the ring nitrogen atoms render alkoxy or aryloxy-substituted cyclotriphosphazenes inert to iodomethane at room temperature or lead to the rearrangement of the alkoxyphosphazene to the N-alkyloxophosphazene at higher temperatures [26].

The transition metal chemistry of cyclophosphazenes has also attracted great interest. The nature of cyclophosphazene-adducted compounds usually depends both on the phosphazene base and the corresponding Lewis acid. For example, for the  $\text{N}_6\text{P}_6(\text{NMe}_2)_{12} \cdot \text{CuCl}_2$ , Lewis acid is not bonded to a particular ring atom. However, it is located on the ring and is attached to more than one nitrogen atom [27]. A mono protonated (amino) *spiro* cyclic cyclotriphosphazene salt was synthesized and its crystal structure was clarified. The protonation occurs at one of the nitrogen atoms adjacent to the spiro phosphorus atom of the  $\text{P}_3\text{N}_3$  ring (Figure 11). The protonation caused elongation of the P-N bonds in the ring and puckering of the phosphazene ring. In the crystal lattice,  $2n$  cyclophosphazanium cations are connected by  $n[\text{PtCl}_4]^{2-}$  anions with N-H...Cl hydrogen bonds to generate a linear polymeric structure [28]. A great number of cyclophosphazanium cations with metal anions, such as  $[\text{HN}_3\text{P}_3(\text{NMe}_2)_6]_2[\text{Mo}_6\text{O}_{19}]$ ,  $[\text{HN}_3\text{P}_3(\text{NMe}_2)_6]_2[\text{CoCl}_4]$ ,  $[\text{MeN}_4\text{P}_4\text{Me}_8][\text{Cr}(\text{CO})_5]$ ,  $[\text{HN}_4\text{P}_4\text{Me}_8][\text{CoCl}_4]$ ,  $[\text{H}_2\text{N}_4\text{P}_4\text{Me}_8][\text{PtCl}_4]$  and  $[\text{H}_2\text{N}_5\text{P}_5\text{Me}_{10}][\text{CuCl}_4]$ , have been obtained.

## 2.2. Phosphazene-based ionic liquids in which quaternization occurs on a pendant group of phosphazene bonded to a phosphorus atom

Due to the more sterically suitable positions of the nitrogen atoms of the phosphazene ring, the alkylation occurred at the exocyclic nitrogen atoms Rapko and Feistel presented the parameters in their study on the dialkyl cation of hexakisdimethylamino cyclotriphosphazene ( $[N_3P_3(NMe_2)_6(Me)_2]^{2+}[(BF_4^-)_2]$ ), (Figure 12). The position of the alkylation was investigated by hydrolytic degradation of the obtained cyclotriphosphazene salts [29].

Allcock et al. synthesized phosphazanium iodide salts by quaternization of several cyclic phosphazenes either at side-group sites or at the skeletal nitrogen atom (Figure 13). With the exception of piperidino derivatives, in which case the reactive sites were the skeletal nitrogen atoms, quaternization occurred at the side-group sites. The compound  $N_3P_3(OC_6H_5)_5N(CH_3)_2$  was not quaternized, since the side-group nitrogen atoms are directly attached to the phosphazene ring due to their protected or inactivated nature [30].

## 2.3. Applications of phosphazene-based ionic liquids

PzILs are prepared by quaternization of a wide variety of phosphazenes either at the side-group or at the skeletal nitrogen atoms. These ILs have been used as anticancer, antibacterial reagents [31–34], adsorbents and surface modifiers of fluorescent nanoparticles [35], lubricants [36, 37], chemosensors for metal ions [38], electrolyte solutions for energy storage devices [39–41], as gate dielectric layer for OFETs [42], or as polyelectrolytes [26, 43, 44].

### 2.3.1. Anticancer, antibacterial reagents

Several studies have been performed on cyclotriphosphazene-based protic molten salts (PMOSs) synthesized with cyclotriphosphazenes and bulky organic acids. Recently, aminocyclotriphosphazenes have received greater attention due to their anti-cancer agent properties [45, 46]. In contrast to cyclotriphosphazene derivatives, there are not many studies related to cyclotriphosphazene salts as antimicrobial and anticancer agents [31–34]. Phosphazanium salts are very soluble in common apolar and polar organic solvents and some are quite soluble in water. Solubility in biological liquid is very important in pharmacological studies.

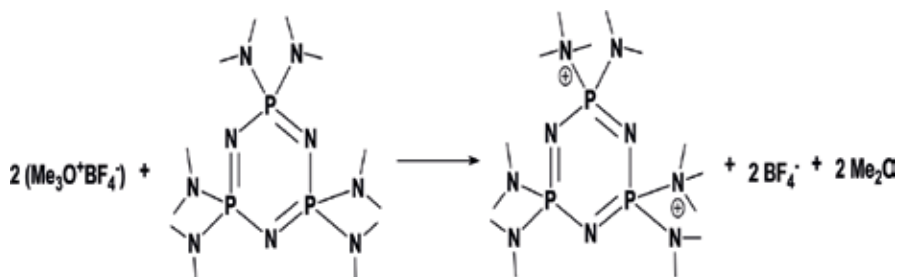


Figure 12. The synthesis of dimethyl hexakisdimethylamino cyclotriphosphonitrilium difluoroborate.

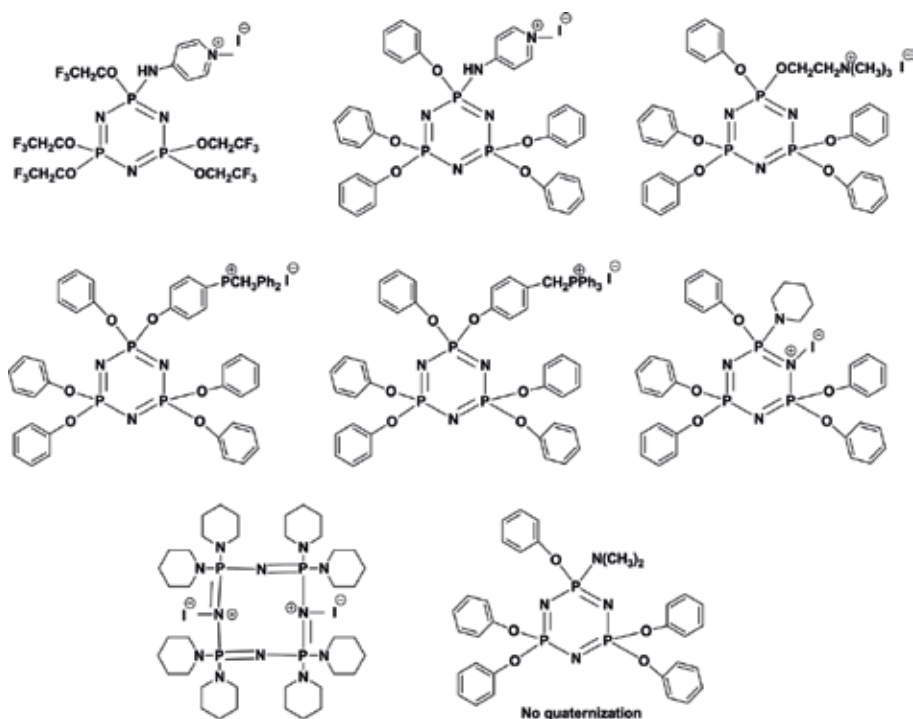


Figure 13. Various cyclotriphosphazene iodide salts.

Therefore, studies on the biological and anti-cancer activities of the salts of cyclotriphosphazenes are likely to attract great interest because of their organic solvent/water solubility and various PMOS diversity with different properties.

Akbaş et al. prepared the salicylic acid salts (1–6) of pyrrolidine and piperidine substituted cyclotriphosphazenes (Figure 14). The crystallographic data of 5 clearly indicate that the nitrogen of the phosphazene ring was protonated (Figure 15). The antimicrobial and cytotoxic activities of the phosphazene salts (1–6) were also investigated. Compounds 5 and 6 appear to be good candidates for anti-cancer agents because they have significant cytotoxic activity against DLD-1 cancer cells. All of the compounds have an antimicrobial effect on bacterial and yeast strains between 312 and 625  $\mu\text{M}$  (bacterial strains) and 19.5–312  $\mu\text{M}$  (yeast strains) and compounds 4–6 are found to be most effective against yeast strains [31].

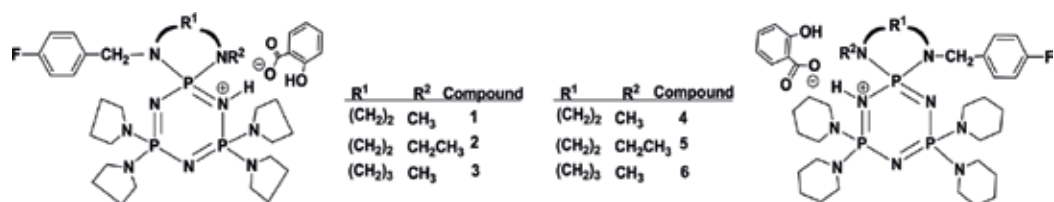


Figure 14. Salicylic acid salts of the mono(4-fluorobenzyl)spirocyclotriphosphazenes.



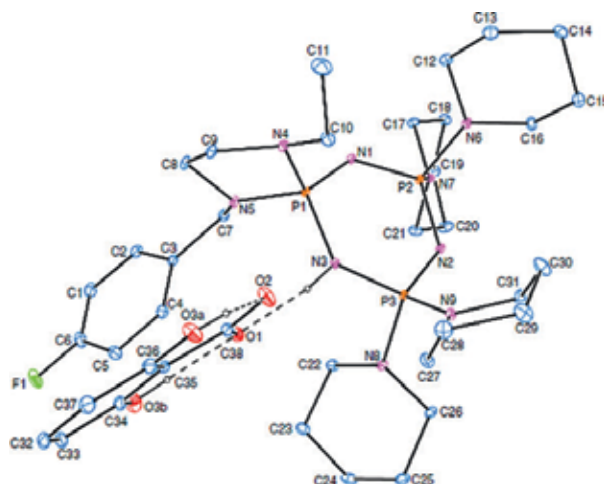


Figure 15. The crystal structure of compound 5.

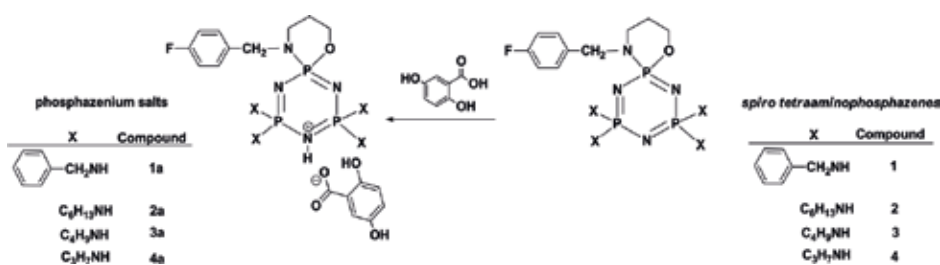


Figure 16. The synthesis of 4-fluorobenzylspiro(N/O)cyclotriphosphazenum salts.

Elmas et al. synthesized phosphazenum salts (**1a-4a**) from the reactions of the phosphazene bases (**1-4**) with gentisic acid (Figure 16). The crystallographic data of **4a** unambiguously indicate that the nitrogen of the phosphazene ring is monoprotonated (Figure 17). Also, In vitro antimicrobial activities of compounds were investigated and the PILs (**1a**, **3a** and **4a**) were found to be significantly active against *C. albicans* [32].

Akbaş et al. obtained the PILs or PMOSs (**1-3**) from the reactions of  $[N_3P_3(NC_4H_8)_6]$  with the gentisic, decanoic and boric acids (Figure 18). Their biological activity in cultured cell lines was investigated. The binding of **1,2** or **3** to calf thymus (CT-DNA) and bovine serum albumin (BSA) led to remarkable changes in spectral characteristics. The potent low cytotoxic, strong apoptotic, and effective DNA topoisomerase inhibitory characteristics of these PILs revealed that they can be a good candidate for anticancer drugs [33].

Okumuş et al. obtained the PMOSs from the reactions of tetrapyrrolidino- and tetrapiperidino-substituted cyclotriphosphazenes with the gentisic and  $\gamma$ -resorcylic acids (Figure 19). The crystallographic result of **1b** and **2b** exhibited that the N atom of the phosphazene ring adjacent to the spiro precursor was mono protonated (Figure 20). In addition, their

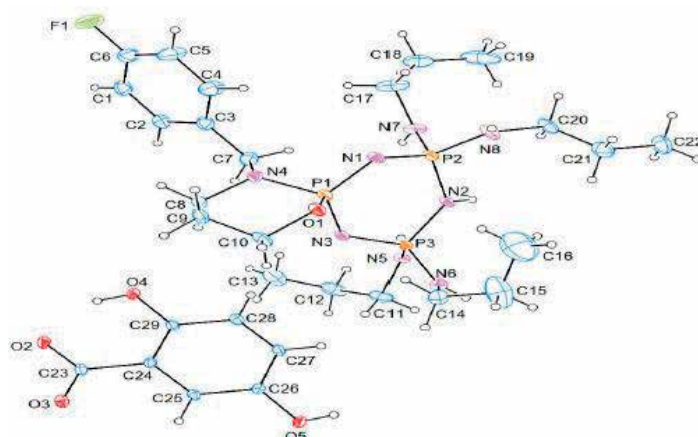


Figure 17. The crystal structure of compound 4a.

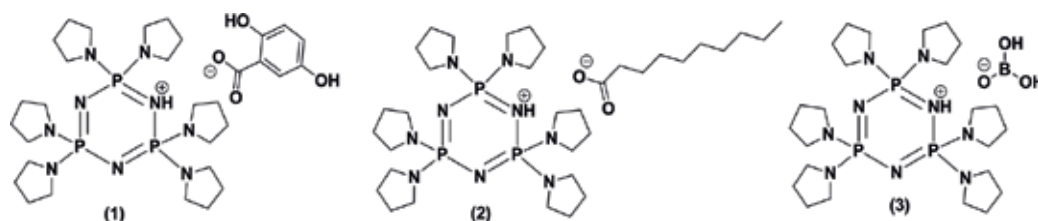


Figure 18. The syntheses of the PILs (1-3) with  $[N_3P_3(NC_4H_9)_6]$  and gentisic, decanoic and boric acids, respectively.

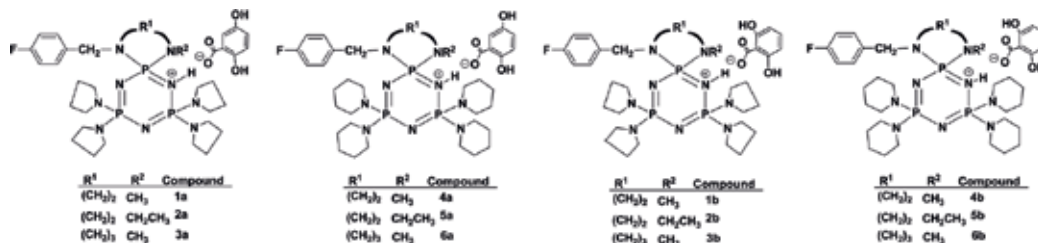


Figure 19. The gentisic and  $\gamma$ -resorcylic acid salts of the tetrapyrrolidino and tetrapiperidino mono(4-fluorobenzyl) spirocyclotriphosphazenes.

cytotoxic and antiproliferative activities against A549, Hep3B and normal FL cell lines were investigated. The findings also displayed that the PMOS (**1b-6b**) were strong antiproliferatives and they had excusable cytotoxic activities against the cells [34].

### 2.3.2. Adsorbents and surface modifiers of fluorescent nanoparticles

Veldboer et al., quaternized the cyclotriphosphazenes having terminal tertiary amino functions with methyl iodide (**Figure 21**) and the resulting salts were studied as surface modifiers for lanthanide phosphate nanoparticles. It was observed that the quaternized cyclic

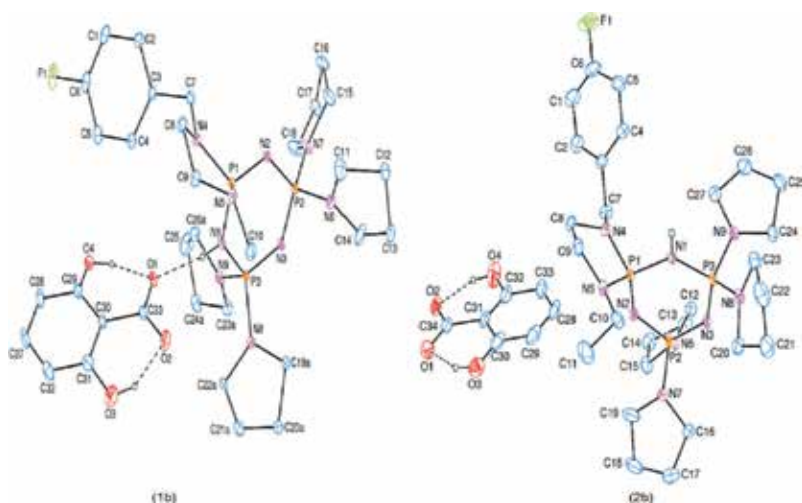


Figure 20. The crystal structure of **1b** and **2b**.

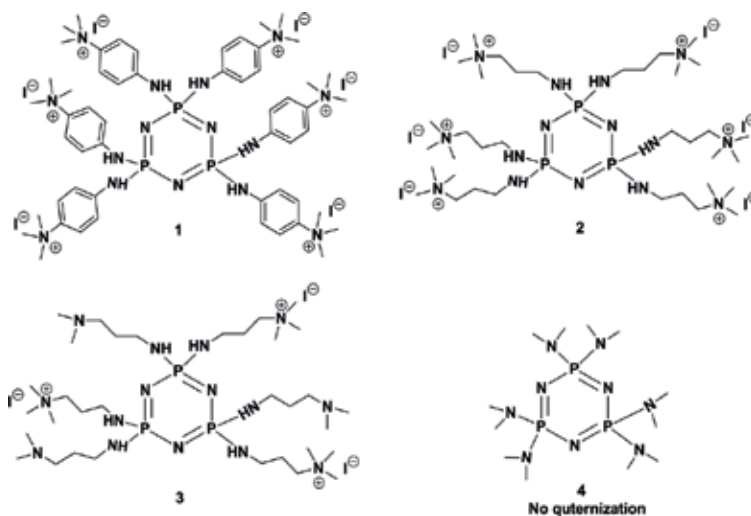


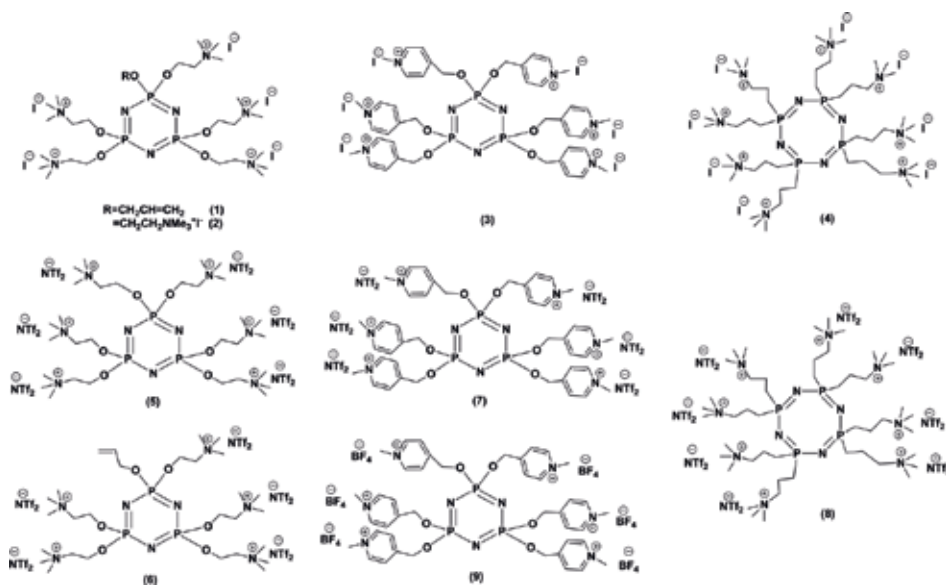
Figure 21. The synthesis of cyclotriphosphazenum iodide salts.

phosphazenes were well suited for coupling to the nanocrystalline surface and a strategy for surface modification of cyclotriphosphazenes containing cationic substituents was developed. A good solubility of nanoparticles in an aqueous medium is a significant precondition for the prediction of bioanalytical applications such as fluorescent immunoassays. This is the main purpose of specially designed molecule surface modifiers. The stable nanocrystal-linker complexes in methanol were formed with compounds **3** and **4**, while the fully quaternized cyclic phosphazenes **1** and **2** interact strongly with nanoparticles, resulting in an agglomeration. It was found that aromatic groups may interfere with the UV absorption in nanocrystals, but no significant effect of aliphatic side chains was observed [35].

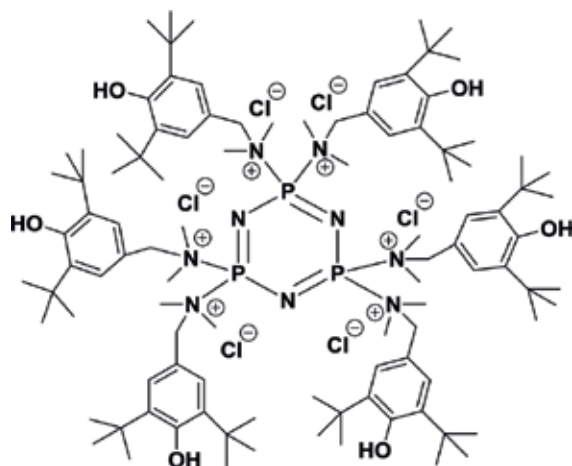
## 2.3.3. Lubricants

Omotowa et al. investigated the tribological properties of PzILs containing trimethylammonium and N-methylpyridinium chains (**Figure 22**). (Dimethylamino)ethoxy, pyridylmethoxy, or (dimethylamino)propoxy side groups linked to the phosphorus in the phosphazene ring were quaternized at the side group nitrogen with iodomethane to obtain polyiodo salts. Subsequently, polyquaternary PZILs were formed with salts such as  $\text{LiN}(\text{SO}_2\text{CF}_3)_2$  or  $\text{NaBF}_4$  by the anions exchange reaction. These PzILs were investigated for use as lubricants for aircraft gas turbine engines and as additives in water lubrication of silicon nitride ceramics. Friction and wear properties of water with 5–8 (0.25 weight %) as boundary lubricant additives were tested on silicon nitride ceramic interfaces. It was observed that these PzILs lead to a decrease in the running-in period. The PzILs, 5–8, are more viscous than the free cyclophosphazene bases and are highly viscous for use as oils. For a faster transition to low friction, ionic liquids with higher solubility must be used [36].

Recently, additives obtained from phosphazene having polar functions which can interact with tribological surfaces, have been developed. Singh et al. obtained The  $\text{PzP}(-\text{NHP})_6$  salt with  $\text{N}_3\text{P}_3\text{Cl}_6$  and 2,6-di-*tert*-butyl-4-(dimethylaminomethyl) phenol (**Figure 23**). This compound contains a phosphazene ring containing polar nitrogen and phosphorus atoms surrounded by hindered phenolic substituents with *tert*-butyl groups. Due to these properties, it can show an affinity for a metal surface to form a surface film which leads to anticorrosion, antiwear, and antifriction properties together with antioxidant characteristics. Reportedly, the  $\text{PzP}(-\text{NHP})_6$  additive exhibits excellent antioxidant properties, and moderate anticorrosion, antiwear and antifriction properties. A doping concentration of 3000 ppm  $\text{PzP}(-\text{NHP})_6$  decreased the average wear scar diameter (AWS) and average friction coefficient by 15.81% and ~27.27%, respectively, in comparison to those for the blank polyol base oil [37].



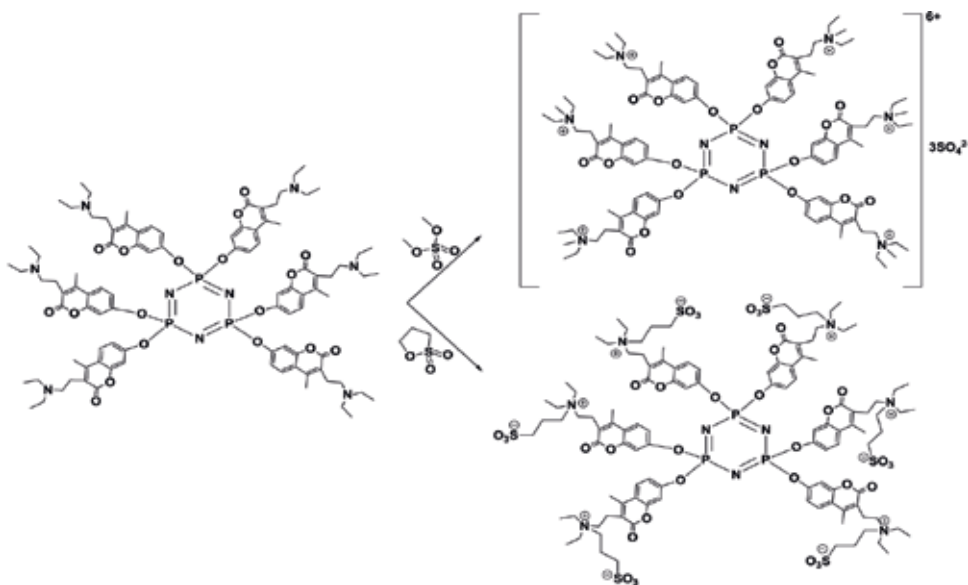
**Figure 22.** PzILs containing trimethylammonium and N-methylpyridinium chains.



**Figure 23.** The structure of the PzP(-NHP)<sub>6</sub> salt.

### 2.3.4. Chemosensors for metal ions

Çiftçi et al. obtained the quaternized cationic and zwitterionic derivatives of 3-[2-(diethyl-amino)ethyl]-7-oxy-4-methylcoumarin substituted trimeric and tetrameric derivatives with dimethyl sulfate and 1,3-propanesultone, respectively (**Figure 24**). Quaternized ionic and zwitterionic compounds display excellent solubility in water and the effects of metal ions on the fluorescent behavior of the cytophosphazene salts were investigated using these compounds



**Figure 24.** The quaternization of coumarin-substituted cyclophosphazene derivatives.

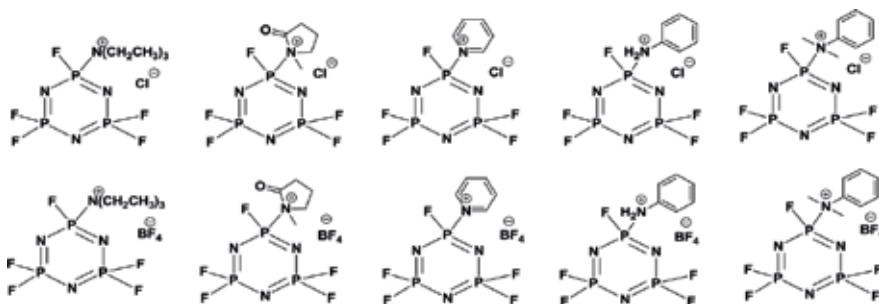
as chemosensors for metal ions. The results showed that cyclophosphazenum salts exhibit highly selective fluorescence chemosensor behavior for  $\text{Fe}^{3+}$  ions in aqueous solution [38].

### 2.3.5. Electrolyte solutions for energy storage devices

The ionic liquid also serves as an ion source for the formation of an electric double layer when electrolytes are used for the electrical double layer capacitor. Thus, an additional supporting electrolyte is not required. The PzIL is decomposed during combustion to produce a nitrogen gas, a phosphate ester, and the like. Because of this nitrogen gas, phosphate ester and the like, the ionic compound overcomes the risk of low combustion. Further, when the ionic compound contains a halogen, the halogen acts as an active radical during the accidental combustion to reduce the risk of burning. Moreover, when the ionic compound contains an organic substituent, the oxygen has a protective effect, as it forms a carbide during combustion. When the ionic compound is in a liquid state at room temperature, it can be used as an electrolyte for an electric double layer capacitor, a lithium-ion battery or a dye-sensitized solar cell, a reaction solvent for an organic synthesis, an extracting solvent for an organic compound and a magnetic fluid. If the ionic compound is in a solid state at room temperature, it can be used as a salt. It exhibits high non-combustibility in both of the liquid and solid states and can significantly suppress the risk of combustion in the application. For this purpose, various PzILs have been synthesized (**Figure 25**) [39–41].

### 2.3.6. A gate dielectric layer for OFETs

Organic field effect transistors (OFETs) are very attractive with their potential applications in a wide area, as flexible and low cost electronic devices. Conventional electrolytes are not stable with their solvents and it is difficult to stabilize the electrolyte concentration. However, ionic liquids are attractive as a gate dielectric layer for OFETs with superior properties such as high thermal and chemical stability, non-volatility, non-toxicity and high polarizability. For this purpose, PzILs have been synthesized. The chain nitrogen atoms of free cyclotriphosphazene bases were quaternized by treatment with methyl iodide to give phosphazenum salts, PzIL1-PzIL4. Subsequently, polyquaternary PZILs have been formed with  $\text{LiN}(\text{SO}_2\text{CF}_3)_2$  (**Figure 26**). These PzILs have been used as the dielectric layer in OFETs. Due to the high dielectric effect of PzILs, the fabricated OFETs have operated in the low voltage ranges. On/



**Figure 25.** The conversion of chloropentafluorocyclotriphosphazenes to PzILs.

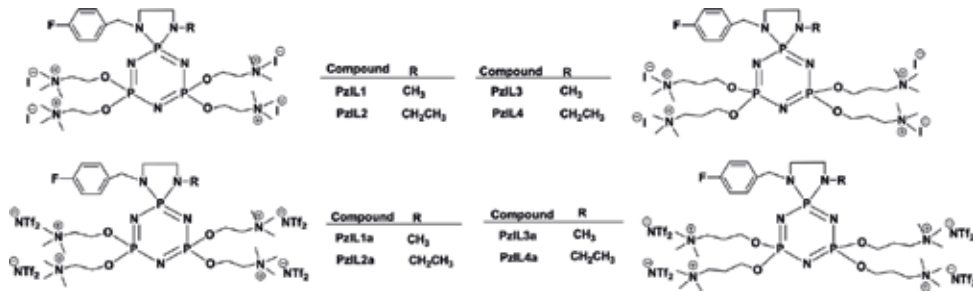


Figure 26. The chemical structure of mono(4-fluorobenzyl)cyclotriphosphazene ionic liquids.

off ratios of these OFETs are about  $10^2$ . The low value of on–off ratio could be caused by the increasing thickness and doping level of active organic layer [42].

### 2.3.7. Polyelectrolytes

Linear polyphosphazenes containing quaternary ammonium side groups have the potential for application as a polycation component in the formation of ordering polyelectrolyte multilayers. Polyelectrolyte multilayers comprise of ionically modified polyphosphazenes by layer-by-layer assembly of a cationic (PAZ<sup>+</sup>) and an anionic (PAZ<sup>-</sup>) polyphosphazene (Figure 27). The dc conductivity values of the PAZ<sup>+</sup>/PAZ<sup>-</sup> films were found to be ten times greater than those of the PAH/PSS multilayers when these multilayers were compared to those of poly(sodium-4-styrenesulfonate) (PSS) and poly(allylamine hydrochloride) (PAH) [43].

Polyelectrolytes were obtained by quaternization of the poly- alkoxy- and aryloxy- phosphazenes with strong alkylating reagents (Figure 28). Because of the lower electron donating abilities of the alkoxy and aryloxy side groups compared to the alkylamino side groups, quaternization is only carried out with methyl trifluoromethanesulfonate (MeOTf). Quaternary poly(alkoxyphosphazenes) have a high ionic conductivity without the need for plasticizers or additional salts [26].

Because of the atomic polarization of the iodide anion, it has been found that the iodide salts (ionomer) of poly[bis(methoxyethoxyethoxy)phosphazene] (MEEP) (Figure 29) have a high

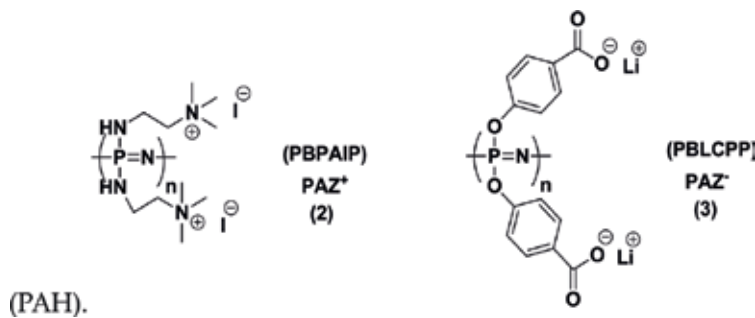


Figure 27. Structures of the (PAZ<sup>+</sup>) (2) and (PAZ<sup>-</sup>) (3) polyphosphazenes.



Figure 28. Quaternization of polymers.

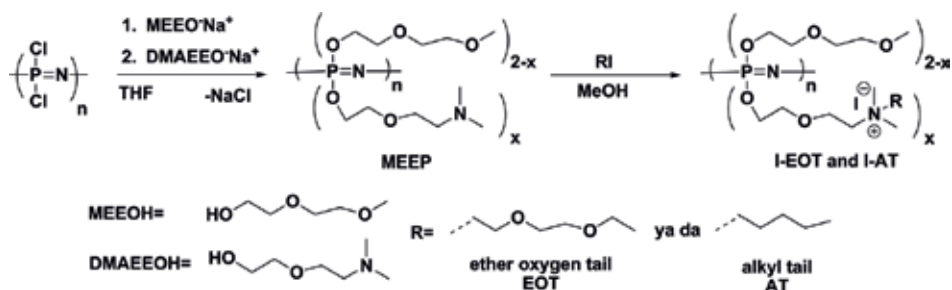


Figure 29. Synthetic route for the polyphosphazenes and their salts.

frequency dielectric constant,  $\epsilon_\infty$  (highest value  $\epsilon_\infty=11$ ). These MEEP-based polyphosphazene salts have a room temperature dc conductivity of  $10^{-6} \text{ S}\cdot\text{cm}^{-1}$ . If the segmental mobility can be increased, they may have a potential for application in iodide conducting solar cells [44].

### 3. Conclusions

In this chapter, we reported a literature review about phosphazene-based ionic liquids (PzILs), which have received considerable attention in recent years. The design and synthesis of PzILs were introduced, and the recent applications (since 2004) were analyzed and discussed. We believe that further studies on the synthesis and application of new PzILs will be performed in the near future.

### Author details

Ahmet Karadağ<sup>1,2\*</sup> and Hüseyin Akbaş<sup>2</sup>

\*Address all correspondence to: ahmet.karadag@gop.edu.tr

1 Department of Biotechnology, Bartın University, Bartın, Turkey

2 Department of Chemistry, Gaziosmanpaşa University, Tokat, Turkey

### References

- [1] Chandrasekhar V, Thilagar P, Pandian BM. Cyclophosphazene-based multi-site coordination ligands. *Coordination Chemistry Reviews*. 2007;**251**:1045-1074. DOI: 10.1016/j.ccr.2006.07.005



- [2] Jaeger R, Gleria M. Poly(Organophosphazene)s and related compounds: Synthesis, properties and applications. *Progress in Polymer Science*. 1998;**23**:179-276. DOI: 10.1016/S0079-6700(97)00027-0
- [3] Allcock HR. Recent developments in polyphosphazene materials science. *Current Opinion in Solid State & Materials Science*. 2006;**10**(5-6):231-240. DOI: 10.1016/j.cossms.2007.06.001
- [4] Xu G, Lu Q, Yu B, Wen L. Inorganic polymer phosphazene disulfide as cathode material for rechargeable lithium batteries. *Solid State Ionics*. 2006;**177**:305-309. DOI: 10.1016/j.ssi.2005.10.029
- [5] Singh A, Krogman NR, Sethurman S, Nair LS, Sturgeon JL, Brown PW, Laurencin CT, Allcock HR. Effect of side group chemistry on the properties of biodegradable l-alanine cosubstituted polyphosphazenes. *Biomacromolecules*. 2006;**7**:914-918. DOI: 10.1021/bm050752r
- [6] Keller MA, Saba CS. Oxidative stability and degradation mechanism of a cyclotriphosphazene lubricant. *Analytical Chemistry*. 1996;**68**(19):3489-3492. DOI: 10.1021/ac960632x
- [7] Davarcı D, Beşli S, Demirbaş E. Synthesis of a series of triple-bridged cyclotriphosphazene hexa-alkoxy derivatives and investigation of their structural and mesomorphic properties. *Liquid Crystals*. 2013;**40**(5):624-631. DOI: 10.1080/02678292.2013.773093
- [8] Brandt K, Bartczak TJ, Kruszynski R, Porwolik-Czomperlik I. AIDS-related lymphoma screen results and molecular structure determination of a new crown ether bearing aziridinylcyclophosphazene, potentially capable of ion-regulated DNA cleavage action. *Inorganica Chimica Acta*. 2001;**322**:138-144. DOI: 10.1016/S0020-1693(01)00557-6
- [9] Çil E, Tanyıldızı MA, Ozen F, Boybay M, Arslan M, Görgülü AO. Synthesis, characterization, and biological–pharmacological evaluation of new phosphazenes bearing dioxybiphenyl and schiff base groups. *Archiv der Pharmazie - Chemistry in Life Sciences*. 2012;**345**:476-485. DOI: 10.1002/ardp.201100412
- [10] Sun J, Yu Z, Wang X, Wu D. Synthesis and performance of cyclomatrix polyphosphazene derived from trispiro-cyclotriphosphazene as a halogen-free nonflammable material. *ACS Sustainable Chemistry & Engineering*. 2014;**2**:231-238. DOI: 10.1021/sc400283d
- [11] Allcock HR, Kwon S. Covalent linkage of proteins to surface-modified poly (organophosphazenes): Immobilization of glucose-6-phosphate dehydrogenase and trypsin. *Macromolecules*. 1986;**19**:1502-1508. DOI: 10.1021/ma00160a002
- [12] Greish YE, Bender JD, Lakshmi S, Brown PW, Allcock HR, Laurencin CT. Low temperature formation of hydroxyapatite-poly(alkyl oxybenzoate)phosphazene composites for biomedical applications. *Biomaterials*. 2005;**26**:1-9. DOI: 10.1016/j.biomaterials.2004.02.016
- [13] Gering K L, Harrup M K, Rollins H W. Ionic liquids, electrolyte solutions including the ionic liquids, and energy storage devices including the ionic liquids. *Pat. Appl. Pub.* 2013; US 2013/0089793A1:1-11
- [14] Feakins D, Last WA, Shaw RA. 855. Structure and basicity. Part II. The basicity of fully aminolysed cyclotriphosphazatrienes and cyclotetraphosphazatetraenes in nitrobenzene and water. *Journal of the Chemical Society*. 1964:4464-4471. DOI: 10.1039/JR9640004464

- [15] Feakins D, Last WA, Neemuchwala N, Shaw RA. 503. Structure and basicity. Part III. The basicity of homogeneously substituted cyclotriphosphazatrienes and cyclotetra-phos-phazetraenes. *Journal of the Chemical Society*. 1965;2804-2811. DOI: 10.1039/JR9650002804
- [16] Feakins D, Last WA, Nabi SN, Shaw RA. Structure and basicity. Part IV. Aminochlorocyclotriphosphazatrienes. *Journal of the Chemical Society A*. 1966:1831-1834. DOI: 10.1039/J19660001831
- [17] Moeller T, Kokalis SG. The Lewis-base behaviour of some hexa-n-alkylamino triphosphonitriles. *Journal of Inorganic and Nuclear Chemistry*. 1963;**25**(7):875-881. DOI: 10.1016/0022-1902(63)80375-9
- [18] Zhang Y, Tham FS, Reed CA. Phosphazene cations. *Inorganic Chemistry*. 2006;**45**:10446-10448. DOI: 10.1021/ic062077f
- [19] Mani NV, Wagner AJ. The crystal structure of compounds with (N-P)<sub>n</sub> rings. VIII. Dichlorotetrakis(isopropylaminocyclotriphosphazatriene hydrochloride, N<sub>3</sub>P<sub>3</sub>Cl<sub>2</sub>(NHPri)<sub>4</sub>·HCl. *Acta Cryst*. 1971;**B27**:51-58. DOI: 10.1107/S0567740871001699
- [20] Alberti M, Marecek A, Zak Z, Pastera P. Reaction of [P<sub>3</sub>N<sub>3</sub>Cl<sub>4</sub>(NH<sub>2</sub>)<sub>2</sub>] with [HN(POCl<sub>2</sub>)<sub>2</sub>]; the crystal structure of the phosphazanium salt ([P<sub>3</sub>N<sub>3</sub>HCl<sub>4</sub>(NH<sub>2</sub>)<sub>2</sub>]<sup>+</sup> [N(POCl<sub>2</sub>)<sub>2</sub>]<sup>-</sup>). *Zeitschrift für Anorganische und Allgemeine Chemie*. 1995;**621**:1771-1774. DOI: 10.1002/zaac.19956211027
- [21] Tun ZM, Heston AJ, Panzner MJ, Medvetz DA, Wright BD, Savant D, Dudipala VR, Banerjee D, Rinaldi PL, Youngs WJ, Tessier CA. Group 13 Lewis acid adducts of [PCl<sub>2</sub>N]<sub>3</sub>. *Inorganic Chemistry*. 2011;**50**(18):8937-8945. DOI: 10.1021/ic201075z
- [22] Tun ZM, Heston AJ, Panzner MJ, Scionti V, Medvetz DA, Wright BD, Johnson NA, Li L, Westemiotis C, Savant D, Rinaldi PL, Youngs WJ, Tessier CA. Group 13 super-acid adducts of [PCl<sub>2</sub>N]<sub>3</sub>. *Inorganic Chemistry*. 2016;**55**(7):3283-3293. DOI: 10.1021/acs.inorgchem.5b02341
- [23] Benson MA, Zacchini S, Boomishankar R, Chan Y, Steiner A. Alkylation and acylation of cyclotriphosphazenes. *Inorganic Chemistry*. 2017;**46**(17):7097-7108. DOI: 10.1021/ic7009463
- [24] Furuyama R, Fujita T, Funaki SF, Nobori T, Nagata T, Fujiwara K. New high-performance catalysts developed at mitsui chemicals for polyolefins and organic synthesis. *Catalysis Surveys from Asia*. 2004;**8**:61-71. DOI: 10.1023/B:CATS.0000015115.09940.4e
- [25] Nobori T, Hayashi T, Shibahara A, Saeki T, Yamasaki S, Ohkubo K. Development of novel molecular catalysts "phosphazene catalysts" for commercial production of highly advanced polypropylene glycols. *Catalysis Surveys from Asia*. 2010;**14**:164-167. DOI: 10.1007/s10563-010-9098-0
- [26] Chen C, Hess AR, Jones AR, Liu X, Barber GD, Mallouk TE, Allcock HR. Synthesis of new polyelectrolytes via backbone quaternization of poly(aryloxy- and alkoxyphosphazenes) and their small molecule. *Macromolecules*. 2012;**45**:1182-1189. DOI: 10.1021/ma202619j

- [27] Marsh WC, Trotter J. Crystal and molecular structure of chloro[dodeca(dimethylamino)-cyclohexaphosphazene-NNNN]-copper(II)dichlorocuprate(I) ( $[\text{N}_6\text{P}_6(\text{NMe}_2)_{12}\text{CuIICl}]^+\text{CuIICl}_2^-$ ). *Journal of the Chemical Society A*. 1971;1482-1486. DOI: 10.1039/J19710001482
- [28] Chandrasekaran A. A salt of a protonated (amino)spirocyclic cyclotriphosphazene. *Acta Cryst*. 1994;**C50**:1692-1694. DOI: 10.1107/S0108270194003859
- [29] Rapko JN, Feistel GR. The synthesis and structure of a dialkyl cation of hexakisdimethylaminocyclotriphosphazatriene. *Chemical Communications (London)*. 1968:474-475. DOI: 10.1039/C19680000474
- [30] Allcock HR, Levin ML, Austin PE. Quaternized cyclic and high polymeric phosphazenes and their interactions with tetracyanoquinodimethane. *Inorganic Chemistry*. 1986;**25**:2281-2288. DOI: 10.1021/ic00234a002
- [31] Akbaş H, Okumuş A, Karadağ A, Kılıç Z, Hökelek T, Koç LY, Açık L, Aydın B, Türk M. Phosphorus–nitrogen compounds part 32. Structural and thermal characterizations, antimicrobial and cytotoxic activities, and in vitro DNA binding of the phosphazanium salts. *Journal of Thermal Analysis and Calorimetry*. 2016;**123**:1627-1641. DOI: 10.1007/s10973-015-5001-6
- [32] Elmas G, Okumuş A, Kılıç Z, Gönder LY, Açık L, Hökelek T. The syntheses and structural characterizations, antimicrobial activity and in vitro DNA binding of 4-fluorobenzylspiro(N/O)cyclotriphosphazenes and their phosphazanium salts. *JOTCSA*. 2016;**3**(3):25-46. DOI: 10.18596/jotcsa.04055
- [33] Akbaş H, Karadağ A, Aydın A, Destegül A, Kılıç Z. Synthesis, structural and thermal properties of the hexapyrrolidinocyclotriphosphazenes-based protic molten salts: Antiproliferative effects against HT29, HeLa, and C6 cancer cell lines. *Journal of Molecular Liquids*. 2017;**230**:482-495. DOI: 10.1016/j.molliq.2017.01.067
- [34] Okumuş A, Akbaş H, Karadağ A, Aydın A, Kılıç Z, Hökelek T. Antiproliferative effects against A549, Hep3B and FL cell lines of cyclotriphosphazene-based novel protic molten salts: Spectroscopic, crystallographic and thermal results. *ChemistrySelect*. 2017;**2**(18):4988-4999. DOI: 10.1002/slct.201700497
- [35] Veldboer K, Karataş Y, Vielhaber T, Karst U, Wiemhöfer H. Cyclic phosphazenes for the surface modification of lanthanide phosphate-based nanoparticles. *Zeitschrift für Anorganische und Allgemeine Chemie*. 2008;**634**:2175-2180. DOI: 10.1002/zaac.200800297
- [36] Omotowa BA, Phillips BS, Zabinski JS, Shreeve JM. Phosphazene-based ionic liquids: Synthesis, temperature-dependent viscosity, and effect as additives in water lubrication of silicon nitride ceramics. *Inorganic Chemistry*. 2004;**43**(17):5466-5471. DOI: 10.1021/ic049483o
- [37] Singh RK, Kukrety A, Saxena RC, Chouhan A, Jain SL, Ray SS. Phosphazene-based novel organo-inorganic hybrid salt: Synthesis, characterization and performance evaluation as multifunctional additive in polyol. *RSC Advances*. 2017;**7**:13390-13397. DOI: 10.1039/C6RA26186H

- [38] Çiftçi GY, Şenkuytu E, Bulut M, Durmuş M. Novel coumarin substituted water soluble cyclophosphazenes as "turn-off" type fluorescence chemosensors for detection of Fe<sup>3+</sup> ions in aqueous media. *Journal of Fluorescence*. 2015;**25**:1819-1830. DOI: 10.1007/s10895-015-1672-4
- [39] Otsuki M, Kanno H. Ionic compound. US Patent. 2010;**7**(718,826):1-10
- [40] Otsuki M, Kanno H. Non-aqueous electrolyte for battery and non-aqueous electrolyte battery comprising the same as well as electrolyte for electric double layer capacitor and electric double layer capacitor comprising the same. US Patent 2011;**7,951;495**:1-10
- [41] Gering KL, Harrup MK, Rollins HW. Ionic liquids, electrolyte solutions including the ionic liquids, and energy storage devices including the ionic liquids. *Pat. Appl. Pub.* 2013; US 2013/0089793A1:1-11
- [42] Akbaş H, Karadağ A, Destegül A, Çakırlar Ç, Yerli Y, Tekin K C, Malayoğlu U, Kılıç Z. Syntheses, spectroscopic, thermal and dielectric properties of phosphazene based ionic liquids: Tribological behavior and OFET application. *Journal of Molecular Liquids*. 2018;In Review
- [43] Akgöl Y, Hofmann C, Karataş Y, Cramer C, Wiemhöfer H, Schönhoff M. Conductivity spectra of polyphosphazene-based polyelectrolyte multilayers. *The Journal of Physical Chemistry. B*. 2007;**111**:8532-8539. DOI: 10.1021/jp068872w
- [44] Bartels J, Hess A, Shiau H, Allcock HR, Colby RH, Runt J. Synthesis, morphology, and ion conduction of polyphosphazene ammonium iodide ionomers. *Macromolecules*. 2015;**48**:111-118. DOI: 10.1021/ma501634b
- [45] Görgülü AO, Koran K, Özen F, Tekin S, Sandal S. Synthesis, structural characterization and anti-carcinogenic activity of new cyclotriphosphazenes containing dioxybiphenyl and chalcone groups. *Journal of Molecular Structure*. 2015;**1087**:1-10. DOI: 10.1016/j.molstruc.2015.01.033
- [46] Akbaş H, Okumuş A, Kılıç Z, Hökelek T, Süzen Y, Koç LY, Açık L, Çelik ZB. Phosphorus-nitrogen compounds part 27. Syntheses, structural characterizations, antimicrobial and cytotoxic activities, and DNA interactions of new phosphazenes bearing secondary amino and pendant (4-fluorobenzyl)spiro groups. *European Journal of Medicinal Chemistry*. 2013;**70**:294-307. DOI: 10.1016/j.ejmech.2013.09.046

---

# **Tribochemical Reactions of Halogen-Free Ionic Liquids on Nascent Steel Surface**

---

Shouhei Kawada, Seiya Watanabe,  
Shinya Sasaki and Masaaki Miyatake

Additional information is available at the end of the chapter

<http://dx.doi.org/10.5772/intechopen.77352>

---

## **Abstract**

Ionic liquids are expected to show applicability as novel lubricants. However, halogen anion-based ionic liquids cause severe corrosive wear. To preclude this, this chapter describes the use of halogen-free anion-based ionic liquids as lubricants. The study investigated the tribological performances and lubricating mechanisms of sulfur, phosphorus, and cyanoanion-based ionic liquids. Sulfur and phosphorus anion-based ionic liquids formed reaction films on worn surfaces; the sulfur- and phosphorus-containing films exhibited low-friction coefficients and specific wear rates, respectively. The steric hindrance of the ionic liquids affected their tribochemical reaction behaviors. Cyanoanion-based ionic liquids also showed low-friction coefficients; however, their values were higher than those of halogen anion-based ionic liquids. To achieve low friction, tribochemical reaction of the ionic liquids and adsorption of anions on the worn surface were required. The stability of the cyanoanion-based ionic liquids against the nascent steel surface was related to the thermal stability. These halogen-free anion-based ionic liquids and formed tribolayer films differ in physical and chemical properties. When these ionic liquids are applied as lubricants in the industry, it is important to choose ionic liquids depending on the sliding conditions.

**Keywords:** tribology, lubricants, halogen-free ionic liquids, tribochemical reaction, quadrupole mass spectrometer

---

## **1. Introduction**

Global warming is an important issue that cannot be ignored. The Intergovernmental Panel on Climate Change (IPCC) has reported increases in the global average temperature [1]. This

---

meeting reported that the global average temperature increased by 0.85°C from 1880 to 2012 [1]. Some measures must be taken quickly to resolve this problem. The *Conférence de Paris de 2015 sur le climat* (COP21) established the target values of CO<sub>2</sub> release reduction, which is the most significant matter in global warming. The United States of America and Japan each set the goal to reduce CO<sub>2</sub> release by more than 25% by 2025–2030. Meanwhile, the European Union, Russian Federation, China, and India set significant reduction targets exceeding 35%. To achieve these targets, high efficiency of mechanical systems is required. One method to increase efficiency is the reduction of friction loss in sliding parts. In order to achieve this, the development of new technologies, such as novel lubricants, materials, and lubrication state controls, are needed. Regarding novel materials, the research on the tribological performance of diamond-like carbon (DLC) has been the most energetic [2–5]. The development of novel synthetic oils as lubricants has also been remarkable. Among these, ionic liquids such as lubricants have received much attention [6–14]. Ionic liquids are organic salts consisting of cations and anions that form liquid phases at temperatures below 100°C. They have the attractive physical and chemical properties of high thermal stability, low vapor pressure, and flame resistance [15–17]. In addition, their properties can be controlled by changing the combinations of cations and anions [8]. In the tribology field, ionic liquids were first considered for use in extreme environmental conditions, such as high temperatures, vacuum, and high contact pressures, where existing lubricants cannot be used [7, 8]. Ionic liquids exhibit high heat resistance compared to existing lubricants such as perfluoropolyether (PFPE) and poly- $\alpha$ -olefin [7]. Recently, reports on ionic liquids under ordinary temperatures and pressures have increased [6, 11–13]. The increase in the variety of ionic liquids triggered this trend. However, the detailed lubricating mechanisms and the relationship between the chemical structures of ionic liquids and tribological performances are still unclear. To apply ionic liquids as lubricants, it is necessary to understand lubricating mechanisms.

Regarding the tribological performances of ionic liquids, most investigations have used fluoride or chloride anion-based ionic liquids, such as chloride [Cl], tetrafluoroborate [BF<sub>4</sub>], hexafluorophosphate [PF<sub>6</sub>], and bis(trifluoromethane)sulfonamide [TFSI] [7, 8, 10–13]. These kinds of anions form metallic halides on worn surfaces, and these reactants achieve good tribological performances [7, 8]. These anions exhibit lower friction coefficients than PFPE [7]. However, the hydrolysis of metallic halides causes severe corrosive wear [8]. In addition, [BF<sub>4</sub>] and [PF<sub>6</sub>] anions generate hydrogen fluoride by hydrolysis with water or atmospheric moisture [18–20]. To preclude the appearance of these bad properties, this chapter describes experiments considering the application of two kinds of halogen-free ionic liquids. One is sulfur or phosphorus anion-based ionic liquids, which form reaction films on worn surfaces. The other is cyanoanion-based ionic liquids, which form adsorption films on worn surfaces. The tribological performances of these ionic liquids were investigated by sliding tests. In addition, the relationship between the chemical structures of the ionic liquids and tribochemical reaction is discussed by using quadrupole mass spectrometry (Q-MS).

## 2. Sulfur or phosphorus anion-based ionic liquids

Sulfur and phosphorus are widely used as extreme-pressure additives, such as zinc dialkyl dithiophosphate (ZDDP) [21–23]. These elements exhibit low-friction coefficients, low wear,

or both. From this information, it is considered that sulfur or phosphorus anion-based ionic liquids can be applied in the industry as alternatives to halogen anion-based ionic liquids. This section investigated tribological performances and the effect of alkyl chain lengths of the anions on their tribochemical reactions.

## 2.1. Experimental details

### 2.1.1. Ionic liquids

Four kinds of sulfur and three kinds of phosphorus anion-based ionic liquids were used as lubricants. **Table 1** lists the chemical names and molecular structures of these ionic liquids: 1-ethyl-3-methylimidazolium hydrogen sulfate ([EMIM][HSO<sub>4</sub>]), 1-ethyl-3-methylimidazolium methyl sulfate ([EMIM][MSU]), 1-ethyl-3-methylimidazolium ethyl sulfate ([EMIM][ESU]), 1-ethyl-3-methylimidazolium n-octyl sulfate ([EMIM][OSU]), 1-ethyl-3-methylimidazolium dimethyl phosphate ([EMIM][DMP]), 1-ethyl-3-methylimidazolium diethyl phosphate ([EMIM][DEP]), and 1-ethyl-3-methylimidazolium dibutyl phosphate ([EMIM][DBP]). All ionic liquids were commercial materials. [EMIM][HSO<sub>4</sub>], [EMIM][ESU], and [EMIM][OSU] were purchased from Merck Chemicals, Germany, as “Synthesis (S)” grade (halide content <1000 ppm, water content <10,000 ppm). [EMIM][MSU], [EMIM][DMP], [EMIM][DEP], and [EMIM][DBP] were purchased from IoLiTec, Germany, as “HP” grade (water content <5000 ppm). In addition, 1-butyl-3-methylimidazolium hexafluorophosphate ([BMIM][PF<sub>6</sub>]), containing halogens, was used for comparison.

### 2.1.2. Physical and chemical properties of ionic liquids

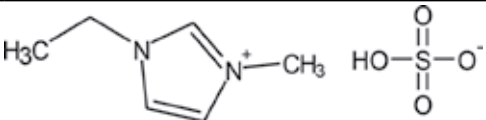
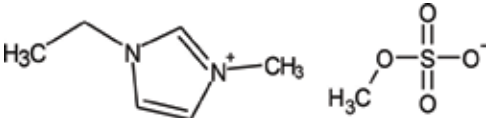
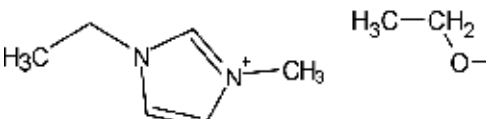
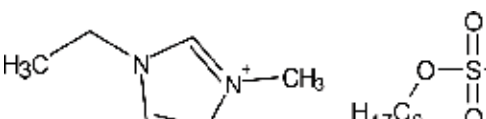
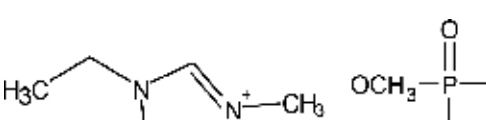

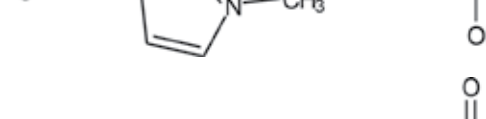
All ionic liquids are liquid in phase at room temperature. **Table 2** lists the viscosities and thermal decomposition temperatures of the used ionic liquids. The viscosities of all the ionic liquids were measured using a tuning-fork vibration-type viscometer (SV-1A, A&D Company, Japan). The thermal decomposition temperatures of the ionic liquids were defined as the points at which 10% weight loss occurred by thermogravimetric analysis. The programming rate was 10°C/min, the environment was N<sub>2</sub>, and the measurement range was 50–500°C.

### 2.1.3. Sliding tests

The tribological performances of all ionic liquids were evaluated using a ball-on-disk sliding tester [9]. For the specimens, a  $\phi$  24 mm  $\times$   $t$  7.9 mm disk and a  $\phi$  4-mm ball of bearing steel (AISI 52100, hardness of HRC 60) were used. The surface roughness of the disk specimens and corresponding balls were each  $R_a$  0.05  $\pm$  0.01  $\mu$ m. They were ultrasonically cleaned twice with a mixed solution of 1:1 petroleum benzene and acetone for 20 min. The sliding tests were performed with a normal load of 3.5 N and sliding speed of 52.3 mm/s for 2 h under vacuum conditions (2.0  $\times$  10<sup>-5</sup> Pa). After the sliding tests, the worn surfaces of the ball specimens were observed and the specific wear rates were measured by optical microscopy (OM, VHX-100, Keyence, Japan).

### 2.1.4. Analysis

The tribochemical reactions of the ionic liquids were estimated using Q-MS (MKS Instruments, Inc.). The measurable mass-to-charge ratio ( $m/e$ ) range of the Q-MS was 1–200, using an ion

Chemical name	Molecular structure
1-Ethyl-3-methylimidazolium hydrogen sulfate	
1-Ethyl-3-methylimidazolium methyl sulfate	
1-Ethyl-3-methylimidazolium ethyl sulfate	
1-Ethyl-3-methylimidazolium n-octyl sulfate	
1-Ethyl-3-methylimidazolium dimethyl phosphate	
1-Ethyl-3-methylimidazolium diethyl phosphate	
1-Ethyl-3-methylimidazolium dibutyl phosphate	

**Table 1.** Names and molecular structures of the sulfur and phosphorus anion-based ionic liquids.

source sensitivity of  $3.8 \times 10^{-7}$  A/Pa with a secondary electron multiplier. The partial pressure of the ions was converted from the ion currents using the conversion rate of  $N_2$  by the Q-MS software. The  $m/e$  ratios, derived from the decomposition of ionic liquids before and after the friction tests, were measured. The temporal resolution was approximately 1 s. After the sliding tests, the disk specimens were ultrasonically cleaned with a mixed solution of 1:1 petroleum benzene and acetone for 10 min. The disk specimens were analyzed by X-ray photoelectron spectroscopy (XPS, QUANTERAII, ULVAC-PHI, Inc., Japan) with a monochromatic Al  $K\alpha$  X-ray source (1486.6 eV). All the spectra were referenced relative to the C 1 s peak (285.0 eV).



Ionic liquid	Viscosity [mPa s]		Decomposition temperature [°C]
	40°C	70°C	
[EMIM][HSO <sub>4</sub> ]	327.8	93.6	312.8
[EMIM][MSU]	41.0	17.6	309.6
[EMIM][ESU]	41.8	18.2	314.9
[EMIM][OSU]	169.2	47.9	296.6
[EMIM][DMP]	75.5	28.4	294.2
[EMIM][DEP]	110.3	37.6	229.8
[EMIM][DBP]	251.6	58.6	355.5

**Table 2.** The viscosities and thermal decomposition temperatures of the sulfur and phosphorus anion-based ionic liquids.

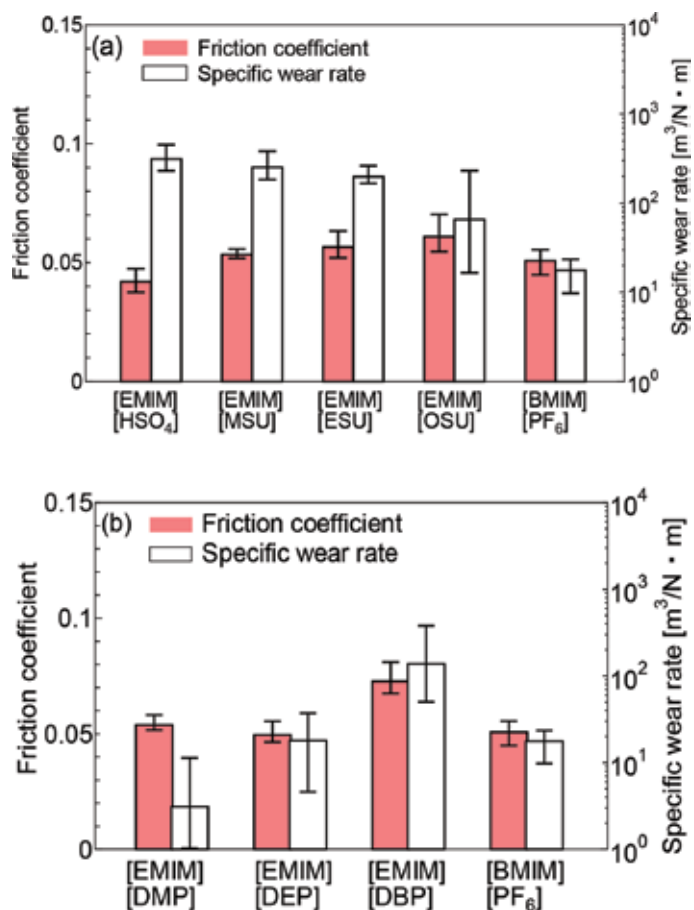
## 2.2. Results

### 2.2.1. Tribological performances of sulfur and phosphorus anion-based ionic liquids

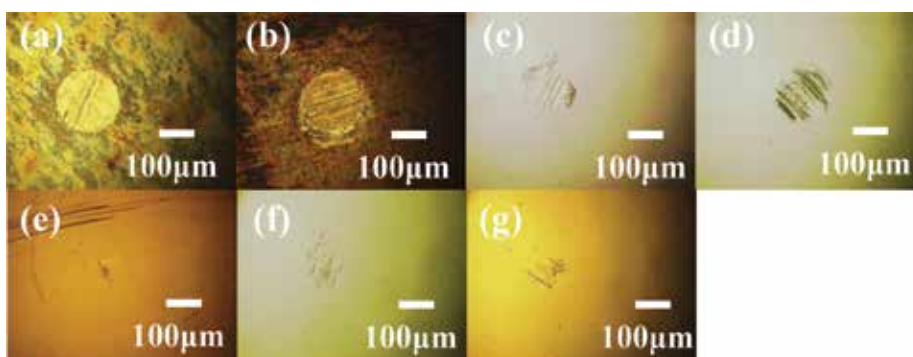
**Figure 1** shows the average friction coefficients in the last 5 min of testing and the specific wear rates of the ball specimens. The results for the sulfur anion-based ionic liquids confirm the relationship between the alkyl chain lengths of the anions and the liquids' tribological performances. The friction coefficients are increased as the alkyl chains become longer. Meanwhile, the specific wear rates of the ball specimens are decreased as the alkyl chains become longer. The friction coefficient of [EMIM][HSO<sub>4</sub>] is approximately 0.04, smaller than that of [BMIM][PF<sub>6</sub>]. However, the specific wear rate is very high. Other sulfur anion-based ionic liquids exhibit higher friction coefficients and specific wear rates than [BMIM][PF<sub>6</sub>]. For the phosphorus anion-based ionic liquids, the friction coefficients and specific wear rates both show increasing tendencies as the alkyl chains become longer. The friction coefficients of [EMIM][DMP] and [EMIM][DEP] exhibit almost the same value as [BMIM][PF<sub>6</sub>]. Furthermore, the [EMIM][DMP] exhibits a very low specific wear rate. [EMIM][DMP] showed the greatest tribological performance of all the ionic liquids. **Figure 2** shows the worn surface images of the ball specimens. Chemical wear is confirmed with [EMIM][HSO<sub>4</sub>] and [EMIM][MSU].

### 2.2.2. Tribochemical reaction behaviors via Q-MS

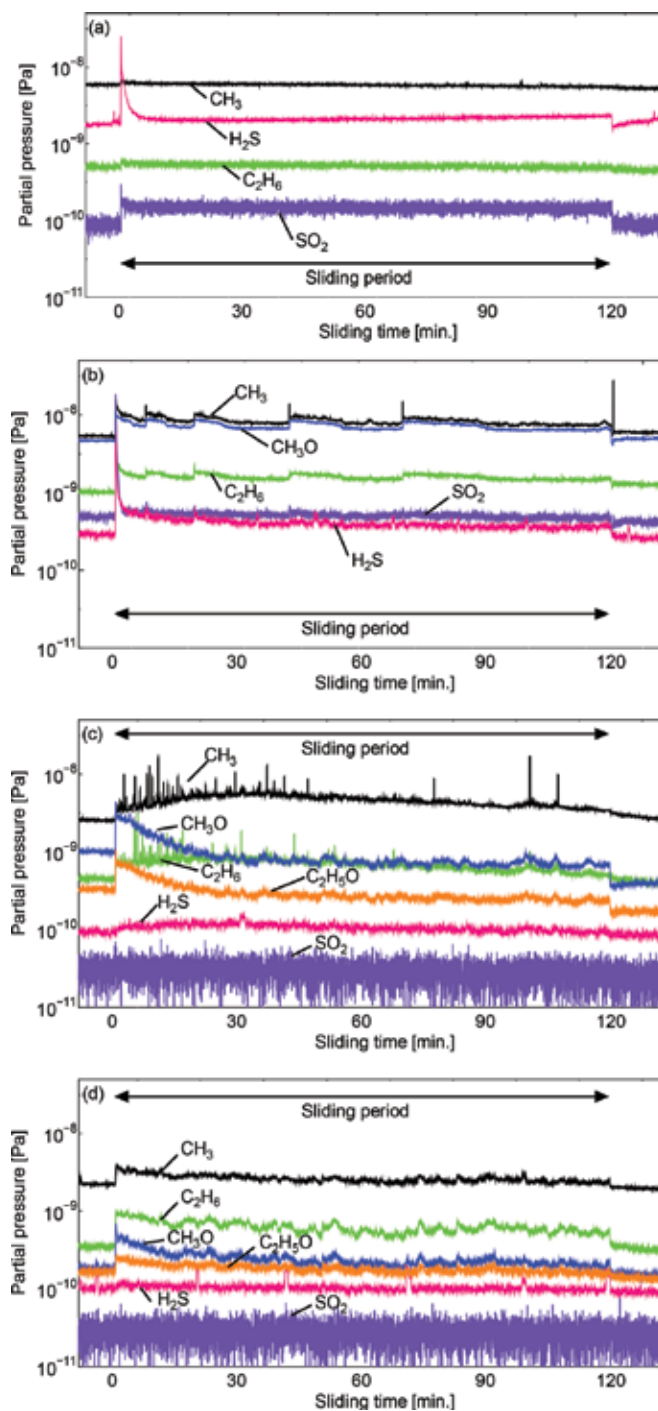
The outgassing of the ionic liquids due to sliding was measured by Q-MS. The main kinds of outgassing were as follows: CH<sub>3</sub> (m/e = 15) and C<sub>2</sub>H<sub>6</sub> (m/e = 30) were derived from the cations, while H<sub>2</sub>S (m/e = 34), CH<sub>3</sub>O (m/e = 31), C<sub>2</sub>H<sub>5</sub>O (m/e = 45), SO<sub>2</sub> (m/e = 64), and PO<sub>3</sub> (m/e = 79) were derived from the anions [24]. Q-MS was used to track the detailed outgassing behaviors of these materials. **Figures 3** and **4** show the outgassing behaviors of the sulfur and phosphorus anion-based ionic liquids, respectively. For [EMIM][HSO<sub>4</sub>], outgassing derived from the cation is slight. In addition, outgassing of H<sub>2</sub>S derived from the anion is significant in the initial sliding period. On the other hand, the outgassing of SO<sub>2</sub> derived from the anion is detected throughout the sliding period. For [EMIM][MSU], the outgassing of CH<sub>3</sub>, C<sub>2</sub>H<sub>6</sub>, and



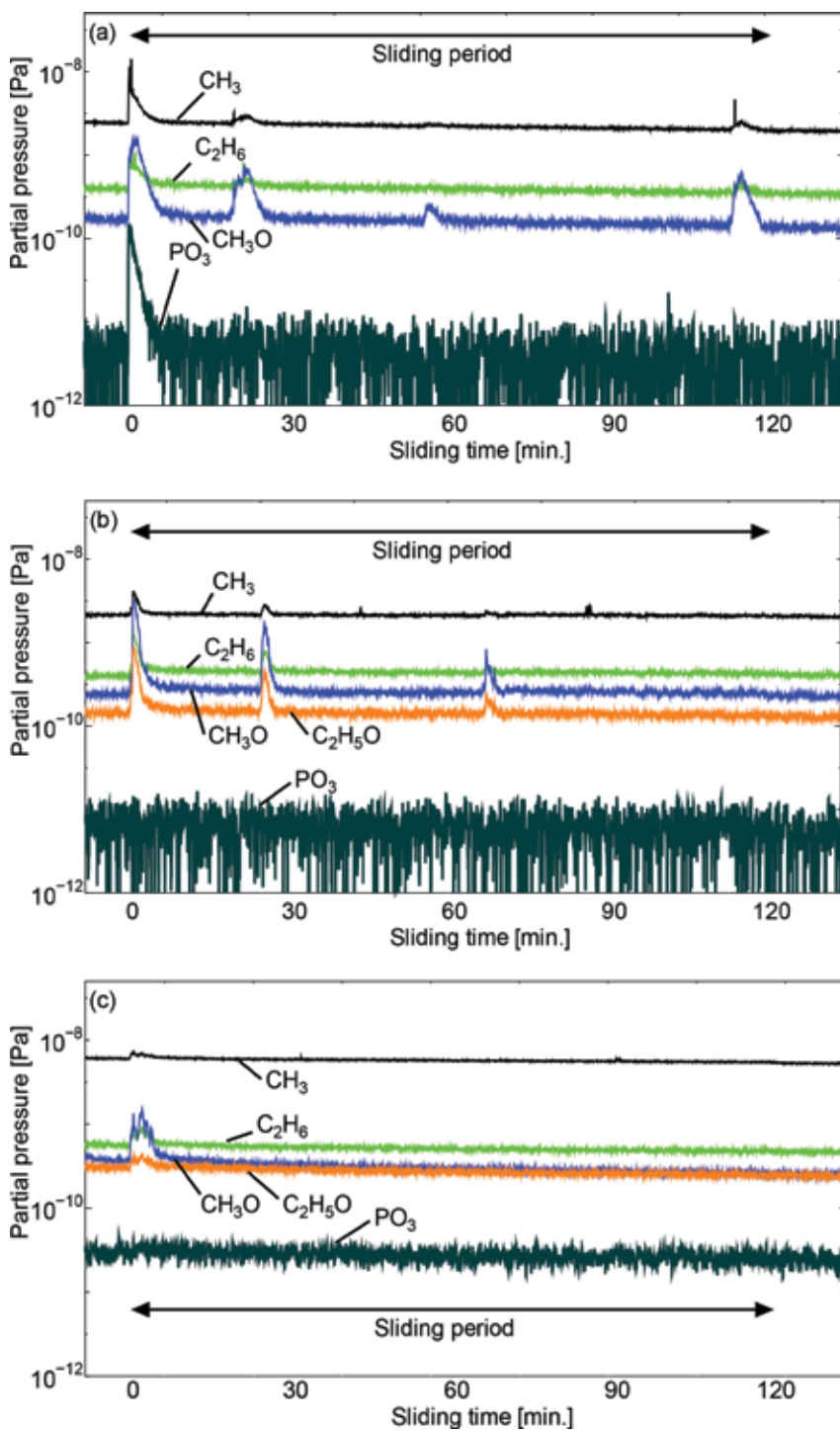
**Figure 1.** The average friction coefficients in the last 5 min of testing and specific wear rates of the tested ionic liquids. (a) Sulfur anion-based ionic liquids and (b) phosphorus anion-based ionic liquids.



**Figure 2.** The worn surface images of ball specimens tested with the ionic liquids. (a) [EMIM][HSO<sub>4</sub>], (b) [EMIM][MSU], (c) [EMIM][ESU], (d) [EMIM][OSU], (e) [EMIM][DMP], (f) [EMIM][EDP], and (g) [EMIM][DBP].



**Figure 3.** The outgassing behaviors of sulfur anion-based ionic liquids. (a) [EMIM][HSO<sub>4</sub>], (b) [EMIM][MSU], (c) [EMIM][ESU], and (d) [EMIM][OSU].



**Figure 4.** The outgassing behaviors of phosphorus anion-based ionic liquids. (a) [EMIM][DMP], (b) [EMIM][DEP], and (c) [EMIM][DBP].

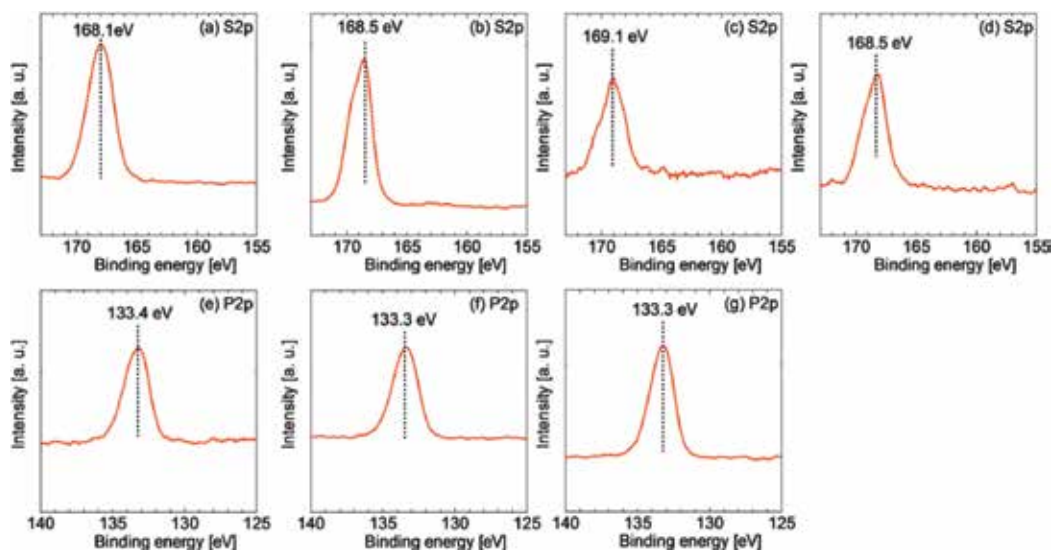
CH<sub>3</sub>O is detected with unstable behavior. The outgassing of H<sub>2</sub>S and SO<sub>2</sub> is high in the initial sliding period, like that of [EMIM][HSO<sub>4</sub>]. For [EMIM][ESU], the outgassing of CH<sub>3</sub> and C<sub>2</sub>H<sub>6</sub> also shows unstable behavior. The outgassing of CH<sub>3</sub>O and C<sub>2</sub>H<sub>5</sub>O is high in the initial sliding period. However, the outgassing of H<sub>2</sub>S and SO<sub>2</sub> is hardly detected, unlike with [EMIM][HSO<sub>4</sub>] and [EMIM][MSU]. For [EMIM][OSU], it is interesting to note that the outgassing of CH<sub>3</sub>, C<sub>2</sub>H<sub>6</sub>, CH<sub>3</sub>O, and C<sub>2</sub>H<sub>5</sub>O is slight and shows stable behavior, but the outgassing of SO<sub>2</sub> is not detected.

### 2.2.3. XPS analysis

**Figure 5** shows the S 2p and P 2p spectra of the sulfur and phosphorus anion-based ionic liquids, respectively. For the sulfur anion-based ionic liquids, the FeSO<sub>4</sub> peak (168–169 eV) is observed on the worn surface; however, FeS and FeS<sub>2</sub> (162–163 eV) peaks are not observed [25–27]. On the other hand, the worn surfaces of phosphorus anion-based ionic liquids show the peak of FePO<sub>4</sub> (133–134 eV) [28–30].

### 2.3. Lubricating mechanisms

From the results of the sliding tests with sulfur anion-based ionic liquids, [EMIM][HSO<sub>4</sub>] exhibited a very low-friction coefficient, but a high specific wear rate and chemical wear. It is well known that chemical wear induces a low-friction coefficient and high wear volume. Among the phosphorus anion-based ionic liquids, [EMIM][DMP] exhibited the greatest tribological performance. Q-MS analysis indicated that the outgassing derived from the anion was small compared to that from the cation. This result indicated that the anion components remained on and reacted with the worn surface. It is well known that reaction films derived from sulfur



**Figure 5.** The spectra of S 2p and P 2p from worn surfaces treated with different ionic liquids. (a) [EMIM][HSO<sub>4</sub>], (b) [EMIM][MSU], (c) [EMIM][ESU], (d) [EMIM][OSU], (e) [EMIM][DMP], (f) [EMIM][EDP], and (g) [EMIM][DBP].

achieve low friction, while those derived from phosphorous achieve low wear volumes [21–24]. These reaction films were confirmed by XPS analysis. Regarding the tribochemical reaction behaviors, ionic liquids with short alkyl chain lengths (e.g., [EMIM][HSO<sub>4</sub>] and [EMIM][MSU]) showed high reactivities with the worn surfaces. It is possible that the heat of friction dominates the tribochemical reactions of the lubricants. However, no relationship between thermal stability and reactivity existed. It is well known that the sliding surface has a high chemical activity derived from the uncovered nascent surface, which functions as a catalytic substance [24, 31]. Thus, the ionic liquids with short alkyl chain lengths easily underwent catalytic degradation on the nascent steel surfaces because the ionic liquids made easy contact with the chemically active sites of the nascent steel surfaces and then achieved low-friction coefficients. For long alkyl chain lengths, the steric hindrance of the anions induced by the alkyl chains decreased the degree of contact with the nascent surface and slowed the tribochemical reactions.

## 2.4. Summary

The sulfur anion-based ionic liquids exhibited low-friction coefficients, while the phosphorus anion-based ionic liquids exhibited low specific wear rates. The sulfur and phosphorus anion-based ionic liquids reacted with the steel surface to achieve low friction and low wear volume, respectively. Ionic liquids with short alkyl chain lengths easily underwent catalytic degradation on the nascent steel surfaces and reacted easily.

## 3. Cyanoanion-based ionic liquids

The cyanoanion-based ionic liquids consist of light elements (e.g., hydrogen, boron, carbon, and nitrogen). These ionic liquids are expected to reduce environmental burdens when compared to halogen, sulfur, and phosphorus anion-based ionic liquids. However, information on the tribological performances of these ionic liquids is scarce. This section reports the lubricating mechanism of cyanoanion-based ionic liquids.

### 3.1. Experimental details

#### 3.1.1. Lubricants

Six kinds of cyanoanion-based ionic liquids were used as lubricants. **Table 3** lists the chemical names and molecular structures of the used ionic liquids: 1-ethyl-3-methylimidazolium dicyanamide ([EMIM][DCN]), 1-butyl-3-methyl pyrrolidinium dicyanamide ([BMPL][DCN]), 1-ethyl-3-methylimidazolium tricyanomethanide ([EMIM][TCC]), 1-butyl-3-methyl pyrrolidinium tricyanomethanide ([BMPL][TCC]), 1-ethyl-3-methylimidazolium tetracyanoborate ([EMIM][TCB]), and 1-butyl-3-methyl pyrrolidinium tetracyanoborate ([BMPL][TCB]). All ionic liquids were commercial materials. [EMIM][DCN], [BMPL][DCN], [EMIM][TCB], and [BMPL][TCB] were purchased from Merck Chemicals, Germany, as “High Purity (HP)” grade (halide content <100 ppm, water content <1000 ppm). [EMIM][TCC] and [BMPL][TCC] were purchased from IoLiTec, Germany, as “HP” grade (water content <1000 ppm). In addition, 1-butyl-3-methylimidazolium hexafluorophosphate ([BMIM][PF<sub>6</sub>]), containing halogen elements, was used for comparison.

Chemical name	Molecular structure
1-Ethyl-3-methylimidazolium dicyanamide	
1-Butyl-3-methyl pyrrolidinium dicyanamide	
1-Ethyl-3-methylimidazolium tricyanomethanide	
1-Butyl-3-methyl pyrrolidinium tricyanomethanide	
1-Ethyl-3-methylimidazolium tetracyanoborate	
1-Butyl-3-methyl pyrrolidinium tetracyanoborate	

**Table 3.** Chemical names and molecular structures of cyanoanion-based ionic liquids.

### 3.1.2. Physical and chemical properties of ionic liquids

All ionic liquids are liquid in phase at room temperature. **Table 4** lists the viscosities and thermal decomposition temperatures of the used ionic liquids. The measurement methods were the same as those given in Section 2.1.2.

### 3.1.3. Sliding tests

Testing was performed in the same methods outlined in Section 2.1.3.

Ionic liquid	Viscosity [mPa s]		Decomposition temperature [°C]
	40°C	70°C	
[EMIM][DCN]	9.7	5.1	298.23
[BMPL][DCN]	15.4	7.1	283.73
[EMIM][TCC]	10.0	5.4	349.0
[BMPL][TCC]	19.4	9.1	320.8
[EMIM][TCB]	10.6	5.2	412.3
[BMPL][TCB]	25.1	10.3	376.7

**Table 4.** The viscosities and thermal decomposition temperatures of the used ionic liquids.

### 3.1.4. Analysis

The tribochemical reactions of the ionic liquids were estimated using Q-MS (MKS Instruments, Inc.). After the sliding tests, the disk specimens were ultrasonically cleaned with a mixed solution of 1:1 petroleum benzine and acetone for 10 min. The worn disk surfaces were analyzed by time-of-flight secondary-ion mass spectrometry (ToF-SIMS). The primary ion source was  $\text{Au}_3^+$ , impact energy was 30 kV, measured area was  $300 \times 300 \mu\text{m}$ , mass resolution was  $1955 \text{ m}/\delta\text{m}$ , spatial resolution was  $3 \mu\text{m}$ , and dosage was  $4.09 \times 10^{10} \text{ ion}/\text{cm}^2$ .

## 3.2. Results

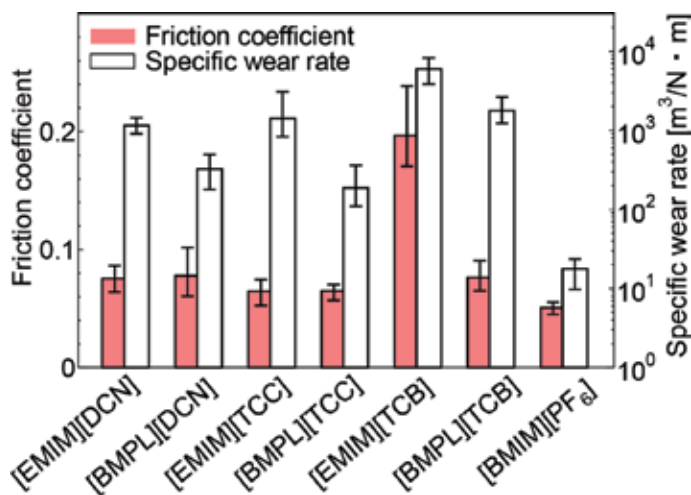
### 3.2.1. Tribological performance

**Figure 6** shows the average friction coefficients in the last 5 min of testing and specific wear rates of the ball specimens. [EMIM][TCB] exhibits the highest friction coefficient of 0.18. The other cyanoanion-based ionic liquids exhibit equivalent low-friction coefficients of approximately 0.07. However, this value is higher than that of [BMIM][PF<sub>6</sub>]. For the specific wear rate, the [BMPL] cation exhibits a smaller value than the [EMIM] cation for the same anion. In addition, chemical wear was observed with none of the ionic liquids, thus, imaging of the ball specimens was omitted.

### 3.2.2. Tribochemical reaction via Q-MS

The main kinds of outgassing are as follows:  $\text{CH}_3$  ( $m/e = 15$ ),  $\text{C}_2\text{H}_6$  ( $m/e = 30$ ),  $\text{C}_3\text{H}_8$  ( $m/e = 44$ ), and  $\text{C}_4\text{H}_{10}$  ( $m/e = 58$ ) are derived from the cations [31]. Q-MS traced the detailed outgassing behaviors of these materials. Outgassing derived from anions was not confirmed. This indicated that anions remained on the worn surfaces. **Figure 7** shows the outgassing behavior of each ionic liquid. When [EMIM][DCN] and [BMPL][DCN] are used, the outgassing shows stable behavior throughout the sliding period. With [EMIM][TCC], the outgassing behavior is particularly interesting. Much outgassing with sliding is detected until 30 min have elapsed, then the outgassing behavior is stabilized. For [BMPL][TCC], the outgassing behavior shows





**Figure 6.** The average of friction coefficients in the last 5 min and specific wear rates of the tested ionic liquids.

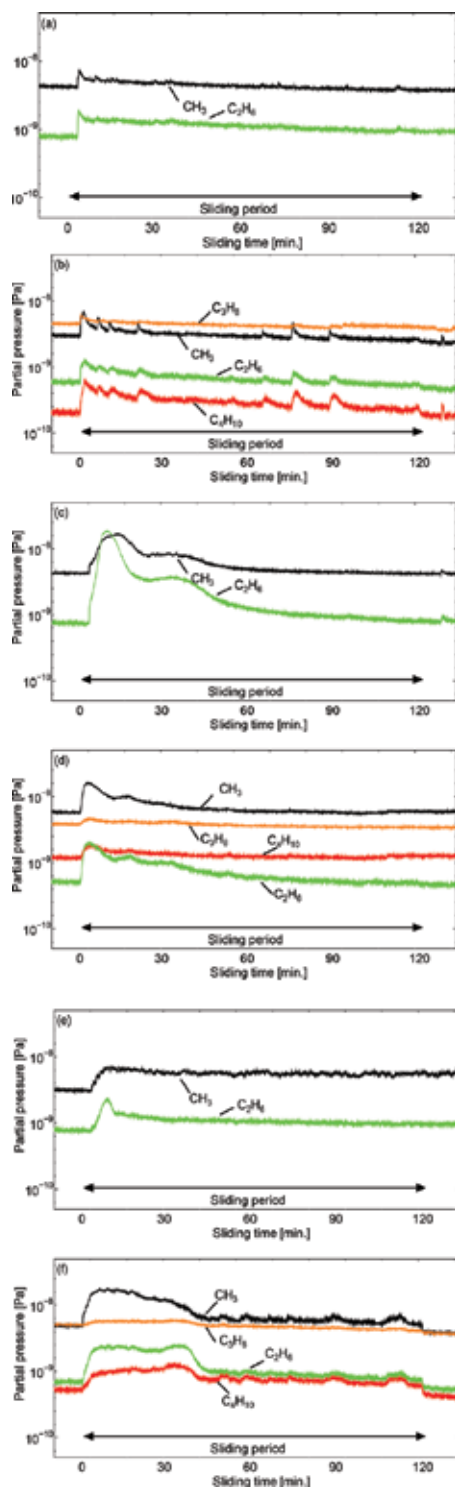
tendencies similar to those of [EMIM][TCC]. For [EMIM][TCB], the amount of outgassing is initially large before stabilizing. With [BMPL][TCB], much outgassing is detected in the first 30 min of sliding, before stabilizing.

### 3.2.3. ToF-SIMS analysis

Q-MS indicated that the anions remained on the worn surfaces. To obtain information from the worn surfaces, mapping imaging was conducted. **Figure 8** shows mapping images of the surfaces tested with each ionic liquid. For [EMIM][TCB], which showed the highest friction coefficient, both ions show low intensities on the worn area. However, for the other ionic liquids, the adsorption of anions on the worn areas is confirmed. The cations are not observed on the worn surfaces, unlike the anions.

### 3.3. Lubricating mechanisms

From the results of the sliding tests, [EMIM][TCB] exhibited the highest friction coefficient. Other ionic liquids exhibited low-friction coefficients. The [BMPL] cation group exhibited a low specific wear rate when compared to the [EMIM] cation group. Q-MS analysis indicated that the anions remained on the worn surfaces. Adsorption film formation was confirmed by ToF-SIMS analysis. Regarding the tribochemical reaction behavior, [EMIM][TCC], [BMPL][TCC], and [BMPL][TCB] decomposed easily on the nascent steel surfaces and exhibited low-friction coefficients. However, [EMIM][TCB] was stable when compared to the other ionic liquids and exhibited a high-friction coefficient. These ionic liquids did not have large differences in chemical structure. Thus, the effect of steric hindrance on the tribochemical reaction was very small and another influence was extant. It is considered that the stability of the cyanoanion-based ionic liquids was important in the tribochemical reactions. [EMIM][TCB] had the highest thermal stability of the cyanoanion-based ionic liquids, and it is believed that



**Figure 7.** The outgassing behaviors of cyanoanion-based ionic liquids. (a) [EMIM][DCN], (b) [BMPL][DCN], (c) [EMIM][TCC], (d) [BMPL][TCC], (e) [EMIM][TCB], and (f) [BMPL][TCB].

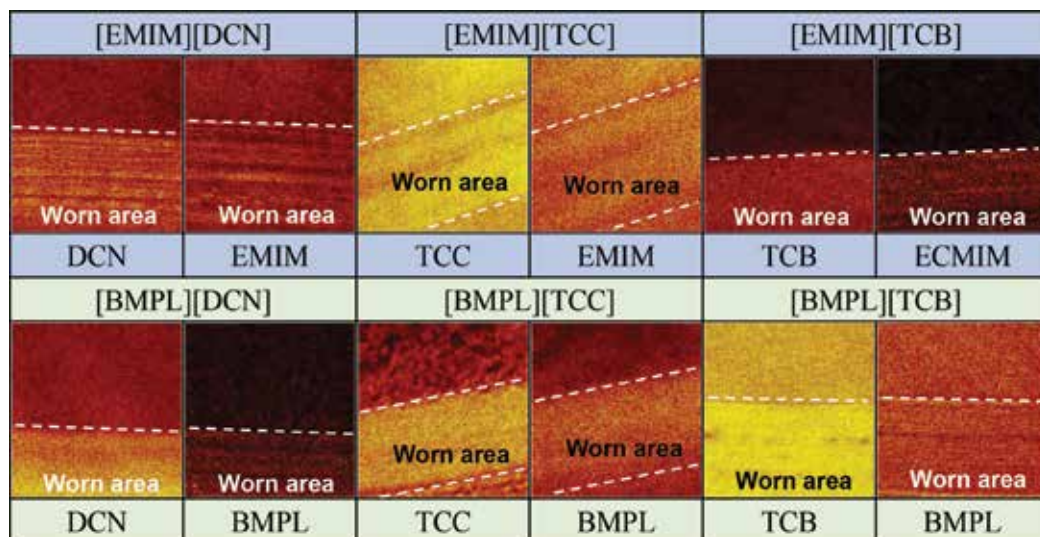


Figure 8. The mapping images (300 × 300 μm) of each ion on the worn surfaces by ToF-SIMS.

[EMIM][TCB] was stable against nascent surface. From these results, it was considered that realizing low friction required the tribochemical decomposition of the ionic liquids and adsorption of anions.

### 3.4. Summary

The tribological performances were different according to the structures of the cyanoanion-based ionic liquids. To achieve low friction, the tribochemical reaction of the ionic liquids and adsorption of anions were required. The stability of the cyanoanion-based ionic liquids against the nascent steel surfaces was related to the results of thermal stability for each liquid.

## 4. Conclusions

This chapter reported investigations of the tribological performances of halogen-free ionic liquids and discussed the lubricating mechanisms of such liquids. As compared with halogen anion-based ionic liquids, the sulfur anion-based ionic liquids exhibited low-friction coefficients, and the phosphorus anion-based ionic liquids exhibited low specific wear rates. [EMIM][DMP] exhibited a particularly low-friction coefficient and specific wear rate. The main kind of outgassing under sliding was from the cation component. The anion remained on and reacted with the worn surface. The anion with short alkyl chain length reacted easily with the worn surface and achieved high tribological performance. Sulfur and phosphorus anion-based ionic liquids show potential as novel lubricants.

The cyanoanion-based ionic liquids also showed low-friction coefficients of less than 0.1; however, these remained higher than those of halogen anion-based ionic liquids. To achieve low

friction, tribochemical reactions with the worn surface and the adsorption of anions on the worn surface were required. The thermal stability and tribochemical reactivity were found to be related.

The sulfur and phosphorus anion-based ionic liquids and cyanoanion-based ionic liquids formed different tribological films. These films had different physical and chemical properties. When these ionic liquids are applied as lubricants in the industry, it is important to select the ionic liquid type depending on the sliding condition. For example, because the sulfur and phosphorus anion-based ionic liquids have high viscosities, they are suitable for sliding in the low-velocity regime. In addition, they are suitable for high contact pressures because they form reaction films. On the other hand, the cyanoanion-based ionic liquids are expected to show applicability for sliding parts exposed to large temperature changes, because their viscosity indices are high.

## Acknowledgements

This work was supported by a Grant-in-Aid for JSPS Fellows No. 15 J05958 and JSPS KAKENHI Grant Numbers, JP16H02310, JP26630041.

## Conflict of interest

The authors declare no conflict of interest.

## Author details

Shouhei Kawada<sup>1\*</sup>, Seiya Watanabe<sup>2</sup>, Shinya Sasaki<sup>1</sup> and Masaaki Miyatake<sup>1</sup>

\*Address all correspondence to: s-kawada@rs.tus.ac.jp

<sup>1</sup> Tokyo University of Science, Tokyo, Japan

<sup>2</sup> Kungliga Tekniska Högskolan, Stockholm, Sweden

## References

- [1] Stocker TF, Qin D, Plattner G-K, Tignor MMB, Allen SK, Boschung J, Nauels A, Xiam Y, Bex V, Midgley PM. Climate Change 2013—The Physical Science Basis. Cambridge: Cambridge University Press; 2014. 1552 p. DOI: 10.1017/CBO9781107415324
- [2] Okubo H, Tsuboi R, Sasaki S. Frictional properties of DLC films in low-pressure hydrogen conditions. *Wear*. 2015;**340-341**:2-8. DOI: 10.1016/j.wear.2015.03.018

- [3] Okubo H, Oshima K, Tsuboi R, Tadokoro C, Sasaki S. Effects of hydrogen on frictional properties of DLC films. *Tribology Online*. 2015;**10**:397-403. DOI: 10.2474/trol.10.397
- [4] Okubo H, Sasaki S. *In situ* Raman observation of structural transformation of diamond-like carbon films lubricated with MoDTC solution: Mechanism of wear acceleration of DLC films lubricated with MoDTC solution. *Tribology International*. 2017;**113**:399-410. DOI: 10.1016/j.triboint.2016.10.009
- [5] Okubo H, Watanabe S, Tadokoro C, Sasaki S. Ultralow friction of a tetrahedral amorphous carbon film lubricated with an environmentally friendly ester-based oil. *Tribology Online*. 2016;**11**:102-113. DOI: 10.2474/trol.11.102
- [6] Okubo H, Kawada S, Watanabe S, Sasaki S. Tribological performance of halogen-free ionic liquids in steel–steel and DLC–DLC contacts. *Tribology Transactions*. 2018;(1):71-79. DOI: 10.1080/10402004.2016.1272731
- [7] Suzuki A, Shinka Y, Masuko M. Tribological characteristics of imidazolium-based room temperature ionic liquids under high vacuum. *Tribology Letters*. 2007;**24**:307-313. DOI: 10.1007/s11249-007-9235-8
- [8] Kondo Y, Yagi S, Koyama T, Tsuboi R, Sasaki S. Lubricity and corrosiveness of ionic liquids for steel-on-steel sliding contacts. *Proceedings of the Institution of Mechanical Engineers, Part J: Journal of Engineering Tribology*. 2012;**226**:991-1006. DOI: 10.1177/1350650112456127
- [9] Kawada S, Watanabe S, Kondo Y, Tsuboi R, Sasaki S. Tribochemical reactions of ionic liquids under vacuum conditions. *Tribology Letters*. 2014;**54**:309-315. DOI: 10.1007/s11249-014-0342-z
- [10] Ye C, Liu W, Chen Y, Yu L. Room-temperature ionic liquids: a novel versatile lubricant. *Chemical Communications*. 2001:2244-2245. DOI: 10.1039/B106935G
- [11] Kamimura H, Kubo T, Minami I, Mori S. Effect and mechanism of additives for ionic liquids as new lubricants. *Tribology International*. 2007;**40**:620-625. DOI: 10.1016/j.triboint.2005.11.009
- [12] Mahrove M, Pagano F, Pejaković V, Valea A, Kalin M, Igartua A, Tojo E. Pyridinium based dicationic ionic liquids as base lubricants or lubricant additives. *Tribology International*. 2015;**82**:245-254. DOI: 10.1016/j.triboint.2014.10.018
- [13] Pejaković V, Kronberger M, Kalin M. Influence of temperature of tribological behaviour of ionic liquids as lubricants and lubricant additives. *Lubrication Science*. 2014;**26**:107-115. DOI: 10.1002/ls.1233
- [14] Kawada S, Sato K, Watanabe S, Sasaki S. Lubricating property of cyano-based ionic liquids against hard materials. *Journal of Mechanical Science and Technology*. 2017;**31**:5745-5750. DOI: 10.1007/s12206-017-1116-y
- [15] Wilkes JS. A short history of ionic liquids—From molten salts to neoteric solvents. *Green Chemistry*. 2002;**4**:79-80. DOI: 10.1039/B110838G

- [16] Rogers RD, Seddon KR. Ionic liquids—Solvents of the future? *Science*. 2003;**302**:792-793. DOI: 10.1126/science.1090313
- [17] Seddon KR. Ionic liquids: A taste of the future. *Nature Materials*. 2003;**2**:363-365. DOI: 10.1038/nmat907
- [18] Wamser CA. Hydrolysis of fluoboric acid in aqueous solution. *Journal of the American Chemical Society*. 1948;**70**:1209-1215. DOI: 10.1021/ja01183a101
- [19] Swatloski RP, Holbrey JD, Rogers RD. Ionic liquids are not always green: hydrolysis of 1-butyl-3-methylimidazolium hexafluorophosphates. *Green Chemistry*. 2003;**5**:361-363. DOI: 10.1039/B304400A
- [20] Arias-Pardilla J, Espinosa T, Bermudez MD. Ionic liquids in surface protection. *Electrochemistry in Ionic Liquids*. 2015;**2**:533-561. DOI: 10.1007/978-3-319-15132-8\_19
- [21] Okubo H, Watanabe S, Tadokoro C, Sasaki S. Effects of concentration of zinc dialkyl-dithiophosphate on the tribological properties of tetrahedral amorphous carbon films in presence of organic friction modifiers. *Tribology International*. 2016;**94**:446-457. DOI: 10.1016/j.triboint.2015.10.008
- [22] Okubo H, Watanabe S, Tadokoro C, Sasaki S. Effects of structure of zinc dialkyldithiophosphates on tribological properties of tetrahedral amorphous carbon film under boundary lubrication. *Tribology International*. 2016;**98**:26-40. DOI: 10.2474/trol.12.221
- [23] Okubo H, Tadokoro C, Sasaki S. Tribological properties of a tetrahedral amorphous carbon (ta-C) film under boundary lubrication in the presence of organic friction modifiers and zinc dialkyldithiophosphate (ZDDP). *Wear*. 2015;**332-333**:1293-1302. DOI: 10.1016/j.wear.2015.01.023
- [24] Kawada S, Watanabe S, Tadokoro C, Sasaki S. Effects of alkyl chain length of sulfate and phosphate anion-based ionic liquids on tribochemical reactions. *Tribology Letters*. 2018;**66**. DOI: 10.1007/s11249-017-0962-1
- [25] Totolin V, Ranetcais N, Hamciuc V, Shore N, Dörr N, Ibanescu C, Simionescu BC, Harabagiu V. Influence of ionic structure and tribological properties of poly(dimethylsiloxane-alkylene oxide) graft copolymers. *Tribology International*. 2013;**67**:1-10. DOI: 10.1016/j.triboint.2013.06.015
- [26] Lu Q, Wang H, Ye C, Liu W, Xue Q. Room temperature ionic liquid 1-ethyl-3-hexylimidazolium-bis(trifluoromethylsulfonyl)-imide as lubricant for steel-steel contact. *Tribology International*. 2004;**37**:547-552. DOI: 10.1016/j.triboint.2003.12.003
- [27] Zhao W, Pu J, Yu Q, Zeng Z, Wu X, Wue Q. A novel strategy to enhance micro/nano-tribological properties of DLC film by combining micro-pattern and thin ionic liquids film. *Colloids Surface A*. 2013;**428**:70-78. DOI: 10.1016/j.colsurfa.2013.03.047
- [28] Nelson AJ, Glenis S, Frank AJ. XPS and UPS investigation of PF<sub>6</sub> doped and undoped poly 3-methyl thiophene. *The Journal of Chemical Physics*. 1987;**87**:5002-5006. DOI: 10.1063/1.452815

- [29] Wang Z, Xia Y, Liu Z, Wen Z. Conductive lubricating grease synthesized using the ionic liquid. *Tribology Letters*. 2012;**46**:33-42. DOI: 10.1007/s11249-012-9915-x
- [30] Wang H, Lu Q, Ye C, Liu W, Cui Z. Friction and wear behaviors of ionic liquid of alkyl-imidazolium hexafluorophosphates as lubricants for steel/steel contact. *Wear*. 2004; **256**:44-48. DOI: 10.1016/S0043-1648(03)00255-2
- [31] Kawada S, Watanabe S, Tadokoro C, Tsuboi R, Sasaki S. Lubricating mechanism of cyano-based ionic liquids on nascent steel surface. *Tribology International*. 2018;**119**:474-780. DOI: 10.1016/j.triboint.2017.11.019





---

## State of the Art Characterization

---



---

# Progress in Green Solvents for the Stabilisation of Nanomaterials: Imidazolium Based Ionic Liquids

---

Zikhona Tshemese, Siphamandla C. Masikane,  
Sixberth Mlowe and Neerish Revaprasadu

Additional information is available at the end of the chapter

<http://dx.doi.org/10.5772/intechopen.80062>

---

## Abstract

For over a decade, ionic liquids (ILs) have attracted enormous attention from scientists across the globe. The history of these compounds traces back to 1914 where the inception of the first IL with a melting point of 12°C was made. Years later, a progression of the remarkable related compounds have been discovered. Out of many analogous compounds realized from time to time, the imidazolium class of ionic liquid is the most studied because of their air and moisture stability. The physicochemical properties of ILs differ significantly depending on the anionic/cationic species and alkyl chain length. ILs have found application in many scientific fields the most recent being good solvents and stabilizing agents in the nanomaterial synthesis. Studies have showed that ILs not only stabilize as synthesized nanomaterials but also provide environmentally green routes towards nanomaterials engineering.

**Keywords:** ionic liquids, green solvent, nanomaterials, imidazolium-based ionic liquid, stabilization, capping agents

---

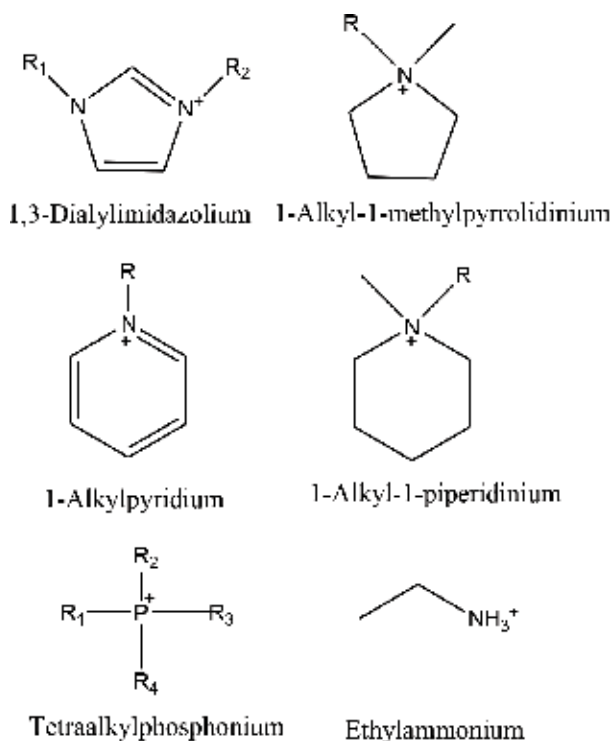
## 1. Introduction

Nanomaterials have penetrated numerous multidisciplinary research fields in both science and engineering domains, leading to the development of next generation products which have already made a debut in the commercial marketplace [1]. To date, synthetic methods and protocols remain of fundamental importance in accessing and harnessing unique properties of materials as their particle sizes approach the nanometer size regime. Suspended nanomaterials are usually desired due to their suitability with various applications and they are

---

easily prepared from chemical approaches. These approaches provide opportunities in tailoring and tuning the properties of the nanomaterials to suit desired applications by tweaking reaction parameters. Two main reaction parameters have received attention, namely, (1) the type and nature of the precursor/s [2–4], as well as (2) the nature of the solvent used during and after completion of the fabrication process [5–7]. Nanomaterials have, however, received their share of potential negative implications on the environment and its inhabitants [8]. Thus, efforts in devising eco-friendly reaction protocols have been seen as a proper response. In this chapter, imidazolium-based ILs are reviewed as green solvents over conventional organic solvents for use in the synthesis of nanomaterials.

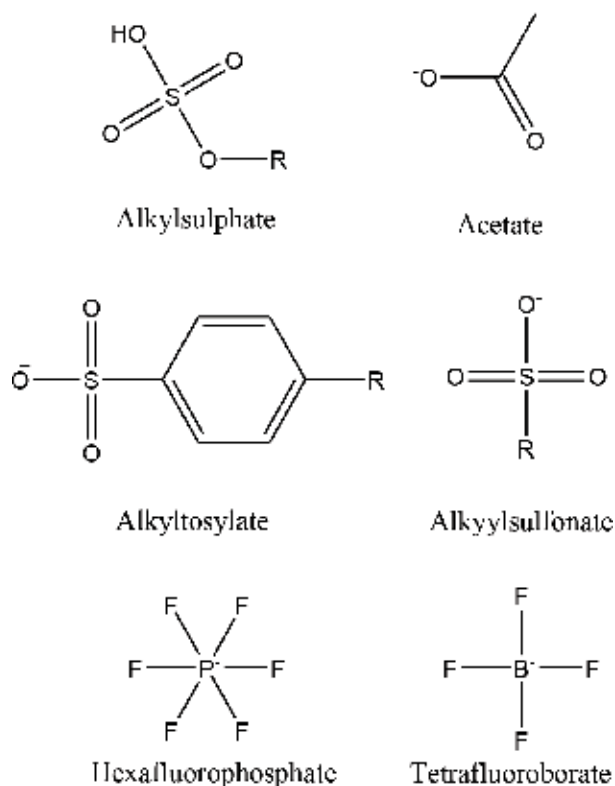
The general use of conventional organic solvents in various laboratory and industrial processes has presented issues over the years. For example, in pharmaceutical production, the high energy consumption (*ca.* 60% of the overall energy) and 50% of the post-treatment greenhouse gas emissions are attributed to the incorporation of organic solvents in the production process [9, 10]. Thus, the search for alternative green solvents that do not compromise the process and quality of the end-product has become popular. As a result, different tools, methods and guidelines have been established to ascertain the proper selection of alternative solvents for synthesis; Ghandi [11] has categorized these solvents into three classes, namely: (i) preferred, (ii) usable and (iii) desirable. Ionic liquids are among solvents have become a central focus as alternatives to toxic solvents and subsequently exploited in various reactions.



**Figure 1.** Commonly used cations for ILs synthesis.

Ionic liquids (ILs) are generally molten salts composed of organic cations and organic or inorganic anions, with characteristic melting points below 100°C. They possess unique physicochemical properties such as low viscosity [12], negligible vapor pressure [13], non-flammability [14], good thermal and chemical stability [15], high ionic conductivity [16], and tunable solubility for both organic and inorganic molecules. They are thus regarded as environmentally-friendly and may lead to the formation of novel materials that have never been achieved by conventional solvents or even water. ILs are normally characterized by their cationic components of which imidazolium [17], pyridinium [18], ammonium [19], pyrrolidinium [20], piperidinium [21] and phosphonium [22] cations with different alkyl chain lengths being the most common (**Figure 1**). Examples of some commonly used anions are shown in **Figure 2**. ILs can be classified further into groups, *viz.* polyionic liquids (PILs) [23, 24], room temperature ionic liquids [25–27], task-specific ionic liquids [28, 29] and supported ionic liquid membranes [30, 31]. IL composites are also known, such as the metal organic frameworks-supported ILs [32, 33].

The complexity and suitability of ILs in various applications have been debated over the years. Many questions have been asked about the complexity (and sometimes even the simplicity) associated with the usefulness of ionic liquids in various fields of science specifically their use as solvents. However, the hybrid ionic nature of ILs and the resultant intermolecular interactions



**Figure 2.** Most familiar anionic species used in ILs synthesis.

give rise to a complex set of phenomena, creating an area of study that is both interesting and challenging. Furthermore, they have been extensively studied and researched as potential solvents for inorganic nanomaterial synthesis, organic chemical reactions, polymer synthesis and electrochemical applications [34–38]. Thus, the aim of this chapter is to rather highlight the recent developments and breakthroughs in exploiting the interesting physicochemical properties of ILs in the world of nanomaterials. The scope will be restricted to the use of room temperature ILs as green solvents for the synthesis and stabilization of inorganic nanomaterials. Prior to this, the physicochemical properties of ILs will be briefly outlined.

## 2. Physicochemical properties of ILs

The physicochemical properties of ILs (e.g. viscosity, melting point, hydrophobicity, solvation, and catalytic activity) can be tuned by changing the alkyl chain length in the cationic and/or the anion groups [39, 40]. Task specific or targeting ILs can be synthesized by careful choice and combination of the cationic and anionic groups, to suit a specific application. A catalysis-themed review article by Sheldon [35], for example, outlines the potential use of ILs as both reaction media and catalysts. The former was, however, found to have a profound effect on the catalytic activities and selectivity.

### 2.1. Viscosity

Greater van der Waals forces and hydrogen bonding are typical attributes of materials exhibiting high viscosities [41, 42]. Generally, ILs are highly viscous than most common molecular solvents, with viscosity ranging between 10 and 500 mPa s at room temperature [43]. The cation structure influences the IL viscosity with minimal values reported for ethylmethylimidazolium, EtMeIm<sup>+</sup> ILs. Furthermore, EtMeIm<sup>+</sup> ILs have adequate side chain mobility and low molecular weight. Generally, the viscosity of ILs increases with alkyl chain length and degree of fluorination [44]. Anions also have an influence over the viscosity of ILs, e.g. [BMIm]PF<sub>6</sub> = 312 mPa [45], [BMIm]BF<sub>4</sub> = 154 mPa [46] and [BMIm]TF<sub>2</sub>N = 52 mPa [44].

### 2.2. Conductivity

ILs have relatively good ionic conductivities compared to organic solvents and electrolytic systems (up to about 10 mS cm<sup>-1</sup>) [43]. Susan et al. [47] first demonstrated that fused ammonium salts can be used as proton conductors in polymer membrane fuel cells [47]. According to Greaves et al. [48], “ionic conductivity is a transport property and is governed by the degree of dissociation of the ions, viscosity, ion mobility, and ionic charge”. These aforementioned factors depend on the effective ion sizes and shapes. Furthermore, ionic conductivity of ILs is inversely proportional to viscosity and molar volume [48].

### 2.3. Melting point

The general description of ILs is that of ionic salts that are in a liquid phase below an arbitrary temperature of 100°C; the majority of ILs are solids at standard room temperature. From a

practical point of view, ILs are desirable in their molten state e.g. transportation of ILs across multiple unit operations in industrial applications is most effective in their liquid phase. ILs exhibiting of significantly lower melting points or "room temperature ILs" ( $T_m < 25^\circ\text{C}$ ) are critically important to researchers searching for new industrial applications [49]. One main reason for their demand is their usage as solvents or absorbents for separation tasks involving selective dissolution of solutes in gas (e.g.  $\text{CO}_2$ ), liquid (e.g. toluene), or solid (e.g. cellulose) states. They are also widely considered as liquid solvents to promote chemical reactions [50].

## 2.4. Density

ILs are generally denser than water, with values ranging from 1 to  $1.6 \text{ g cm}^{-3}$  and their densities decrease with increase in alkyl chain length in the cation [51]. For example, ILs composed of substituted imidazolium-type cations and  $\text{CF}_3\text{SO}_3^-$  anion display densities of 1.39, 1.33, 1.29 and  $1.27 \text{ g cm}^{-3}$  for  $[\text{EMIm}]^+$ ,  $[\text{EEIm}]^+$ ,  $[\text{BMIm}]^+$  and  $[\text{BEIm}]^+$ , respectively [52]. The densities of ILs are also affected by the nature of anions, e.g. the densities of 1-butyl-3-methylimidazolium-type ILs with different anions, such as  $\text{BF}_4^-$ ,  $\text{PF}_6^-$ , TFA and  $\text{Tf}_2\text{N}^-$  in literature are recorded to be 1.12, 1.21, 1.36 and  $1.43 \text{ g cm}^{-3}$ , respectively [44, 53]. The order of increasing density with respect to anions is:  $[\text{CH}_3\text{SO}_3]^- \approx [\text{BF}_4]^- < [\text{CF}_3\text{CO}_2]^- < [\text{CF}_3\text{SO}_3]^- < [\text{C}_3\text{F}_7\text{CO}_2]^- < [(\text{CF}_3\text{SO}_2)_2\text{N}]^-$ , in Ref. [52].

## 2.5. Electrochemical window

The electrochemical window allows ILs to be used in the electrodeposition of semiconductors and metals. The electrochemical window, by definition, is the electrochemical potential range over which the electrolyte is neither reduced nor oxidized at an electrode. Thus, the magnitude of the electrochemical value determines the solvent's electrochemical stability. The electrodeposition of elements and compounds in water is limited by its low electrochemical window of only about 1.2 V. On the contrary, ILs have significantly larger electrochemical windows, for example, 4.15 V for  $[\text{BMIm}]\text{PF}_6$  at a platinum electrode, 4.10 V for  $[\text{BMIm}]\text{BF}_4$  and 5.5 V for  $[\text{BMP}]\text{Tf}_2\text{N}$  at a glassy carbon electrode [54, 55]. Generally, the wide electrochemical windows of ILs have opened the new horizon for the electrodeposition-assisted synthesis of metals and semiconductors at room temperature, which were previously achieved only from molten salts at high reaction temperatures.

## 2.6. Thermal stability

Most solvents are thermally stable at high temperatures only for short durations; long time exposure habitually leads undesirable decomposition [43]. On the other hand, ILs are known to be thermally stable up to  $450^\circ\text{C}$ . Their thermal stability is limited by the strength of their hydrocarbon bonds [43]. It is common knowledge that ILs with larger proton transfer energies prematurely decompose before reaching their boiling points with varying decomposition temperatures ranging between 100 and  $360^\circ\text{C}$  [56]. Protic ILs with a bis(trifluoromethane) sulfonamide anion and alkylammonium, imidazolium and a range of other heterocyclic cations are identified as the most stable ILs due to their bond strength resulting from resonance stabilization [57]. Specifically, ILs such as 1-ethyl-3-methyl-imidazolium tetrafluoroborate, 1-butyl-3-methyl-imidazolium tetrafluoroborate and 1,2-dimethyl-3-propyl imidazolium

bis(trifluorosulfonyl)imide are thermally stable up to 445, 423 and 457°C, respectively [43]. The anionic components is known to predominantly contribute to the thermal stability of the ILs over the cationic counterparts. Furthermore, the hydrophilicity of the anions decreases thermal stability of the ILs [58].

### 3. Imidazolium-based ionic liquids

ILs with the 1,3-dialkylimidazolium cation are by far the most studied class of ILs due to their interesting properties. The class can interact with various chemical species, as they offer hydrophobic or hydrophilic regions and a high directional polarizability. The structural organization of these solvents can be used as 'entropic drivers' for spontaneous, well-defined, and prolonged ordering of nanoscale structures. Certainly, the unique combination of flexibility towards other molecules (and phases) with strong hydrogen-bond-driven structures make ILs potential key tools in the preparation of a new generation of chemical nanostructures [13].

### 4. Imidazolium-based ionic liquids in nanomaterial synthesis

Generally, ILs have chemical attributes such as non-volatility, negligible vapor pressure and most importantly, high thermal stability [59]. The majority of the fabrication protocols require heat to be applied, thus controlling both nucleation and growth rates to ensure monodispersity in suspended nanomaterials [60]. Functional groups of organic solvents determine stability and coordination mode towards nanomaterials [5]. Similarly, the composition of the ILs (combination of organic cation with organic or inorganic anion) play a major role in determining the final chemical attributes. The early reports have demonstrated ILs as dual-action reagents, i.e. as both solvent media and template or structure/shape-directing agent [61, 62]. Furthermore, the recovery of ILs after completion of nanomaterials synthesis strengthens their classification as eco-friendly solvents. The negligible vapor pressure feature enables reactions in ILs to proceed in ambient pressure when subjected to synthetic protocols common for hydro- and solvothermal methods, hence the reactions are rather termed ionothermal synthesis [59].

In recent years the advantages of incorporating ILs in the synthesis of inorganic nanomaterials have been thoroughly demonstrated, due to their unique physicochemical properties [63, 64]. Several ILS-incorporated methods and protocols have been reported for the fabrication of inorganic nanomaterials. Synthetic reactions, in the presence of ILs, offers nanomaterials to display exceptional and/or unique properties [34].

#### 4.1. Electrostatic stabilization of nanomaterials by ILs

Ionic compounds such as carboxylates, polyoxoanions and fluorides usually generate double layers between the nanoparticles, thereby introducing repulsive forces between individual nanoparticles. Thus, electrostatic repulsions prevent aggregations and agglomeration of nanoparticles suspended in the solution phase. This type of electrostatic stabilization is sensitive to reaction parameters such as pH, concentration and temperature. This has been demonstrated in metal nanoparticles stabilized by ILs composed of sulfonium, tertiary butyl



ammonium, phosphonium and imidazolium moieties [65]. A graphical illustration of this kind of stabilization is shown in **Figure 3**.

#### 4.2. Steric stabilization of nanomaterials by ILs

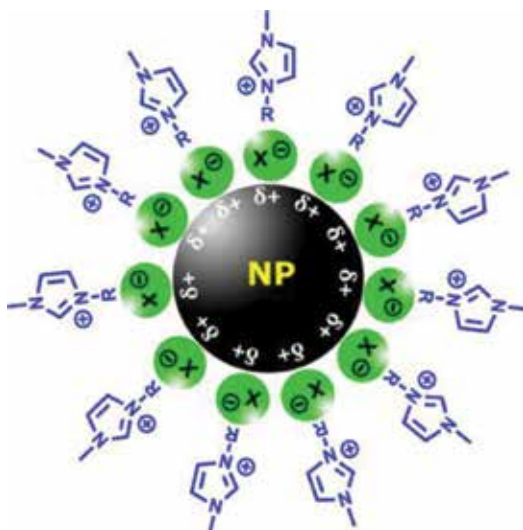
Steric stabilization of nanoparticles is another significant parameter. This usually happens through the use of surfactants, alcohols and a variety of polymers/oligomers. These compounds are adsorbed on the nanoparticle's surface, thereby forming a protective layer [66]. When the nanoparticles are sterically stabilized, their free motion in solution is limited. Furthermore, the thickness of the protective layer has an important role in the stabilization process and greatly depends on the alkyl chain length and nature of the stabilizing agent, where applicable [65].

#### 4.3. A combination of electrostatic and steric stabilization of nanomaterials by ILs

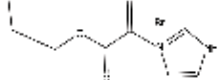
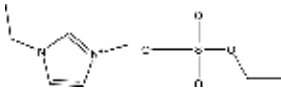
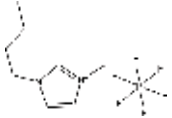
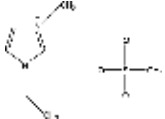
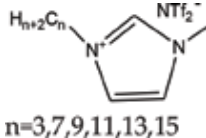
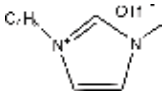
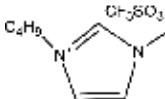
Both electrostatic and steric stabilization processes can co-exist in the stabilization of nanoparticles in solution phase. Ionic surfactants with long alkyl chains ordinarily provide this type of stabilization. This is mostly achieved through ILs which have polar heads groups which generate electric double layer around the nanoparticle and a lipophilic tail group providing the steric repulsions between nanoparticles [65]. Examples of IL-stabilized nanoparticles are listed in **Table 1**.

#### 4.4. Practical examples of imidazolium-based ILs used in the synthesis of nanomaterials

The diversity of ILs presents a challenge is identifying the relationship/trend between their physiochemical properties and morphological (also crystal phase) control of the nanomaterials. It is for these reasons ILs have been used in conjunction with conventional organic solvents to synthesize nanomaterials [68, 74, 75]. Since the influence of ILs on the



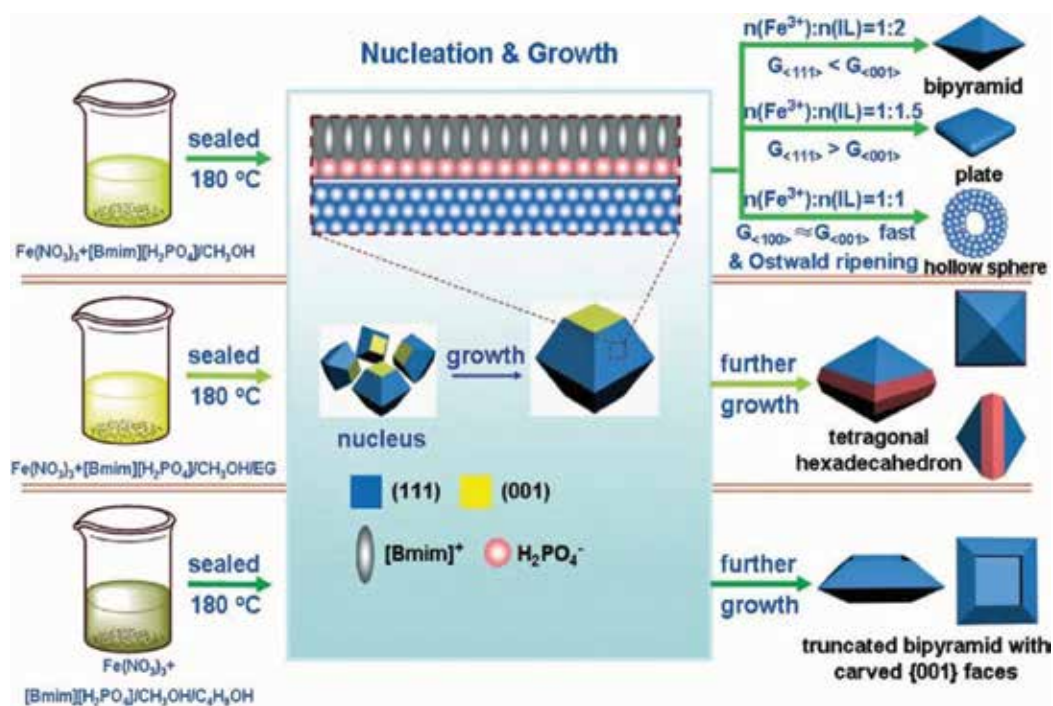
**Figure 3.** Electrostatic stabilization of nanoparticles by the imidazolium based ILs. Reproduced from Ref. [65] with permission granted by Springer.

IL used	NP synthesized	Size (nm)	IL name and reference
	Al <sub>2</sub> O <sub>3</sub> , TiO <sub>2</sub> , Fe <sub>3</sub> O <sub>4</sub>	80–100	1-methacryloyloxypropyl-3-methylimidazolium bromide [67]
	ZnSe	70–100	1-butyl-3-methylimidazolium methyl sulfate [68]
	PbS	100	1-n-butyl-3-methylimidazolium hexafluorophosphate [69]
	CdS, PbS	2–15, 102–160	1-ethyl-3-methylimidazolium methanesulfonate [70]
	Ni	4.9–5.9	1-alkyl-3-methylimidazolium N-bis(trifluoromethane sulfonate) [71]
	Au	140	n-butyltrimethylammonium N-bis(trifluoromethylsulfonate)imide [72]
	Ir	2.4–2.6	1-n-butyl-3-methyl trifluoromethane sulfonate [73]

**Table 1.** Examples of nanoparticles stabilized by imidazolium based ILs.

properties of nanomaterials is not predictable at this stage, there are efforts in conducting investigations for the sake of rather establishing databases. A good example is the work by Duan et al. [76] where ILs are demonstrated as both solvent and shape-directing agent in the synthesis of  $\gamma$ -AlOOH and well-dispersed  $\text{NH}_4\text{Al}(\text{OH})_2\text{CO}_3$  nanostructures. The same group extended the study on ferric giniite crystals (**Figure 4**) which revealed interesting photocatalytic behavior which could only be linked to exposed facets of the crystals, as opposed to the surface area [77]. There are reports that have documented evidence of imidazolium-based ILs having acted as capping agents [78, 79]. Zheng and co-workers [79, 80] have given plausible reasons that support capping through interaction modes of imidazolium-based ILs with TiO<sub>2</sub> nanoparticles, for example, hydrogen bonding between the positively charged (due to delocalization) position-2 H atom in the imidazole ring with O on the TiO<sub>2</sub> surface.

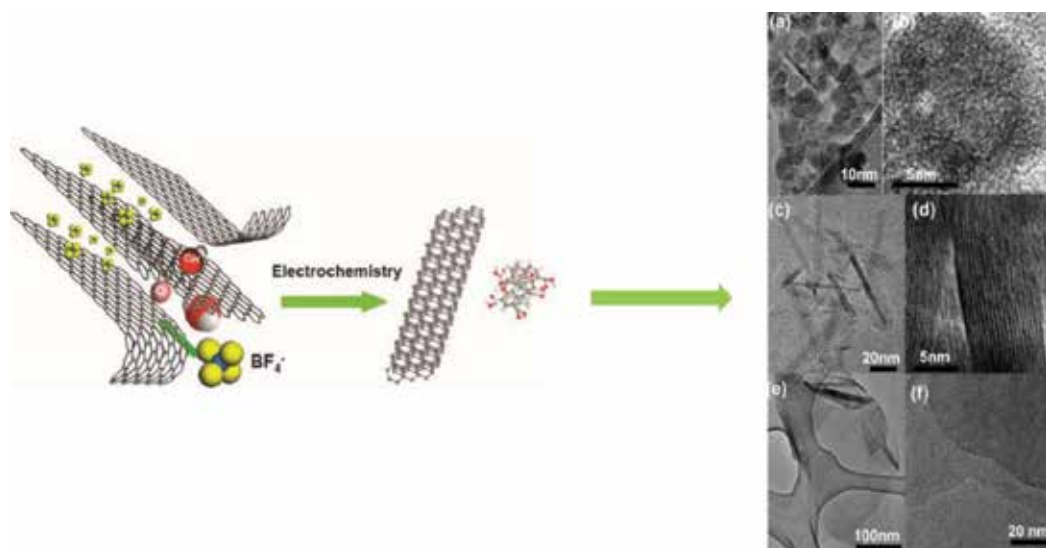
IL-nanomaterial composites have also been reported for use in biological applications, e.g. the study by Alavi-Tabari et al. [81] demonstrates the use of 1-butyl-3-methylimidazolium



**Figure 4.** Synthesis of ferric giniite crystals exhibiting different shapes as a result of varying reaction parameters. Reproduced from Ref. [70] with permission from the Royal Society of Chemistry.

tetrafluoroborate IL to form IL-ZnO composites for potential activity enhancement of doxorubicin and dasatinib for breast anticancer remedies. In their study the outcome showed that ZnO-NPs/BMTFB/CPE reveals two different oxidation signals for the simultaneous examination of doxorubicin and dasatinib, which eventually showed a good linear relationship between the oxidation peak current of doxorubicin and its concentration. They concluded that ZnO-NPs/BMTFB/CPE showed good capacity for analysis of doxorubicin and dasatinib in injection and serum samples. Husanu et al. [82] reported an easy synthetic method focusing on preparing citrate-based ILs which showed a dual-action feature, an ability to act as both capping agents and reducing agents towards the preparation of inorganic nanomaterials.

Although the topic “ILs in the synthesis of nanomaterials” is not of novel origin, the ‘novelty’ is observed where a new class of ILs is prepared through the incorporation of new anionic groups. This subsequently results in the synthesis of nanomaterials bearing desired properties. For example; 3-(hydroxypropyl)-3-methylimidazolium bis(salicylato)borate (OHMimBScB) IL has been used for the covalent grafting of carbon quantum dots via a bottom up approach [83]. Since ILs have strong adsorption capabilities, the surface on the carbon quantum dots was protected against friction, which then improved their stability efficiency in tribological evaluations. Saien and Hashemi [84] used 1-hexadecyl-3-methyl imidazolium chloride IL as a surfactant to study its interaction with  $\text{Fe}_3\text{O}_4$  nanoparticles in a biphasic oil/water system. In a study by Okoli et al. [85] it was found that the sole use of ILs without additional co-surfactants is capable of producing good quality (monodispersity with narrow size distribution) metal alloy nanoparticles which displayed enhanced catalytic activities.



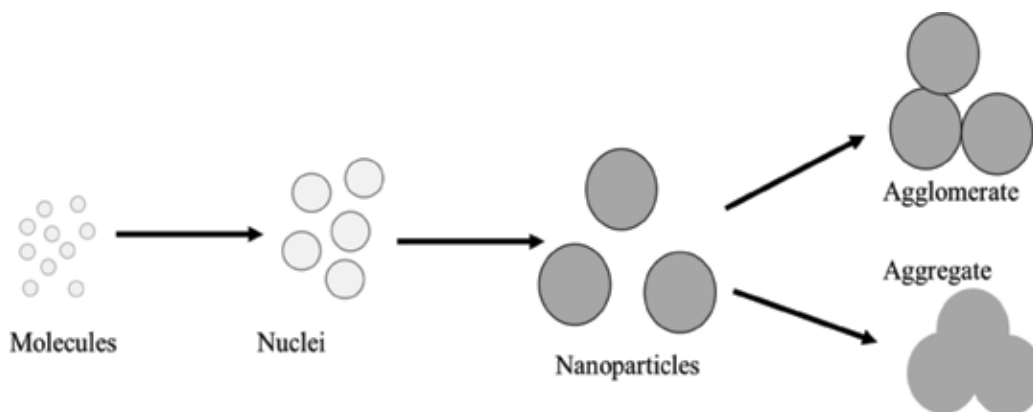
**Figure 5.** The electrochemical exfoliation of graphite into (a and b) carbon nanoparticles, (c and d) carbon nanoribbons and (e and f) graphene sheets. Reprinted with permission from Ref. [87]. Copyright 2009 American Chemical Society.

A pre-concentration technique based on the use of graphene oxide (GO) functionalized with an IL was established for the determination of Hg traces in water [86]. In this study, the hybrid IL-GO nanomaterial was fabricated by a simple procedure, where the IL used was 1-butyl-3-dodecylimidazolium bromide ( $[C_4C_{12}im]Br$ ). The incorporation of  $[C_4C_{12}im]Br$  led to high sorption performances on Hg. Furthermore, functionalization of the imidazolium ring with long alkyl chains increased the retention competence of GO for the analyte, consequently providing additional physicochemical properties that were beneficial for the extraction of Hg and its control at trace levels.

Other interesting reports include the use of ILs as a solvent medium in the electrochemical exfoliation of graphite to obtain nanomaterials of significant technological importance i.e. fluorescent carbon nanoribbons, nanoparticles and graphene (**Figure 5**) [87]. ILs are most suited for this task due to their broad electrochemical window, as well as high dielectric constant necessary to counteract stacking in nanomaterials resulting from van der Waals interactions. Furthermore, imidazolium-based IL-capped carbon quantum dots have been prepared by pyrolysis [88]. Recently, imidazolium-based IL has been used to exfoliate 2D transition metal chalcogenide,  $WS_2$  nanosheets [89]. Prechtel et al. [90] demonstrated the use of ILs as both stabilizing and reducing agents in the preparation of metal nanoparticles from organometallic complexes. Similarly, citrate-modified ILs were recently used to prepare IL-capped Ag nanoparticles [90].

## 5. Tuning the properties of nanomaterials (NMs) through the use of IBILs

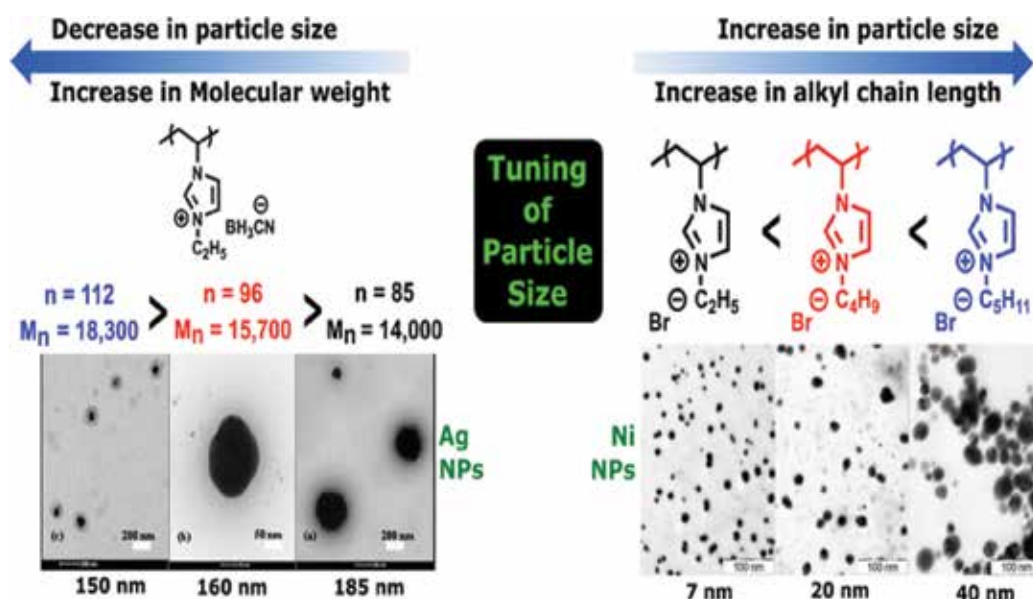
Stabilization of nanoparticles using different media has been necessary to suit various applications. The medium plays a key role in modifying and tuning the chemical and physical



**Figure 6.** Mechanism of nanoparticle production using colloidal methods. The methods differ in the way the starting molecules are generated by chemical reaction/precipitation. The nuclei may be amorphous or crystalline and lead to amorphous or crystalline nanoparticles. Because of their intrinsic instability, the nanoparticles may form agglomerates that can be easily redispersed or form non-dispersible aggregate clusters.

properties of the nanomaterials [91, 92]. Various synthetic routes such as colloidal methods use solvent-mediated chemical procedures to form colloids via self-assembly or other processes related to the tuning of physicochemical properties [93]. The former process usually proceeds via the homogeneous nucleation of particles and subsequent particle growth by condensation, coagulation and arrest of particles (**Figure 6**).

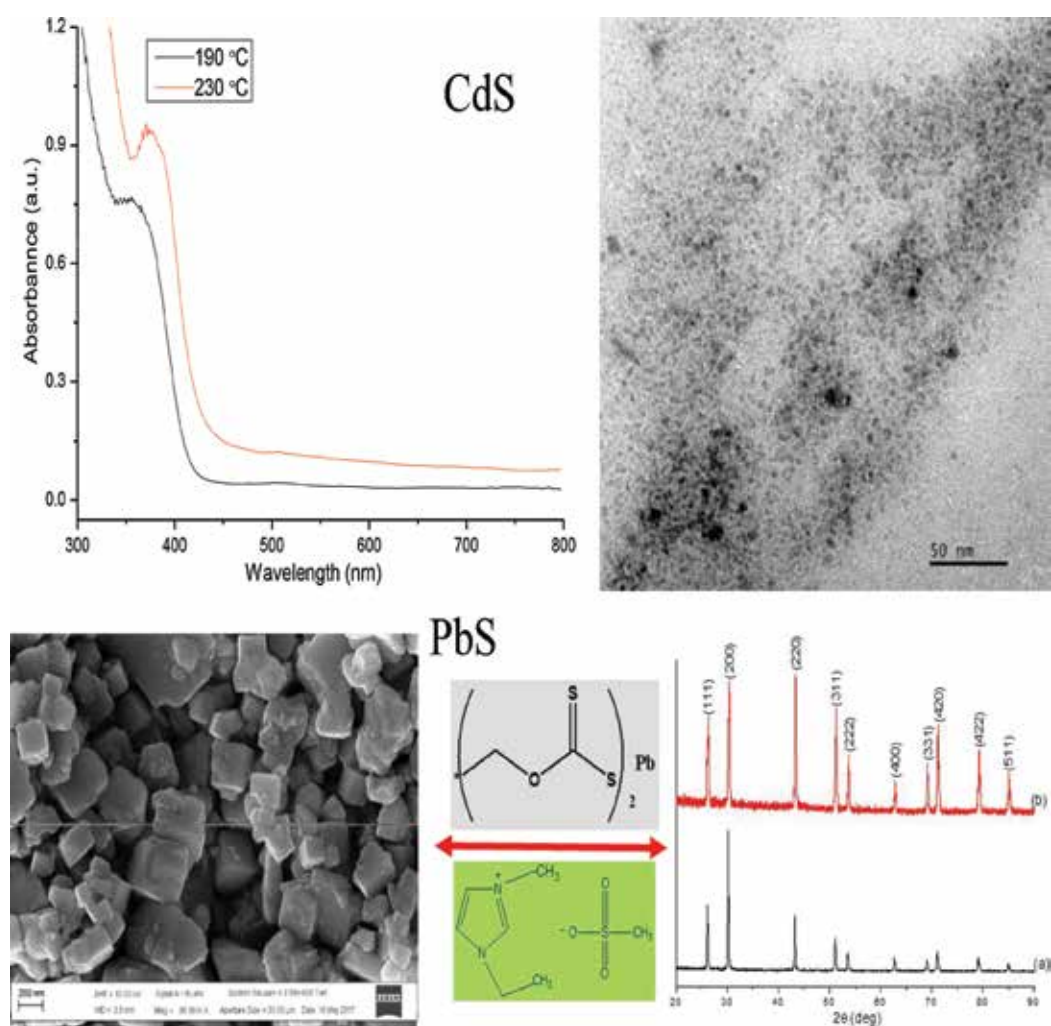
Imidazolium-based ILs have been reported to improve the electric conductivity of multi-walled carbon nanotubes for electrochemical or electro catalytic applications [65]. Covalent interaction linkage ensures improved oxidation and hydrogenation reactions. Imidazolium-based



**Figure 7.** Tuning of nanoparticles size by imidazolium based ionic liquid (reprinted with permission from Refs. [65, 95, 97]).

ILs provide surface stabilization of nanoparticles over a long period of time with insignificant or no change in particle size and size distribution, providing re-usable or recyclability capabilities in applications such as catalysis [65]. Photocatalyst stabilized by imidazolium-based ILs are known to bind strongly and could be easily separated from the reaction mixture without contamination or significant loss in catalytic performance [65].

Interestingly, small-sized Cu nanoparticles (6.6 nm) have reportedly been synthesized *in situ* using [BMIM][PF<sub>6</sub>] and [BMIM][BF<sub>4</sub>] ILs as stabilizing agent and later used in cycloaddition catalytic reactions between azides and alkynes [94]. The particle size of imidazolium-based IL-capped nanoparticles can be easily tuned by varying the molecular weight, alkyl chain lengths and substituents on the imidazolium ring [71, 95]. Gracia et al. [96] demonstrated



**Figure 8.** Top = optical properties and transmission electron microscopy image of 1-ethyl-3-methylimidazolium methanesulfonate stabilized CdS nanoparticles. Bottom = scanning electron microscope image, structure of the IL and X-ray diffraction patterns of 1-ethyl-3-methylimidazolium methanesulfonate stabilized PbS nanoparticles (reprinted with permission from Refs. [70, 98]).

the decrease of Ag nanoparticle sizes with an increase of the molecular weight of P[ViEtIm][BH<sub>3</sub>CN] IL. In another report, Vijayakrishna et al. [97] studied the effect of alkyl chain lengths in the imidazolium-based poly-ILs of the general formula (P[ViRIm][OH]) where R = ethyl, butyl and pentyl, on particle sizes of magnetic Ni nanoparticles; average particle sizes increased with alkyl chain length (**Figure 7**).

The type of functional group present in the IBIL determines the mode of interaction with the nanoparticle. Furthermore, tweaking of the reaction parameters has become a common practice to manipulate these interaction modes, thus, enabling particle size and shape-directing capabilities. The chemical structure of 1-ethyl-3-methylimidazolium IL, in the recent study, afforded covalent, coordinate, electrostatic/steric or weak chemisorption interactions via their cations and counter anions (**Figure 8**) to produce CdS and PbS nanoparticles [70, 98]. The 1-ethyl-3-methylimidazolium IL efficiently produced very small and well dispersed CdS quantum dots in the size range of  $2.3\text{--}4.3 \pm 0.265$  nm, attributed to the presence of both cationic and anionic components [70]. Cubic-shaped and highly crystalline PbS nanoparticles in the particle size range of  $64 \pm 18$  nm were synthesized using the same 1-ethyl-3-methylimidazolium IL (**Figure 8**) [98].

## 6. Conclusion

Ionic liquids (ILs), imidazolium-based ILs (IBILs) in particular, have been exploited in various applications including its use as both reactants and stabilizing agents in the synthesis of functional nanomaterials. The remarkable merit of IBILs and ILs in general is their diversified design which involves a vast selection of cations and anions species. The physicochemical properties of ILs play a major role in improving, modifying and tuning important properties of nanomaterials such as particle size and morphology to suit various applications. Interestingly, the physicochemical properties of ILs further provide unique stability for nanomaterials, which guarantees longer shelf life. In addition, ILs are known to be less toxic, thus enabling them to be used as alternative eco-friendly candidates in various studies as means of applying green chemistry principles. The properties of ILs change with cation/anion composition and there is currently no model to predict its interactions and subsequent influence on the properties of nanomaterials. Hence, an increasing interest observed in evaluating ILs as both reactants and stabilizing agent in the synthesis of different classes of nanomaterials.

## Acknowledgements

Z. Tshemese, S. Mlowe, N. Revaprasadu and S.C. Masikane wishes to thank the National Research Foundation—South Africa (NRF) for financial support.

## Conflict of interest

We declare no conflict of interest.

## Author details

Zikhona Tshemese<sup>1</sup>, Siphamandla C. Masikane<sup>1</sup>, Sixberth Mlowe<sup>1,2\*</sup> and Neerish Revaprasadu<sup>1</sup>

\*Address all correspondence to: sixb2809@gmail.com

1 Chemistry Department, University of Zululand, KwaDlangezwa, South Africa

2 Chemistry Department, University of Dar es Salaam, Dar es Salaam, Tanzania

## References

- [1] Vance ME, Kuiken T, Vejerano EP, McGinnis SP, Hochella MF Jr, Rejeski D, Hull MS. Nanotechnology in the real world: Redeveloping the nanomaterial consumer products inventory. *Beilstein Journal of Nanotechnology*. 2015;**6**:1769
- [2] Kumar S, Nann T. Shape control of II–VI semiconductor nanomaterials. *Small*. 2006;**2**(3):316-329
- [3] Tian L, Yao Tan H, Vittal JJ. Morphology-controlled synthesis of Bi<sub>2</sub>S<sub>3</sub> nanomaterials via single-and multiple-source approaches. *Crystal Growth and Design*. 2007;**8**(2):734-738
- [4] Wooten AJ, Werder DJ, Williams DJ, Casson JL, Hollingsworth JA. Solution-liquid-solid growth of ternary Cu-In-Se semiconductor nanowires from multiple- and single-source precursors. *Journal of the American Chemical Society*. 2009;**131**(44):16177-16188
- [5] Green M. The nature of quantum dot capping ligands. *Journal of Materials Chemistry*. 2010;**20**(28):5797-5809
- [6] Garnweitner G, Niederberger M. Organic chemistry in inorganic nanomaterials synthesis. *Journal of Materials Chemistry*. 2008;**18**(11):1171-1182
- [7] Al-Salim N, Young AG, Tilley RD, McQuillan AJ, Xia J. Synthesis of CdSe nanocrystals in coordinating and noncoordinating solvents: Solvent's role in evolution of the optical and structural properties. *Chemistry of Materials*. 2007;**19**(21):5185-5193
- [8] Buzea C, Pacheco I, Robbie K. Biointerphases 2. *MR17*. 2017;**2**(4):17-71
- [9] Slater CS, Savelski M. A method to characterize the greenness of solvents used in pharmaceutical manufacture. *Journal of Environmental Science and Health Part A*. 2007;**42**(11):1595-1605
- [10] Rundquist EM, Pink CJ, Livingston AG. Organic solvent nanofiltration: A potential alternative to distillation for solvent recovery from crystallisation mother liquors. *Green Chemistry*. 2012;**14**(8):2197-2205
- [11] Ghandi K. A review of ionic liquids, their limits and applications. *Green and Sustainable Chemistry*. 2014;**4**(1):44-53



- [12] Seddon KR. Ionic liquids for clean technology. *Journal of Chemical Technology and Biotechnology*. 1997;**68**(4):351-356
- [13] Earle MJ, Esperança JM, Gilea MA, Lopes JNC, Rebelo LP, Magee JW, Seddon KR, Widegren JA. The distillation and volatility of ionic liquids. *Nature*. 2006;**439**(7078):831-834
- [14] Ye C, Liu W, Chen Y, Yu L. Room-temperature ionic liquids: A novel versatile lubricant. *Chemical Communications*. 2001;**21**:2244-2245
- [15] He Z, Alexandridis P. Nanoparticles in ionic liquids: Interactions and organization. *Physical Chemistry Chemical Physics*. 2015;**17**(28):18238-18261
- [16] Noda A, Hayamizu K, Watanabe M. Pulsed-gradient spin-echo <sup>1</sup>H and <sup>19</sup>F NMR ionic diffusion coefficient, viscosity, and ionic conductivity of non-chloroaluminate room-temperature ionic liquids. *The Journal of Physical Chemistry B*. 2001;**105**(20):4603-4610
- [17] Freire MG, Neves CM, Marrucho IM, Coutinho JA, Fernandes AM. Hydrolysis of tetrafluoroborate and hexafluorophosphate counter ions in imidazolium-based ionic liquids. *The Journal of Physical Chemistry A*. 2009;**114**(11):3744-3749
- [18] Gao H, Luo M, Xing J, Wu Y, Li Y, Li W, Liu Q, Liu H. Desulfurization of fuel by extraction with pyridinium-based ionic liquids. *Industrial & Engineering Chemistry Research*. 2008;**47**(21):8384-8388. DOI: 10.1021/ie800739w
- [19] Kogelnig D, Stojanovic A, Galanski M, Groessl M, Jirsa F, Krachler R, Keppler BK. Greener synthesis of new ammonium ionic liquids and their potential as extracting agents. *Tetrahedron Letters*. 2008;**49**(17):2782-2785
- [20] Pont A-L, Marcilla R, De Meazza I, Grande H, Mecerreyes D. Pyrrolidinium-based polymeric ionic liquids as mechanically and electrochemically stable polymer electrolytes. *Journal of Power Sources*. 2009;**188**(2):558-563
- [21] Paduszyński K, Domańska U. Experimental and theoretical study on infinite dilution activity coefficients of various solutes in piperidinium ionic liquids. *The Journal of Chemical Thermodynamics*. 2013;**60**:169-178
- [22] Breitbach ZS, Armstrong DW. Characterization of phosphonium ionic liquids through a linear solvation energy relationship and their use as GLC stationary phases. *Analytical and Bioanalytical Chemistry*. 2008;**390**(6):1605-1617
- [23] Qian W, Texter J, Yan F. Frontiers in poly (ionic liquid)s: Syntheses and applications. *Chemical Society Reviews*. 2017;**46**(4):1124-1159
- [24] Rojas MF, Bernard FL, Aquino A, Borges J, Dalla Vecchia F, Menezes S, Ligabue R, Einloft S. Poly (ionic liquid) s as efficient catalyst in transformation of CO<sub>2</sub> to cyclic carbonate. *Journal of Molecular Catalysis A: Chemical*. 2014;**392**:83-88
- [25] Hallett JP, Welton T. Room-temperature ionic liquids: Solvents for synthesis and catalysis. 2. *Chemical Reviews*. 2011;**111**(5):3508-3576

- [26] Bara JE, Carlisle TK, Gabriel CJ, Camper D, Finotello A, Gin DL, Noble RD. Guide to CO<sub>2</sub> separations in imidazolium-based room-temperature ionic liquids. *Industrial & Engineering Chemistry Research*. 2009;**48**(6):2739-2751
- [27] Lei Z, Dai C, Yang Q, Zhu J, Chen B. UNIFAC model for ionic liquid-CO (H<sub>2</sub>) systems: An experimental and modeling study on gas solubility. *AIChE Journal*. 2014;**60**(12):4222-4231
- [28] Gurkan BE, de la Fuente JC, Mindrup EM, Ficke LE, Goodrich BF, Price EA, Schneider WF, Brennecke JF. Equimolar CO<sub>2</sub> absorption by anion-functionalized ionic liquids. *Journal of the American Chemical Society*. 2010;**132**(7):2116-2117
- [29] Ruckart KN, O'Brien RA, Woodard SM, West KN, Glover TG. Porous solids impregnated with task-specific ionic liquids as composite sorbents. *The Journal of Physical Chemistry C*. 2015;**119**(35):20681-20697
- [30] Wickramanayake S, Hopkinson D, Myers C, Hong L, Feng J, Seol Y, Plasynski D, Zeh M, Luebke D. Mechanically robust hollow fiber supported ionic liquid membranes for CO<sub>2</sub> separation applications. *Journal of Membrane Science*. 2014;**470**:52-59
- [31] Scovazzo P, Havard D, McShea M, Mixon S, Morgan D. Long-term, continuous mixed-gas dry fed CO<sub>2</sub>/CH<sub>4</sub> and CO<sub>2</sub>/N<sub>2</sub> separation performance and selectivities for room temperature ionic liquid membranes. *Journal of Membrane Science*. 2009;**327**(1-2):41-48
- [32] Khan NA, Hasan Z, Jhung SH. Ionic liquids supported on metal-organic frameworks: Remarkable adsorbents for adsorptive desulfurization. *Chemistry-A European Journal*. 2014;**20**(2):376-380
- [33] Vicent-Luna JM, Gutiérrez-Sevillano JJ, Anta JA, Calero S. Effect of room-temperature ionic liquids on CO<sub>2</sub> separation by a Cu-BTC metal-organic framework. *The Journal of Physical Chemistry C*. 2013;**117**(40):20762-20768
- [34] Li Z, Jia Z, Luan Y, Mu T. Ionic liquids for synthesis of inorganic nanomaterials. *Current Opinion in Solid State and Materials Science*. 2008;**12**(1):1-8
- [35] Sheldon R. Catalytic reactions in ionic liquids. *Chemical Communications*. 2001;**23**:2399-2407
- [36] Huddleston JG, Willauer HD, Swatoski RP, Visser AE, Rogers RD. Room temperature ionic liquids as novel media for 'clean' liquid-liquid extraction. *Chemical Communications*. 1998;**16**:1765-1766
- [37] Enders Dickinson V, Williams ME, Hendrickson SM, Masui H, Murray RW. Hybrid redox polyether melts based on polyether-tailed counterions. *Journal of the American Chemical Society*. 1999;**121**(4):613-616
- [38] Kubisa P. Application of ionic liquids as solvents for polymerization processes. *Progress in Polymer Science*. 2004;**29**(1):3-12
- [39] Ngo HL, LeCompte K, Hargens L, McEwen AB. Thermal properties of imidazolium ionic liquids. *Thermochimica Acta*. 2000;**357**:97-102

- [40] Bradley A, Hardacre C, Holbrey J, Johnston S, McMath S, Nieuwenhuyzen M. Small-angle X-ray scattering studies of liquid crystalline 1-alkyl-3-methylimidazolium salts. *Chemistry of Materials*. 2002;**14**(2):629-635
- [41] Varma R. Solvent-free organic syntheses. Using supported reagents and microwave irradiation. *Green Chemistry*. 1999;**1**(1):43-55
- [42] Davoodnia A, Heravi MM, Safavi-Rad Z, Tavakoli-Hoseini N. Green, one-pot, solvent-free synthesis of 1, 2, 4, 5-tetrasubstituted imidazoles using a Brønsted acidic ionic liquid as novel and reusable catalyst. *Synthetic Communications*. 2010;**40**(17):2588-2597
- [43] Endres F, El Abedin SZ. Air and water stable ionic liquids in physical chemistry. *Physical Chemistry Chemical Physics*. 2006;**8**(18):2101-2116
- [44] Bonhôte P, Dias A-P, Papageorgiou N, Kalyanasundaram K, Grätzel M. Hydrophobic, highly conductive ambient-temperature molten salts. *Inorganic Chemistry*. 1996;**35**(5):1168-1178
- [45] Carda-Broch S, Berthod A, Armstrong D. Solvent properties of the 1-butyl-3-methylimidazolium hexafluorophosphate ionic liquid. *Analytical and Bioanalytical Chemistry*. 2003;**375**(2):191-199
- [46] Seddon KR, Stark A, Torres M-J. Influence of chloride, water, and organic solvents on the physical properties of ionic liquids. *Pure and Applied Chemistry*. 2000;**72**(12):2275-2287
- [47] Susan MA, Noda A, Mitsushima S, Watanabe M. Brønsted acid-base ionic liquids and their use as new materials for anhydrous proton conductors. *Chemical Communications*. 2003;**8**:938-939
- [48] Greaves TL, Weerawardena A, Fong C, Krodziewska I, Drummond CJ. Protic ionic liquids: Solvents with tunable phase behavior and physicochemical properties. *The Journal of Physical Chemistry B*. 2006;**110**(45):22479-22487
- [49] Mehrkesh A, Karunanithi A. Predicting Melting point and Viscosity of Ionic Liquids Using New Quantum Chemistry Descriptors. arXiv preprint arXiv:161200879. 2016
- [50] Cole AC, Jensen JL, Ntai I, Tran KLT, Weaver KJ, Forbes DC, Davis JH. Novel Brønsted acidic ionic liquids and their use as dual solvent-catalysts. *Journal of the American Chemical Society*. 2002;**124**(21):5962-5963
- [51] Marsh K, Boxall J, Lichtenthaler R. Room temperature ionic liquids and their mixtures—A review. *Fluid Phase Equilibria*. 2004;**219**(1):93-98
- [52] Tanaka K. In: Wasserscheid P, Welton T, editors. *Ionic Liquids in Synthesis*. Weinheim: Wiley-VCH; 2003. Wiley-VCH W. Search PubMed
- [53] Huddleston JG, Visser AE, Reichert WM, Willauer HD, Broker GA, Rogers RD. Characterization and comparison of hydrophilic and hydrophobic room temperature ionic liquids incorporating the imidazolium cation. *Green Chemistry*. 2001;**3**(4):156-164

- [54] Schröder U, Wadhawan JD, Compton RG, Marken F, Suarez PA, Consorti CS, de Souza RF, Dupont J. Water-induced accelerated ion diffusion: Voltammetric studies in 1-methyl-3-[2,6-(S)-dimethylocten-2-yl] imidazolium tetrafluoroborate, 1-butyl-3-methylimidazolium tetrafluoroborate and hexafluorophosphate ionic liquids. *New Journal of Chemistry*. 2000;**24**(12):1009-1015
- [55] MacFarlane D, Meakin P, Sun J, Amini N, Forsyth M. Pyrrolidinium imides: A new family of molten salts and conductive plastic crystal phases. *The Journal of Physical Chemistry B*. 1999;**103**(20):4164-4170
- [56] Greaves TL, Drummond CJ. Protic ionic liquids: Properties and applications. *Chemical reviews*. 2008;**108**(1):206-237
- [57] Nazari S, Cameron S, Johnson MB, Ghandi K. Physicochemical properties of imidazopyridine protic ionic liquids. *Journal of Materials Chemistry A*. 2013;**1**(38):11570-11579
- [58] Irge DD. Ionic liquids: A review on greener chemistry applications, quality ionic liquid synthesis and economical viability in a chemical processes. *American Journal of Physical Chemistry*. 2016;**5**:74-79
- [59] Duan X, Ma J, Lian J, Zheng W. The art of using ionic liquids in the synthesis of inorganic nanomaterials. *CrystEngComm*. 2014;**16**(13):2550-2559
- [60] Kwon SG, Hyeon T. Formation mechanisms of uniform nanocrystals via hot-injection and heat-up methods. *Small*. 2011;**7**(19):2685-2702
- [61] Cooper ER, Andrews CD, Wheatley PS, Webb PB, Wormald P, Morris RE. Ionic liquids and eutectic mixtures as solvent and template in synthesis of zeolite analogues. *Nature*. 2004;**430**(7003):1012
- [62] Taubert A. CuCl Nanoplatelets from an ionic liquid-crystal precursor. *Angewandte Chemie*. 2004;**116**(40):5494-5496
- [63] Antonietti M, Kuang D, Smarsly B, Zhou Y. Ionic liquids for the convenient synthesis of functional nanoparticles and other inorganic nanostructures. *Angewandte Chemie International Edition*. 2004;**43**(38):4988-4992
- [64] Taubert A. Inorganic materials synthesis-a bright future for ionic liquids? *Acta Chimica Slovenica*. 2005;**52**(3):183
- [65] Manojkumar K, Sivaramakrishna A, Vijayakrishna K. A short review on stable metal nanoparticles using ionic liquids, supported ionic liquids, and poly (ionic liquids). *Journal of Nanoparticle Research*. 2016;**18**(4):1-22
- [66] Roucoux A, Schulz J, Patin H. Reduced transition metal colloids: A novel family of reusable catalysts? *Chemical Reviews*. 2002;**102**(10):3757-3778
- [67] Sajjadi H, Modaressi A, Magri P, Domańska U, Sindt M, Mieloszynski J-L, Mutelet F, Rogalski M. Aggregation of nanoparticles in aqueous solutions of ionic liquids. *Journal of Molecular Liquids*. 2013;**186**:1-6

- [68] Biswas K, Rao CeNeR. Use of ionic liquids in the synthesis of nanocrystals and nanorods of semiconducting metal chalcogenides. *Chemistry—A European Journal*. 2007;**13**(21):6123-6129
- [69] Zhao X-L, Wang C-X, Hao X-P, Yang J-X, Wu Y-Z, Tian Y-P, Tao X-T, Jiang M-H. Synthesis of PbS nanocubes using an ionic liquid as the solvent. *Materials Letters*. 2007;**61**(26):4791-4793
- [70] Tshemese Z, Mlowe S, Revaprasadu N, Deenadayalu N. Synthesis of CdS quantum dots in an imidazolium based ionic liquid. *Materials Science in Semiconductor Processing*. 2017;**71**:258-262
- [71] Migowski P, Machado G, Texeira SR, Alves MC, Morais J, Traverse A, Dupont J. Synthesis and characterization of nickel nanoparticles dispersed in imidazolium ionic liquids. *Physical Chemistry Chemical Physics*. 2007;**9**(34):4814-4821
- [72] Redel E, Walter M, Thomann R, Vollmer C, Hussein L, Scherer H, Krüger M, Janiak C. Synthesis, stabilization, functionalization and, DFT calculations of gold nanoparticles in fluoruous phases (PTFE and ionic liquids). *Chemistry-A European Journal*. 2009;**15**(39):10047-10059
- [73] Fonseca GS, Machado G, Teixeira SR, Fecher GH, Morais J, Alves MC, Dupont J. Synthesis and characterization of catalytic iridium nanoparticles in imidazolium ionic liquids. *Journal of Colloid and Interface Science*. 2006;**301**(1):193-204
- [74] Wang Y, Yang H. Oleic acid as the capping agent in the synthesis of noble metal nanoparticles in imidazolium-based ionic liquids. *Chemical Communications*. 2006;**24**:2545-2547
- [75] Salas G, Santini CC, Philippot K, Collière V, Chaudret B, Fenet B, Fazzini PF. Influence of amines on the size control of in situ synthesized ruthenium nanoparticles in imidazolium ionic liquids. *Dalton Transactions*. 2011;**40**(17):4660-4668
- [76] Duan X, Kim T, Li D, Ma J, Zheng W. Understanding the effect models of ionic liquids in the synthesis of NH<sub>4</sub>-Dw and  $\gamma$ -AlOOH nanostructures and their conversion into porous  $\gamma$ -Al<sub>2</sub>O<sub>3</sub>. *Chemistry-A European Journal*. 2013;**19**(19):5924-5937
- [77] Duan X, Li D, Zhang H, Ma J, Zheng W. Crystal-facet engineering of ferric Giniite by using ionic-liquid precursors and their enhanced Photocatalytic performances under visible-light irradiation. *Chemistry-A European Journal*. 2013;**19**(22):7231-7242
- [78] Ding K, Miao Z, Liu Z, Zhang Z, Han B, An G, Miao S, Xie Y. Facile synthesis of high quality TiO<sub>2</sub> nanocrystals in ionic liquid via a microwave-assisted process. *Journal of the American Chemical Society*. 2007;**129**(20):6362-6363
- [79] Zheng W, Liu X, Yan Z, Zhu L. Ionic liquid-assisted synthesis of large-scale TiO<sub>2</sub> nanoparticles with controllable phase by hydrolysis of TiCl<sub>4</sub>. *ACS Nano*. 2008;**3**(1):115-122
- [80] Liu X, Ma J, Zheng W. Applications of ionic liquids (ILs) in the convenient synthesis of nanomaterials. *Reviews on Advanced Materials Science*. 2011;**27**:43-51

- [81] Alavi-Tabari SA, Khalilzadeh MA, Karimi-Maleh H. Simultaneous determination of doxorubicin and dasatinib as two breast anticancer drugs uses an amplified sensor with ionic liquid and ZnO nanoparticle. *Journal of Electroanalytical Chemistry*. 2018;**811**:84-88
- [82] Husanu E, Chiappe C, Bernardini A, Cappello V, Gemmi M. Synthesis of colloidal Ag nanoparticles with citrate based ionic liquids as reducing and capping agents. *Colloids and Surfaces A: Physicochemical and Engineering Aspects*. 2018;**538**:506-512
- [83] Shang W, Cai T, Zhang Y, Liu D, Sun L, Su X, Liu S. Covalent grafting of chelated orthoborate ionic liquid on carbon quantum dot towards high performance additives: Synthesis, characterization and tribological evaluation. *Tribology International*. 2018;**121**:302-309
- [84] Saien J, Hashemi S. Long chain imidazolium ionic liquid and magnetite nanoparticle interactions at the oil/water interface. *Journal of Petroleum Science and Engineering*. 2018;**160**:363-371
- [85] Okoli CU, Kuttiyiel KA, Cole J, McCutchen J, Tawfik H, Adzic RR, Mahajan D. Solvent effect in sonochemical synthesis of metal-alloy nanoparticles for use as electrocatalysts. *Ultrasonics Sonochemistry*. 2018;**41**:427-434
- [86] Sotolongo AC, Martinis EM, Wuilloud RG. An easily prepared graphene oxide-ionic liquid hybrid nanomaterial for micro-solid phase extraction and preconcentration of Hg in water samples. *Analytical Methods*; 2018;**10**:338-346
- [87] Lu J, Yang J-X, Wang J, Lim A, Wang S, Loh KP. One-pot synthesis of fluorescent carbon nanoribbons, nanoparticles, and graphene by the exfoliation of graphite in ionic liquids. *ACS Nano*. 2009;**3**(8):2367-2375
- [88] Wang B, Song A, Feng L, Ruan H, Li H, Dong S, Hao J. Tunable amphiphilicity and multifunctional applications of ionic-liquid-modified carbon quantum dots. *ACS Applied Materials & Interfaces*. 2015;**7**(12):6919-6925
- [89] Tan Y, Li M, Ye X, Wang Z, Wang Y, Li C. Ionic liquid auxiliary exfoliation of WS<sub>2</sub> nanosheets and the enhanced effect of hollow gold nanospheres on their photoelectrochemical sensing towards human epididymis protein 4. *Sensors and Actuators B: Chemical*. 2018;**262**:982-990
- [90] Prechtel MH, Campbell PS, Scholten JD, Fraser GB, Machado G, Santini CC, Dupont J, Chauvin Y. Imidazolium ionic liquids as promoters and stabilising agents for the preparation of metal (0) nanoparticles by reduction and decomposition of organometallic complexes. *Nanoscale*. 2010;**2**(12):2601-2606
- [91] Kohler N, Sun C, Wang J, Zhang M. Methotrexate-modified superparamagnetic nanoparticles and their intracellular uptake into human cancer cells. *Langmuir*. 2005;**21**(19):8858-8864
- [92] Bertorelle F, Wilhelm C, Roger J, Gazeau F, Ménager C, Cabuil V. Fluorescence-modified superparamagnetic nanoparticles: Intracellular uptake and use in cellular imaging. *Langmuir*. 2006;**22**(12):5385-5391

- [93] Shenhar R, Norsten TB, Rotello VM. Polymer-mediated nanoparticle assembly: Structural control and applications. *Advanced Materials*. 2005;**17**(6):657-669
- [94] Mohan B, Woo H, Jang S, Lee S, Park S, Park KH. Synthesis of monodisperse Cu nanoparticles in ionic liquids: A synthetic and catalytic approach of in situ nanoparticles. *Solid State Sciences*. 2013;**22**:16-20
- [95] Kim K-S, Demberelnyamba D, Lee H. Size-selective synthesis of gold and platinum nanoparticles using novel thiol-functionalized ionic liquids. *Langmuir*. 2004;**20**(3):556-560
- [96] Gracia R, Vijayakrishna K, Mecerreyes D. Poly (ionic liquid)s with redox active counter-anions: All-in-one reactants and stabilizers for the synthesis of functional colloids. *Reactive and Functional Polymers*. 2014;**79**:54-58
- [97] Vijayakrishna K, Charan K, Manojkumar K, Venkatesh S, Pothanagandhi N, Sivaramakrishna A, Mayuri P, Kumar AS, Sreedhar B. Ni nanoparticles stabilized by poly (ionic liquids) as chemoselective and magnetically recoverable catalysts for transfer hydrogenation reactions of carbonyl compounds. *ChemCatChem*. 2016;**8**(6):1139-1145
- [98] Tshemese Z, Khan MD, Mlowe S, Revaprasadu N. Synthesis and characterization of PbS nanoparticles in an ionic liquid using single and dual source precursors. *Materials Science and Engineering: B*. 2018;**227**:116-121





---

## State of the Art Polymerization

---



---

# Ionic Polymerization in Ionic Liquids

---

Yibo Wu

Additional information is available at the end of the chapter

<http://dx.doi.org/10.5772/intechopen.77183>

---

## Abstract

Ionic liquids have emerged as a new class of solvents for ionic polymerization due to their low volatility, chemical stability, high conductivity, wide electrochemical window. The advantages and limitations of application of ionic liquids as solvents for ionic polymerization processes are critically discussed in this chapter. The field of cationic polymerization in ionic liquid has undergone rapid growth in recent years. The most important types of cationic monomers, such as styrene and its derivatives, vinyl ethers and isobutylene have been polymerized in ionic liquids; even undergo living polymerization. Corresponding elementary reactions of cationic polymerization in ionic liquids were proposed. Methyl methacrylate and styrene can undergo anionic polymerization in ionic liquids. However, ionic liquids seem unsuitable solvents for anionic polymerization.

**Keywords:** ionic liquid, cationic polymerization, anionic polymerization, elementary reactions, ionic environment

---

## 1. Introduction

Ionic liquids are organic salts, and their physical and chemical properties can be fine-tuned by selection of the cation and anion. The most significant properties of ionic liquids are their negligible vapor pressure. So, ionic liquids have been recognized as green solvents alternative to volatile organic solvents. Application of ionic liquids in chemical processes has blossomed within the last decade. Although radical polymerization, electrochemical polymerization, and polycondensation in ionic liquids have been investigated by many researchers, there has been little study on the application of ionic liquids in ionic polymerization. Ionic liquids are regarded as highly polar but non-coordinating solvents, enabling them as ideal solvents for ionic polymerization.

Ionic polymerization is referred to as a classic cationic when the active terminal group is positively charged, or as a pseudocationic if this group forms the positive end of active dipole. By the same token we refer to ionic polymerization as a classic anionic when the charge of the active group is negative, or as a pseudoanionic when the active group forms the negative end of an active dipole. Whenever electrically charged end-groups are formed, suitable counterions have to be present in the polymerizing system to ensure its electric neutrality. So, the counterions chaperon the growing active to form ion-pairs during the initiation and propagation reaction. These ion-pairs usually exist in three thermodynamically distinct forms, which are referred to as tight ion-pairs, loose ion-pairs and free ion-pairs, and plays an important role for determination of polymerization characteristic. For example, in cationic polymerization, if this counterion is too nucleophilic, it will attack the carbenium ion to form a covalently bond, which in principle does not initiate to cationic monomers. So, the ion environment of ionic liquid must affect balance of ion pairs owing to the high polarity and high charge density, and then influence polymerization process.

Moreover, properties of ionic liquids such as melting point, polarity, viscosity, and solubility of monomers, which can be fine-tuned by the adequate selection of the cation and anion constituents, also significantly affect the feasibility and regularity of ionic polymerization. High polarity of ionic liquid contributes to stabilize the cationic active center, but it also exhibits the low solubility for cationic monomers. Thus, desirable ionic liquids hope to achieve polar and non-polar balance scale, which can provide a moderately polar environment to solubilize cationic monomers and a polar environment to stabilize carbocation. In this chapter, the mechanism of polymerization, advantages and limitations of application of ionic liquids as solvents for ionic polymerization processes are critically discussed.

## 2. Cationic polymerization in ionic liquids

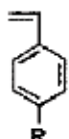
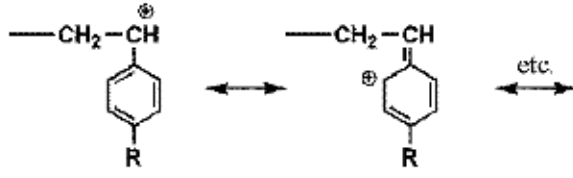
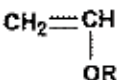
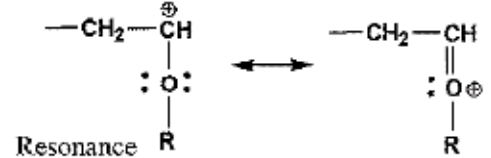
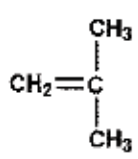
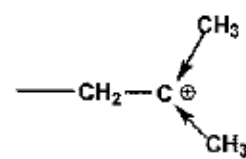
Cationic polymerization is an important technique to produce (co)polymers with predictable molecular weight and monomer sequence. Especially, living/controlled cationic polymerization represents an attractive technique for the synthesis of well-defined polymers, such as telechelic, star polymer, graft copolymer, etc. Industrialization products, such as bromide functionalized poly(isobutylene-*co-p*-methylstyrene) random copolymer, butyl rubber and poly(styrene-*b*-isobutylene-*b*-styrene) thermoplastic elastomer, play an important role in the tire industry, coronary stent, chewing gum and other fields. However, during the preparation of these products by traditional cationic polymerization, halogenated alkane (e.g., methyl chloride) usually used as solvents and cause environmental pollution due to its toxicity, volatile and corrosively. So it should be replaced by green solvents. In addition, various Lewis acids (e.g.,  $\text{BF}_3$ ,  $\text{SnCl}_4$ ,  $\text{TiCl}_4$ ,  $\text{AlCl}_3\text{O}i\text{Bu}_2$ , and  $\text{AlCl}_3$ ) were used as coinitiator in cationic polymerization. It is difficult to separate these Lewis acid catalysts from the reaction products, and reuse/disposal of these catalysts is also a big challenge to industry.

Ionic liquid is regarded as the ideal medium of cationic polymerization, which can be recycled and no pollution to the environment. So, applications of ionic liquids in cationic

polymerizations have great theoretical and practical significance for the development of environment-friendly and low-energy consumption. The most important monomers polymerizing through cationic mechanism are styrene and its derivatives, vinyl ethers and isobutylene (IB). The commonness of these cationic monomers is that the active species can be stabilized by the substituents on the olefinic group. And the way of stabilization of the corresponding carbocation are shown in **Table 1** [1]. We discuss cationic polymerization of these monomers in ionic liquids respectively in following sections.

## 2.1. Styrene and its derivatives

Styrene is a well-known, commercially available vinyl monomer that undergoes polymerization via cationic as well as radical, anionic, and coordination pathways. More recently, developed air- and water-stable neutral ionic liquids (for instance, 1-butyl-3-methylimidazoliumhexafluorophosphate ([BMIM][PF<sub>6</sub>]) [2–4] and trihexyltetradecylphosphonium bis(trifluoromethanesulfonyl)amide ([P<sub>6,6,6,14</sub>][NTf<sub>2</sub>])) [5] have been applied in cationic polymerization. Moreover, cationic polymerization of styrene in N-butyl-N-methylpyrrolidiniumbis-(trifluoromethanesulfonyl)amide ([P<sub>14</sub>][NTf<sub>2</sub>]) [6] ionic liquid with organoborate acids as initiators indicates some living/controlled characteristics.

Monomer	Carbenium ion stabilization
 Styrenics	 Resonance
 Vinyl ether	 Resonance
 Isobutylene	 Inductive effect

**Table 1.** Cationic monomers and stabilization of the corresponding active species.

In the traditional cationic polymerization of styrene, the lack of strongly electron-donating groups renders the growing carbocation unstable and thus results in side reactions, such as chain transfer accompanied by  $\beta$  proton elimination and Friedel–Crafts alkylation on the phenyl ring of the monomer unit. However, the polymerization mechanism of styrene and its derivatives cationic polymerizations in ionic liquids is still vague.

Usually, the low solubilities of the monomers in ionic liquids impede the efficiency of these polymerization reactions. In order to search for suitable ionic liquids for styrene and its derivatives, we firstly screened and selected target ionic liquids by quantum chemically based computations (the COSMO-RS method) [7]. The COSMO-RS method was successfully used to screen potential ionic liquids as solvents with respect to the solubility of *p*-methylstyrene used in cationic polymerization (Figure 1). We also have demonstrated that COSMO-RS is a valuable tool for the preliminary screening of solvents for cationic monomers without the need for extensive experimental data. The guiding principle of the selection of suitable ionic liquids for use in cationic polymerization was obtained from COSMO-RS calculations. The monomer solubilities in ionic liquids are highly dependent on physical and chemical properties which determine by anion and cation in ionic liquid. Larger nonpolar regions of the cation or anion in ionic liquids result in higher monomer solubility for cationic monomers, for example, longer alkyl chains of the cation or anion contributes to higher *p*-methylstyrene solubilities in imidazolium-based ionic liquids.

It is instructive to compare the organic solvents and ionic liquids in cationic polymerizations. So, we comprehensively compared the cationic polymerizations of styrene [8] and *p*-methylstyrene [9] in ionic liquids with those in organic solvents employing a series of

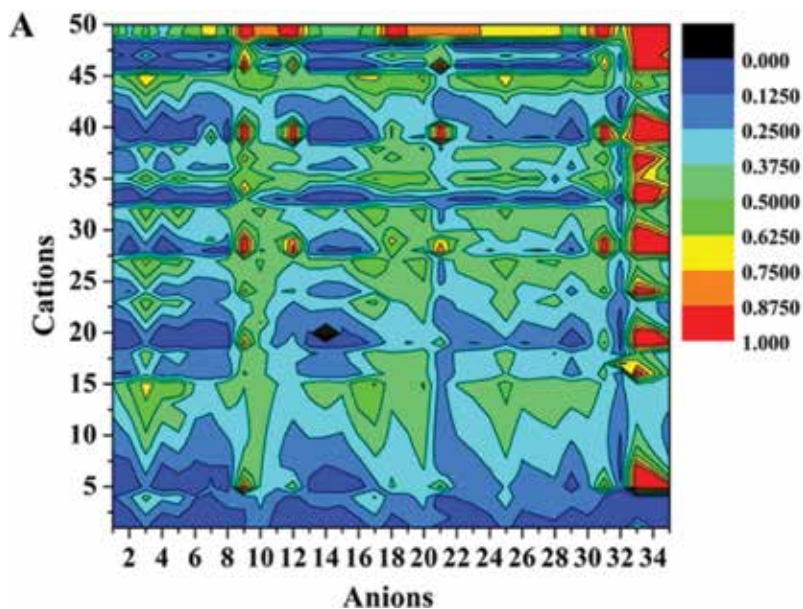


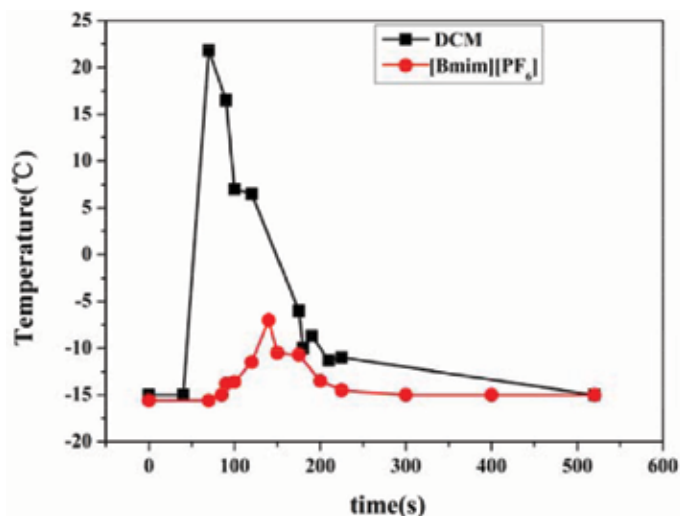
Figure 1. Predicted solubilities of *p*-methylstyrene in 1750 types (50 cations  $\times$  35 anions) of ionic liquids.

initiating systems. Considering that the effect of polymerization by the initiator, styrene cationic polymerization initiated by water exhibited lower yield and lower  $M_n$  compared with *a,a*-dimethylbenzyl chloride and 2-chloro-2,4,4-trimethylpentane. It was speculated that the low initiating efficiency might occur by the formation of hydrogen bonding for water in the imidazole-based ionic liquid. Water is more likely to initiate cationic polymerization in organic solvents.

The polymerization rate of styrene and *p*-methylstyrene in ionic liquids rely mainly on solvent polarity and viscosity. We found that initial polymerization rate of styrene in ionic liquid was similar to that in dichloromethane which resulting from interactions between viscosity and polarity factors of ionic liquids. The [bmim][PF<sub>6</sub>] ionic liquid had a considerably higher normalized solvent polarity  $E_N^T$  as compared to dichloromethane. On the one hand, the high the polarity of solvent give rise to the faster the reaction rate in cationic polymerization; on the other hand, the high viscosity of ionic liquid reduces the monomer diffusion and thus slow down the rate of polymerization. So, the polymerization rate in ionic liquids was similar to that in dichloromethane, which was a consequence of viscosity and polarity of ionic liquid.

Styrene and *p*-methylstyrene cationic polymerizations proceeded in a milder exothermic manner in ionic liquids than in traditional organic solvents. The milder reactions in ionic liquid may be due to the relatively higher heat capacity of the ionic liquid. The relatively higher heat capacity of ionic liquid could absorb more heat during the cationic polymerization.

On basis of terminal structure and kinetics of polymerization, we proposed the corresponding elementary reactions of styrene and *p*-methylstyrene cationic polymerization in ionic liquids, as shown in **Figures 1** and **2**, respectively.

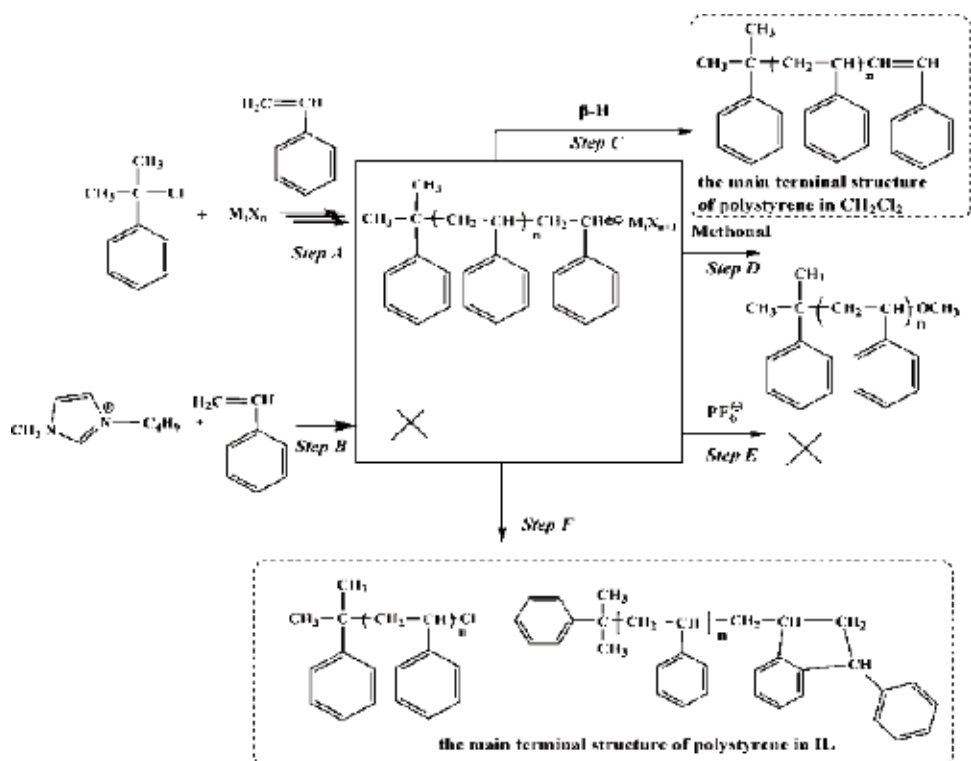


**Figure 2.** Temperature changes vs. time plots for cationic polymerization of styrene with CumCl/Lewis acid initiating system in ionic liquid and dichloromethane at  $-15^{\circ}\text{C}$  operating temperature, (black square) dichloromethane, (red circle) [Bmim][PF<sub>6</sub>].

In initiation reactions, ion-pairs of carbocation and counterion were first formed by complexation reactions between coinitiator Lewis acid and initiator. Comparing with cation of ionic liquid, the carbocation in ion-pairs was easier to attack the styrene or *p*-methylstyrene to initiate cationic polymerization. Also, because of anion of ionic liquid was very weakly nucleophilic species, the counterion of ion-pairs was more closely to carbocation and made them approachable to interact with growing active center. Therefore, we assumed that at least one portion of chain termination reactions directly took place toward counterion rather than anion of ionic liquid. So, the anions or cations of the ionic liquids did not participate in any elementary reactions in the whole cationic polymerization. Despite all this, the anion of ionic liquid could stabilize the propagating carbocation active by dispersing the charge of carbocation. But it was still insufficient to stabilize the propagating carbocation to achieve a controlled/living cationic polymerization.

The terminal structure of polystyrenes analyzed by  $^1\text{H-NMR}$  spectroscopy and MALDI-TOF spectra which clearly indicated that main chain termination reactions in ionic liquid directly took place toward halide-based counterion or toward Friedel-Crafts reaction, rather than  $\beta$ -hydrogen elimination reaction (**Figure 3**).

The sterical hindrance of counteranion influenced the insertion of monomer molecules into the propagating carbocation. Thus, the interaction between propagating carbocation and



**Figure 3.** Polymerization pathway of cationic polymerization of styrene with CumCl/Lewis acid in [bmim][PF<sub>6</sub>].

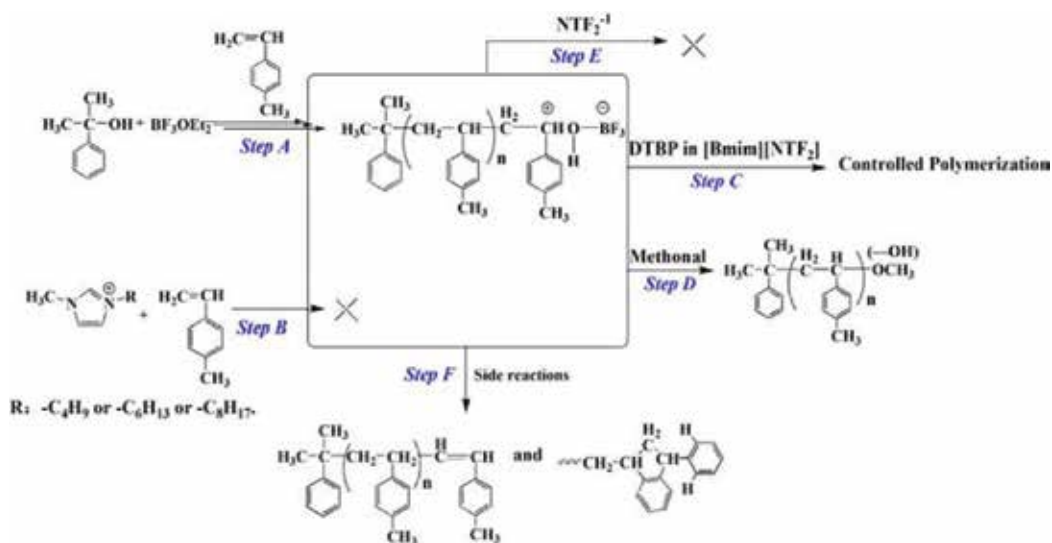


metal halide-based counterion was directly responsible for stereoregulation. Due to the existence interaction between growing carbocation with anion of ionic liquid, the interaction between the growing carbocation and counteranion become weaker. So, sterical hindrance of counteranion was reduced in ionic liquid which led to lower stereoregulation (**Figure 4**).

MacFarlane [5] has successfully demonstrated that the a controlled cationic polymerization of styrene has been achieved in  $[C_4m\text{pyr}][\text{NTf}_2]$  ionic liquid using bis(oxalato)boric acid (HBOB) as initiators. The hydrophobic nature of the  $[C_4m\text{pyr}][\text{NTf}_2]$  ionic liquid allowed relatively easy to achieve styrene cationic polymerization. The molecular weights of polystyrenes obtained in  $[C_4m\text{pyr}][\text{NTf}_2]$  ionic liquid increased with decreasing HBOB concentration with narrow polydispersity and were predominantly syndiotactic. In another study cationic polymerization of styrene initiated with  $\text{AlCl}_3$  in ionic liquid ( $[\text{bmim}][\text{PF}_6]$ ), supercritical  $\text{CO}_2$  and organic solvent ( $\text{CH}_2\text{Cl}_2$ ) was investigated [4]. The only conclusion was that polymerization rates and molecular weights were higher than in organic solvent.

## 2.2. Vinyl ethers

The cationic polymerization of vinyl ethers under “non-living “ conditions, has been known for many years and been used commercially [10]. These polymerizations are characterized by extremely high polymerization rates and the occurrence of chain transfer and termination reactions with the formation of different kinds of unsaturated end-groups. In additional, vinyl ethers are among the most reactive monomers in conventional (dry conditions) cationic polymerization, even more reactive than pMOS. So, chain transfer reaction is more likely to occur in vinyl ethers cationic polymerization. Low temperatures are usually employed in an attempt to reduce side reactions that destroy the propagating centers. In order to meet



**Figure 4.** Proposed mechanism for the cationic polymerization of *p*-methylstyrene with the CumOH/  $\text{BF}_3\text{OEt}_2$  initiating system in  $\text{NTf}_2^-$  based ionic liquids.

the requirements of low temperature for vinyl ethers cationic polymerizations, we mainly focused on the low-melting-point ionic liquids, such as [omim][BF<sub>4</sub>] ionic liquid.

In order to further understand the ion environment and its effect on cationic polymerization, we compared the characteristics of IBVE cationic polymerization in organic molecule medium. **Table 2** showed the data of IBVE polymerization in dichloromethane in the same condition as [omim][BF<sub>4</sub>]. Comparing with those obtained in ionic liquid, the yields of poly(IBVE)s obtained in organic molecule medium were lower (~30%). These indicated that IBVE cationic polymerizations were more likely to participate chain transfer and chain termination reactions in organic molecule medium. In addition, The  $M_n$  of poly(IBVE)s obtained in ionic liquid were much higher than that in organic molecule medium. The ionic liquid had a considerably higher normalized solvent polarity  $E_T^N$  as compared to organic molecule medium, such as dichloromethane. Usually, the higher the polarity of solvent gives in cationic polymerization, the higher the  $M_n$  of poly(IBVE) obtained.

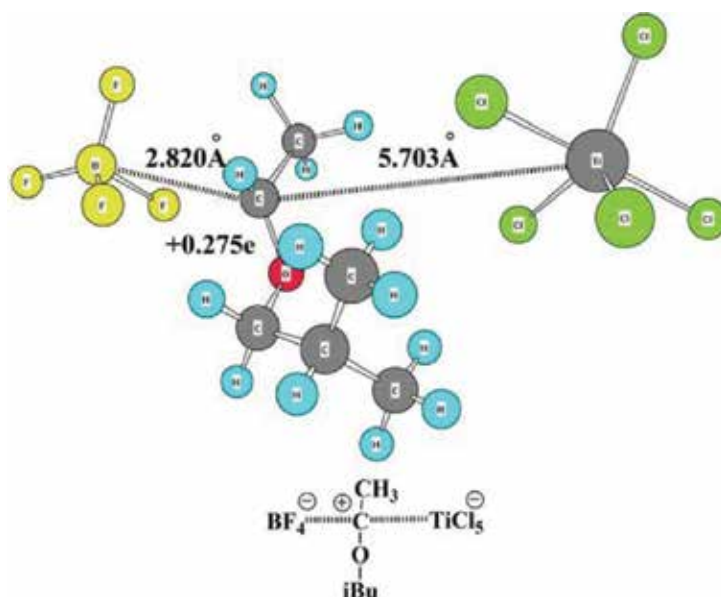
Like that of styrene, the cationic polymerization of IBVE in dichloromethane system proceeded in a highly exothermic manner. For example, in IBVE-HCl/TiCl<sub>4</sub> initiating system, the exothermic peak reached to 24°C. However, the exothermic peak in [omim][BF<sub>4</sub>] ionic liquid reached to 9°C with ~90% monomer conversion. The temperature rise and fall periods were slower than that in dichloromethane. IBVE cationic polymerization in ionic liquid proceed in mild exothermic reactions may be due to the relatively higher viscosity and higher heat capacity of the ionic liquids. The high viscosity could slow down the reaction rate; the relatively higher heat capacity could absorb more heat during the cationic polymerization.

From reaction kinetics analysis, we found that the first-order plots of  $\ln([M_0]/[M])$  vs. time were not linear for isobutyl vinyl ether (IBVE) cationic polymerization in [omim][BF<sub>4</sub>] ionic liquid. Analyzing from end microstructure, the side reactions took place by chain-breaking via predominant  $\beta$ -proton elimination from  $-\text{CH}_2-$  in the growing carbocation and then by protic reinitiation to create a new polymer chain, resulting in the formation of polymer chains with exo-olefin terminal group. Once 2,6-di-tert-butylpyridine was used;  $\beta$ -proton had been trapped. Thus, the polymerization in ionic liquid exhibited some characteristics of a living/controlled process (**Figure 5**).

Entry	Solvent	Coinitiator	Time (min)	Conv. (%)	Mn	Mw	Mw/Mn
1	Dichloromethane	Al <sub>2</sub> Et <sub>3</sub> Cl <sub>3</sub>	1.5	20	21,880	40,700	1.86
2	Dichloromethane	SnCl <sub>4</sub>	2.5	27	16,490	31,500	1.91
3	Dichloromethane	TiCl <sub>4</sub>	2.5	29	13,200	24,000	1.82
4	[omim][BF <sub>4</sub> ]	Al <sub>2</sub> Et <sub>3</sub> Cl <sub>3</sub>	10.0	82	38,010	65,380	1.72
5	[omim][BF <sub>4</sub> ]	SnCl <sub>4</sub>	15.0	76	21,070	38,140	1.81
6	[omim][BF <sub>4</sub> ]	TiCl <sub>4</sub>	15.0	83	18,140	36,600	2.02

Conditions: Initiator: [IBVE-HCl] = 0.003 M, [IBVE] = 1.04 M, the molar ratio of coinitiator to IBVE-HCl = 16, T = 0°C; Mn(theor) = 34,300 g/mol.

**Table 2.** Cationic polymerizations of IBVE using various coinitiators in ionic liquid and dichloromethane.



**Figure 5.** The optimized geometries of metal halide-based counterion, propagating carbocation and anion of ionic liquid.

The long-lived species were observed in monomer addition experiments. The [omim][BF<sub>4</sub>] ionic liquid did not participate elementary reactions during IBVE cationic polymerization. However, [omim][BF<sub>4</sub>] should affect not only the stability of active center but also the interaction between propagating carbocation and counterion. We want to understand what was the cause of production of the long-lived species. The density functional theory was used to study the interactions among propagating active center, counterion and ionic liquid.

According to the geometry, the propagating carbocations of the poly(IBVE)s in [omim][BF<sub>4</sub>] interacted with not only metal halide-based counterions, but also soft Lewis basic BF<sub>4</sub> anions. It was also noted that the charge on the propagating carbocation in ionic liquid was separated by its interaction with anion of ionic liquid leading to form relative stabilized propagating carbocation. However, these interactions were still insufficient to stabilize the propagating carbocation to achieving a controlled polymerization.

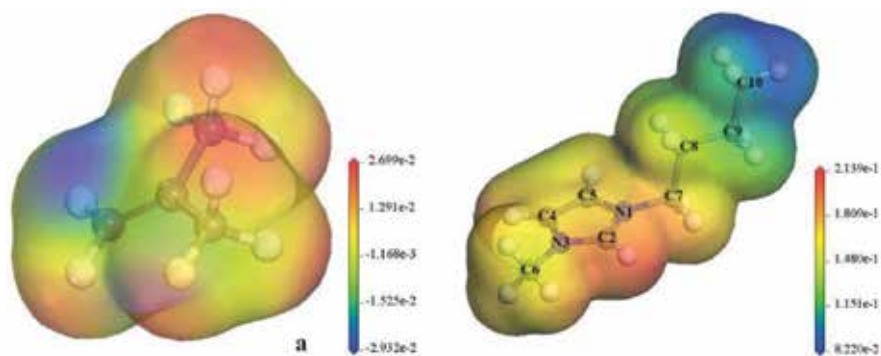
### 2.3. Isobutylene

Among cationic monomers, isobutylene is no doubt the most extensively studied one as it polymerizes only by cationic mechanism. In comparison with silicones or polyphosphazenes, polyisobutylene-based products exhibit such unique properties as chemical resistance, low permeability, good thermal and oxidative stability, mechanical dampening. The high- ( $M_n > 120,000$  g/mol), medium- ( $M_n = 40,000$ – $100,000$  g/mol) and, low-molecular weight ( $M_n < 5000$  g/mol) polyisobutylenes (PIB) have been achieved commercial success and were widely used in the world.

Low molecular weight polyisobutylene possessing an exo-olefin terminal group (so-called highly reactive polyisobutylene, HR PIB) is a key intermediate in the manufacturing of

motor oil and fuel additives, with worldwide production in excess of 750,000 tons per year. The cationic polymerizations of HR PIB in ionic liquids were described only in a patent literatures [11–14] and only limited information was available. The use of acidic chloroaluminate ionic liquids as catalysts for low molecular weight polyisobutylene ( $M_n = 1000$  g/mol) in n-heptane should be particularly noteworthy. But, unfortunately, little information about the molecular weight distribution and microstructure of polyisobutylene oligomers was available. Recently, Kostjuk [15] has present new catalysts for the synthesis of HR PIB based on the combination of a chloroaluminate ionic liquids and diisopropyl ether, which allow to synthesize PIBs with a high content of exo-olefin end groups ( $\geq 90\%$ ) and relatively narrow MWD ( $M_w/M_n \leq 2.0$ ) (**Figure 6**).

Indeed, we did not find suitable ionic liquids for isobutylene cationic polymerization to synthesize the high-, medium- $M_n$  polyisobutylene. Generally, isobutylene is hard to dissolve in ionic liquids. The number of possible combinations of anions and cations in ionic liquids are very numerous. The properties of ionic liquids can be fine-tuned by selection of the cation and anion. It is difficult to discuss their properties in general because their properties depend on the structure of cation and anion. So, in order to screen the potential neutral ionic liquid solvent for isobutylene cationic polymerization, we used density functional theory calculations to investigate the inter-ionic interactions of ionic liquids and the interactions of ionic liquids with isobutylene [16]. The geometry was explained by the change of total energy, inter-molecular distance and ESP charge. The most stable gas-phase structures of ion pairs (IPs) and IPs-IB indicated that hydrogen bonding with the C2-hydrogen on the imidazole ring played a dominating role in the formation of IPs. The addition of IB did not change the dominant interactions of IPs. Compared with previous literature, the dissolution mechanism of IB in ionic liquids is that IB molecules occupy the free space of the cavities which are primarily created by small angular rearrangements of the anions. The potential solvent for IB polymerization is the ionic liquid with weaker interactions of anion and ion pair with IB. This work was motivated by the selection of ionic liquids as polymerization solvents. This study will also provide a broad range for future studies on cationic polymerizations in ionic liquids.



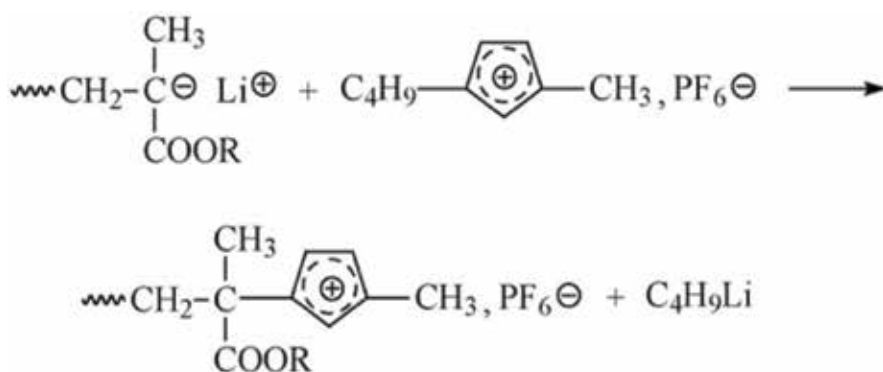
**Figure 6.** The electrostatic potentials (ESP) surface of isobutylene (IB, a) and [Bmim]<sup>+</sup> (b).

### 3. Anionic polymerization in ionic liquids

#### 3.1. Methyl methacrylate

Generally, anionic polymerizations need strict dehydration and oxygen-free conditions. Ionic liquids can be easy to dry under vacuum at high temperature due to their negligible volatility [17, 18]. So, cumbersome handling procedures for conventional volatile solvent such as distillation in the presence of drying agents was no need for ionic liquid. In order to understand mechanism and characteristics of anionic polymerization in ionic liquids, the methyl methacrylate (MMA) anionic polymerizations were carried out in ionic liquids by using alkyl lithium initiators such as *n*-butyllithium (*n*-BuLi) and diphenylhexyl lithium (DPHLi). The results were compared with those obtained for polymerization reactions in conventional solvents such as tetrahydrofuran (THF) and toluene. The MMA anionic polymerization in [NTf<sub>2</sub>]<sup>-</sup> based ionic liquids did not yield polymers because the initiator were be deactivated by attacking on the trifluoromethyl group. However, as compared with in tetrahydrofuran, the MMA anionic polymerization proceeded in [C<sub>4</sub>mim][PF<sub>6</sub>]<sup>-</sup> ionic liquid with lower monomer conversion. The reaction between the initiator and the imidazolium cation and high polymerization temperature resulted in lower yields. Analyzing from the <sup>1</sup>H-NMR spectrum, the alkyl lithium initiator withdrawn hydrogen atom at the imidazolium ring, which was the main cause of deactivating initiator. The tacticity of PMMA initiating by DPHLi in [C<sub>4</sub>mim][PF<sub>6</sub>]<sup>-</sup> was rich in mm triads. These results indicated that the propagation carbocation of PMMA in [C<sub>4</sub>mim][PF<sub>6</sub>]<sup>-</sup> has a similar terminal structure with that in toluene.

Another side-reaction in anionic MMA polymerization initiated by alkyl lithium initiators was observed by Kubisa [19]. Analyzing the terminal structure by MALDI-TOF, it was found that chain transfers to ionic liquids were easy to occur at the early stages of propagation polymerization. The chain transfer reaction in ionic liquid is shown in **Figure 7**. Although MMA anionic polymerization put a limit on molecular weights (M<sub>n</sub> < 2000) in ionic liquid, all the PMMAs contained ionic end-groups derived from ionic liquids, which should be pay enough attention.



**Figure 7.** Chain transfer to ionic liquid in anionic polymerization of methyl methacrylate.

### 3.2. Styrene

Styrene anionic polymerization initiated by butyllithium (BuLi) or sodium acetate (NaAc) in phosphonium-based ionic liquids has been reported by MacFarlane [20]. Although relatively high initiator concentration was used, polystyrene yield was still lower (10 ~ 20%). Yields could be improved by addition of butyl imidazolium butane sulfonate zwitterion. Moreover, molecular weights kept to high (up to 400,000) with molecular weight distribution in the range of 1.4–2.1. This indicated that phosphonium-based ionic liquids were more suitable as solvents for styrene anionic polymerization than imidazolium-based ionic liquids.

## 4. Conclusion

In recent years, an enormous progress has been made in the development of ionic polymerizations in ionic liquid. The polymerization reactions for cationic and anionic monomers were realized in ionic liquids. Some cationic polymerizations in ionic liquid indicated some living/controlled characteristics. However, only the control of molecular weight and polydispersity have been achieved. Telechelic polymers, macromonomers, block copolymers, polymer networks, star-shaped polymers have not been described in ionic liquids. So, in development of mechanism of living cationic polymerization, scientists need to strengthen scientific research further. Ionic liquids seem unsuitable solvents for anionic polymerization. Is it possible to find suitable ionic liquids for anionic polymerization by “designer-solvents”? The further theoretical studies are needed and the guiding roles of the relevant theories should be brought into full play.

## Acknowledgements

This work was supported by the National Science Foundation of China (51573020), Beijing Natural Science Foundation (2172022).

## Conflict of interest

The authors report no conflicts of interest in this work.

## Author details

Yibo Wu

Address all correspondence to: wuyibo@bipt.edu.cn

Department of Material Science and Engineering, Beijing Key Lab of Special Elastomeric Composite Materials, Beijing Institute of Petrochemical Technology, Beijing, China

## References

- [1] Goethals EJ, Prez FD. Carbocationic polymerizations. *Progress in Polymer Science*. 2007; **32**(2):220-246. DOI: 10.1016/j.progpolymsci.2007.01.001
- [2] Biedroń T, Kubisa P. Cationic polymerization of styrene in a neutral ionic liquid. *Journal of Polymer Science, Part A: Polymer Chemistry*. 2004;**42**:3230-3235. DOI: 10.1002/pola.20158
- [3] Baćko M, Biedroń T, Kubisa P. Polymerization processes in ionic liquids. Cationic polymerization of styrene. *Macromolecular Symposia*. 2006;**240**:107-113. DOI: 10.1002/masy.200650814
- [4] Bueno C, Cabral V, Cardozo-Filho L, Dias M, Antunes O. Cationic polymerization of styrene in scCO<sub>2</sub> and [bmim][PF<sub>6</sub>]. *Journal of Supercritical Fluids*. 2009;**48**:183-187. DOI: 10.1016/j.supflu.2008.09.023
- [5] Vijayaraghavan R, MacFarlane D. Organoborate acids as initiators for cationic polymerization of styrene in an ionic liquid medium. *Macromolecules*. 2007;**40**:6515-6520. DOI: 10.1021/ma070668z
- [6] Vijayaraghavan R, Macfarlane DR. Living cationic polymerisation of styrene in an ionic liquid. *Chemical Communications*. 2004;**6**:700-701. DOI: 10.1039/b315100j
- [7] Zhang XQ, Guo WL, Wu YB, Li W, Li SX, Shang YW, Zhang JH. Solubility of monomers for chain polymerization in ionic liquids predicted by the conductor-like screening model for real solvents. *Industrial and Engineering Chemistry Research*. 2017;**56**:14694-14703. DOI: 10.1021/acs.iecr.7b04235
- [8] Han L, Wu YB, Yang D, Wang H, Zhang XQ, Wei XL, Guo WL, Li SX. Characteristics and mechanism of styrene cationic polymerization in 1-butyl-3-methylimidazolium hexafluorophosphate ionic liquid. *RSC Advances*. 2016;**6**:105322-105330. DOI: 10.1039/C6RA22284F
- [9] Zhang XQ, Guo WL, Wu YB, Gong LF, Li W, Li XN, Li SX, Shang YW, Yang D, Wang H. Cationic polymerization of p-methylstyrene in selected ionic liquids and polymerization mechanism. *Polymer Chemistry*. 2016;**7**:5099-5112. DOI: 10.1039/c6py00796a
- [10] Wu YB, Han L, Zhang XQ, Mao J, Gong LF, Guo WL, Gu K, Li SX. Cationic polymerization of isobutyl vinyl ether in an imidazole-based ionic liquid: Characteristics and mechanism. *Polymer Chemistry*. 2015;**6**:2560-2568. DOI: 10.1039/C4PY01784F
- [11] Ambler PW, Hodgson PKG, Stewart NJ. (BP Chem. Ltd) EP, 0558187 1993
- [12] Abdul-Sada A, Ambler PW, Hodgson PKG, Seddon KR, Stewart NJ. (BP Chem. Ltd) WO, 9521871. 1995
- [13] Abdul-Sada A, Seddon KP, Stewart NJ. (BP Chem. Ltd) WO, 9521872. 1995
- [14] Murphy V. (Symyx Tech. Inc.) WO, 00/32685. 2000

- [15] Vasilenko IV, Bereziianko IA, Shiman DI, Kostjuk SV. New catalysts for the synthesis of highly reactive polyisobutylene: Chloroaluminate imidazole-based ionic liquids in the presence of diisopropyl ether. *Polymer Chemistry*. 2016;**7**:5615-5619. DOI: 10.1039/c6py01325b
- [16] Li XN, Guo WL, Wu YB, Li W, Gong LF, Zhang XQ, Li SX, Shang YW, Yang D, Wang H. Investigation of the interactions between 1-butyl-3-methylimidazolium-based ionic liquids and isobutylene using density functional theory. *Journal of Molecular Modeling*. 2018;**24**:83. DOI: 10.1007/s00894-018-3586-y
- [17] Kubisa P. Ionic liquids as solvents for polymerization processes—progress and challenges. *Progress in Polymer Science*. 2009;**34**:1333-1347. DOI: 10.1016/j.progpolymsci.2009.09.001
- [18] Kokubo H, Watanabe M. Anionic polymerization of methyl methacrylate in an ionic liquid. *Polymers for Advanced Technologies*. 2008;**19**:1441-1444. DOI: 10.1002/pat.1210
- [19] Biedron T, Kubisa P. Chain transfer to ionic liquid in an anionic polymerization of methyl methacrylate. *Journal of Polymer Science Part A: Polymer Chemistry*. 2007;**45**:4168-4172. DOI: 10.1002/pola.22256
- [20] Vijayaraghavan R, Pringle JM, MacFarlane DR. Anionic polymerization of styrene in ionic liquids. *European Polymer Journal*. 2008;**44**(6):1758-1762. DOI: 10.1016/j.eurpolymj.2008.02.028



---

# Ionic Liquids for Desulphurization: A Review

---

Syamsul Bahari Abdullah, Hanida Abdul Aziz and Zakaria Man

Additional information is available at the end of the chapter

<http://dx.doi.org/10.5772/intechopen.79281>

---

## Abstract

The literature survey has shown that not much work has been reported on the interaction mechanism of ionic liquids (ILs) with sulfur in model oil system. In recently published work, the interaction was predicted using COSMO-RS where the strength of hydrogen bond of anion should be reduced in order to increase thiophene extraction capacity. On the other hand, the same researchers also found that the smaller sized cations would lead to higher selectivity, which could lower the capacity and vice versa. While others have reported that the absorption capacity of sulfur compounds in ILs are strongly dependent on the chemical structures, physical properties and compactness between the cation and the anion of the ILs. However, these conclusions lead to a broad selection of ILs for extractive desulphurization process.

**Keywords:** ionic liquids, sulfur compounds, extractive desulphurization, absorption capacity

---

## 1. How do ILs interact with sulfur compounds?

Within recent years, ILs has gained increasing interest for application to different kinds of processes, amongst those is as separation media for LLE processes. Basically the optimization in LLE process or technique is mostly influenced by the interaction mechanism between the solute and solvent. Therefore, for desulphurization process it is vital to identify the interaction mechanism between sulfur compounds (solute) and ILs (solvent) since the interaction mechanism will determine the extraction efficiency and recycling capability of the ILs. Since the number of conceivable combinations between cations and anions are almost unlimited, and sole experimental screening is impossible, the use of simulation tools becomes important. Since ILs are a relatively new class of compounds, the use of common activity coefficient model for

---

example group contribution method like UNIFAC is complicated, because it requires the input of interaction parameters, which for ILs have not been fully determined thus far. In order to describe the interaction mechanism and behavior of ILs, the dielectric continuum model COSMO-RS has been introduced, and it is gaining more interest for ILs prediction for various applications [1, 2].

### 1.1. Interaction mechanism in COSMO-RS

COSMO-RS is independent of specific interaction parameters; therefore it is a promising approach for ILs. The name of COSMO-RS is derived from “**C**onductor-like-**S**creening-**M**odel” (COSMO) and its extension RS stands for “real solvents”. This approach belongs to the class of quantum chemistry of continuum solvation models (CSMs). CSMs are an extension of the basic quantum chemistry where a molecule in solution is described through a quantum chemical calculation of the solute molecule with an approximate representation of the surrounding solvent as a continuum. The solute is treated as if embedded in a dielectric medium via a molecular surface or cavity that is constructed around the molecule [3].

COSMO-RS uses only structural information of the molecules for the priori prediction of activity coefficients and other thermophysical data; thus the program is independent of specific interaction parameters. In COSMO-RS, a number of quantum chemical calculations are combined with statistical thermodynamics in order to enable the prediction of thermodynamic properties without any experimental data [4].

COSMO-RS is a combination of electrostatic theory of locally interacting molecular surface descriptors, which are computed by quantum chemical method (QM) with exact statistical thermodynamics methodology. In other words, it integrates concepts from quantum chemistry, dielectric continuum models, electrostatic forces interactions and statistical thermodynamics. It is based upon information evaluated by QM-COSMO calculations, which describe discrete surface around a molecule embedded in a virtual conductor. It treats a liquid as an ensemble of closely packed ideally screened molecules, where the molecular surface is in close contact with one another. Assuming that each molecule is still enclosed by virtual conductor, the interaction energies of the surface pairs are defined in terms of screening charge densities (SCDs), where  $\sigma$  and  $\sigma'$  of the respective surface segments. The SCDs measure electrostatic screening of the solute molecule by its surrounding and the back-polarization of the solute molecule [2–5].

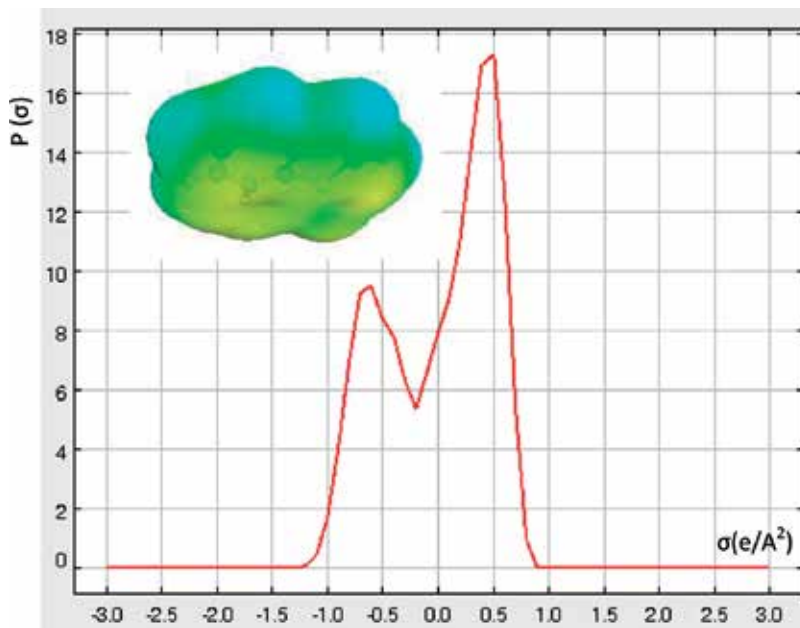
Meanwhile, the statistical thermodynamic provides a link between the microscopic surface interaction energy and the macroscopic thermodynamic properties of a liquid. Since in COSMO-RS all molecular interactions are viewed as consisting of local pair-wise interactions of surface segments, the statistical averaging can be done in the ensemble of interacting surface pieces. In order to describe the composition of the surface segment ensemble which depends on  $\sigma$ , it is sufficient to consider histograms of the SCDs, the so-called  $\sigma$ -profiles. Such probability distribution gives the relative amount of surface with polarity  $\sigma$  for a molecule [5].

The COSMO-RS prediction that starts with QM-COSMO calculation is performed on the density functional theory (DFT) level, utilizing the BP functional with RI (resolution of identity) approximation and a triple- $\zeta$  valence polarized (TZVP) basis set. These QM-COSMO

calculations are done in a Turbomole program package. The geometries of all molecules involved in these calculations are first fully optimized and the calculations are only performed once for each compound. The result of the COSMO calculation which is the charge distribution on the molecular surface is stored in the so-called COSMO-files, which are collected in the database. COSMO-RS calculations are then performed using COSMOtherm program, which provides an efficient and flexible implementation of the COSMO-RS method. Thus in combination with a large database of solvents including ILs, COSMO-RS allows fast and efficient large scale solvent screening [4–6].

In COSMO-RS, the bulk of a liquid phase is considered to be built of closely packed molecular cavities, and each molecule is divided into discrete segments, where each segment is assigned with a screening charge density,  $\sigma_i$ . Then, the interactions between the molecules are reduced to the interactions of the molecular segments, or rather the interactions of the screening charge densities. In order to describe the entire molecule and molecular properties the screening charge density distribution of a molecule, the so called  $\sigma$ -profile as shown in **Figure 1** is used [6].

Initially, the assumption has been made that a liquid consists of close packed molecules, as a logical consequence, the properties of this liquid can also be described by means of the  $\sigma$ -profiles. Next, based on the  $\sigma$ -profiles, the  $\sigma$ -potential,  $\mu(\sigma)$  of a molecule is calculated. The  $\sigma$ -potential is the central equation in COSMO-RS where all other equations for the calculation of thermodynamic data are based on. Additionally, electrostatic interactions ( $E_{\text{misfit}}$ ) and hydrogen bond interactions ( $E_{\text{HB}}$ ) between the molecular surfaces pieces are described in dependence of  $\sigma$ . Therewith, the screening charge distribution profile holds all the information which is necessary for COSMO-RS [5–7].



**Figure 1.** Screening charge distribution and  $\sigma$ -profile of BT.

Activity coefficient at infinite dilution,  $\ln(\gamma_i^{\text{inf}})$  is an important parameter in order to study the deviation from ideal behavior in a mixture of ILs + sulfur compound in hydrocarbon. Basically, it provides information regarding non-ideality of the chosen species in a mixture. The value describes the extreme case in which only solute-solvent interaction contributes to non-ideality that has practical implications in chemical and industrial processes. In the case of desulphurization, it provides information about interaction between solvent, where in this case is ILs (solvent) and solute i.e. sulfur compounds. This is a useful tool for solvent selection for extractive desulphurization process. The separation factor of species to be separated at infinite dilution is sufficient for determining the suitability of an IL as solvent for selective extraction. Experimentally, the activity coefficient at infinite dilution of some ILs in hydrocarbons, polar and non-polar solvents is measured using either gas-liquid chromatography or the dilutor technique [5–8].

Several thermodynamic models are available such as NRTL and UNIFAC for predicting activity coefficient at infinite dilution, but the accuracy of the measurement needs to be improved in order to enhance the prediction. Besides that, new experimental data are required to generate quantitative interaction parameter, which hinders the use of these models [8]. On the other hand, COSMO-RS is a novel and efficient model for priori prediction of activity coefficient at infinite dilution for a mixture of ILs from thermodynamic aspects as it relies on optimized molecular structure as the only information; no experimental data is needed [9].

The predicted activity coefficient values obtained through COSMO-RS using different or modified parameterization have been done by Banerjee group to predict potential ILs for separation of sulfur compounds (thiophene, BT and DBT), by means of selectivity, capacity and performance index at infinite dilution. In the first study, they selectively screened out 264 suitable ILs (from 24 anions and 11 cations) and found that smaller sized cations have higher selectivity, but lower capacity and vice versa [10]. They identified that for fluorinated anions, the removal of sulfur compound (thiophene) increases with the increase of the van der Waals volume. While a smaller cation with a sterically shielded large anion gave high extraction efficiency. In a second study they screened out 168 suitable ILs based on the permutations of 28 anions and 6 cations, and found that the cation without aromatic ring combined with anions having sterical shielding effect such as thiocyanate, acetate and chloride proved to be the most favorable ILs [11]. However, their predictions were not consistent with the literatures. This shows that COSMO-RS has a limitation to some extent. For example, COSMO-RS may not be able to represent the  $\pi$ - $\pi$  interaction effect which has resulted in inconsistent result between prediction and experiment. Therefore, there is a need to introduce new predictive approach for selecting appropriate ILs for desulphurization via interaction mechanism.

## 1.2. Interaction mechanism in extractive desulphurization

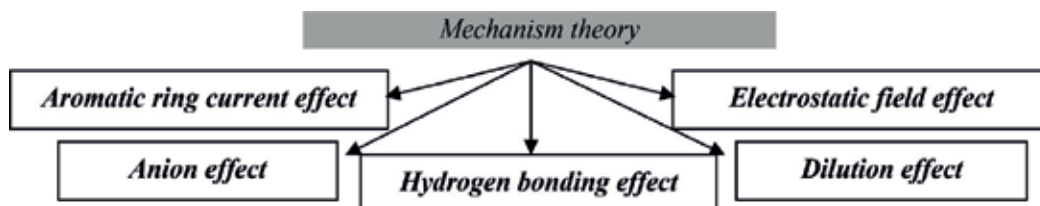
ILs consist of complex ions with multiple types of interaction, where each solute molecule will possess somewhat different solute-solvent interactions due to the various acidic, basic, electron donating and electron withdrawing properties. There are several possible contributing mechanism theories in extractive desulphurization as listed in **Figure 2**.

- Aromatic ring current effect (i.e.,  $\pi$ - $\pi$  interaction and CH- $\pi$  interaction) occurs between aromatic-type-cation of ILs and aromatic sulfur compound.
- Electrostatic field effect (i.e., Columbic interaction) occurs when bonding between the anion and cation of ILs becomes weaker because of their structures (most probably due to the length of substituted alkyl side-chain on the cation), which makes it more easier for insertion or interaction of aromatic sulfur compound in/with ILs.
- Hydrogen bonding effect occurs due to the H-bond donation of cation part of ILs to the sulfur atom of aromatic sulfur.
- Anion effect.
- Dilution effect.

The CH- $\pi$  interaction between the imidazolium cation and aromatic ring of sulfur compound becomes one of the major mechanisms during sulfur extraction as indicated by chemical quantum simulation [10, 11] and NMR observations [12]. By using quantum chemical calculation approach (namely ab initio calculations correlated with experimental results), it was suggested that the positively charged atoms of the imidazolium cation can be the most approachable to the negatively charged atoms of the sulfur compounds, producing a maximal Columbic interaction [13, 14]. On the other hand, the formation of hydrogen bonding between acidic hydrogen of the imidazolium cation and the sulfur compound is weak due to poor H-bond acceptor by the sulfur compound, but becomes stronger with increasing alkyl side-chain length. The anion and dilution effects (the dilution of ILs by sulfur compound insertion) are not the dominant factors in determining the absorption capacity and selectivity of sulfur compounds in model oil/imidazolium based-ILs systems [12, 15, 16].

Meanwhile, the specific  $\pi$ - $\pi$  interaction due to aromatic current effects was first predicted between imidazolium cation and sulfur compound (thiophene) using NMR analysis approach [12]. The aromatic current effect is largely affected by the size of the cation itself and the length of alkyl side-chain substituted on the cation. Since then, it was predicted by many researchers that the stronger selective extraction of aromatic sulfur compounds resulted from the  $\pi$ - $\pi$  interaction between the imidazolium-based ILs and aromatic sulfur ring [17–21].

There was also a suggestion that  $\pi$ - $\pi$  interaction between the unsaturated bonds of sulfur and the imidazole ring leads to the formation of liquid clathrate. Liquid clathrate is a semi-ordered liquid formed by associative interactions between ILs and aromatic sulfur compounds which



**Figure 2.** Possible contributing theories of interaction mechanism in extractive desulphurization by ILs.

separate the cation-anion packing interactions to a sufficient degree resulting in the formation of localized cage-structures; in this case ILs are trapping the aromatic sulfur compounds. With too little interaction, the ILs are simply completely miscible or immiscible with the aromatic sulfur compound, whereas, if the cation-anion interaction of ILs are too great, then crystallization of the ILs occurs [22–25]. Since the aromatic sulfur compounds e.g. DBT, BT, 3-methylthiophene are conjugated structure, the lone pairs on the sulfur atom or the  $\pi$ -electrons on the aromatic sulfur compound ring preferentially insert into the molecular structure of the ILs. The steric effect between the interacting compounds also influences the interaction mechanism involved [26, 27].

## 2. Selection of ILs for extractive desulphurization

Preliminary selection and screening of suitable ILs by relying on physical, chemical and thermodynamic properties have been intensively investigated and reported in literatures. However, the reported predictive tools for selecting potential ILs are still not satisfactory, as these tools still lack the capability to identify the correct combination of cations and anions matchup for a particular application; this needs further investigations.

### 2.1. Predictive approach

Due to the enormous number of possible combinations of cations and anions to produce ILs, an accurate prediction for a particular application is necessary. Predictive approach will reduce cost and time as opposed to trial and error using experimental work. One of the predictive approaches is COSMO-RS which is based on quantum chemistry approach. Recently this approach is being applied especially in predicting physical, chemical and thermodynamic properties plus interaction mechanism of potential ILs [25–28]. A recent study which employed COSMO-RS was carried out by Banerjee group, in which different or modified parameterization were used to predict potential ILs for diesel desulphurization, by means of selectivity and capacity at infinite dilution. They selectively screened out 168 suitable ILs (from 28 anions and 6 cations) mostly for extracting thiophene, BT and DBT from simulated diesel composition [11–29]. The attempted investigation via COSMO-RS showed that 4-ethyl-4-methylmorpholinium gave the best performance for desulphurization in combination with anions such as thiocyanate (CNS), acetate ( $\text{CH}_3\text{COO}$ ), bis(trifluoromethylsulfonyl)imide ( $\text{NTf}_2$ ) and triflate ( $\text{CF}_3\text{SO}_3$ ). However, their predictions did not match well with the experimental results from the literatures; for instance Holbrey et al. who reported that ( $\text{CF}_3\text{SO}_3$ ) and ( $\text{NTf}_2$ ) anions showed poor results in removing DBT from *n*-dodecane phase, while Wang et al. indicated that ( $\text{CH}_3\text{COO}$ ) anion gave average performance in removing thiophene from *n*-heptane phase.

### 2.2. Experimental approach

The screening of appropriate combination of cation/anion for ILs was first attempted by Bosmann and co-worker. They justified that from three types of cations ([emim], [bmim] and

ILs	Experimental description	
[3-mebupy][N(CN) <sub>2</sub> ]	DBT (%)	GC-analysis
[bmim][C(CN) <sub>3</sub> ]	86	Extraction condition
[4-mebupy][N(CN) <sub>2</sub> ]	86	Speed: 1200 rpm
[4-mebupy][SCN]	85	Time: 15 min
[bmim][N(CN) <sub>2</sub> ]	84	Vol. Ratio: 1/1
[bmim][SCN]	77	
[emim][N(CN) <sub>2</sub> ]	70	
[omim][BF <sub>4</sub> ]	57	
[opy][BF <sub>4</sub> ]	70	
[beim][DBP]	66	
[bmim][DBP]	63	
[eeim][DEP]	62	
[hpy][BF <sub>4</sub> ]	62	
[omim][DMP]	59	
[emim][DEP]	57	
[obim][DBP]	57	
[beim][DEP]	55	
[oeim][DEP]	54	
[emim][DMP]	54	
[hmim][DMP]	54	
[hbim][DBP]	51	
[bbim][DBP]	50	
[heim][DEP]	47	
[bmim][DMP]	47	
[bpy][BF <sub>4</sub> ]	41	
[mmim][DMP]	44	
[emim][DBP]	33	
[bmim][BF <sub>4</sub> ]	32	
Hansmeier et al., Green chemistry	16	
[C <sub>4</sub> mim][BF <sub>4</sub> ]	DBT (%)	GC-MS and HPLC
[C <sub>4</sub> mim][OcSO <sub>4</sub> ]	47	Extraction condition;
[C <sub>4</sub> mim][CF <sub>3</sub> SO <sub>3</sub> ]	63	Time: 60 min
[C <sub>4</sub> mim][PF <sub>6</sub> ]	50	Settling: 15 min
[C <sub>4</sub> mim][NTf <sub>2</sub> ]	53	Temp.: 40° C
[C <sub>4</sub> mim][SCN]	50	(equal volume ratio)
[C <sub>4</sub> mim][CH <sub>3</sub> CO <sub>2</sub> ]	66	
[C <sub>4</sub> py][NTf <sub>2</sub> ]	61	
[C <sub>4</sub> py][BF <sub>4</sub> ]	55	
[C <sub>4</sub> <sup>4</sup> mpy][NTf <sub>2</sub> ]	43	
[C <sub>4</sub> <sup>4</sup> mpy][BF <sub>4</sub> ]	76	
[C <sub>4</sub> <sup>4</sup> mpy][SCN]	70	
[C <sub>4</sub> <sup>4</sup> mpy][CF <sub>3</sub> SO <sub>3</sub> ]	79	
[C <sub>4</sub> <sup>3</sup> mpy][NTf <sub>2</sub> ]	72	
[C <sub>4</sub> <sup>3</sup> mpy][BF <sub>4</sub> ]	77	
[C <sub>4</sub> <sup>3</sup> mpy][SCN]	70	
[C <sub>4</sub> <sup>3</sup> mpy][CF <sub>3</sub> SO <sub>3</sub> ]	83	
[C <sub>4</sub> <sup>2,4</sup> dmpy][NTf <sub>2</sub> ]	69	
[C <sub>4</sub> <sup>2,5</sup> dmpy][NTf <sub>2</sub> ]	83	
[C <sub>4</sub> mpyrr][NTf <sub>2</sub> ]	81	
Holbrey et al., Green Chemistry	47	
	<i>n</i> -dodecane	

**Table 1.** Results of DBT removal using some ILs in extractive desulphurization.

[omim]) with [BF<sub>4</sub>] as anion and seven types of anions ([PF<sub>6</sub>], [CF<sub>3</sub>SO<sub>3</sub>], [BF<sub>4</sub>], [Cl], [MeSO<sub>4</sub>], [MeSO<sub>3</sub>] and [OSO<sub>4</sub>]) with [bmim] as cation, [omim] and [OSO<sub>4</sub>] depicted better extractability for DBT removal. It was later proved that the combination of these cation-anion, [omim][OSO<sub>4</sub>] has high viscosity at ambient conditions. Further work was carried out which indicated that [bmim][OSO<sub>4</sub>] has the best extractability of some sulfur compounds (Eßer et al.; Nie et al.). Later, Holbrey and co-worker screened out 20 ILs for extracting DBT and revealed that 1-butyl-dimethylpyridinium bis(trifluoromethylsulfonyl)imide ([bdmpy][NTf<sub>2</sub>]) yielded the highest DBT removal (83%) from *n*-dodecane. Recently, [bmim] tricyanomethane ([C(CN)<sub>3</sub>] has been found to yield higher DBT removal (86%) as compared to previous works [28, 29]. The result of both research studies are summarized in **Table 1**.

### 3. Extractive desulphurization

When a separation by distillation is ineffective or very difficult, liquid–liquid extraction (LLE) is one of the main alternatives to be considered. Close boiling point mixtures or substances that are unstable at the temperature of distillation, even under a vacuum condition, may often be separated by extraction which utilizes the chemical differences instead of vapor pressure differences. One of the major uses of extraction is to separate petroleum products that have different chemical structures, but have about the same boiling range. In liquid–liquid extraction, two phases must be brought into good contact to permit transfer of solute and then be separated [29, 30].

Extraction is a process in which a liquid mixture (of normally two species that contain the solute and the feed carrier) is contacted in a mixer with a third liquid (normally the solvent) that is immiscible or nearly immiscible with the feed carrier component. When the liquids are contacted, the solute is transferred from the feed carrier into the solvent. It is because during mixing process, bonds between solute and feed carrier are broken and possible new bonds are formed between solute and solvent. The energy, which may or may not be required in breaking the bonds between the solute and feed carrier or in forming the bonds between the solute and solvent, depends on the type of interaction.

The combined mixture is then allowed to settle into two phases that are then separated by gravity in a decanter. When a solute transfers from one phase to another, the transfer rate generally decreases with time until the second phase is saturated with the transferred solute, holding as much as it can hold at the prevailing process condition. When the concentrations of the solute in each phase no longer changes with time, the phases are said to be at equilibrium. The effectiveness of any of the separation processes described depends on both how the solute is distributed between the phases at equilibrium and on the rate at which the system approaches equilibrium from its initial state. The extract is the layer of solvent plus extracted solute and the raffinate is the layer from which the solute has been removed from the feed carrier substance [31, 32].

Recently, ILs has been applied in the petrochemical industry especially in catalytic processes, extractive distillation and LLE process for example upgrading heavy oils for desulphurization.



Their negligible vapor pressure allows the extracted product to be separated from the ILs through low pressure distillation with potential energy savings. In addition, as a result of their negligible vapor pressure, they are able to be regenerated for reuse.

The use of ILs for selective extraction of sulfur compounds from diesel is first described by Bosmann et al. in 2001 [33]. Based on the initial idea to extract the sulfur compound by chemical interaction, the extraction of DBT with Lewis and Brønsted acidic ILs was majorly investigated. They indicated that such Lewis-acid based interactions enhance the extraction power of ILs that permit complex formation of sulfur compound and ILs. They also identified that extraction of actual diesel is much more complicated due to the complex chemical composition of diesel which includes many different sulfur compounds and other impurities like organic nitrogen and oxygen compounds [34].

### 3.1. Extractive desulphurization on model oil

As mentioned previously, due to the limited efficiency of HDS towards aromatic sulfur compounds, a number of research have been focused on extracting them, mainly thiophene, BT, DBT and their derivatives. By using various types of ILs through various anion/cation combinations, some researchers have found that extraction process alone could remove up to 86% sulfur in model oil and 30% in actual diesel, which due to the steric hindrance of various sulfur compounds [25]. There are various types of model oil that have been investigated including aliphatics (*n*-hexane, *n*-heptane, *n*-octane, *n*-dodecane) and aromatics (toluene). In evaluating desulphurization performance, besides removal percentage, sulfur partition coefficient ( $K_N$ ) gives a better insight in terms of explaining the relationship between ILs amount and its structure against desulphurization performance [25, 27].  $K_N$  is defined as the ratio of sulfur concentration on weight basis in ILs to sulfur concentration in hydrocarbons, which the higher  $K_N$  the better the desulphurization performance of that ILs [33, 34].

Taib and Murugesan [35] in their report said that at ambient condition operation, sulfur compounds with  $C_5$  aromatic ring were observed to favorably absorb over  $C_6$  aromatics sulfur, while sulfur with non-aromatic structures were poorly absorbed by imidazolium-based ILs. Eßer and co-worker reported in their article that, even though the concept of extraction in desulphurization seemed feasible, but selective extraction of nitrogen-containing compounds and aromatic hydrocarbons still needs further investigation. Although quite a few researchers preferred pyridinium-based [36] and ammonium based ILs [37] for extractive desulphurization, it seems that the extraction ability is less promising. Some have been noticed to be comparable to imidazolium-based ILs if the anions matchup is just appropriate [38].

### 3.2. Extractive desulphurization on model fuel

Extractive desulphurization has been performed on model fuel containing up to 25% aromatics. Basically naphthalene, methylnaphthalene, indole, pyridine and tetralin are the most common aromatics used for preparing model fuel. The extraction efficiency is relatively high, and competing removal of aromatics and sulfur compounds was not detected based on model fuel containing *n*-dodecane/indole/DBT using [BMIm][OSO<sup>-</sup>] as extractant. Further

investigations showed that ILs gave higher removal of molecules that have higher density of aromatic  $\pi$ -electrons. Cross-miscibility of the studied aromatics in the ILs produced an unwanted effect, whereby high cross-miscibility will demonstrate a loss of fuel or at least contribute to an increase of process costs [39]. However, the effect of aromatic hydrocarbons such as benzene and xylene needs further research in order to understand the selective extraction process.

### 3.3. Extractive desulphurization on actual diesel

An approach based on extraction for removing sulfur compounds from actual diesel using ILs have been investigated by many researchers [39]. Compared to model oil or model fuel, the extraction from actual diesel is much more complicated due to its complex chemical composition including many different sulfur compounds and other impurities such as nitrogen and oxygen-containing compounds. For example, the removal of sulfur from model oil is 64% but in actual diesel this percentage is drastically reduced to 24.3% when the same ILs is applied. The obvious or most sterically hindered sulfur species would still remain in the actual diesel even though after several extraction steps. However, it has been proven that extractive desulphurization of actual diesel with ILs is still possible, although the operating expenses such as the number of theoretical extraction steps may vary in order to reach ultra-low concentration of sulfur [40].

## 4. Regeneration of spent ILs

Besides being efficient for extraction process, regeneration or recyclability of spent ILs is equally important since ILs has been recognized as environmentally benign solvent. Since ILs is quite expensive as compared to some conventional organic solvents, finding an alternative way to recycle spent ILs is the key for cost effectiveness in order to ensure the feasibility of using ILs at a larger scale application.

Undoubtedly, regeneration has become a fundamental issue from economic point of view. However, this is not only limited to the operating cost, but also concerning environmental issues such as disposal, biodegradable and toxicity. In general, ILs has a higher density compared to organic solvents or water; therefore, many ILs form separate phases when mixed with organic or aqueous solution. This behavior makes ILs as feasible for regeneration, which in turn presents potential economic viability of desulphurization process using ILs. In addition, the process is considered as being environmental benign since no waste is generated [33–40].

In conclusion, extractive desulphurization process using selective ILs as the extractant is still in need of further research, starting from screening of suitable ILs for desulphurization, synthesis of ILs, physical property analysis of ILs, single batch extraction study encompassing process optimization up to actual diesel application, and including regeneration of spent ILs.

## Author details

Syamsul Bahari Abdullah<sup>1\*</sup>, Hanida Abdul Aziz<sup>2</sup> and Zakaria Man<sup>3</sup>

\*Address all correspondence to: [syamsul@ump.edu.my](mailto:syamsul@ump.edu.my)

1 Faculty of Chemical and Natural Resources Engineering, Universiti Malaysia Pahang, Gambang, Pahang, Malaysia

2 Faculty of Engineering Technology, Universiti Malaysia Pahang, Gambang, Pahang, Malaysia

3 Centre of Research in Ionic Liquids (CORIL), Chemical Engineering Department, Universiti Teknologi PETRONAS, Bandar Seri Iskandar, Tronoh, Perak, Malaysia

## References

- [1] Klamt A, Eckert F. COSMO-RS: A novel and efficient method for the a priori prediction of thermophysical data of liquids. *Fluid Phase Equilibria*. 2000;**172**:43-72
- [2] Diedenhofen M, Eckert F, Klamt A. Prediction of infinite dilution activity coefficients of organic compounds in ionic liquids using COSMO-RS. *Journal of Chemical & Engineering Data*. 2003;**48**:475-479
- [3] Eckert F, Klamt A. Fast solvent screening via quantum chemistry: COSMO-RS approach. *AIChE Journal*. 2002;**48**:369-385
- [4] Banerjee T, Khanna A. Infinite dilution activity coefficients for trihexyltetradecyl phosphonium ionic liquids: Measurements and COSMO-RS prediction. *Journal of Chemical & Engineering Data*. 2006;**51**:2170-2177
- [5] Palomar J, Torrecilla JS, Ferro VR, Rodriguez F. Development of an a priori ionic liquid design tool: Ionic liquid selection through the prediction of COSMO-RS molecular descriptor by inverse neural network. *Industrial & Engineering Chemistry Research*. 2009;**48**:2257-2265
- [6] Gmehling H, Gmehling J. Performance of a conductor-like screening model for real solvents model in comparison to classical group contribution methods. *Industrial & Engineering Chemistry Research*. 2005;**44**:1610-1624
- [7] Klamt A. Conductor-like screening model for real solvents: A new approach to the quantitative calculation of solvation phenomena. *Journal of Physical Chemistry*. 1995;**99**:2224-2235
- [8] Mohanty S, Banerjee T, Mohanty K. Quantum chemical based screening of ionic liquids for the extraction of phenol from aqueous solution. *Industrial & Engineering Chemistry Research*. 2010;**49**:2916-2925

- [9] Garcia-Chavez LY, Hermans AJ, Schuur B, de Haan AB. COSMO-RS assisted solvent screening for liquid-liquid extraction of mono ethylene glycol from aqueous streams. *Separation and Purification Technology*. 2012;**97**:2-10
- [10] Kumar AAP, Banerjee T. Thiophene separation with ionic liquids for desulphurization: A quantum chemical approach. *Fluid Phase Equilibria*. 2009;**278**:1-8
- [11] Anantharaj R, Banerjee T. COSMO-RS based predictions for the desulphurization of diesel oil using ionic liquids: Effect of cation and anion combination. *Fuel Processing Technology*. 2011;**92**:39-52
- [12] Su BM, Zhang S, Zhang ZC. Structural elucidation of thiophene interaction with ionic liquids by multinuclear NMR spectroscopy. *Journal of Physical Chemistry*. 2004;**108**:19510-19517
- [13] Nie Y, Li C, Meng H, Wang Z. N,N-dialkylimidazolium dialkylphosphate ionic liquids: Their extractive performance for thiophene series compounds from fuel oils versus the length of alkyl group. *Fuel Processing Technology*. 2008;**89**:978-983
- [14] Zhou J, Mao J, Zhang S. Ab initio calculations of the interaction between thiophene and ionic liquids. *Fuel Processing Technology*. 2008;**89**:1456-1460
- [15] Liu X, Zhou G, Zhang X, Zhang S. Molecular dynamics simulation of desulfurization by ionic liquids. *AIChE Journal*. 2010;**56**:2983-2996
- [16] Nie Y, Li C, Sun A, Meng H, Wang Z. Extractive desulfurization of gasoline using imidazolium-based phosphoric ionic liquids. *Energy & Fuels*. 2006;**20**:2083-2087
- [17] Nie Y, Li C, Wang Z. Extractive desulfurization of fuel oil using alkylimidazole and its mixture with dialkylphosphate ionic liquids. *Industrial & Engineering Chemistry Research*. 2007;**46**:5108-5112
- [18] Mochizuki Y, Sugawara K. Removal of organic sulfur from hydrocarbon resources using ionic liquids. *Energy & Fuels*. 2008;**22**:3303-3307
- [19] Chu X, Hu Y, Li J, Liang Q, Liu Y, Zhang X, Peng X, Yue W. Desulfurization of diesel fuel by extraction with  $[\text{BF}_4]^-$ -based ionic liquids. *Chinese Journal of Chemical Engineering*. 2008;**16**:881-884
- [20] Ko NH, Lee JS, Huh ES, Lee H, Jung KD, Kim HS, Cheong M. Extractive desulfurization using Fe-containing ionic liquids. *Energy & Fuels*. 2008;**22**:1687-1690
- [21] Crowhurst L, Mawdsley PR, Perez-Arlandis JM, Salter PA, Welton T. Solvent—Solute interactions in ionic liquids. *Physical Chemistry Chemical Physics*. 2003;**5**:2790-2794
- [22] Holbrey JD, Reichart WM, Nieuwenhuyzen M, Sheppard O, Hardarce C, Rogers RD. Liquid clathrate formation in ionic liquid—Aromatic mixtures. *Chemical Communications*. 2003:476-477
- [23] Eßer J, Wassercheid P, Jess A. Deep desulfurization of oil refinery streams by extraction with ionic liquids. *Green Chemistry*. 2004;**6**:316-322

- [24] Cassol CC, Umpierre AP, Ebeling G, Ferrera B, Chiaro SSX, Dupont J. On the extraction of aromatic compounds from hydrocarbons by imidazolium ionic liquids. *International Journal of Molecular Sciences*. 2007;**8**:593-605
- [25] Jiang X, Nie Y, Li C, Wang Z. Imidazolium-based alkylphosphate ionic liquids—A potential solvent for extractive desulfurization of fuel. *Fuel*. 2008;**87**:79-84
- [26] Hansmeier AR, Meindersma GW, de Haan AB. Desulfurization and denitrogenation of gasoline and diesel fuels by means of ionic liquids. *Green Chemistry*. 2011;**13**:1907-1913
- [27] McCabe WL, Smith JC, Harriott P. *Unit Operations of Chemical Engineering*. 6th ed. United States: McGraw Hill Companies; 2001
- [28] McCain WD. *The Properties of Petroleum Fluids*. 2nd ed. United States: PennWell Publishing Company; 1990
- [29] Planeta J, Karasek P, Roth M. Distribution of sulfur-containing aromatics between [hmim][Tf<sub>2</sub>N] and supercritical CO<sub>2</sub>: A case study for deep desulfurization of oil refinery streams by extraction with ionic liquids. *Green Chemistry*. 2006;**8**:70-77
- [30] Stanislaus A, Marafi A, Rana MS. Recent advances in the science and technology of ultra low sulfur diesel (ULSD) production. *Catalysis Today*. 2010;**153**:1-68
- [31] Bosmann A, Datsevich L, Jess A, Lauter A, Schmitz C, Wasserscheid P. Deep desulfurization of diesel fuel by extraction with ionic liquids. *Chemical Communications*. 2001:2494-2495
- [32] Brennecke JF, Maginn EJ. Ionic liquids: Innovative fluids for chemical processing. *AIChE Journal*. 2001;**47**:2384-2389
- [33] Zhang S, Zhang ZC. Novel properties of ionic liquids in selective sulfur removal from fuels at room temperature. *Green Chemistry*. 2002;**4**:376-379
- [34] Gao H, Luo M, Xing J, Wu Y, Li Y, Li W, Liu Q, Liu H. Desulfurization of fuel by extraction with pyridinium-based ionic liquids. *Industrial & Engineering Chemistry Research*. 2008;**47**:8384-8388
- [35] Taib MM, Murugesan T. Experimental study on the extractive desulfurization of model fuel using hydroxyl ammonium ionic liquids. *Asia-Pacific Journal of Chemical Engineering*. 2011
- [36] Alonso L, Arce A, Francisco M, Soto A. (Liquid + liquid) equilibria of [C<sub>8</sub>mim][NTf<sub>2</sub>] ionic liquid with a sulfur-component and hydrocarbons. *Journal of Chemical Thermodynamics*. 2008;**40**:265-270
- [37] Huang C, Chen B, Zhang J, Liu Z, Li Y. Desulfurization of gasoline by extraction with new ionic liquids. *Energy & Fuels*. 2004;**18**:1862-1864
- [38] Kuhlmann E, Haumann M, Jess A, Seeberger A, Wasserscheid P. Ionic liquids in refinery desulfurization: Comparison between biphasic and supported ionic liquid phase suspension processes. *ChemSusChem*. 2009;**2**:969-977

- [39] Wang X, Han M, Wan H, Yang C, Guan G. Study on extraction of thiophene from model gasoline with bronsted acidic ionic liquids. *Frontiers of Chemical Science and Engineering*. 2011;**5**:107-112
- [40] Zhang S, Zhang Q, Zhang ZC. Extractive desulfurization and denitrogenation of fuels using ionic liquids. *Industrial & Engineering Chemistry Research*. 2004;**43**:614-622

---

## State of the Art Applications

---





---

# Applications of Ionic Liquids in Elastomeric Composites: A Review

---

Anna Sowinska and Magdalena Maciejewska

Additional information is available at the end of the chapter

<http://dx.doi.org/10.5772/intechopen.76978>

---

## Abstract

Ionic liquids (ILs) are organic salts that are liquid at ambient temperatures. ILs are considered a versatile class of chemicals because their properties can be easily tailored for specific applications. Due to their negligible vapor pressure, non-flammability, and thermal stability in the temperature range for preparation and processing of elastomeric composites, ILs are being used increasingly in the field of elastomer science and technology. In this review, the advantages of ILs as functional additives for elastomeric composites are discussed, with special emphasis on their use as dispersing agents for fillers, components of conducting rubber composites, crosslinkers or components of crosslinking systems.

**Keywords:** ionic liquids, elastomer, composites, dispersion degree, conductive composites

---

## 1. Introduction

ILs are generally defined as salts with melting temperatures lower than 100°C [1]. Recently, IL research has been one of the most rapidly growing fields in chemistry and in industry, mainly due to many unique properties of ionic liquids. ILs can solvate a large variety of organic polar and nonpolar compounds, and they show potentially “environmentally friendly” characteristics due to their negligible vapor pressure and non-flammability [2, 3]. Therefore, ILs are used as “green” solvents for numerous applications [4]. Moreover, their chemical and physical properties can be tuned for a wide range of potential applications by varying their cation and anion components. The anti-electrostatic properties of ILs have also been described [5]. Recently, ILs have not only been employed as solvents for various types of polymerizations [6–8] but they

---

have also been used to dissolve polymers (cellulose [9], silk fibroin [10] and starch [11]) to create new polymer composites [12], as plasticizers for many kinds of polymers [13] or for the preparation of polymer gels [14] and finally as effective wood preservatives [15]. The applications of ILs as novel electrolytes for electrochemical polymerization have also been reviewed [16]. ILs, due to their high-boiling points (300–450°C, which are also their decomposition temperatures), their low vapor pressure, their low volatility, their ability to create nonexplosive mixtures of their vapors with air, and their high flash-point, can be used successfully in elastomer technologies.

This chapter presents an overview of different applications of ILs in elastomeric composites. The main applications of ILs in elastomer technology include the improvement of fillers and the dispersion of other solids in the elastomer matrix, the preparation of conducting rubber composites, or using ILs as crosslinkers or other components of crosslinking systems (e.g., activators or vulcanization accelerators).

## 2. Use of ILs to improve the dispersion of solids in elastomers

The basic requirement for the reinforcement effect is to produce a homogeneous dispersion of the filler particles in the elastomeric matrix that results in good interphase adhesion [17]. However, most fillers exhibit a high degree of agglomeration, which makes it technologically difficult to obtain a homogenous dispersion in the elastomer. The unique chemical structure of ILs promotes the dispersion of nanoparticles in polymers owing to the surface modification of the nanoparticles with the ILs, which increases the interactions between filler particles and the elastomer matrices, especially in the case of silica, clays, carbon black and carbon nanotubes (CNTs). Because ILs are nonvolatile and nonflammable, the process of carbon nanotube modification and incorporation into an elastomeric matrix could be environmentally friendly. Moreover, ILs act as a lubricant; so, the process of modification is not accompanied by structural disruption of CNTs [18].

In 2007, Fukushima and co-workers reported a novel use for ILs as modifiers for carbon nanotubes, which enabled the production of soft composite materials that contained CNTs [19]. The use of ILs allowed for the noncovalent and covalent modifications of CNTs and for the formation of polymer composites with improved physical properties. In the presence of ILs, CNT bundles were reduced and unrolled. The result was fine bundles of CNTs that formed a network structure in the elastomeric matrix. This was related to the possible specific interactions between the imidazolium cation of ILs and the  $\pi$ -electronic carbon nanotube surface. The use of ILs during the processing of CNTs did not require solvents and did not alter the structure of the  $\pi$ -conjugated nanotube.

Subramaniam et al. reported an effect of the 1-butyl-3-methylimidazolium bis(trifluoromethylsulfonyl)imide (BmiTFSI) on the properties of polychloroprene rubber (CR) composites that contained multi-walled carbon nanotubes (MWCNTs) and suggested an optimum weight ratio (MWCNTs:BmiTFSI) to achieve an appropriate balance between mechanical and electrical properties of the composites [20]. After the modification process, the structure of the carbon nanotubes was well maintained, indicating a physical interaction between  $\pi$ -electrons on the MWCNT surface and the imidazolium cation of the BmiTFSI. This improved the dispersion of

the MWCNT in the CR elastomer, and as a consequence, increased the filler network, which was supported by strain sweep measurements. The optimum MWCNT/BmiTFSI ratio was reported to be 1:5. Higher loading of BmiTFSI caused deterioration of the composites mechanical properties. It was concluded that the use of an imidazolium ionic liquid resulted in increased electrical conductivity, as well as a reinforcing effect of the nanotubes in the CR elastomer. Addition of BmiTFSI-modified MWCNTs increased the tensile modulus and hardness of the CR composites, which clearly promoted dispersion of the nanotubes in the elastomeric matrix.

Das et al. [21] confirmed that the addition of ILs ensures better interactions between rubber and the MWCNTs, and therefore, improves the compatibility between the nanotubes and the elastomer and, consequently, their dispersibility in the elastomeric matrix. ILs, such as 1-allyl-3-methylimidazolium chloride (AMICI), were used to blend the styrene-butadiene (S-SBR) and polybutadiene rubber (BR) that contained MWCNTs. Using 3 phr, AMICI-functionalized MWCNTs caused a three-fold increase in the composites' tensile strength. Despite such small quantities of MWCNTs, the sample was stretched up to 456% without mechanical failure. Therefore, it was clear that an AMICI with a double bond in the structure produced the best reinforcing activity for composites containing 3 phr of MWCNTs. Moreover, it was suggested that AMICI acted as a coupling agent between the CNTs and the rubber chains and, hence, that the twisted structure of the CNTs held a certain amount of rubber and enhanced the three-dimensional interactions of the CNTs with the elastomeric matrix. A specific interaction between the MWCNTs and the rubber matrices in the presence of AMICI was postulated. The double bond of AMICI was presumably chemically linked with the double bond of the diene rubber chains by sulfur bridges, which then interacted with the  $\pi$ -electrons of the CNTs due to delocalization of the  $\pi$ -electrons in the imidazolium cation of AMICI. Transmission electron microscopic images confirmed the improved dispersion of MWCNTs that were functionalized with AMICI in the rubber matrix. Moreover, this ionic liquid promoted the formation of MWCNT clusters with a cellular structure in the elastomeric matrix that confirmed the strong adhesion of carbon nanotubes to the rubber phase and a special bound rubber aggregation in the reported composites.

One of the most effective reinforcing fillers for rubber compounds is carbon black (CB) with the surface of graphitic structures, which possess delocalized  $\pi$ -electrons. Particles of CB can interact with ILs in a manner similar to CNTs. Kreyenschulte et al. [22] investigated the interactions of AMICI with different types of carbon black and demonstrated strong interactions between AMICI and CB, as well as an improvement of the filler's dispersion in the elastomers. CB formed a bucky gel with AMICI, and an increase in the glass transition temperature ( $T_g$ ) of ionic liquid was observed. This effect was more apparent when the CB was graphitized; thus, a larger fraction of the CB surface was coated with graphitic crystals that can interact with AMICI via cation  $\pi$ -interactions. AMICI-modified carbon blacks were applied as fillers for S-SBR/BR composites and ethylene-propylene-diene rubber (EPDM). AMICI was premixed with CB, using ethanol and an ultrasonic treatment, and then dried before mixing with elastomers. As mentioned above, Fukushima et al. have reported that CNTs are able to build so-called bucky gels by physical crosslinking of nanotube bundles by mediating the molecular ordering of imidazolium-based ILs [23]. To study this behavior, which can be caused by CB or by its mixture with AMICI, analysis of the frequency dependence of the storage modulus and the loss modulus was performed which revealed significant differences. Hydrodynamic

reinforcement of the elastomers in the presence of CB particles that were modified with ILs could not explain the differences in the frequency dependencies of the storage and the loss modulus. Therefore, it was concluded that particles of CB can form gels in the presence of ILs, similar to CNTs. AMICI appeared to react either with vulcanization systems or with the double bonds of the rubber matrix, especially for EPDM, which decreased the crosslink density and thus affected the mechanical properties of the composites. For S-SBR/BR blends with AMICI-modified CB, the elongation at break was increased slightly, but there was no influence on the rupture strength. For EPDM vulcanizates, AMICI-CB caused a huge increase in the elongation at break and a significant increase in the rupture strength compared to samples without ILs.

Silicone rubber is a special rubber with improved electrical insulation, high elasticity and flexibility, and low modulus. Xu, Wang, et al. fabricated a novel, flexible piezoresistive material by mechanical grinding and two-roll mixing of silicone-rubber (SR), conductive CB and the ionic liquid 1-hexadecyl-3-methylimidazolium bromide (HdmiBr) that was applied to improve the dispersibility of the filler in SR matrix [24]. CB and HdmiBr were effectively co-grounded in a mortar and mixed with silicone rubber. A uniform dispersion of CB particles was observed in both composites (CB/SR and CB-HdmiBr/SR), but the size of the CB particles in the SR that contained ionic liquid was much smaller. Some of the HdmiBr was distributed on the surface of the CB, and attractive interactions between the imidazolium cation of the HdmiBr and the  $\pi$ -electrons on the CB surface were reported to improve the compatibility between the SR matrix and the CB and, consequently, the extent of dispersion in the elastomer. Additionally, these composites were characterized by a lower percolation threshold compared with the composite without HdmiBr. About 5 vol.% of CB-HdmiBr filler was sufficient to obtain higher piezoresistivity, shorter time of relaxation, and better cyclic repeatability of the composites, due to the plasticizing effect of the HdmiBr which resulted in the forced motion of the CB particles in the SR elastomeric network.

ILs were also reported to interact with a specific type of filler—graphene. A perfect form of graphene consists ideally of a flat, single layer material. However, in reality, some ripples are formed due to thermal fluctuations, which along with associated waviness, may affect its ability to reinforce composite materials [25]. Generally, elastomer/graphene and graphite composites can be fabricated by solution mixing, melt blending, and in situ polymerization methods, but it is difficult to incorporate chains of rubber macromolecules directly into the interlayers of graphite. There are many surfactants that can facilitate the dispersion of graphene in polymers [26]. The increased recognition gained by ILs is due to their unique capacity of imparting surface charges to the graphene sheet and thereby increasing colloidal stability [27].

Xiong et al. demonstrated that adding modified ionic liquid graphene oxide (GO-ILs) to bromobutyl rubber (BIIR) improved the thermal stability and thermal conductivity of the BIIR [28]. The thermal stability of BIIR has always been a concern because of the double bonds, which could be generated by eliminating HBr from its backbone [29]. Suitably prepared GO was modified with 1-butyl-3-methylimidazolium hexafluorophosphate ( $\text{BmiPF}_6$ ) and then incorporated into a BIIR matrix.  $\text{BmiPF}_6$  was successfully intercalated into the interlayer of GO, resulting in an increased degree of GO exfoliation, which consequently improved the dispersion in the BIIR matrix due to the strong interfacial interactions between GO- $\text{BmiPF}_6$  and BIIR rubber chains.

Addition of GO intercalated with BmiPF<sub>6</sub> increased the thermal stability of composites as well as the T<sub>g</sub> of BIIR, due to the attractive interactions of the elastomer chains with the large surface area of the GO-BmiPF<sub>6</sub>. Moreover, an improvement of the thermal conductivity of GO-BmiPF<sub>6</sub>/BIIR nanocomposites was observed compared with that of the unfilled BIIR.

Silica is widely used as a filler for elastomers because of its excellent mechanical properties, high thermal and chemical stability, a suitable pore structure, the presence of silanol groups on the surface and its high specific surface area [30]. ILs can be used to modify the surface of silica [31], mainly due to the  $\pi$ - $\pi$  interactions between the cations and anions of the ILs with active sites on the silica's surface [32]. Generally, nanoparticles of silica after modification with ILs are monodispersed and smooth spheres. The structure of the applied ILs significantly influences the surface and properties of modified silica nanoparticles, thereby improving the hydrophobicity to encourage the stability of dispersions and suspensions of this filler in proper dispersants [33].

ILs can be used to increase the degree of dispersion of silica fillers and vulcanization activators (zinc oxide) nanoparticles, as was reported by Maciejewska et al. [34]. The addition of ILs (salts of benzylimidazolium, alkylpyridinium, alkylpyrrolidinium, or alkylpiperidinium) produced a homogeneous dispersion of silica and zinc oxide nanoparticles in the SBR rubber. This resulted in reduced time and temperature of vulcanization and increased the crosslink density, thermal stability of vulcanizates and their aging resistance under the influence of UV radiation.

ILs with specific structures can be employed as interfacial modifiers for various silica-filled polymer composites [35]. Lei and Tang reported using 1-methylimidazolium methacrylate (MimMa) as a modifier for SBR to improve the dispersion of silica and increase the interfacial interactions between SBR and the filler [36]. MimMa was polymerized radically and grafted onto rubber chains during vulcanization, forming the graft product poly(SBR-g-MimMa), to enhance the compatibility between MimMa and SBR. As a consequence, the mechanical performance of SBR/silica composites was improved effectively. With increasing MimMa loading, the abrasion resistance, tensile strength, tear strength, and the modulus at 300% relative elongation were improved. The composites can be used as damping materials owing to increased mechanical loss under dynamic load. The strong interactions between MimMa and silica were partially linked, due to hydrogen bonding between the imidazolium cation of the MimMa and the Si-O-Si groups of silica, and partially to hydrogen bonding between the anion of the MimMa and the Si-OH groups on the silica's surface, which was well-described in [37]. SEM and TEM confirmed the improved dispersion of silica in the IL-functionalized SBR, and that agglomerates with reduced size were uniformly distributed into the SBR matrix. This was attributed to interfacial interactions that were induced by the incorporation of functional MimMa into the rubber chains. The presence of MimMa affected the vulcanization behavior of SBR compounds. With an increasing loading of MimMa, the value of minimum rheometric torque during vulcanization was consequently lowered, and the maximum torque required a maximum of 1 phr MimMa and then decreased significantly for higher content of this ionic liquid. It was expected that MimMa would cover the silica surface and reduce the adsorption of dicumyl peroxide (DCP) onto the silica, but on the other hand, it would consume a portion of the DCP during the vulcanization process.

The improved dispersion of silica nanoparticles in the SBR elastomer was confirmed by Maciejewska and Zaborski [38] for ILs with benzalkonium or didecyldimethylammonium cations and saccharinate, acesulfame, or lactate anions, which contributed to a considerable increase in the mechanical properties of the SBR composites.

Over the last two decades, the published literature regarding polymer composites with layered silicates, especially montmorillonite (MMT) and halloysite and nanoclays, has grown [39, 40]. MMT is a hydrophilic material that can be used as a filler in polymeric nanocomposites to enhance mechanical strength, modulus, heat resistance, anti-flammability, anti-gas permeability, and service life at elevated temperatures [41]. However, the key factor that is required to achieve these properties of polymer composites is ensuring a homogeneous dispersion of MMT in the polymer matrix accompanied with the exfoliation of MMT layers. The modification of clays with ILs can be considered as a green method because it does not require a solvent [42] or a melt intercalation process [43] to be successfully completed.

Fontana et al. [44] reported the use of MMT mechano-chemically co-intercalated with hexadecyltrimethylammonium bromide (HDTMA) and the ionic liquid 1-methyl-3-octylimidazolium bis(trifluoromethanesulfonyl)imide (OMImTf<sub>2</sub>N) as a filler for acrylonitrile-butadiene elastomers (NBR). Applying MMT intercalated with ILs improved the thermal stability of the NBR composites, which was explained by the extra interactions between the cations present in the clay layers and the elastomer chains. Based on SEM analysis, it was shown that the presence of ILs was necessary to improve the dispersion of the MMT into rubber. There were numerous agglomerates in the vulcanizate with small amounts of OMImTf<sub>2</sub>N, but after increasing its loading, the dispersion of MMT became more homogeneous. Therefore, it was confirmed that the organophilization of MMT enhanced the interfacial interactions between the MMT and NBR elastomer, due to the higher compatibility of intercalated MMT with the elastomeric matrix. MMT modified with ILs added to NBR was classified as a good reinforcing filler, which improved the efficiency of the vulcanization process, and consequently, the mechanical and physical properties of the elastomer.

Halloysite nanotubes (HNTs) are naturally occurring types of mineral clays with a nanotubular structure and were studied as promising fillers for polymer composites. Overcoming the poor interfacial interactions between polymers and HNTs remains a great challenge for processing polymer/HNTs nanocomposites with desired performance [45]. Guo et al. reported that BmiPF<sub>6</sub> was strongly adsorbed onto HNT surfaces and consequently improved the strength of interfacial bonding and the dispersion of the HNTs in the elastomeric matrix [46]. It was reported that clays may adsorb ILs by an ion exchange mechanism [47]. The authors claimed that ILs may be adsorbed onto HNT surfaces by hydrogen bonding between hydrogen atoms of the imidazolium ring of the ionic liquid and the surface siloxane groups of the HNTs. The IL-coated HNTs (m-HNTs) were used as a reinforcement for SBR. The rheometric torque during vulcanization of SBR composites increased with loading of HNTs, probably due to the increase in the crosslink density of the vulcanizates and the improved interaction between SBR and m-HNTs. Moreover, using m-HNTs, the scorch time and the optimal vulcanization time of SBR compounds shortened in comparison with neat SBR. This resulted from the adsorption of IL on the surface of the HNTs, which restricted the adsorption of curing

agents on its surface, thus increasing the efficiency of vulcanization. When an IL was absorbed on the HNT, the interfacial bonding and the dispersion were improved, and consequently, the tensile strength of the SBR vulcanizates increased.

The same authors investigated two other functional ILs, 1-methylimidazolium mercaptopropionate (MimMP) and bis(1-methylimidazolium) mercaptosuccinate (BMimMS), as modifiers for tailoring the interfacial structure of SBR/HNTs composites [48]. Incorporation of functional groups, e.g., double bonds and thiol groups, into IL molecules improved the performance of rubber composites. MimMP was reported to interact with Al-O, Si-OH and Al-OH on the HNT's surface by hydrogen bonding. Hydrogen bonding between Si-O, Al-OH, or Si-OH and the imidazolium cation of BMimMS was also confirmed. With loading of functional ILs, the scorch time of SBR was reduced due to restricted adsorption of curatives on the HNT's surface. Additionally, the presence of a thiol group in the ILs could activate the vulcanization significantly by effectively lowering the activation energy of this process. Incorporation of ILs increased the maximum torque values during vulcanization, which was attributed to the filler networking into the SBR matrix and filler-rubber interfacial interactions by hydrogen bonding, as well as to increasing the vulcanizates crosslink density with ILs loading. It was also confirmed that incorporation of MimMP or BMimMS into SBR/HNTs composites effectively restrained the agglomeration of HNTs in the elastomer matrix, especially in the case of BMimMS which promoted the fine and homogeneous dispersion of filler. The addition of functional ILs improved considerably the tensile and tear strengths of the vulcanizates. Possible explanations that were proposed for this phenomenon included: the increased crosslink density of SBR, the improved dispersion of HNTs in the rubber matrix, and the strengthened interfacial interactions between HNTs and SBR. The efficiency of the described functional ILs in modifying SBR/HNTs vulcanizates was also enhanced compared with other modifiers [49].

Furthermore, it was reported that the addition of hydrophobic ILs, such as 1-hexyl-3-methylimidazolium tetrafluoroborate (HMIMBF<sub>4</sub>), 1-methyl-3-octylimidazolium hexafluorophosphate (OMIMPF<sub>6</sub>), and 1-methyl-3-methylimidazolium hexafluorophosphate (HMIMPF<sub>6</sub>), to elastomeric blends based on an ethylene-propylene copolymer (EPM), prevented the agglomeration of magnetic fillers, such as Fe<sub>2</sub>O<sub>3</sub>, and improved the degree of their dispersion. ILs were introduced with other ingredients to the pre-plasticized rubber. The elastomeric composites that were produced exhibited good magnetic and mechanical properties. Moreover, uniformly distributed particles of magnetite protected the composites against elevated temperatures and UV rays [50].

### 3. Conducting rubber composites containing ILs

Solid polymer electrolytes (SPEs) have been used in various electrochemical devices such as sensors, actuators, supercapacitors, and rechargeable batteries [51]. To improve their mechanical properties, SPEs based on elastomers, such as natural rubber (NR), NBR or SBR containing lithium salts, were developed. This is an effective process for obtaining polymer electrolytes with high tensile strength and elasticity. However, due to their high ionic conductivity, good electrochemical stability, and non-volatility, ILs could be applied successfully as novel electrolytes as an alternative to commonly used lithium salts [52].

Marwanta et al. [35] used NBR as a matrix and ILs as an ion source for SPEs. N-ethylimidazolium salts of tetrafluoroborate (EImBF<sub>4</sub>), bis(trifluoromethanesulfonyl)imide (EImTFSI) and benzenesulfonate (EImBS) were included as electrolytes. The EImTFSI was the only one miscible with NBR, which was confirmed by the single T<sub>g</sub> present in the DSC curve. This was attributed to ion-dipole interactions between the nitrile groups of NBR and EImTFSI ions. The best miscibility of ILs with TFSI anions was confirmed by Likozar [53] for hydrogenated nitrile elastomers. In the case of other ILs, completely phase-separated composites were obtained. The T<sub>g</sub> of NBR/EImTFSI composites decreased with increasing ionic liquid content, thereby demonstrating the plasticizing effect of ILs on the elastomeric matrix. The conductivity of NBR/EImTFSI composites increased with EImTFSI content, which resulted from both the increased carrier ion number and the low T<sub>g</sub> of the composites. Moreover, the composites containing from 10 to 50 phr of EImTFSI exhibited good elasticity and high ionic conductivity (up to  $1.2 \times 10^{-5}$  S/cm at 30°C). The addition of lithium salts with the TFSI anion (LiTFSI) produced NBR conductive composites with even better mechanical strength than the composites without lithium salts. However, in this case, the composites revealed microscopic phase separation that was induced by the addition of a lithium salt. Li<sup>+</sup> ions in the LiTFSI should function as couplers between the NBR and the EImTFSI, since they can interact with both nitrile groups in the elastomer and the TFSI anion from the LiTFSI. As a result of microphase separation in the NBR/EImTFSI/LiTFSI composites, their ionic conductivity was approximately 100 times greater than that of composites without lithium salt, and the conductivity increased with the content of this salt up to 20 mol%.

Ion conductive elastomeric composites were also prepared by mixing NBR with lithium salts and ILs with an alkylimidazolium cation and a TFSI anion, where both cation and anion were tethered in the form of a zwitterion [54]. Addition of 9.2 wt% zwitterion enhanced the ionic conductivity approximately 8-fold compared with composites without zwitterions. The zwitterion was thought to provide additional high ion conductive paths that could improve the ionic conductivity. Moreover, zwitterions can effectively reduce the interaction between nitrile groups of the NBR and Li<sup>+</sup> ions of the lithium salt as a result of a strong interaction between zwitterions and lithium ions. The reduction of NBR/Li<sup>+</sup> interactions could increase the number of free Li<sup>+</sup> ions that can enhance the ionic conductivity of the NBR composites. No less important was microphase separation of the prepared composites, which was responsible for creating an ion conduction path. Flexible and mechanically stable NBR-based SPEs were also fabricated using BmiTFSI [55]. The highest ionic conductivity was achieved with composites that contained NBR with 40 mol% acrylonitrile. ILs were reported to act as electrolytes and plasticizers that enhanced the mobility of the elastomer chains and also increased the ionic conductivity.

Another approach that could produce a soft, flexible SPE with good dimensional stability made use of interpenetrating polymer networks (IPNs) that were formed by two crosslinked polymers, such as NBR and poly(ethylene oxide) (PEO) and the ionic liquid N-ethylmethylimidazolium bis(trifluoromethanesulfonyl)imide (EmiTFSI) as the electrolyte [56]. EmiTFSI was chosen because of its high affinity for polymers with polar groups, which rendered it compatible with NBR and PEO [58]. Swelling of NBR/PEO IPNs with EmiTFSI produced materials with an ionic conductivity greater than  $10^{-4}$  S/cm at room temperature. Such materials could be used successfully in actuators and other electrochemical devices.



Matchawet et al. fabricated elastomeric composites with increased electrical conductivity using epoxidized natural rubber (ENR) and 1-ethyl-3-methylimidazolium chloride (EmiCl) as the ionic liquid [57]. The electrical conductivity of ENR composites increased from  $10^{-8}$  S/m (for neat ENR) to  $10^{-4}$  S/m for the composites with 7 phr of EmiCl, due to the mobility of cations and anions in the EmiCl, which served as additional charge carriers. The effect of EmiCl on both the curing behavior of ENR and its crosslink density was also reported. The scorch time and optimal vulcanization time significantly decreased for EmiCl loadings below 5 phr and then increased with the content of EmiCl due to the microphase separation of the EmiCl that was dispersed in the ENR matrix. The addition of EmiCl increased the crosslink density of ENR, probably as a result of  $\pi$ - $\pi$  and dipole interactions in the ENR with the imidazolium moiety of the EmiCl. The disadvantage of using EmiCl was the significant reduction of tensile strength and elongation at break of the ENR.

Hydrophobic ILs, such as BmiTFSI, were used to produce composites of carboxylated nitrile rubber (XNBR) that contained hydrotalcite (HT), which exhibited an increase in the ionic conductivity from  $10^{-10}$  S/cm (neat XNBR) to  $10^{-7}$  S/cm [58]. Moreover, BmiTFSI did not affect the tensile strength or elongation at break of XNBR significantly, although a plasticizing effect of BmiTFSI was confirmed. The improvement of the ionic conductivity of XNBR/HT composites resulted not only from the ionic conductivity of BmiTFSI and its concentration but was also influenced by the plasticizing effect of the ionic liquid, which increased the mobility of the rubber chain segments of the XNBR that contained BmiTFSI. Additionally, BmiTFSI improved the dispersion of HT in the elastomeric matrix.

In recent years, the use of MWCNTs has increased as a method for producing conductive elastomeric composites [21, 59, 60]. Unfortunately, because of their tendency to agglomerate due to van der Waals interactions between individual nanotubes, a fine, uniform dispersion of MWCNTs and their network formation in the elastomer is a significant challenge from a technological point of view. Different techniques have been applied to disperse MWCNTs in polymer matrices, including functionalization with the use of harmful solvents. In addition to the harmful effect of these volatile organic solvents, they also have several disadvantages, such as destruction of the  $\pi$ -electron network of MWCNTs, resulting in a reduction of their inherent electrical conductivity [61]. To preserve the  $\pi$ -electrons on the surface of MWCNTs and to maintain the inherent electrical conductivity, ILs can be used to non-covalently modify the surface of nanotubes [21, 59]. Subramaniam et al. reported the development of new elastomeric conductors that employ CR rubber and MWCNTs that were modified with ILs [59]. BmiTFSI was used for surface modification of the MWCNTs and the resultant mix was directly admixed into CR without the use of an organic solvent. The Raman spectrum confirmed the interactions between  $\pi$ -electrons of the nanotubes and cations of the BmiTFSI, or the perturbation of  $\pi$ - $\pi$  stacking of multi-walls of the nanotubes. Therefore, it was concluded that the modified MWCNTs were activated physically, without a chemical impairment of the nanotubes. The use of modified MWCNTs produced CR composites whose electrical conductivity increased with the amount of filler. Moreover, the higher the ratio of MWCNTs to BmiTFSI, the higher was the conductivity of the obtained composites. The increase in the conductivity of the CR composites was attributed to a synergistic effect of electrons and ions as well as to an improved dispersion and formation of a percolating network by the BmiTFSI-modified

MWCNTs. The dispersion of MWCNTs in the CR matrix was enhanced with an increasing proportion of BmiTFSI due to a reduction in the intertubular attraction between nanotubes in the presence of the BmiTFSI. The network formation of the exfoliated nanotubes in the elastomer matrix is destroyed with an increase in the strain amplitude in DMA measurements, as confirmed by the Payne effect.

Sabu et al. developed SBR composites that can attenuate electromagnetic radiation. To achieve this, MWCNT surfaces were modified with the 1-benzyl-3-methylimidazolium chloride (BenMICI) and subsequently incorporated in the SBR matrix [60]. The cation- $\pi$  interaction between the imidazolium cation of the BenMICI and the  $\pi$  electronic surface of the carbon nanotubes that resulted in the reduction of the size of the MWCNT agglomerates after modification, and an improvement of their dispersion in the elastomer matrix, has been reported. An increase in the dielectric constant of SBRs that contain MWCNTs was observed due to the large difference between dielectric permittivity of the elastomer matrix and the nanotubes, which caused the accumulation of charge carriers at the elastomer/carbon nanotubes interphase. Electrical percolation was determined between 3 and 5 wt% MWCNTs. At this concentration of MWCNTs, a sudden and sharp increase in the conductivity was observed, indicating the formation of an electrically conductive three-dimensional continuous network of carbon nanotubes. Moreover, SBR composites that contain MWCNTs that are functionalized with BenMICI exhibited the shielding effect to electromagnetic radiation, which increased with the content of the MWCNTs. After the percolation threshold, the formation of continuous networks of MWCNTs enhanced the mobility of charge carriers; as a result, the attenuation of electromagnetic radiation by absorption was observed. This was reported to be a synergistic effect of BenMICI that is in electrical contact with carbon nanotubes [61]. The shielding effectiveness increased with an increase of the ratio between MWCNTs and the BenMICI, because the ionic liquid provides additional charge carriers that increase the polarizability of the SBR composites. Therefore, the combination of ILs with MWCNTs produced a new soft rubber material that is suitable for the attenuation of electromagnetic radiation. The same authors reported developing highly conducting and mechanically durable SBR composites that contained MWCNTs that were modified with the 1-ethyl-2,3-dimethylimidazolium bis(trifluoromethylsulfonyl)imide [62]. The significant increase in the dielectric constant of SBR composites was attributed to the uniform dispersion of the MWCNTs in the elastomeric matrix, resulting in the formation of micro capacitor networks of carbon nanotubes in the presence of ILs. The cation- $\pi$  interactions between ILs and MWCNTs were also confirmed.

MWCNTs pretreated with BmiTFSI were also used to produce stretchable conductive polymer nanocomposites (CPCs) of thermoplastic elastomers (polyester-based thermoplastic polyurethanes TPU) [63] that could be used as strain sensors. It was reported that entangled single-walled CNTs or MWCNTs bundles could be exfoliated into much finer bundles by grinding them with BmiTFSI, after which a gel-like material was formed. Physical interactions or the formation of chemical bonds between BmiTFSI-modified MWCNTs and TPU chains enhanced the uniform dispersion of the MWCNTs in the TPU matrix; as a result, the composites were able to withstand high strain as opposed to the TPU without BmiTFSI. The resulting CPCs exhibited a high level of strain (100%) without a noticeable degradation of the conductivity after many stretching/relaxing cycles. Their resistivity was reported to be recoverable, and the strain sensing properties were stable.

#### 4. Use of ILs for crosslinking elastomers

Catalytic activity of ILs in interfacial reactions and their dispersing action could be used successfully as elastomer crosslinkers [64] or other components of crosslinking systems [37, 65–67].

Behera et al. [64] fabricated a novel ionic liquid-crosslinked flexible polyurethane elastomer using a one-pot polymerization method. Tris(2-hydroxyethyl)methylammonium methylsulfate (THMAMS) was used as a crosslinker. FT-IR analysis confirmed the presence of THMAMS in the polyurethane backbone, which significantly suppressed the hydrogen bonding interactions of the obtained polyurethane elastomer. As a result, a highly flexible and tough elastomeric material was obtained with a much lower  $T_g$  than the linear thermoplastic polyurethane elastomer (TPU) or the elastomer that was crosslinked using a non-ionic crosslinker. Moreover, THMAMS-crosslinked polyurethane elastomers exhibited significantly higher tensile strengths and elongation at break, and lower hardness, compared with conventional TPUs or elastomers prepared without THMAMS as the crosslinker. The higher tensile strength of THMAMS-crosslinked elastomers was reported to be due to the inter-ionic interaction between hard segments.

ILs with a suitably designed structure could be successfully applied as accelerators in the sulfur vulcanization of unsaturated elastomers [65–68]. These ILs consist of the 2-mercaptobenzo-thiazolate anion derived from the traditionally used 2-mercaptobenzothiazole (MBT) vulcanization accelerator and various organic cations, mainly benzalkonium, alkylammonium or phosphonium and alkylimidazolium. All of these are thermally stable at commonly used vulcanization temperatures (150–180°C). Benzalkonium, tetradecyltriethylphosphonium, or alkylimidazolium 2-mercaptobenzothiazolates were used in the vulcanization of silica-filled NBR as an alternative to the traditionally used MBT accelerator [66]. This resulted in a two- or even three-fold (for benzalkonium salt) reduction in the NBR vulcanization time at 160°C while maintaining the torque increase during vulcanization and a crosslink density slightly higher or comparable to that of the rubber compound crosslinked in the presence of MBT. Therefore, it was concluded that these ILs acted as vulcanization accelerators. Moreover, vulcanizates containing most of these ILs exhibited tensile strengths higher than or similar to that of NBR vulcanized with MBT. Additionally, vulcanizates with ILs exhibited an increased resistance to thermo-oxidative aging. The activity of azolanic ILs and their influence on vulcanization kinetics resulted from not only the catalytic effect of ILs but also the improvement in the degree of dispersion of curatives in the NBR composites. It is also very important that by using salts of MBT as vulcanization accelerators, approximately 30–70% less MBT was introduced into the rubber compound than by using pure MBT. The activity of benzalkonium and alkylammonium 2-mercaptobenzothiazolates as vulcanization accelerators was also studied for SBR composites that were filled with pyrogenic silica [67]. The increase in vulcanization efficiency in the presence of ILs can be attributed not only to the aforementioned factors, such as catalytic activity and the improved degree of curative dispersion in the elastomer, but also to the adsorption of ILs on the silica surface, which reduces the ability of the silica to adsorb curatives and water. Therefore, it is possible that ILs could play roles as both accelerators and shielding agents, increasing the efficiency of vulcanization. An important aspect of IL applications is the improvement in SBR resistance to thermo-oxidative aging

and long-term UV radiation that resulted from a reduction in the increase in crosslink density due to aging factors. The greatest activity, from this point of view, was exhibited by alkylammonium salts of MBT. ILs can also be applied as components of new systems that activate the sulfur vulcanization of unsaturated elastomers (SBR, NBR, and EPDM). These systems are based on the use of nanosized ZnO in combination with ILs with different cations and anions [38, 69–71]. Obtaining a homogeneous dispersion of zinc oxide nanoparticles in an elastomer is a technological challenge. Selecting the appropriate dispersing agents remains an unresolved issue. ILs could be useful in this role. Moreover, due to catalytic activity in interfacial reactions, ILs could additionally increase the crosslinking efficiency and reduce the time and temperature of vulcanization. For example, commercially available 1-ethyl-3-methylimidazolium or 1-butyl-3-methylimidazolium bromides, chlorides, tetrafluoroborates, and hexafluorophosphates with nanosized ZnO were used to activate the vulcanization of SBR filled with pyrogenic silica [69, 71]. Nanosized ZnO, despite its 60% lower content in the SBR compound than that of micro-ZnO, reduced the vulcanization time by 20 min and increased the crosslink density of the vulcanizates. ILs, especially chlorides and hexafluorophosphates, produced a further reduction in the vulcanization time to 12 min, and additionally increased the number of crosslinks in the elastomer network. Moreover, ILs decreased the onset temperature of the SBR vulcanization process by 20–30°C compared to that of rubber compounds without ionic liquids. The tensile strength of SBR vulcanizates that contain ZnO nanoparticles and alkylimidazolium salts was similar to or higher than the TS value of conventionally crosslinked vulcanizates. Furthermore, an improvement in the resistance of SBR to thermo-oxidative aging and UV radiation was achieved by reducing the intensity of the crosslinking reactions during the aging process. The activity of ILs and their influence on the useful properties of vulcanizates depends on the type of elastomer. In the case of SBR, the most significant effect was obtained with chlorides, whereas for EPDM elastomer, the most active ILs were chlorides and tetrafluoroborates. This could be a result of the superior miscibility of these ILs with SBR and EPDM elastomers, which was also observed during the preparation of rubber compounds using two roll mills.

The next area of interest of new systems for activating sulfur vulcanization is related to the application of ILs to the GRAS group (generally regarded as safe). These ILs are generally recognized as environmentally friendly and safe for human health. ILs of interest for this purpose include anions of nonnutritive sweeteners such as saccharinate and acesulfame, or pharmaceutically active anions such as lactate [72–74]. These are currently used as additives in food or pharmaceutical products and are approved by most national health agencies. Moreover, these ILs are thermally stable at vulcanization temperatures (160°C). It was observed that, similar to the ILs discussed above, these salts exhibited catalytic activity during the vulcanization process and improved the degree of dispersion of zinc oxide nanoparticles and filler (silica) in SBR [38]. It can be postulated that the IL/ZnO interactions consist of hydrogen bonding between Zn-OH or Zn-O located on the outside of the zinc oxide crystals and the anion or cation, respectively, of the ionic liquid. Similar interactions were described for Si-OH (Al-OH) or Si-O (Al-O) groups present on HNTs [48]. Hydrogen bonding in IL/ZnO results in reduced interactions between zinc oxide particles, preventing them from agglomerating. The GRAS ILs used in this research produced a 4-fold reduction in the SBR vulcanization

time with respect to that of the rubber compounds that contained micro-sized ZnO, and a two-fold reduction compared with compounds that contained nano-sized ZnO. The greatest activity in the crosslinking process was produced with didecyldimethylammonium lactate (DDAL), which allowed for the shortest time, lowest temperature, and highest energy effect of vulcanization, thereby demonstrating the high intensity of the vulcanization process. All of the GRAS ILs that were studied improved the tensile strength of vulcanizates. They did not affect the dynamic properties of SBR at temperatures above 25°C or the resistance of SBR to thermo-oxidative aging or long-term UV radiation. A similar relationship was observed with alkylimidazolium, pyrrolidinium, piperidinium, and pyridinium salts [34, 70].

The accelerating effect of ILs on the curing process was also reported by Marzec et al. for XNBR/HT composites that contain 1-butyl-3-methylimidazolium tetrachloroaluminate ( $\text{BmiAlCl}_4$ ) [58]. This ionic liquid considerably shortened the scorch time and optimal vulcanization time of rubber compounds. Moreover, XNBR/HT composites with  $\text{BmiAlCl}_4$  exhibited higher crosslink densities than the reference without an ionic liquid, and the crosslink density increased with the concentration of the  $\text{BmiAlCl}_4$ .

The effect of the type and concentration of hydrophilic imidazolium ILs, such as 1-ethyl-3-methylimidazolium thiocyanate ( $\text{EmiSCN}$ ) and 1-methyl-3-octylimidazolium chloride ( $\text{OmiCl}$ ), on the curing kinetics of NBR filled with silica was also studied [75]. The torque values during vulcanization of rubber compounds were reported to be inversely proportional to the content of ILs due to their plasticizing action. The accelerating effect of ILs was demonstrated because their inclusion caused a reduction in the scorch time and significantly shortened the curing time of rubber compounds. However, NBR composites with high loadings of both ILs (20 and 30 phr) exhibited reversion during vulcanization. The tensile strength decreased with increasing amounts of both ILs, whereas the elongation at break was the highest for NBRs containing 30 phr of ILs, which was attributed to their plasticizing effect.

## 5. Additional applications of ILs in elastomeric composites

Apart from the main applications of ILs in elastomer composites described above, there are other interesting reports that concern additional applications of ILs in elastomer science or technology.

Tang et al. [76] utilized the phosphonium ionic liquid octadecyltriphenylphosphonium iodide (ODtppI) in a silica-filled SBR matrix as a novel catalyst for the silanization reaction between silica and bis(3-triethoxysilylpropyl)-tetrasulfide (TESPT), a commonly used silane in the tire industry. The silanization of silica plays a vital role in enhancing the compatibility between silica and a rubber matrix, and hence the improvement of the composites' properties. ODtppI reacted with silanol groups on the silica surface to yield more nucleophilic silanolate anions, which promoted a condensation reaction with the ethoxy groups of TESPT, and as a result, improved the extent of silanization. Consequently, the dispersion of silica in the SBR matrix and the interfacial interaction between silica and rubber chains were improved. Moreover, treatment of the silica surface with ODtppI rendered it more hydrophobic; the silica surface thus

became more compatible with a nonpolar hydrocarbon rubber matrix. The SBR composites that contained silica functionalized with TESPT in the presence of an ODtppI exhibited shorter optimal vulcanization times and higher crosslink densities compared with SBR filled with pure silica or with TESPT-modified silica without ODtppI. It was confirmed that silanization prevented the adsorption of curing agents onto the silica surface. Additionally, the phosphonium cation of the ODtppI could act as a secondary accelerator, thereby increasing the curing rate and enhancing the crosslink density of the SBR. Moreover, TESPT acts as a sulfur donor that increases the amount of covalent crosslinks in the elastomer network. Finally, the resulting SBR composites exhibited greater tensile strength, abrasion resistance, or decreased energy loss during rolling of the rubber wheel.

Mouawia et al. [77] developed a process for controlling the metathetic depolymerization of NR in trihexyl-(tetradecyl)phosphonium chloride or N,N'-dioctylimidazolium bromide. This process can produce telechelic polyisoprene oligomers from waste tires. The depolymerization of NR was performed using olefin metathesis reactions in the IL phase under soft conditions, e.g., low temperature, the quantity of ILs, and short reaction times, which promoted the efficient production of telechelic oligomers with low Ru contamination. The catalytic IL phase could be recycled five times, and in each cycle, an efficient and controlled depolymerization of NR to polyisoprene oligomers occurred.

Chen et al. [78] developed highly stretchable, nonvolatile, transparent, and stable ionogels by radical polymerization of acrylic acid in the 1-ethyl-3-methylimidazolium ethylsulfate. This ionogel consisted of a three-dimensional polymer network, which provided an elastic solid form, and the IL enabled electrical conduction. The conductivity of the ionogel was adequate to fabricate electromechanical transducers when used with a dielectric elastomer. Additionally, this ionogel exhibited a low elastic modulus, a large rupturing stretch as well as good mechanical reversibility and negligible degradation after cyclic stretches of large amplitude. These studies confirmed the possibility of using ILs as nonvolatile compliant ionic conductors for dielectric elastomeric transducers.

## 6. Conclusions

Owing to their unique properties, such as thermal and chemical stability, low vapor pressure, non-flammability and high ionic conductivity, ILs have attracted much attention for applications not only in thermoplastics or resins composites, but also in elastomer technologies. An analysis of the recent literature reports indicates that ILs are widely used in elastomeric composites as dispersing agents of fillers, conductive additives, crosslinkers or components of the crosslinking system (vulcanization accelerators or activators), catalysts for the silanization reaction, solvents for the depolymerization of natural rubber, or for the production of highly stretchable ionogels. Because the structure of ILs can be designed for specific applications, it can be expected that the use of ILs in elastomeric composites will continue to increase.

## Acknowledgements

The authors wish to acknowledge the French companies TOTAL S.A. and HUTCHINSON S.A. for supporting this work.

## Conflict of interest

The authors declare no conflict of interest.

## Author details

Anna Sowinska and Magdalena Maciejewska\*

\*Address all correspondence to: [magdalena.maciejewska@p.lodz.pl](mailto:magdalena.maciejewska@p.lodz.pl)

Institute of Polymer and Dye Technology, Lodz University of Technology, Lodz, Poland

## References

- [1] Wasserscheid P, Welton T, editors. *Ionic Liquids in Synthesis*. New York: Wiley-VCH; 2008. ISBN 978-3-527-31239-9
- [2] Holbrey JD, Seddon KR. Ionic liquids. In: *Clean Products Processes*. 1st ed. Belfast: Springer-Verlag; 1999. pp. 223-236. DOI: 10.1007/s100980050036
- [3] Kubisa P. Ionic liquids in the synthesis and modification of polymers. *Journal of Polymer Science Part A: Polymer Chemistry*. 2005;**43**:4675-4683. DOI: 10.1002/pola.20971
- [4] Singha NK, Pramanik NB, Behera PK, Chakrabarty A, Mays JW. Tailor-made thermoreversible functional polymer via RAFT polymerization in an ionic liquid: A remarkably fast polymerization process. *Green Chemistry*. 2016;**18**:6115-6122. DOI: 10.1039/C6GC01677D
- [5] Pernak J, Czepukowicz A, Pozniak R. New ionic liquids and their antielectrostatic properties. *Industrial & Engineering Chemistry Research*. 2001;**40**:2379-2383. DOI: 10.1021/ie000689g
- [6] Yuan C, Guo J, Sia Z, Yan F. Polymerization in ionic liquid-based microemulsions. *Polymer Chemistry*. 2015;**6**:4059-4066. DOI: 10.1039/C5PY00423C
- [7] Vijayaraghavan R, MacFarlane DR. Living cationic polymerization of styrene in an ionic liquid. *Chemical Communications*. 2004;**6**:700-701. DOI: 10.1039/B315100J

- [8] Sarbu T, Matyjaszewski K. ATRP of methyl methacrylate in the presence of ionic liquids with ferrous and cuprous anions. *Macromolecular Chemistry and Physics*. 2001;**202**:3379-3391. DOI: 10.1002/1521-3935(20011101)202:17
- [9] Sun N, Rahman M, Qin Y, Maxim ML, Rodriguez H, Rogers RD. Complete dissolution and partial delignification of wood in the ionic liquid 1-ethyl-3-methylimidazolium acetate. *Green Chemistry*. 2009;**11**:646-655. DOI: 10.1039/B822702K
- [10] Phillips DM, Drummy LF, Conrady DG, Fox DM, Naik RR, Stone MO, Trulove PC, De Long HC, Mantz RA. Dissolution and regeneration of bombyx mori silk fibroin using ionic liquids. *Journal of the American Chemical Society*. 2004;**126**:14350-14351. DOI: 10.1021/ja046079f
- [11] Biswas A, Shogren RL, Stevenson DG, Willett JL, Bhowmik PK. Ionic liquids as solvents for biopolymers: Acylation of starch and zein protein. *Carbohydrate Polymers*. 2006;**66**:546-550. DOI: 10.1016/j.carbpol.2006.04.005
- [12] Regmi BP, Speller NC, Anderson MJ, Brutus JO, Merid Y, Das S, El-Zahab B, Hayes DJ, Murray KK, Warner IM. Molecular weight sensing properties of ionic liquid-polymer composite films: Theory and experiment. *Journal of Materials Chemistry*. 2014;**2**:4867-4878. DOI: 10.1039/C3TC32528H
- [13] Lu X, Huang J, He G, Yang L, Zhang N, Zhao Y, Qu J. Preparation and characterization of cross-linked poly(butylene succinate) by multifunctional toluene diisocyanate-trimethylolpropane polyurethane prepolymer. *Industrial & Engineering Chemistry Research*. 2013;**52**:13677-13684. DOI: 10.1021/ie4020342
- [14] Yuan J, Schlaad H, Giordano C, Antonietti M. Double hydrophilic diblock copolymers containing a poly(ionic liquid) segment: Controlled synthesis, solution property, and application as carbon precursor. *European Polymer Journal*. 2011;**47**:772-781. DOI: 10.1016/j.eurpolymj.2010.09.030
- [15] Pernak J, Smiglak M, Griffin ST, Hough WL, Wilson TB, Pernak A, Zabielska-Matejuk J, Fojutowski J, Kita K, Rogers RD. Long alkyl chain quaternary ammonium-based ionic liquids and potential applications. *Green Chemistry*. 2006;**8**:798-806. DOI: 10.1039/B604353D
- [16] Lin B, Qiu L, Lu J, Yan F. Cross-linked alkaline ionic liquid-based polymer electrolytes for alkaline fuel cell applications. *Chemistry of Materials*. 2010;**22**:6718-6725. DOI: 10.1021/cm102957g
- [17] Sabu T, Ranimol, S. *Rubber Nanocomposites: Preparation, Properties, and Applications*. Singapore: John Wiley & Sons; 2010
- [18] Hilt O, Brom HB, Ahlskog M. Localized and delocalized charge transport in single-wall carbon-nanotube mats. *Physical Review B*. 2000;**R5129**(R):61. DOI: 10.1103/PhysRevB.61.R512
- [19] Fukushima T, Aid T. Ionic liquids for soft functional materials with carbon nanotubes. *Chemistry – A European Journal*. 2007;**13**:5048-5058. DOI: 10.1002/chem.200700554



- [20] Subramaniam K, Das A, Steinhauser D, Klüppel M, Heinrich G. Effect on ionic liquid on dielectric mechanical and dynamic mechanical properties of multi-walled carbon nanotubes/polychloroprene rubber composites. *European Polymer Journal*. 2011;**47**:2234-2243. DOI: 10.1016/j.eurpolymj.2011.09.021
- [21] Das A, Stockelhuber KW, Jurk R, Fritzsche J, Klüppel M, Heinrich G. Coupling activity of ionic liquids between diene elastomers and multi-walled carbon nanotubes. *Carbon*. 2009;**47**:3313-3321. DOI: 10.1016/j.carbon.2009.07.052
- [22] Kreyenschulte H, Richter S, Götze T, Fischer D, Steinhauser D, Klüppel M, Heinrich G. Interaction of 1-allyl-3-methylimidazolium chloride and carbon black and its influence on carbon black filled rubbers. *Carbon*. 2012;**50**:3649-3658. DOI: 10.1016/j.carbon.2012.03.037
- [23] Fukushima T, Kosak A, Ishimura Y, Yamamoto T, Takigawa T, Ishii N, Aida T. Molecular ordering of organic molten salts triggered by single-walled carbon nanotubes. *Science*. 2003;**300**:2072-2074. DOI: 10.1126/science.1082289
- [24] Xu P, Wang X, Hu Y, Ding Y. Piezoresistive properties of nanocomposites based on silicone rubber and ionic liquid-functionalized carbon black. *Material Letters*. 2016;**182**:218-222. DOI: 10.1016/j.matlet.2016.06.097
- [25] Young RJ, Kinloch IA, Gong KS, Novoselov KS. The mechanics of graphene nanocomposites: A review. *Composites Science and Technology*. 2012;**72**:1459-1476. DOI: 10.1016/j.compscitech.2012.05.005
- [26] Sadasivuni KK, Ponnamma D, Thomas S, Grohens Y. Evolution from graphite to graphene elastomer composites. *Progress in Polymer Science*. 2014;**39**:749-780. DOI: 10.1016/j.progpolymsci.2013.08.003
- [27] Yang H, Shan C, Li F, Han D, Zhang Q, Niu L. Covalent functionalization of polydisperse chemically-coverted graphene sheets with amine-terminated ionic liquid. *Chemical Communications*. 2009;**26**:3880-3882. DOI: 10.1039/B905085J
- [28] Xiong X, Wang J, Jia H, Fang E, Ding L. Structure, thermal conductivity, and thermal stability of bromobutyl rubber nanocomposites with ionic liquid modified graphene oxide. *Polymer Degradation and Stability*. 2013;**98**:2208-2214. DOI: j.polymdegradstab.2013.08.022
- [29] Vitiello R, Tesser R, Turco G, Santacesaria E, Compagnone G, Di Serio M. A critical review on analytical methods and characterization of butyl and bromobutyl rubber. *International Journal of Polymer Analysis and Characterization*. 2017;**22**:348-360. DOI: 10.1080/1023666X.2017.1297887
- [30] Dunlap CJ, Carr PW, McNaff CV, Stoll D. Zirconia stationary phases for extreme separations. *Analytical Chemistry*. 2001;**73**:598A-607A. DOI: 10.1021/ac012530z
- [31] Nassivera T, Eklund AG, Landry CC. Size-exclusion chromatography of low molecular-mass polymers using mesoporous silica. *Journal of Chromatography A*. 2002;**973**:97-101. DOI: 10.1016/S0021-9673(02)01200-1

- [32] Hanai T, Homma H. Computational chemical prediction of the retention factor of aromatic acid. *Journal of Liquid Chromatography & Related Technologies*. 2002;**25**:1661-1676. DOI: 10.1081/JLC-120005713
- [33] Zhang Y, Zhen B. Fast response and monodisperse silica nanoparticles modified with ionic liquid towards electrophoretic displays. *Dyes and Pigments*. 2018;**148**:270-275. DOI: 10.1016/j.dyepig.2017.09.014
- [34] Maciejewska M, Krzywania-Kaliszewska A, Zaborski M. Elastomer composites containing ionic liquids. *Polimery*. 2015;**7-8**:501-507. DOI: 10.14314/polimery.2015.501
- [35] Marwanta E, Mizumo T, Nakamura N, Ohno H. Improved ionic conductivity of nitrile-rubber/ionic liquid composites. *Polymer*. 2005;**46**:3795-3800. DOI: 10.1016/j.polymer.2005.02.113
- [36] Lei YD, Tang ZH, Guo BC, Zhu LX, Wan JJ, Jia DM. Synthesis of novel functional liquid and its application as a modifier in SBR/silica composites. *eXPRESS Polymer Letters*. 2010;**4**:692-703. DOI: 10.3144/expresspolymlett.2010.84
- [37] Zhou Y, Schattka JH, Antonietti M. Room temperature ionic liquids as template to monolithic mesoporous silica with wormlike pores via a sol-gel nano-casting technique. *Nano Letters*. 2004;**4**:477-481. DOI: 10.1021/nl025861f
- [38] Maciejewska M, Zaborski M. Thermal analysis and mechanical methods applied to studying properties of SBR compounds containing ionic liquids. *Polymer Testing*. 2017;**61**:349-363. DOI: 10.1016/j.polymertesting.2017.05.041
- [39] Alexandre M, Dubois P. Polymer-layered silicate nanocomposites: Preparation, properties and uses of a new class of materials. *Materials and Engineering Science*. 2000;**28**:1-65. DOI: 10.1016/S0927-796X(00)00012-7
- [40] Vaia RA, Ishii H, Giannelis EP. Synthesis and properties of two-dimensional nanostructures by direct intercalation of polymer melts in layered silicates. *Chemistry of Materials*. 1994;**5**:1694-1696. DOI: 10.1021/cm00036a004
- [41] Liang Y, Cao W, Zhang X, Tan Y. Preparation and properties of nanocomposites based on different polarities of nitrile-butadiene rubber with clay. *Journal of Applied Polymer Science*. 2009;**112**:3087-3094. DOI: 10.1002/app.29575
- [42] Ha JU, Xanthos M. Functionalization of nanoclays with ionic liquids for polypropylene composites. *Polymer Composites*. 2009;**30**:534-542. DOI: 10.1002/pc.20583
- [43] Letaief S, Elboki TA, Detellier C. Reactivity of ionic liquids with kaolinite: Melt intercalation of ethyl pyridinium chloride in an urea-kaolinite pre-intercalate. *Journal of Colloid and Interface Science*. 2006;**302**:254-258. DOI: 10.1016/j.jcis.2006.06.008
- [44] Fontana JP, Camilo FC, Bizeto MA, Faez R. Evaluation of the role of an ionic liquid as organophilization agent into montmorillonite for NBR rubber composite production. *Applied Clay Science*. 2013;**83**:203-209. DOI: 10.1016/j.clay.2013.09.002

- [45] Du ML, Guo BC, Jia DM. Carboxylated butadiene-styrene rubber/halloysite nanotube: Nanocomposites: Interfacial interaction and performance. *Polymer*. 2008;**49**:4871-4876. DOI: 10.1016/j.polymer.2008.08.042
- [46] Guo BC, Liu XL, Zhou WY, Lei YD, Jia DM. Adsorption of ionic liquid onto halloysite nanotubes: Mechanism and reinforcement of the modified clay to rubber. *Journal of Macromolecular Science*. 2010;**49**:1029-1043. DOI: 10.1080/00222341003609823
- [47] Mroziak W, Jungnickel C, Skup M, Urbaszek P, Stepnowski P. Determination of the adsorption mechanism of imidazolium-type ionic liquids onto kaolinite, implications for their fate and transport in the soil environment. *Environmental Chemistry*. 2008;**5**:299. DOI: 10.1071/EN08015
- [48] Lei Y, Tang Z, Guo B, Jia D. Functional thiol ionic liquids as a novel interfacial modifiers in SBR/HNTs composites. *Polymer*. 2011;**52**:1337-1344. DOI: 10.1016/j.polymer.2011.01.024
- [49] Guo B, Lei Y, Chen F, Liu X, Du M, Jia D. Styrene-butadiene rubber/halloysite nanotubes nanocomposites modified by methacrylic acid. *Applied Surface Science*. 2008;**255**:2715-2722. DOI: 10.1016/j.apsusc.2008.07.188
- [50] Masłowski M, Zaborski M. The influence of surfactants and ionic liquids on the mechanical and magnetic properties of ethylene-propylene copolymers filled with micrometer and nanometer magnetite. *Polimery*. 2011;**56**:743-748
- [51] Gray FM. *Solid Polymer Electrolytes: Fundamentals and Technological Applications*. New York: Wiley-VCH; 1991
- [52] Forsyth S, Golding J, MacFarlane DR, Forsyth M. N-methyl-N-alkylpyrrolidinium tetrafluoroborate salts: Ionic solvents and solid electrolytes. *Electrochimica Acta*. 2001;**46**:1753-1757. DOI: 10.1016/S0013-4686(00)00781-7
- [53] Likozar B. The effect of ionic liquid type on the properties of hydrogenated nitrile elastomer/hydroxyl-functionalized multi-walled carbon nanotube/ionic liquid composites. *Soft Matter*. 2011;**7**:970-977. DOI: 10.1039/c0sm00759e
- [54] Marwanta E, Mizumo T, Ohno H. Improved ionic conductivity of nitrile rubber/ $\text{Li}(\text{CF}_3\text{SO}_2)_2\text{N}$  composites by adding imidazolium-type zwitterion. *Solid State Ionics*. 2007;**178**:227-232. DOI: 10.1016/j.ssi.2006.12.022
- [55] Cho M, Seo H, Nam J, Choi H, Koo J, Lee Y. High conductivity and mechanical strength of solid polymer electrolytes based on NBR/ionic liquid and its application to an electrochemical actuator. *Sensors and Actuators B: Chemical*. 2007;**128**:70-74. DOI: 10.1016/j.snb.2007.05.032
- [56] Goujon LJ, Khaldi A, Maziz A, Plesse C, Nguyen GTM, Aubert P-H, Vidal F, Chevrot C, Teyssié D. Flexible solid polymer electrolytes based on nitrile butadiene rubber/poly(ethylene oxide) interpenetrating polymer networks containing either LiTFSI or EMITFSI. *Macromolecules*. 2011;**44**:9683-9691. DOI: 10.1021/ma201662h

- [57] Matchawet S, Kaesaman A, Vennemann N, Kumerlöve C, Nakason C. Effects of imidazolium ionic liquid on cure characteristics, electrical conductivity and other related properties of epoxidized natural rubber vulcanizates. *European Polymer Journal*. 2017;**87**:344-359. DOI: 10.1016/j.eurpolymj.2016.12.037
- [58] Marzec A, Laskowska A, Boiteux G, Zaborski M, Gain O, Serghei A. Properties of carboxylated nitrile rubber/hydrotalcite composites containing imidazolium ionic liquids. *Macromolecular Symposia*. 2014;**341**:7-17. DOI: 10.1002/masy.201300149
- [59] Subramaniam K, Das A, Heinrich G. Development of conducting polychloroprene rubber using imidazolium based ionic liquid modified multi-walled carbon nanotubes. *Composites Science and Technology*. 2011;**71**:1441-1449. DOI: 10.1016/j.compscitech.2011.05.01
- [60] Jiji A, Mohammed AP, Priti X, Suryasarathi B, Soney CG, Nandakumar K, Sabu T. Investigation into dielectric behaviour and electromagnetic interference shielding effectiveness of conducting styrene butadiene rubber composites containing ionic liquid modified MWCNT. *Polymer*. 2017;**112**:102-115. DOI: 10.1016/j.polymer.2017.01.078
- [61] Phan CH, Jaafar M, Koh YH. Mild functionalization of carbon nanotubes filled epoxy composites: Effect on electromagnetic interferences shielding effectiveness. *Journal of Applied Polymer Science*. 2015;**132**:42557. DOI: 10.1002/app.42557
- [62] Jiji A, Mohammed AP, Lekshmi K, Nandakumar K, Soney CG, Sabu T. Developing highly conducting and mechanically durable styrene butadiene rubber composites with tailored microstructural properties by a green approach using ionic liquid modified MWCNTs. *RSC Advances*. 2016;**6**:32493-32504. DOI: 10.1039/C6RA01886F
- [63] Lin L, Liu S, Zhang Q, Li X, Ji M, Deng H, Fu Q. Towards tunable sensitivity of electrical property to strain for conductive polymer composites based on thermoplastic elastomer. *ACS Applied Materials and Interfaces*. 2013;**5**:5815-5824. DOI: 10.1021/am401402x
- [64] Behera PK, Usha KM, Guchhait PK, Jehnichen D, Das A, Voit B, Singha NK. A novel ionomeric polyurethane elastomer based on ionic liquid as crosslinker. *Royal Society of Chemistry Advance*. 2016;**6**:99404-99413. DOI: 10.1039/C6RA21650A
- [65] Maciejewska M, Walkiewicz F, Zaborski M. Novel ionic liquids as accelerators for the sulphur vulcanisation of butadiene-styrene elastomer composites. *Industrial & Engineering Chemistry Research*. 2013;**52**:8410-8415. DOI: 10.1021/ie303167z
- [66] Pernak J, Walkiewicz F, Maciejewska M, Zaborski M. Ionic liquids as vulcanization accelerators. *Industrial & Engineering Chemistry Research*. 2010;**49**:5012-5017. DOI: 10.1021/ie100151n
- [67] Maciejewska M, Walkiewicz F. Ionic liquids in the vulcanization of elastomers. In: Handy S, editor. *Ionic Liquids – Current State of the Art*. Rijeka: InTech Europe; 2015. pp. 591-622. DOI: 10.5772/59064
- [68] Maciejewska M, Zaborski M, Kordala R, Walkiewicz F. Ionic liquids as accelerators in elastomer vulcanization. *Przemysł Chemiczny*. 2010;**89**:1470-1474

- [69] Maciejewska M, Zaborski M. Ionic liquids applied to improve the dispersion of solids in elastomers. In: Handy S, editor. *Ionic Liquids – Current State of the Art*. Rijeka: InTech Europe; 2015. pp. 557-589. DOI: 10.5772/58980
- [70] Maciejewska M, Zaborski M. Effect of ionic liquids on the dispersion of zinc oxide and silica nanoparticles, vulcanisation behaviour and properties of NBR composites. *eXPRESS Polymer Letters*. 2014;8:932-940. DOI: 10.3144/expresspolymlett.2014.94
- [71] Maciejewska M, Walkiewicz F, Zaborski M. Ionic liquids as accelerators of elastomer vulcanization. *Przemysł Chemiczny*. 2013;92:1627-1629
- [72] Pernak K, Stefaniak F, Weglewski J. Phosphonium acesulfamate based ionic liquids. *European Journal of Organic Chemistry*. 2005;4:650-652. DOI: 10.1002/ejoc.200400658
- [73] Stasiewicz M, Fojutowski A, Kropacz A, Pernak J. 1-Alkoxymethyl-X-dimethylaminopyridinium-base ionic liquids in wood preservation. *Holzforschung*. 2008;6:309-317. DOI: 10.1515/HF.2008.028
- [74] Hough-Troutman WL, Smigla M, Griffin S, Reichert WM, Mirska I, Jodynis-Liebert J, Adamska T, Nawrot J, Stasiewicz M, Rogers RD. Ionic liquids with dual biological function: Sweet and anti-microbial, hydrophobic quaternary ammonium-based salts. *New Journal of Chemistry*. 2009;33:26-33. DOI: 10.1039/B813213P
- [75] Marzec A, Laskowska A, Boiteux G, Zaborski M, Gain O, Serghei A. The impact of imidazolium ionic liquids on the properties of nitrile rubber composites. *European Polymer Journal*. 2014;53:139-146. DOI: 10.1016/j.eurpolymj.2014.01.035
- [76] Tang Z, Huang J, Wu X, Guo B, Zhang L, Liu F. Interface engineering toward promoting silanization by ionic liquid for high-performance rubber/silica composites. *Industrial & Engineering Chemistry Research*. 2015;54:10747-10756. DOI: 10.1021/acs.iecr.5b03146
- [77] Mouawia A, Nourry A, Gaumont A-C, Pilard J-F, Dez I. Controlled metathetic depolymerisation of natural rubber in ionic liquids: From waste tires to telechelic polyisoprene oligomers. *ACS Sustainable Chemistry & Engineering*. 2017;5:696-700. DOI: 10.1021/acssuschemeng.6b01777
- [78] Chen B, Lu JJ, Yang CH, Yang JH, Zhou J, Chen YM, Suo Z. Highly stretchable and transparent ionogels as non-volatile conductors for dielectric elastomer transducers. *ACS Applied Materials & Interfaces*. 2014;6:7840-7845. DOI: 10.1021/am501130t



---

# Metal Extraction with Ionic Liquids-Based Aqueous Two-Phase System

---

Pius Dore Ola and Michiaki Matsumoto

Additional information is available at the end of the chapter

<http://dx.doi.org/10.5772/intechopen.77286>

---

## Abstract

Although ionic liquids (ILs) have excellent properties, their use as extractants in solvent extraction has not completely overcome the problems encountered when organic solvents are used. In conventional solvent extraction, a hydrophobic IL should be used to establish an IL/water biphasic system to replace the conventional organic solvent with ILs. However, the number of water-immiscible ILs is currently limited, and most contain fluorinated anions which are expensive and environmentally nonbenign. Furthermore, the use of an organic solvent as a diluent agent cannot be avoided because of the very high viscosity of ILs. An IL-based aqueous two-phase system (ATPS) can overcome these drawbacks. This chapter summarizes the use of an IL-based ATPS for the separation of metals used in various areas of human life.

**Keywords:** aqueous two-phase system, metal extraction, solvent extraction, ionic liquid

---

## 1. Introduction

Solvent extraction is the most commonly used method to separate metal ions. This technique is performed by mixing the aqueous phase containing metal salt with an organic phase containing an extraction agent (extractant) [1]. The simplicity with which the parameters controlling extraction, such as pH of the aqueous solution, extractants and diluent, can be changed is a major advantage of solvent extraction [2]. However, it is not environmentally friendly as it requires a large volume of organic solvents which are often toxic and/or flammable. Using ILs, with their excellent properties such as near-zero vapor pressure, good chemical and thermal stability and the tunability of their physicochemical properties by altering the substitutive groups, may overcome the problems of organic solvents [3].

---

In conventional solvent extraction, a hydrophobic IL should be used to create an IL/water biphasic system to replace the conventional organic solvent with ILs. However the number of water-immiscible ILs is currently limited, and most contain fluorinated anions which are expensive and environmentally nonbenign, such as  $\text{PF}_6^-$ , which can decompose to a dangerous HF gas in the presence of water [4]. Furthermore, the use of organic solvent as a diluent cannot be avoided because of the very high viscosity of ILs [5]. On the other hand, the use of ILs as an extractant in conventional solvent extraction has not completely resolved the drawbacks encountered when organic solvents are used as diluents. An IL-based aqueous two-phase system (ATPS) can overcome these disadvantages. This chapter summarizes the use of an IL-based ATPS for the separation of metals. Metals are widely used in many aspects of human life, and their existence in the environment at high concentrations is a cause for concern. For a better understanding of this topic, we will begin with a brief discussion of ILs and ATPSs.

## 2. Extraction of metal ions

Metal ion extraction is a hot topic and is important economically and environmentally. Metals are obtained from ores or scraps through metallurgical processes and then manufactured into final products used by humans, either directly or indirectly. The processing of raw materials into final products produces waste containing metal ions. These products are utilized and later discarded as waste. Metal ion extraction is an effort to recover the metal ions both from ores and from waste due to their limited availability in nature. In addition, metal ion extraction from metal-containing waste can reduce the level of environmental pollution. Therefore, an effective, efficient, economic and environmentally friendly method for the recovery of metal ions from ores and waste is an absolute necessity.

A number of processes have been explored for metal ion recovery, such as precipitation [6], reverse osmosis [7], adsorption [8], ion exchange [9] and solvent extraction using organic solvents [10]. Solvent extraction (liquid-liquid extraction) is the most commonly used method for the separation of metal ions [2]. In this technique, the aqueous solution of metal salt is mixed with an organic solvent containing an extraction agent (extractant). The metal ions form a hydrophobic complex with the extractant and migrate to the organic phase. The migration of complexes from the aqueous to the organic phase is driven by the difference of the complexes' affinity towards the aqueous phase and organic phase, as well as the relative solubility of the complexes in both phases. Solvent extraction can be implemented in a continuous mode and is suitable for the processing of high metal feed concentrations. However, the main disadvantage of this method is that it uses a large amount of organic solvents, such as kerosene, toluene, dichloromethane or diethyl ether, which are often toxic and/or flammable and therefore environmentally unfriendly [2]. Not only are their volatility and flammability an issue, but these organic solvents also have a negative impact on human health if their vapors are emitted into the air. ILs can be used to solve the problem faced when organic solvents are used as extractants in conventional liquid-liquid extraction.

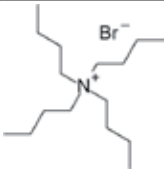
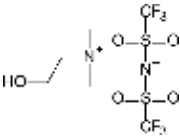
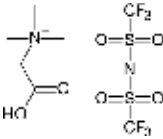


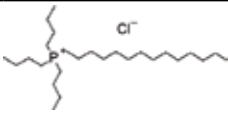
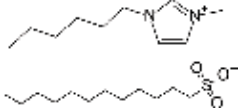
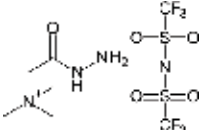
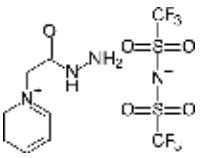
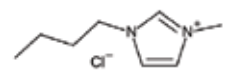
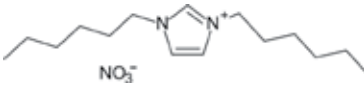
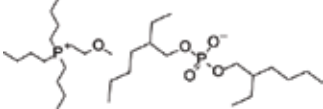
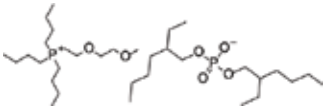
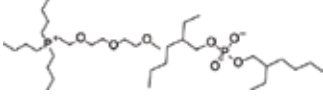
### 3. Ionic liquid and aqueous two-phase system

Ionic liquids (ILs), according to the widely accepted definition, are molten salts under 100°C. The most investigated ILs are comprised of organic cation such as imidazolium, pyridinium, pyrrolidinium, phosphonium and ammonium, and their counterions can be either inorganic (e.g. tetrafluoroborate, hexafluorophosphate, chloride) or organic (e.g. trifluoromethylsulfonate, bis[(trifluoromethyl) sulfonyl]imide) anions [11]. ILs possess many unique physicochemical properties such as low vapor pressure, high thermal stability, high viscosity, good solvation ability, wide electrochemical windows, wide liquid range and tunable polarity [3, 12]. Tuning of these properties by combining the cations and anions makes ILs unique compounds for applications in different areas [13]. With these properties, using ILs instead of organic solvents as extractants in solvent extraction can reduce the negative impact on the environment.

The application of ILs in metal ion extraction is very promising. The main problem is their solubility in the aqueous phase, which can decrease the extraction efficiency. To overcome this issue, a hydrophobic IL can be used. However, hydrophobic ILs are partly soluble in the acidic aqueous solutions from which metal ions are extracted, which results in a costly undesirable loss [14]. In addition, hydrophobic ILs are still limited, and most contain fluorinated anions which can be expensive and environmentally nonbenign [5, 15]. Due to the very high viscosity of ILs, the diffusion of solute from the aqueous to the organic phase probably is slow, thus requiring either a longer stirring time [16] or an organic solvent which can be flammable and toxic as diluent agent. An ATPS can resolve the issues associated with the hydrophobic properties and high viscosity limitations. By using the ATPS, a more hydrophilic IL can be employed as the extractant because this technique needs a water-soluble IL. The ILs used in the ATPS are listed in **Table 1**.

The ATPS was accidentally discovered by Martinus Willem Beijerinck (1896) whilst mixing an aqueous solution of starch and gelatin. However, its real application was developed by Per-Åke

Acronym	Chemical name	Molecule structure	
TBAB	Tetrabutylammonium bromide		(b) (c)
[Chol][NTf <sub>2</sub> ]	Choline bis(trifluoromethylsulfonyl) imide		(a) (d)
[Hbet][NTf <sub>2</sub> ]	Betainium bis(trifluoromethylsulfonyl) imide		(a) (d)

Acronym	Chemical name	Molecule structure	
[P <sub>44414</sub> ][Cl]	Tributyltetradecyl phosphonium chloride		(b) (d)
[C <sub>6</sub> C <sub>1</sub> im][C <sub>12</sub> SO <sub>3</sub> ]	1-Hexyl-3-methyl imidazolium dodecyl sulfonate		(b) (c)
[Nxyzhcm][NTf <sub>2</sub> ] Girard's T cation	(Hydrazinocarbonylmethyl) trimethylammonium bis(trifluoromethylsulfonyl)imide		(b) (d)
[Phcm] [NTf <sub>2</sub> ] Girard's P cation	(Hydrazinocarbonylmethyl)pyridinium bis(trifluoromethylsulfonyl)imide		(b) (d)
[C <sub>4</sub> C <sub>1</sub> im]Cl	1-Butyl-3-methylimidazolium chloride		(b) (c)
[C <sub>6</sub> C <sub>6</sub> im][NO <sub>3</sub> ]	1,3-Dihexylimidazolium nitrate		(b) (d)
[P <sub>444</sub> E][DEHP]	Tri-n-butyl-2-methoxyethylphosphonium bis(2-ethylhexyl)phosphate		(b) (d)
	Tri-n-butyl[2-(2-methoxyethoxy)ethyl]phosphonium bis(2-ethylhexyl)phosphate		
	Tri-n-butyl-[2-[2-(2-methoxyethoxy)ethoxy]ethyl]phosphonium bis(2-ethylhexyl)phosphate		

**Table 1.** Ionic liquids employed in ATPS for separation of metal ions with (a) or without (b) an extra extractant other than IL, with (c) or without (d) a salting-out agent.

Albertsson [17]. Under specific thermodynamic conditions, an ATPS is spontaneously formed by mixing the aqueous solutions of two chemically different hydrophilic polymers or by combining the aqueous solutions of a polymer and an electrolyte, which in turn separate two immiscible aqueous phases in equilibrium—a polymer-enriched top phase and a polymer or an electrolyte-enriched bottom phase [18]. The phase separation of the polymer-polymer

system is derived by the steric exclusion of large aggregates generated by the interaction between the polymer and water. With a polymer-salt ATPS, the salt absorbs a large amount of water, and the similar steric exclusion occurs [19].

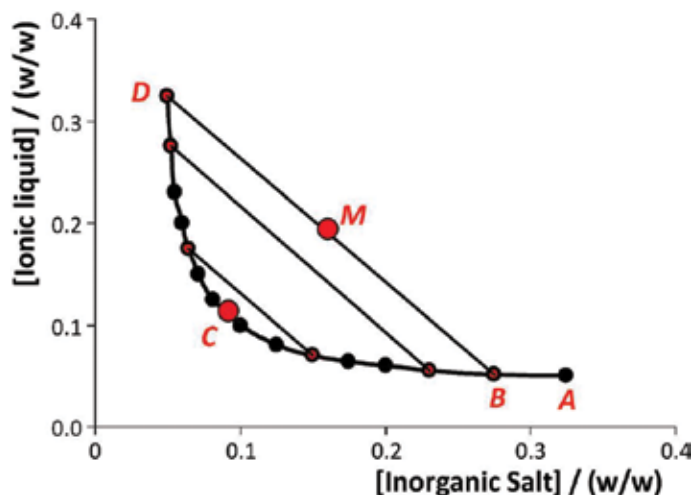
Conventional polymer-based ATPSs have been largely exploited since the 1980s and mainly consist of mixtures of two incompatible polymers or a polymer and a salt that induces salting out. However, the use of polymer-based ATPS for separation is restricted by the similarity in the polarities of the two phases. By using ILs instead of polymer, it is easier to adjust the polarity phases by changing the substitutive groups of ILs [15, 20].

In the past few years, research on biphasic systems with ILs has received crucial attention for the development of novel and more efficient separation processes [21]. The phase separation of systems composed of ILs and water can be induced by temperature. These systems are characterized by either an upper critical solution temperature (UCST) or a lower critical solution temperature (LCST). At a temperature higher than the UCST, the organic phase (ILs) is completely miscible with water, and a homogeneous solution is obtained. Application of this method for metal ion separation allows the reaction between the metal complex and ILs to occur at the entire volume of the solution and does not depend on the metal complex' diffusion from the aqueous to the organic phase, which is slower due to the high viscosity of ILs. Therefore, mixture stirring and organic solvents are unnecessary. In other words, the reaction rate is only determined by the kinetics of the chemical reactions [22]. Upon cooling, the phases separate, and the metal complex is extracted to the organic phase. In a system with an LCST, a homogeneous mixture is formed at temperatures below the LCST, and it returns to a two-phase system when its temperature is higher than the LCST. These temperature-dependent phase transitions, known as homogeneous liquid-liquid extraction (HLL), coalescence extraction or phase-transition extraction, have proven to be highly advantageous in the selective separation of metals [23]. Because HLL is composed mainly of water and no organic solvent is needed, which is a feature of the classical ATPS, we believe that HLL can be categorized as a more recent ATPS. In HLL, a salting-out agent is not needed because phase separation is induced by temperature (temperature-dependent separation). In the next section, we will discuss several articles reporting the extraction of metals using an ATPS composed of ILs with and without a salting-out agent.

## 4. IL-based ATPS for metal separation

### 4.1. ATPS with salting-out agent

As with ATPSs in general, an ATPS composed of ILs and a salting-out agent has a unique phase diagram under a particular set of conditions, such as pH and temperature (**Figure 1**). This phase diagram, known as a binodal curve, is like a fingerprint identifying the potential working area of the ATPS. In this example (**Figure 1**), the total composition of the mixture, the composition of each phase and the critical point are defined as M, D, B and C, respectively. The total mixture compositions above the binodal curve fall into the biphasic regime, whereas mixture compositions below the solubility curve are homogeneous [15]. The salting-out agent



**Figure 1.** Phase diagram for a hypothetical system composed of polymer + inorganic salt + water (weight fraction units).

in ATPS is employed to separate the more hydrophobic agents from the more hydrophilic one. The general salting-out agents used in combination with ILs include inorganic salt [24], carbohydrates [25] and polymer [26]. However, to the best of our knowledge, carbohydrates have not been used as salting-out agents for metal ion extraction in combination with ILs.

Ammonium sulphate was used as a salting-out agent incorporated with tetrabutylammonium bromide (TBAB) for Cr (VI) separation. The results showed that the extraction of Cr (VI) was influenced by pH due to the existence of  $\text{HCrO}_4^-$  as the predominant species at pH 5.5. Therefore, Cr (VI) was satisfactorily extracted into the upper phase at pH 5, where its extraction percentage was found to be 93–98% with the following extraction mechanism:



On the other hand, the extraction percentage of Cr (III) was below 1.0% in all cases, indicating that this system was very selective when used for separating Cr (VI) from Cr (III). The  $(\text{NH}_4)_2\text{SO}_4$  increase resulted in an increase in the extraction of Cr (VI) attributed to the progressive increase in the hydrophobicity of upper phase [27]. This system was also used to separate cadmium from cobalt, copper, iron (III) and zinc. The upper phase permitted the complete extraction of  $\text{Cd}^{2+}$  over the widest possible ranges of pH (1–10) with recovery in the range of 91–99%. Almost complete extraction of  $\text{Cd}^{2+}$  was obtained even though the concentration of  $\text{Cd}^{2+}$  in the mixture was far lower (20  $\mu\text{g}$ ) than the concentration of  $\text{Co}^{2+}$ ,  $\text{Cu}^{2+}$ ,  $\text{Fe}^{3+}$  and  $\text{Zn}^{2+}$  (2 mg for each) which coexisted with  $\text{Cd}^{2+}$ . The proposed method also successfully detected trace Cd in zinc nitrate [28]. In collaboration with tributyl(tetradecyl)phosphonium chloride  $[\text{P}_{44414}][\text{Cl}]$ , a certain concentration of sodium chloride also underwent temperature-induced phase separation (TIPS); thus it can be considered a thermomorphic mixture applicable to HLLC (IL-ABS-HLLE).

A system composed of 40%  $[\text{P}_{44414}][\text{Cl}]$  and lower than 11% NaCl showed the LCST and therefore has been used to separate Co (II) and Ni (II). Ni (II) was only poorly extracted to the IL-rich phase (distribution ratio,  $D = 0.1$ ), and extraction did not improve with increased NaCl

content in the mixture up to 11 wt%. On the other hand, Co (II) extraction improved, with *D* values up to 100 at 11 wt% NaCl. This is because Co (II) easily forms extractable anionic chloride complexes, whilst Ni (II) does not, even at high chloride concentrations [29].

In the case of polymer salting out, Zheng et al. reported the use of polyethylene glycol (PEG) incorporated with 1-hexyl-3-methyl imidazolium dodecyl sulfonate ( $[C_6C_1im][C_{12}SO_3]$ ) IL for the extraction of gold (III) from an aqueous solution. Gold (III) was quantitatively extracted to the IL phase in the range of pH 1.13–1.90 with extraction percentages of 97.56% (PEG 6000), 76.60% (PEG 4000) and 71.83% (PEG 2000) in 5 min, and thereafter the extraction was not related to vibration time. It was also confirmed that the extractability of gold (III) was derived by the reaction between the cation of IL with the gold chloro complex anion [30].

An IL-based ATPS with a salting-out agent was also successfully applied to the separation of radioactive elements. An ATPS composed of 1-butyl-3-methylimidazolium chloride,  $[C_4C_1im]Cl$  and  $K_2HPO_4$  separated no-carrier-added (NCA)  $^{109}Cd$  which was produced by irradiation of the  $^{nat}Ag$  target with a  $\alpha$ -particle from bulk Ag. The salt-rich phase was predominantly alkaline as a result of the hydrolysis of  $K_2HPO_4$  to produce KOH and  $H_3PO_4$ . Therefore, both  $Ag^+$  and  $Cd^{2+}$  were in anionic form, i.e.,  $Ag(OH)_2^-$  and  $Cd(OH)_4^{2-}$  which then reacted with the cation of IL. However, the affinity of  $Ag(OH)_2^-$  to the IL cation is greater than  $Cd(OH)_4^{2-}$ ; thus, the extractability of bulk Ag was higher. Under optimum conditions, the extraction percentage of both the bulk Ag and NCA  $^{109}Cd$  in the IL phase reached 87% for bulk Ag and 4% for NCA  $^{109}Cd$ , respectively, and an overall separation of 91% NCA  $^{109}Cd$  free from bulk Ag was finally achieved by re-extraction twice with 0.1 mL IL to free from the bulk Ag of the salt-rich phase [31].

Thus far in our search, an ATPS with a salting-out agent for metal ion separation is still limited. However, the application of ILs in collaboration with a salting-out agent reported in the above studies confirms that an ATPS consisting of ILs and a salting-out agent is a highly efficient and selective means of separating metal ions.

#### 4.2. ATPS without salting-out agent (HLLC)

Chemical separation methods aim to simplify and miniaturize sample preparation procedures to consume fewer solvents and reagents and drastically reduce laboratory waste [32]. Unconventional liquid-liquid extractions such as HLLC have been developed with this intent [33]. Probably because HLLC does not require a salting-out agent, this method is more often used in metal ion separation than an ATPS with a salting-out agent. IL is mixed with an aqueous solution of metal ions and heated to a temperature higher than the UCST (for mixtures with a UCST) or cooled to lower than the LCST (for mixtures with an LCST) to obtain a homogeneous solution. The temperature of the solution is then returned to its original temperature allowing for phase separation. This technique sometimes requires an extra extractant in addition to the ILs in order to increase the extraction percentage. In this case, the IL only acts as a separator agent. Choline hexafluoroacetylacetonate and betaine, whose structures are shown in **Figure 2**, have been widely applied as extractants for metal ion separation using the HLLC technique.

Choline bis(trifluoromethylsulfonyl)imide  $[Chol][Tf_2N]$ , in combination with choline hexafluoroacetylacetonate  $[Chol][hfac]$  as specific chelating agents mixed with water that displays thermomorphic behaviour with a UCST of 72°C, has been employed for neodymium (III)



**Figure 2.** Molecule structures of the extractants applied in HLE for metal ion extraction.

extraction. The results demonstrate that the heating temperature of mixture greatly influences the extraction percentage. Under heating temperature lower than  $45^\circ\text{C}$ , almost no Nd (III) was extracted. The extraction of Nd (III) was less than 50% at  $60^\circ\text{C}$  due to decreasing viscosity, and by heating the mixture to  $80^\circ\text{C}$  (higher than the UCST), almost 100% of Nd (III) was extracted after shaking for 5 s when  $60 \text{ mmol kg}^{-1}$   $[\text{Chol}][\text{hfac}]$  was contained in the organic phase. Nd (III) was extracted at pH 5.5 and sharply decreased to pH 3–5 because of the protonation of  $[\text{hfac}]^-$  anion. Extraction stoichiometry was confirmed by slope analysis, revealing that Nd (III) was extracted by  $[\text{Chol}][\text{hfac}]$  in a 1:4 ratio [34].

Unlike the variation of the temperature below the UCST, the application of different temperatures around and above the UCST had no influence on the extraction equilibrium and the percentage extraction of Nd (III) by a HLE system composed of betainium bis(trifluoromethylsulfonyl) imide  $[\text{Hbet}][\text{NTf}_2]$  as the organic phase and betaine as the extractant with a UCST of  $55^\circ\text{C}$ . As with the heating temperature, settling temperature tested at  $6\text{--}50^\circ\text{C}$  had no effect on the extractability. The complex formed during extraction can be described as  $[\text{Nd}_2(\text{bet})_3(\text{H}_2\text{O})_y]^{3+}$ .

Electrical neutrality can be achieved by bis(trifluoromethylsulfonyl)imide (or chloride or nitrate) counterions [5]. This similar system was also applied to metal ion separation including  $\text{La}^{3+}$ ,  $\text{Pr}^{3+}$ ,  $\text{Nd}^{3+}$ ,  $\text{Dy}^{3+}$ ,  $\text{Ho}^{3+}$ ,  $\text{Er}^{3+}$ ,  $\text{Y}^{3+}$ ,  $\text{Sc}^{3+}$ ,  $\text{Ga}^{3+}$ ,  $\text{In}^{3+}$ ,  $\text{Mn}^{2+}$ ,  $\text{Ni}^{2+}$ ,  $\text{Cu}^{2+}$ ,  $\text{Zn}^{2+}$  and  $\text{Ag}^+$ ,  $\text{Sc}^{3+}$ ,  $\text{Ga}^{3+}$  and  $\text{In}^{3+}$  were almost completely extracted to the organic phase, and the distribution ratios of  $\text{Mn}^{2+}$ ,  $\text{Ni}^{2+}$ ,  $\text{Zn}^{2+}$  and  $\text{Ag}^+$  are very low (almost no extraction).  $\text{Cu}^{2+}$  was reasonably well extracted to the IL phase, indicating the possibility of separating  $\text{Cu}^{2+}$  from  $\text{Ni}^{2+}$ ,  $\text{Zn}^{2+}$  and  $\text{Mn}^{2+}$ . The distribution ratios for lanthanide ions were about 10 with no significant differences between the different lanthanide ions [16].

Another study of this system specifically focused on scandium (III) extraction from red mud leachates. Individual study on Sc (III) extraction indicates that the distribution of the Sc (III)– $[\text{Hbet}][\text{NTf}_2]$  complex is solely controlled by the difference in solubility in the aqueous phase and the IL phase. Red mud consists of the major elements iron, aluminum, titanium, calcium, sodium and silicon and some minor constituents including scandium and other rare-earth elements. Therefore, the tested metal ions include the rare-earth elements Y (III), La (III), Ce (III), Nd (III), and Dy (III) and the major elements Al (III), Fe (III), Ca (II), Ti (IV) and Na (I) and were compared to the extraction of Sc (III). A high affinity for Sc (III) (extraction percentage,  $\%E > 90\%$ ) as compared to the other rare-earth metal ions ( $\%E$  between 4% and 12% at an initial pH of 3, depending on the rare-earth element) was shown by  $[\text{Hbet}][\text{NTf}_2]$ , as well as a very low affinity for almost all the major elements present in red mud, except for Fe(III), which is very similar to the  $\%E$  of Sc (III). The higher  $\%E$  for Fe (III) and Sc (III) was derived by the smaller ionic radius, and thus there are higher charge densities than the trivalent lanthanide

ions and Y (III). Furthermore, the ATR-FTIR spectra of the IL phase of the extraction mixture, loaded with varying amounts of scandium, showed that coordination of the IL to the scandium ion occurs via the carboxylic acid function of the cation. Sc(III) was extracted in a ligand-to-metal ratio of 3:1, as suggested from the calculations based on the maximum loading [35].

Another mixture having thermomorphic properties with the UCST is demonstrated by the IL analogues of Girard's reagents ( $[N_{xyz}hcm][NTf_2]$ ), in which hcm is hydrazinocarbonylmethyl.  $[N_{222}hcm][NTf_2]$  was selected as the extractant for extraction of four common metal ions, viz.,  $[Ni(OH_2)_6]^{2+}$ ,  $[Co(OH_2)_6]^{2+}$ ,  $[Cu(OH_2)_6]^{2+}$  and  $[Cr(OH_2)_6]^{3+}$ . To create a homogeneous solution, the mixture of IL and aqueous solution of metal ions was heated at 60°C for 20 min. The order of distribution coefficients was Cu (II) (28586) >> Ni (II) (767) > Co (II) (36) > Cr (5.4), which reflects the well-known Irving-Williams series [36]. Nitrate IL (1,3-dihexylimidazolium nitrate,  $[C_6C_6im][NO_3]$ ) was used in metal ion separation for the first time. Most extraction experiments were performed with an aqueous phase containing 6 M  $NaNO_3$ , wherein the solubility of IL was much lower (<0.5 wt%). IL presaturated with a 6 M  $NaNO_3$  solution had a slightly higher viscosity than a water-saturated sample, but the viscosity was still lower than 50 mPa·s at room temperature, which is far lower than water-saturated trihexyltetradecylphosphonium nitrate (265 mPa·s). First-row transition metals were far less efficiently extracted than the rare earths. Among the tested transition metals, no clear trend could be observed; all percentage extractions were around 30%. For the rare earths, as the charge density increased ( $La^{3+} < Nd^{3+} < Sm^{3+} < Sc^{3+}$ ), the %E decreased.

This system was also applied to Sm (III)/Co (II) separation to mimic a  $SmCo_5$  magnet. The higher the molar concentration of  $NaNO_3$ , the more Sm (III) was extracted, facilitated by the inner salting-out effect. At 6 M  $NaNO_3$ , nearly 100% of the Sm (III) was extracted. However, there was also a significant co-extraction of Co (II), of about 30%. The extraction was not affected by the shaking time or the pH of the aqueous solution. La (III)/Ni (II) pairs were investigated to mimic nickel metal hydride batteries. A synthetic solution of 9.6 g L<sup>-1</sup> La (III) and 35.4 g L<sup>-1</sup> Ni (II) was prepared. La (III) was fully extracted, and only 15% of Ni(II) was co-extracted into the IL phase [37].

HLLLE with a UCST has been also applied to U (VI) extraction, which has a strong radioactive nature from the aqueous  $HNO_3$  solution. In this system, betainium bis(trifluoromethylsulfonyl) imide ionic liquid  $[Hbet][Tf_2N]$  does not only act as a solvent but also as an extractant with an extraction percentage of 60%. The *D* value in both HLLLE and conventional liquid-liquid extraction decreased with an increase in the initial  $[HNO_3]$  and were almost consistent with each other. That the carboxyl group of  $[Hbet]^+$  takes part in the extraction of U (VI) has been confirmed by the fact that the *D* value clearly decreases with an increase in  $[H^+]$ ; the plot seems to follow a linear relationship with a slope of 1.2; it is independent of  $[NO_3^-]$ . The decrease in *D* value was derived by decreasing the deprotonated carboxyl group due to the increase in  $[H^+]$ . This mechanism was also confirmed by the fact that the *D* values were almost zero using an unfunctionalized IL ( $[TMPA][Tf_2N]$ ) [38].

Previous applications of an IL-based HLLLE have been a mixture of ILs with water with a UCST. Some ILs that form a homogeneous phase below the critical solution temperature were also applied in metal ion separation. Gras et al. [39] reported the formation of a two-phase system by mixing concentrated hydrochloric acid with tributyl(tetradecyl) phosphonium

chloride ( $[P_{44414}][Cl]$ ), which is water miscible below the critical solution temperature. The use of concentrated hydrochloric acid allows for the simultaneous leaching and extraction of metal ions. This system was used to separate Fe (III), Pt (IV), Ni (II) and Co (II). After stirring in a rotator for 2 hours until complete dissolution, the mixture was then placed in a heating bath for 6 hours until phase separation. Fe (III) and Pt (IV) were close to quantitatively extracted towards the IL-rich phase for all experimental mixtures for temperatures of all system. Co (II) was also efficiently extracted from 75 to 97% in mixtures composed of 10.2% IL, 19% HCl and 70.8% water and 18.6% IL and 15.7% HCl and 65.7% water, respectively, at 50°C, whilst the majority of Ni (II) remained in the HCl-rich phase. The extraction mechanism was derived by the anion exchange between a metalchlorocomplex with  $Cl^-$  of IL. The selectivity of this system was evaluated towards Co (II) and Mn (II), which is relevant for the recycling of NiMH batteries. Mixtures containing 17.8% IL, 25.9% HCl, 56.3%  $H_2O$  and 18.1% IL, 20.8% HCl and 61.1%  $H_2O$  at 50°C yielded a nearly pure Co(II) in the IL-rich phase, with a separation factor of 400 and 376, respectively. These promising results demonstrate that an acidic aqueous biphasic system can be used simply and efficiently for the critical separation of Co (II) and Ni (II) directly from the HCl leachates of NiMH batteries [39].

Another system, composed of IL-water with a dependent temperature homogeneous below the critical solution temperature, was obtained by mixing ether-functionalized ILs with bis(2-ethylhexyl)phosphate (DEHP), which is well known as a metal extractant anion with water. The cations investigated were tri-n-butyl-2-methoxyethylphosphonium ( $[P_{444}E_1]$ ), tri-n-butyl[2-(2-methoxyethoxy) ethyl]phosphonium ( $[P_{444}E_2]$ ) and tri-n-butyl-[2-[2-(2-methoxyethoxy)ethoxy]ethyl] phosphonium ( $[P_{444}E_3]$ ). All synthesized chloride ILs ( $[P_{444}E]Cl$ ) were fully miscible with water, whilst all synthesized DEHP ILs  $[P_{444}E][DEHP]$  displayed LCST-phase behaviour. To determine the distribution ratios, four different aqueous solutions of approximately 5000 ppm of the metal ( $CoCl_2$ ,  $CuCl_2$ ,  $NiCl_2$  and  $ZnCl_2$ ) at a pH of around 3.5 were mixed with the IL  $[P_{444}E_3][DEHP]$  in the homogeneous phase. The distribution ratio of Co (II), Ni (II), Cu (II) and Zn (II) were 4.4, 19, 34 and 25, respectively, which meets the Irving-Williams series. Indium and some rare earths formed the precipitation with the IL probably due to the strong complexation with the anion of IL [40].

## 5. Conclusion

This chapter reviewed several articles discussing the use of an IL-based ATPS for metal ion extraction. In general, an ATPS composed of ILs and a salting-out agent is excellent for metal ion separation because of its efficiency, selectivity and environmental friendliness. Due to the temperature dependence of a mixture comprised of ILs with water, it has been manipulated for metal ion extraction known as homogeneous liquid-liquid extraction (HLL). With this technique, a salting-out agent is not necessary. In some cases, ILs in HLL act as both an extractant and separator agent simultaneously. In other cases, the IL acts only as a separator agent. Therefore, an extractant should be added to the system in order to increase the extraction percentage of metal ions. HLL also showed high efficiency and selectivity in the metal ion extraction. Metal ions can be extracted by both an ATPS and HLL, including transition metals, rare-earth elements and radioactive substances.



## Conflict of interest

No conflict of interest.

## Author details

Pius Dore Ola and Michiaki Matsumoto\*

\*Address all correspondence to: [mmatsumo@mail.doshisha.ac.jp](mailto:mmatsumo@mail.doshisha.ac.jp)

Department of Chemical Engineering and Materials Science, Doshisha University,  
Kyotanabe, Kyoto, Japan

## References

- [1] Kislik V. Solvent Extraction, Classical and Novel Approaches. Amsterdam: Elsevier; 2011
- [2] Hoogerstraete TV, Wellens S, Verachtert K, Binnemans K. Removal of transition metals from rare earths by solvent extraction with an undiluted phosphonium ionic liquid: Separations relevant to rare-earth magnet recycling. *Green Chemistry*. 2013;**15**:919-927. DOI: 10.1039/c3gc40198g
- [3] Matsumoto M. Ionic liquid-based supported liquid membranes. In: Mohanty K, Purkait MK, editors. *Membrane Technology and Applications*. Boca Raton, USA: CRC Press; 2012. pp. 305-316
- [4] Swatloski RP, Holbrey JD, Rogers RD. Ionic liquids are not always green: Hydrolysis of 1-butyl-3-methylimidazolium hexafluorophosphate. *Green Chemistry*. 2003;**5**:361-363. DOI: 10.1039/b304400a
- [5] Hoogerstraete TV, Onghena B, Binnemans K. Homogeneous liquid-liquid extraction of rare earths with the betaine—Betainium bis(trifluoromethylsulfonyl)imide ionic liquid system. *International Journal of Molecular Sciences*. 2013;**14**:21353-21377. DOI: 10.3390/ijms141121353
- [6] Fu F, Xie L, Tang B, Wang Q, Jiang S. Application of a novel strategy-advanced Fenton-chemical precipitation to the treatment of strong stability chelated heavy metal containing wastewater. *Chemical Engineering Journal*. 2012;**189-190**:283-287. DOI: 10.1016/j.cej.2012.02.073
- [7] Lee KP, Arnot TC, Mattia D. A review of reverse osmosis membrane materials for desalination: Development to date and future potential. *Journal of Membrane Science*. 2011;**370**:1-22. DOI: 10.1016/j.memsci.2010.12.036
- [8] Lakherwar D. Adsorption of heavy metals: A review. *International Journal of Environmental Research and Development*. 2014;**4**:41-48

- [9] Nikoloski AN, Ang K. Review of the application of ion exchange resins for the recovery of platinum-group metals from hydrochloric acid solutions. *Mineral Processing and Extractive Metallurgy Review*. 2014;**35**:369-389. DOI: 10.1080/08827508.2013.764875
- [10] Xie F, Zhang TA, Dresinger D, Doyle F. A critical review on solvent extraction of rare earths from aqueous solutions. *Minerals Engineering*. 2014;**56**:10-28. DOI: 10.1016/j.mineng.2013.10.021
- [11] Liu J, Jonsson JÅ, Jiang G. Application of ionic liquids in analytical chemistry. *Trends in Analytical Chemistry*. 2005;**24**:20-27. DOI: 10.1016/j.trac.2004.09.005
- [12] Anderson JL, Armstrong DW. High-stability ionic liquids. A new class of stationary phases for gas chromatography. *Analytical Chemistry*. 2003;**75**:4851-4858. DOI: 10.1021/ac0345749
- [13] Joshi MD, Anderson JL. Recent advances of ionic liquids in separation science and mass spectrometry. *RSC Advances*. 2012;**2**:5470-5484. DOI: 10.1039/c2ra20142a
- [14] Ternova D, Boltoeva M, Cointeaux L, Gaillard C, Kalchenko V, Mazan V, Miroschnichenko S, Mohapatra PK, Ouadi A, Papaiconomou N, Petrova M, Billard I. Dramatic changes in the solubilities of ions induced by ligand addition in biphasic system  $D_2O/DNO_3// [C_1C_4im][Tf_2N]$ : A phenomenological study. *The Journal of Physical Chemistry. B*. 2016;**120**:7502-7510. DOI: 10.1021/acs.jpcc.6b05424
- [15] Freire MG, Cláudio AFM, Araújo JMM, Coutinho JAP, Marrucho IM, Lopes JNC, Rebelo LPN. Aqueous biphasic systems: A boost brought about by using ionic liquids. *Chemical Society Reviews*. 2012;**41**:4966-4995. DOI: 10.1039/c2cs35151j
- [16] Hoogerstraete TV, Onghena B, Binnemans K. Homogeneous liquid-liquid extraction of metal ions with a functionalized ionic liquid. *Journal of Physical Chemistry Letters*. 2013;**4**:1659-1663. DOI: 10.1021/jz4005366
- [17] Iqbal M, Tao Y, Xie S, Zhu Y, Chen D, Wang X, Huang L, Peng D, Sattar A, Shabbir MAB, Hussain HI, Ahmed S, Yuan Z. Aqueous two-phase system (ATPS): An overview and advances in its applications. *Biological Procedures Online*. 2016;**18**:18. DOI: 10.1186/s12575-016-0048-8
- [18] de Lemos LR, Santos IJB, Rodrigues GD, da Silva LHM, da Silva MCH. Copper recovery from ore by liquid-liquid extraction using aqueous two-phase system. *Journal of Hazardous Materials*. 2012;**237-238**:209-214. DOI: 10.1016/j.jhazmat.2012.08.028
- [19] Asenjo JA, Andrews BA. Aqueous two-phase systems for protein separation: A perspective. *Journal of Chromatography. A*. 2011;**1218**:8826-8835. DOI: 10.1016/j.chroma.2011.06.051
- [20] Pereira JFB, Rebelo LPN, Rogers RD, Coutinho JAP, Freire MG. Combining ionic liquids and polyethylene glycols to boost the hydrophobic-hydrophilic range of aqueous biphasic systems. *Physical Chemistry Chemical Physics*. 2013;**15**:19580. DOI: 10.1039/c3cp53701c

- [21] Kohno Y, Ohno H. Ionic liquid/water mixtures: From hostility to conciliation. *Chemical Communications*. 2012;**48**:7119-7130. DOI: 10.1039/c2cc31638b
- [22] Onghena B, Jacobs J, Meervelt LV, Binnemans K. Homogeneous liquid-liquid extraction of neodymium(III) by choline hexafluoroacetylacetonate in the ionic liquid choline bis(trifluoromethylsulfonyl)imide. *Dalton Transactions*. 2014;**43**:11566. DOI: 10.1039/c4dt01340a
- [23] Nockemann P, Thijs B, Pittois S, Thoen J, Glorieux C, Hecke KV, Meervelt LV, Kirchner B, Binnemans K. Task-specific ionic liquid for solubilizing metal oxides. *The Journal of Physical Chemistry. B*. 2006;**110**:20978-20992. DOI: 10.1021/jp0642995
- [24] JNC L. ABS composed of ionic liquids and inorganic salts. In: Freire MG, editor. *Ionic-Liquid-Based Aqueous Biphasic Systems*. Berlin Heidelberg: Springer-Verlag; 2016. pp. 27-35. DOI: 10.1007/978-3-662-52875-4\_2
- [25] da Costa Lopes AM, Bogel-Lukasik R. ABS constituted by ionic liquids and carbohydrates. In: Freire MG, editor. *Ionic-Liquid-Based Aqueous Biphasic Systems*. Berlin Heidelberg: Springer-Verlag; 2016. pp. 37-60. DOI: 10.1007/978-3-662-52875-4\_3
- [26] Sadeghi R. ABS composed of ionic liquids and polymers. In: Freire MG, editor. *Ionic-Liquid-Based Aqueous Biphasic Systems*. Berlin Heidelberg: Springer-Verlag; 2016. pp. 61-88. DOI: 10.1007/978-3-662-52875-4\_4
- [27] Akama Y, Sali A. Extraction mechanism of Cr(VI) on the aqueous two-phase system of tetrabutylammonium bromide and  $(\text{NH}_4)_2\text{SO}_4$  mixture. *Talanta*. 2002;**57**:681-686. DOI: 10.1016/S0039-9140(02)00076-0
- [28] Akama Y, Ito M, Tanaka S. Selective separation of cadmium from cobalt, copper, iron (III) and zinc by water-based two-phase system of tetrabutylammonium bromide. *Talanta*. 2000;**53**:645-650. DOI: 10.1016/S0039-9140(00)00555-5
- [29] Onghena B, Opsomer T, Binnemans K. Separation of cobalt and nickel using athermomorphic ionic-liquid-based aqueous biphasic system. *Chemical Communications*. 2015;**51**:15932-15935. DOI: 10.1039/c5cc06595j
- [30] Zheng Y, Tong Y, Wang S, Zhang H, Yang Y. Mechanism of gold (III) extraction using a novel ionic liquid-based aqueous two phase system without additional extractants. *Separation and Purification Technology*. 2015;**154**:123-127. DOI: 10.1016/j.seppur.2015.09.014
- [31] Ghosh K, Maiti M, Lahiri S, Hussain VA. Ionic liquid-salt based aqueous biphasic system for separation of  $^{109}\text{Cd}$  from silver target. *Journal of Radioanalytical and Nuclear Chemistry*. 2014;**302**:925-930. DOI: 10.1007/s10967-014-3412-7
- [32] Anthemidis AN, Adam ISI. Development of on-line single-drop micro-extraction sequential injection system for electrothermal atomic absorption spectrometric determination of trace metals. *Analytica Chimica Acta*. 2009;**632**:216. DOI: 10.1016/j.aca.2008.10.078
- [33] Anthemidis AN, Ioannou K-IG. Recent developments in homogeneous and dispersive liquid-liquid extraction for inorganic elements determination. A review. *Talanta*. 2009;**80**:413-421. DOI: 10.1016/j.talanta.2009.09.005

- [34] Onghena B, Jacobs J, Meervelt LV, Binnemans K. Homogeneous liquid-liquid extraction of neodymium(III) by choline hexafluoroacetylacetonate in the ionic liquid choline bis(trifluoromethylsulfonyl)imide. *Dalton Transactions*. 2014;**43**:11566-11578. DOI: 10.1039/c4dt01340a
- [35] Onghena B, Binnemans K. Recovery of scandium(III) from aqueous solutions by solvent extraction with the functionalized ionic liquid betainium bis(trifluoromethylsulfonyl)imide. *Industrial and Engineering Chemistry Research*. 2015;**54**:1887-1898. DOI: 10.1021/ie504765v
- [36] Blesic M, Gunaratne HQN, Jacquemin J, Nockemann P, Olejarz S, Seddon KR, Strauss CR. Tunable thermomorphism and applications of ionic liquid analogues of Girard's reagents. *Green Chemistry*. 2014;**16**:4115-4121. DOI: 10.1039/c4gc01159g
- [37] Depuydt D, den Bossche AV, Dehaen W, Binnemans K. Metal extraction with a short-chain imidazolium nitrate ionic liquid. *Chemical Communications*. 2017;**53**:5271. DOI: 10.1039/c7cc01685a
- [38] Mori T, Takao K, Sasaki K, Suzuki T, Arai T, Ikeda Y. Homogeneous liquid-liquid extraction of U(VI) from HNO<sub>3</sub> aqueous solution to betainium bis(trifluoromethylsulfonyl)imide ionic liquid and recovery of extracted U(VI). *Separation and Purification Technology*. 2015;**155**:133-138. DOI: 10.1016/j.seppur.2015.01.045
- [39] Gras M, Papaiconomou N, Schaeffer N, Chainet E, Tedjar F, Coutinho JAP, Billard I. Ionic-liquid-based acidic aqueous biphasic systems for simultaneous leaching and extraction of metallic ions. *Angewandte Chemie, International Edition*. 2018;**57**:1563-1566. DOI: 10.1002/anie.201711068
- [40] Depuydt D, Liu L, Glorieux C, Dehaena W, Binnemans K. Homogeneous liquid-liquid extraction of metal ions with non-fluorinated bis(2-ethylhexyl)phosphate ionic liquids having a lower critical solution temperature in combination with water. *Chemical Communications*. 2015;**51**:14183. DOI: 10.1039/c5cc05649g

---

# Kinetic Assessment of Tetramethyl Ammonium Hydroxide (Ionic Liquid) for Carbon Dioxide, Methane and Binary Mix Gas Hydrates

---

Muhammad Saad Khan, Bavoh B. Cornelius,  
Bhajan Lal and Mohamad Azmi Bustam

Additional information is available at the end of the chapter

<http://dx.doi.org/10.5772/intechopen.77262>

---

## Abstract

This present work highlights the impact of ammonium-based ionic liquid tetramethylammonium hydroxide (TMAOH) on the formation kinetics of carbon dioxide ( $\text{CO}_2$ ), methane ( $\text{CH}_4$ ), and their binary mixed gas (50–50 mole%) hydrates. The TMAOH (IL) is applied in varying concentrations (0.5, 1, and 2 wt%) at different experimental temperatures, i.e., 1 and 4°C. The kinetic experiments are conducted in a high-pressure reactor equipped with two-bladed impeller, to provide sufficient agitation. The experimental pressures of  $\text{CO}_2$ ,  $\text{CH}_4$ , and mixed 50%  $\text{CO}_2$  + 50%  $\text{CH}_4$  were 3.50, 8.0, and 6.50 MPa, respectively. Induction time, the initial apparent rate of formation and the total gas consumed are the kinetic parameters used to evaluate the performance of TMAOH as KHI. The results are further compared with commercial KHI (PVP), at higher subcooling condition of 1°C and 1 wt% of all the studied gaseous systems. Furthermore, the KHI performance of TMAOH is also evaluated via the relative inhibition performance (RIP) compared with other ILs for  $\text{CO}_2$  and  $\text{CH}_4$  hydrates. Results revealed that TMAOH delays the induction time for all the considered systems. The presence of TMAOH also reduced the total gas consumed and the initial rate of hydrate formation in most of the studied systems.

**Keywords:**  $\text{CH}_4$  hydrate,  $\text{CO}_2$  hydrate, ionic liquids, mix gas hydrate, KHI, RIP

---

## 1. Introduction

Gas hydrates are solid crystals formed when gas ( $\text{C}_1$ ,  $\text{C}_2$ ,  $\text{C}_3$ ,  $\text{C}_4$  and  $\text{CO}_2$ ) molecules are trapped inside the hydrogen-bonded water cages under thermodynamically favourable conditions

---

(low-temperature and high-pressure conditions) [1, 2]. Typically, three types of gas hydrate structures are known, sI, sII and sH hydrates, depending on the type and size of the encaged gas molecules. For example, pure  $\text{CH}_4$  and  $\text{CO}_2$  mostly form sI hydrate, while  $\text{C}_2\text{H}_6$  forms sII hydrate.

Gas hydrate formation in the pipelines is considered as one of the most perennial flow assurance problems, which consumes about 70% of flow assurance resources. The accumulation of gas hydrates plugs oil and gas pipelines, disturbing hydrocarbon flow, and causes several safety issues [3–5]. The removal of hydrate plugs from transmission pipeline amount to about 1 million/day shutdown [1]. The hydrate plugging risk increases when producing and transporting high carbon dioxide ( $\text{CO}_2$ ) content natural gas, as  $\text{CO}_2$  readily forms hydrates than methane ( $\text{CH}_4$ ) at the same pressure [6, 7]. High  $\text{CO}_2$  content natural gas reservoirs are frequently encountered in various areas around the world, such as Central European Pannonian Basin, Colombian Putumayo Basin, Gulf of Thailand, South China Sea, Ibleo platform, Taranaki Basin, Sicily, North Sea South Viking Graben and New Zealand [8]. Malaysia is among the leading natural gas exporters in the world [8]. The J5 and K5 gas fields located in offshore Eastern Malaysia produces about 70–87 mol%  $\text{CO}_2$  content natural gas [9]. This significant amount of  $\text{CO}_2$  together with the harsh offshore conditions poses various complications for the exploration and transportation of these enormous reserves. One of the core concerns from  $\text{CO}_2$ -enriched gas systems are their susceptibility to forming gas hydrates in the natural gas production lines [6, 7, 10]. Therefore, in-depth understanding of the mix gas hydrate systems will primarily provide an avenue for safe flow assurance operations when transporting such natural gas systems. Also, this will also provide some fundamental knowledge to design  $\text{CO}_2$  separation system for the natural gas system together with the storage opportunity for  $\text{CO}_2$  captured from richer  $\text{CO}_2$  content natural gas [4, 11, 12].

Four methods can be used to combat gas hydrate formation in flow assurance; this includes removal of water, pressure reduction, thermal heating and chemical injection [4]. In most of the cases, chemical injection is the utmost economical preventive method among the others [8, 13]. These gas hydrate preventive chemicals are known as hydrate inhibitors and are extensively used in oil and gas transmission pipelines. There are three types of gas hydrate inhibitors; thermodynamic hydrate inhibitors (THIs), which mainly shift the hydrate equilibrium curves towards lower-temperature and higher-pressure regions. THIs are mostly required in large concentrations (10–50 wt% of water cuts). Commonly used THIs are methanol and glycols. Although these chemicals are still used in practical field applications till date, they face many drawbacks such as their high operational cost (transportation, storage, injection and pumping quantities and regeneration units) [14, 15].

The drawbacks of above THIs motivated researchers to develop a new kind of hydrate of inhibitors known as low-dosage hydrate inhibitors (LDHIs). This class of inhibitors are typically applied in very less concentration (<2 wt%). LDHIs consist of kinetic hydrate inhibitors (KHIs) and anti-agglomerates (AA). Kinetic hydrate inhibitors (KHIs) are primarily engrossed in delaying the hydrate nucleation time and formation growth rate. It remains quite problematic to evaluate the kinetics of hydrate formation [16–18], exclusively in the presence of KHIs, as it is a very dynamic

and complex process [19]. Commercially employed KHIs are water-soluble polymers such as polyvinylpyrrolidone (PVP) and polyvinyl caprolactam (PVCAP). Karaaslan and Parlaktuna [20] reported that PVP and PEO work as kinetic hydrate inhibitors but have carcinogenic materials which are capable of causing severe health and safety impact on human health. However, the impact of PEO is relatively less compared to PVP [20]. To address these environmental deficiencies of current inhibitors, the quest for greener inhibitors is actively ongoing. Several chemicals such as ILs (mostly imidazolium-based ILs) have been tested for gas hydrate mitigation. ILs could efficiently work as dual-functional hydrate inhibitors (THIs alongside KHIs).

Xiao and Adidharma [21] initiated the research on ILs as gas hydrate inhibitors and found a dual functional effect through imidazolium-based ILs. Since ILs are salts in a molten state, their ability to exhibit electrostatic interaction and form hydrogen bonds with water molecules enhances their hydrate crystalline surface adsorption ability by retarding hydrate nucleation process [21]. Kim and Kang [22] used a high-pressure cell to evaluate pyrrolidinium- and morpholinium-based ionic liquids such as N-hydroxyethyl-N-methyl pyrrolidinium chloride ([HEMP][Cl]), N-hydroxyethyl-N-methyl pyrrolidinium tetrafluoroborate ([HEMP][BF<sub>4</sub>]), N-butyl-N-methyl pyrrolidinium bromide ([BMP][Br]), N-(2-hydroxyethyl)-N-methyl morpholinium bromide ([HEMM][Br]) and N-(2-hydroxyethyl)-N-methyl morpholinium tetrafluoroborate ([HEMM][BF<sub>4</sub>]) that can delay methane hydrate nucleation time than PVP and PVCAP at 0.1, 1 and 10 wt%. Furthermore, Nazari and Ahmadi [23] studied the effects of [BMIM][BF<sub>4</sub>] and [BMIM][MS] on the CH<sub>4</sub> hydrate formation and suggested that [BMIM][BF<sub>4</sub>] acts as better KHI than [BMIM][MS]. However, poor THI behaviour was observed from [BMIM][BF<sub>4</sub>] in comparison with [BMIM][MS]. Norland and Kelland [24] and Lee et al. [25] elucidate that the type of anion/cation has a significant impact on IL effectiveness. They further suggested that ILs synergistically enhance the kinetic inhibition impact of PVCAP [25]. However, quaternary ammonium salts have also reported as potential KHIs, which open the door for the second-generation IL-based KHIs.

An earlier study suggested that quaternary ammonium salts (QAs) can reduce the nucleation time and hydrate growth rate of tetrahydrofuran (THF) hydrates [26]. The inhibition influence of trimethylpentane, trimethyl hexane and trimethyl octane (QAs) is attributed to the presence of alkyl (CH<sub>3</sub>) groups in a polar moiety form, which shows high tendency to be adsorbed on the hydrate crystalline surface [27]. Most QAs were found to exhibit kinetic inhibition and anti-agglomeration tendency. However, prior study from Storr et al. [27] recommended that these chemicals should be tested in mixed gas or natural gas hydrate system to evaluate their suitability for field applications. The best kinetic inhibition performance for the studied QAs on THF hydrates were achieved by tetrapentylammonium bromide (TPAB) followed by tetrabutylammonium bromide (TBAB) [28–30].

On the other hand, a limited number of studies are found on the effect of ammonium-based ionic liquids (AILs) as gas hydrate inhibitors [4, 12, 31–33]. Few studies have reported that AILs could efficiently induce thermodynamic hydrate inhibition [3, 4, 14, 34]; however, kinetic evaluations of AILs are rarely available in open literature [15]. Tariq et al. [15] previously reported that the presence of OH<sup>-</sup> anion in ILs has a higher inhibition effect as it facilitates more water hydrogen bond cleavage, thus delaying hydrate formation nucleation time. As the

search for useful IL hydrate inhibitors is still ongoing, in our recent works [3, 4], tetramethylammonium hydroxide (TMAOH) was reported as an effective THI for both  $\text{CH}_4$  and  $\text{CO}_2$  gases with average suppression temperature ( $\Delta T$ ) of 1.53 and 2.23°C, respectively. However, its ability to delay hydrate formation kinetics has not been investigated in the open literature.

Therefore, herein, the kinetic influence of TMAOH on  $\text{CO}_2$ ,  $\text{CH}_4$  and binary mixed gas hydrate (50–50  $\text{CO}_2 + \text{CH}_4$ ) formation at different concentrations (0.5, 1 and 2 wt%) is comprehensively evaluated and reported for the first time. Induction time, moles consumption and initial apparent rate of hydrate formation are the kinetic parameters that are used to assess the performance of TMAOH at different subcooling experimental temperatures of 1 and 4°C. The obtained results for all gaseous systems are further compared with PVP (commercial KHI) at 1 wt% and 1°C (since the best and commercially applicable concentration of PVP is 1 wt%, and 1°C gives the highest subcooling conditions in the study.) conditions. Also, the performance evaluation of TMAOH via RIP with other ILs is reported. Also, an attempt is made to describe the TMAOH kinetic inhibition mechanism in the presence of the studied hydrate systems.

## 2. Methodology

### 2.1. Materials

**Table 1** shows the materials used in this study. Only deionized water is used for all the sample preparations during the experiments. The sample concentration measurements are performed using a gravimetric analytical balance.

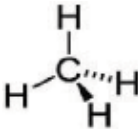
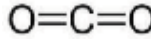
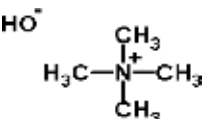
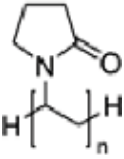
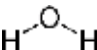
### 2.2. Details of experimental equipment

A high-pressure stainless steel cell [3, 12, 32] with an internal volume of 650 mL, alongside a maximum working pressure of 30 MPa, is used in this study. The cell is immersed in a water bath to regulate the temperature in the cell at desired conditions during experimentations. Two thermocouples are used to measure the temperature inside the cell at an accuracy of  $\pm 0.01^\circ\text{C}$ . To achieve appropriate agitation in the liquid phase, two-bladed pitch impeller stirrer is positioned in the equipment with a constant speed of 400 rpm (optimum speed) in all experimentations. The pressure inside the cell is noticed via a pressure transducer with an accuracy of  $\pm 0.001$  MPa.

### 2.3. Kinetic measurement procedure

Before each experimental run, the cell is meticulously cleaned with distilled water, and then a 100 mL liquid phase sample (with or without TMAOH) is loaded into the cell. The cell is then introduced into the water bath, and the system is put under vacuum for about an hour to ensure there are no traces of the air in the cell. The desired gas is then pressurized into the cell to the desired experimental operating pressures; after that, the system is allowed to stabilize to the desired initial experimental pressure and temperature conditions by leaving it for about an hour. The mechanical stirrer is turned on at 400 rpm, and data logging system is started simultaneously with the commencement of the experiment (i.e. by reducing the



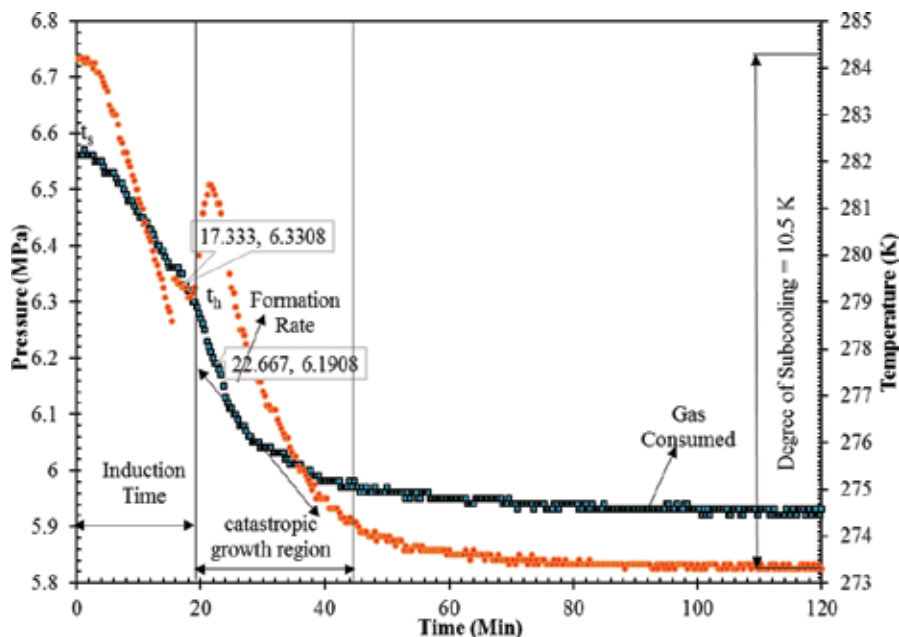
No	Chemical name	Symbol	Purity	Chemical structure
1	Methane	CH <sub>4</sub>	99.99 mole %	
2	Carbon dioxide	CO <sub>2</sub>	99.95 mole %	
3	Mixed gas	CO <sub>2</sub> + CH <sub>4</sub>	50.009–49.991 mole %	—
4	Tetramethylammonium hydroxide	TMAOH	25 wt% aqueous solution	
5	Polyvinylpyrrolidone	PVP	99 wt%	
6	Water	H <sub>2</sub> O	Deionized	

**Table 1.** Materials used for kinetic study of gas hydrates.

system temperature to the experimentally desired subcooling temperature of 1 or 4°C). The experimental pressures are set at 3.50, 8.00 and 6.50 MPa for CO<sub>2</sub>, CH<sub>4</sub> and binary mixed gas 50–50 CH<sub>4</sub> + CO<sub>2</sub> hydrate systems, respectively. The experimental temperatures are kept constant at 1 and 4°C for all studied systems and concentrations. All the experiments are repeated for three times, and averages are reported. The kinetic inhibition influence of TMAOH is assessed within the range of 0.5–2 wt%, similar to the typical industrial application of KHIs.

#### 2.4. Kinetic measurement parameter

In all experiments, the hydrate formation is observed through a sudden pressure drop in the pressure-time plot recorded by the data recording system. The experiments are considered complete after observing a constant pressure in the cell at each experimental temperature for about 3–5 hours. A typical pressure and temperature verse time profile during hydrate formation is illustrated in **Figure 1**. In **Figure 1**, the general hydrate formation process has three major stages: nucleation, crystal/hydrate growth and complete hydrate formation due to mass transfer limitation. The objective of effective KHIs is to increase the hydrate nucleation time (induction time) and at the same time reduce the hydrate crystal growth rate and the total amount of gas consumed into hydrates [35]. Hence, the kinetic inhibition influence of TMAOH is evaluated based on these three parameters.



**Figure 1.** Pressure and temperature vs. time relationship (50–50 mixed gas hydrate).

#### 2.4.1. Induction time measurement

The induction time is the most significant indicator to assess initiation of gas hydrate crystallization and growth. It is the time elapse for the occurrence of visible hydrate crystals of the critically stable-sized hydrate nucleus. Longer induction time than the fluid retention time would result in hydrate-free transportation for hydrocarbons in pipelines [36]. However, induction time is a probabilistic phenomenon which depends upon the heterogeneous nucleation parameters [2]. The nucleation rate could influence by the numerous factors, such as the existence of particles and impurities in the sample, the roughness of the cell wall and the presence of driving force. Thus, diverse experimental approaches would apparently provide different outcomes. For comparison of measurements of the induction time of hydrate inhibitors, the same apparatus is highly recommended/appropriate, and experimental method should be employed [15]. The induction time is measured in this study from the pressure–time data plotted in **Figure 1** as described in the literature [37, 38] as

$$t_i = t_s - t_h \quad (1)$$

where  $t_s$  is the time taken for the system pressure to decrease the experimental pressure and  $t_h$  and  $t_i$  is the actual induction time for hydrate formation (**Figure 1**). Usually, the induction time is recognized by the point at which there is a drastic drop in the reactor pressure accompanied by a corresponding sudden spike in the reactor temperature, thus indicating the onset of hydrate formation (see **Figure 1** at point  $t_h$ ).

### 2.4.2. Initial apparent rate of hydrate formation

The initial apparent rate of hydrate formation determines the rate of hydrate crystallization after the hydrate nucleation [39]. The initial apparent rate is measured with regard to the rate at which the initial moles of gas is consumed into hydrate formation, thereby defining fast hydrate crystal growth that takes place [40]. In these experiments, the initial rate of hydrate formations is accounted for initial 10 min of hydrate formations. The initial apparent rate of hydrate formation can be given by

$$dn/dt = k(n_0 - n_s) \quad (2)$$

where  $k$  is the initial apparent rate of any studied gas,  $n_0$  is the mole of gas at initial stage 0 and  $n_s$  is the initial moles of consumed gas. The Peng-Robinson equation is employed for calculation of compressibility factor  $z$ , and the real gas equation is also used to calculate the mole of consumed gas.

### 2.4.3. Moles of gas consumed

Moles of gas consumed during hydrate formation determine the dissolved gas in hydrate phase which could form hydrate plug in the subsea condition. The total amount of consumed gas for complete hydrate formation is calculated by applying the real gas law [38, 41]:

$$\Delta n_{gas} = \frac{V}{R} \left[ \left( \frac{P}{zT} \right)_0 - \left( \frac{P}{zT} \right)_f \right] \quad (3)$$

where  $V$ ,  $R$ ,  $P$  and  $T$  denote the system gas phase volume, universal gas constant, pressure and temperature, respectively.  $\Delta n_{gas}$  denotes the moles of gas consumed,  $z$  is the compressibility factor of the gas determined from the Peng-Robinson equation of state and the subscripts  $'_0'$  and  $'_f'$  denote the number of  $n$  of moles of gas at the time, zero and time of complete hydrate formation.

In the mixed gas hydrate system, the final gas composition in the gas phase is different from the original mix gas composition due to the guest cage occupancy ratio of the mix gas composition. A gas chromatograph (PerkinElmer) is used to accurately calculate the final composition of the mixed gas in the gas phase after complete hydrate formation. The gas chromatograph results are employed to calculate the moles of mixed gas in the gas phase after hydrate completion (denoted as  $'_f'$  in Eq. (3)). Also, the gas chromatograph values indicated that gas composition is more in the hydrate phase in the presence and absence of TMAOH.

## 3. Results and discussion

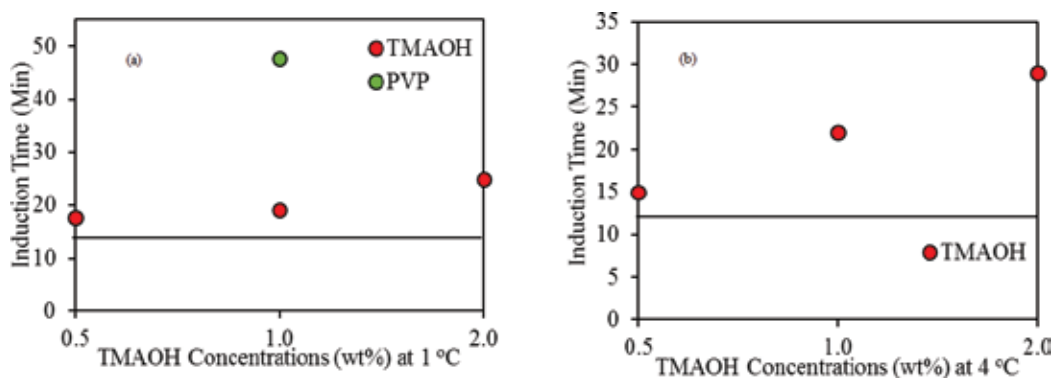
The kinetic inhibition effect of TMAOH on the hydrate induction time, formation growth rate and total gas consumption on the hydrate systems is assessed in this work. This is to efficiently evaluate the kinetic inhibition of TMAOH on the complete hydrate formation and growth stages.

### 3.1. Effect of TMAOH on the kinetics of CO<sub>2</sub> hydrates

The experimental pressure for CO<sub>2</sub> hydrates has been fixed at 3.50 MPa with operating temperatures of 1 and 4°C (subcooling of 8.32 and 5.32°C). These conditions are selected to provide sufficient driving force for hydrate formation as typically encountered in offshore operations of oil and gas production. The effect of various concentrations (0.5, 1 and 2 wt %) of TMAOH on the induction time of CO<sub>2</sub> hydrate at different experimental temperatures (1 and 4°C) is presented in **Figure 2(a)** and **(b)**, respectively. Results reveal that TMAOH could delay the growth of CO<sub>2</sub> hydrates at almost all studied systems by hindering its nucleation process. In the absence of TMAOH, the induction time of water is observed as 14.33 min at 1°C (see **Figure 2(a)**), while 4°C condition showed even lesser induction time of 12.35 min for pure water as evident in **Figure 2(b)**. The presence of 0.5 wt% TMAOH shows a slight improvement in hydrate nucleation time (induction time) with the base sample (pure water) for both 1 and 4°C, which are 23.2 and 21.45%, respectively. Upon increasing the concentration to 1 wt%, the induction time of pure water is improved up to 32.5 and 78.1% at 1 and 4°C, respectively, indicating an inhibition ability of TMAOH at the studied subcooling conditions. However, the inhibition impact at 4°C is relatively higher compared to 1°C, primarily due to the significant driving force existed at 1°C (8.32°C). Further increase in TMAOH concentration to 2 wt% resulted in a negligible delay of CO<sub>2</sub> hydrate induction time compared to the 1 wt% sample. Thus, the optimum TMAOH concentration to delay CO<sub>2</sub> hydrate nucleation is at 1 wt% as shown in **Figure 2**. For comparison purposes, the induction time data is also equated with PVP at 1°C condition in **Figure 2(a)**. The comparison results suggest that PVP still possess better hydrate holding efficacy than studied aqueous TMAOH solution perhaps due to the enhanced polymer linkage on the liquid-gas surface compared to TMAOH.

Since hydrate formation kinetic is a complex phenomenon, it is hard to compare with the previous studies due to the different experimental conditions and apparatus designs. However, [42] found the efficient method to compare different types of the system via relative inhibition power (RIP):

$$RIP = \frac{\text{Induction time of KHI} - \text{Induction time of water}}{\text{Induction time of water}} \quad (4)$$

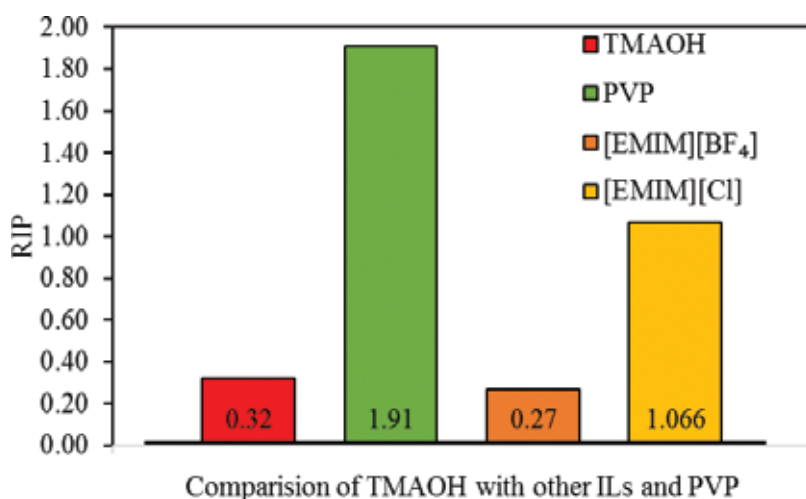


**Figure 2.** Induction time of CO<sub>2</sub> hydrates in the presence of water (straight line) and TMAOH at different experimental temperatures (a) 1 and (b) 4°C.

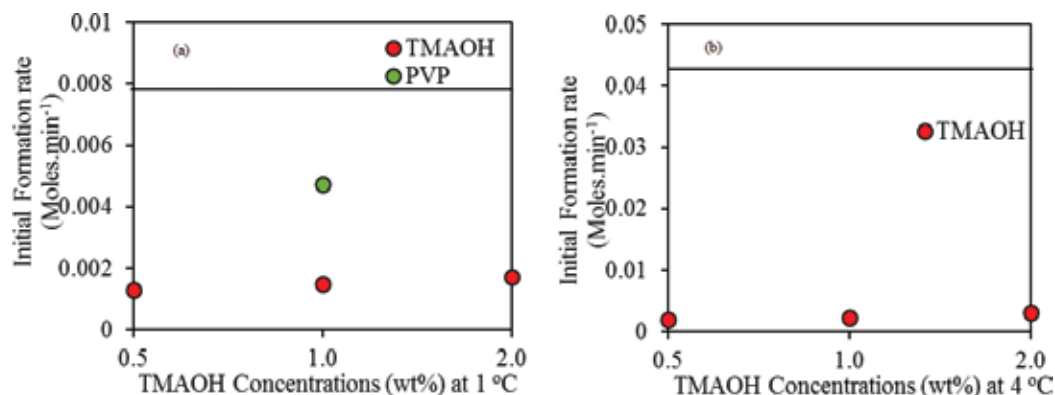
The RIP values determine the kinetic inhibitory efficacy of the KHIs, as the  $RIP > 0$  corresponds to the better inhibitory performance of KHI. The RIP value of 1 wt% TMAOH concentration at a higher subcooling experimental temperature ( $1^\circ\text{C}$ ) is presented in **Figure 3** for  $\text{CO}_2$  hydrate system. The RIP results are further compared with PVP and some reported ILs, namely, [EMIM][Cl] and [EMIM][ $\text{BF}_4$ ] from Bavoh et al. [38] and Chun et al. [43], respectively. The RIP results further enlighten the kinetic inhibition performance of TMAOH. In fact, TMAOH possess enhanced RIP value (0.32) compared to [EMIM][ $\text{BF}_4$ ] (0.27) earlier studied imidazolium-based IL. However, [EMIM][Cl] provides much better inhibition performance due to the presence of  $\text{Cl}^-$  anion in its structure which leads towards better induction time [15]. However, PVP performs better than all studied ILs in **Figure 3**.

**Figure 4** presents the initial rate constant of  $\text{CO}_2$  hydrate formation in the presence of various TMAOH concentrations at 1 and  $4^\circ\text{C}$ , respectively. It is found that the rate of hydrate formation is inhibited in the presence of TMAOH compared with the pure water sample at all studied concentrations (see **Figure 4**). The  $\text{CO}_2$  hydrate formation rate is reduced more at  $4^\circ\text{C}$  experimental temperature than  $1^\circ\text{C}$ , especially at 0.5 wt% system. This is attributed to the higher driving force existed at  $1^\circ\text{C}$  [15, 21]. At both 1 and  $4^\circ\text{C}$ , the samples with 0.5 wt% TMAOH concentration shows the maximum inhibition impact on  $\text{CO}_2$  hydrate formation rates up to 0.0013 and  $0.00065 \text{ min}^{-1}$ , respectively. Unlike the induction time, whose inhibition impact is enhanced with increasing TMAOH concentration, the inhibition impact on  $\text{CO}_2$  formation rate is condensed with increasing TMAOH concentrations from 0.5 to 1 and 2 wt% as shown in **Figure 4**. It is suggested that the hydrate kinetic inhibition impact of TMAOH is concentration and subcooling temperature dependent. The obtained formation rate data of PVP (see **Figure 4(a)**) suggests that 1 wt% TMAOH performed considerably superior to PVP at  $1^\circ\text{C}$  conditions perhaps due to superior steric hindrances ensued in very least formation rates for all the studied  $\text{CO}_2$  systems.

The total moles of  $\text{CO}_2$  consumption during hydrate formation in TMAOH solution is depicted in **Figure 5**. All concentrations of TMAOH solution reduce the  $\text{CO}_2$  uptakes (moles) into hydrate phase. The maximum inhibition effect on mole consumption of TMAOH for  $\text{CO}_2$



**Figure 3.** Influence of 1 wt% TMAOH on relative inhibition power (RIP) of  $\text{CO}_2$  hydrates at  $1^\circ\text{C}$ , the solid line (0.00 RIP) represents pure water, and results are compared with commercial inhibitor (PVP) and ILs.



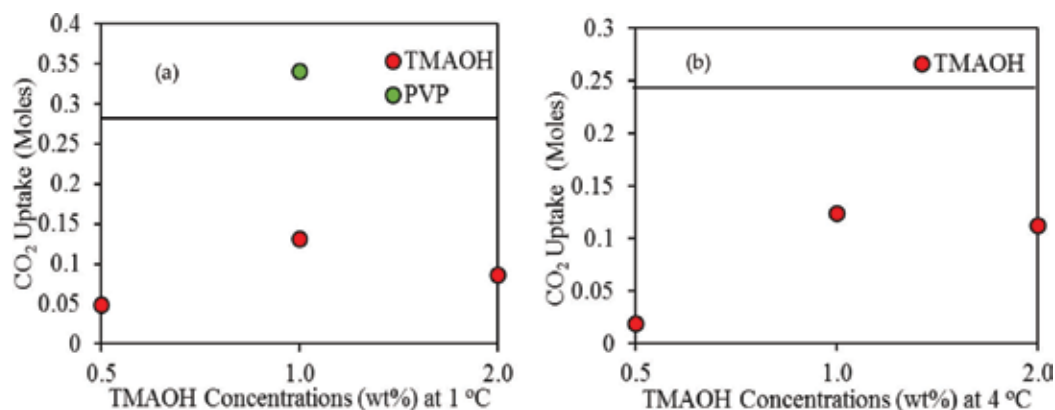
**Figure 4.** The initial apparent rate of CO<sub>2</sub> hydrate formation in the presence of water (straight line) and TMAOH at different temperatures (a) 1 and (b) 4 °C.

hydrate is observed at 1 wt% for both experimental conditions. The CO<sub>2</sub> uptake values are found to be 0.132 and 0.124 moles for 1 and 4 °C, respectively. The complete moles consumed at 4 °C at all concentration are significantly higher than 1 °C, again affirming the effect of the active driving force at 1 °C. This considerable driving force attributed further hydrate formation environs cause the formation of more CO<sub>2</sub> hydrates. Additionally, the CO<sub>2</sub> uptake result of 1 wt% TMAOH is further compared with PVP in **Figure 5(a)**. Referring to the comparison results of CO<sub>2</sub> consumed, it is detected that TMAOH can reduce the mole consumption of CO<sub>2</sub> more than PVP which signifies its usefulness as a potential KHI for CO<sub>2</sub> hydrate formation.

### 3.2. Effect of TMAOH on the kinetics of CH<sub>4</sub> hydrates

CH<sub>4</sub> hydrate formation is a bit different from CO<sub>2</sub> hydrate formation and required higher pressure (8.0 MPa) compared to CO<sub>2</sub> hydrate (3.5 MPa). **Figure 6** presents the influence of TMAOH on the induction time of CH<sub>4</sub> hydrate formation at various concentrations (0.5, 1 and 2 wt%) and different experimental temperatures (1 and 4 °C).

In contrary to CO<sub>2</sub>, higher concentrations of TMAOH do not reflect the linear induction time with mass concentration perhaps due to probabilistic nature of hydrate formation. Similarly,



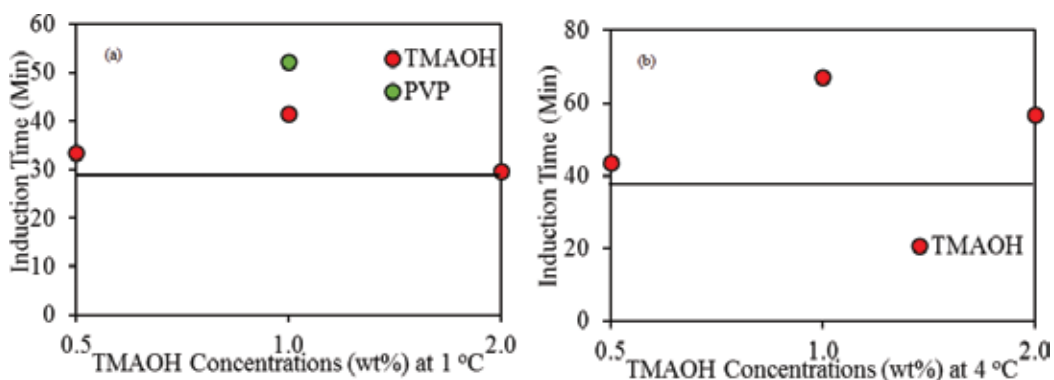
**Figure 5.** Moles of CO<sub>2</sub> consumption in the presence of water (straight line) and TMAOH at different temperatures (a) 1 and (b) 4 °C.

as overseen in CO<sub>2</sub> hydrate systems, the maximum TMAOH inhibition impact is observed at 1 wt% at 1 and 4°C. In the presence of 1 wt% TMAOH, the CH<sub>4</sub> hydrate induction time is enhanced nearly 41.4 and 81.1% for 1 and 4°C, respectively, compared to the pure water sample. However, the presence of 0.5 wt% TMAOH ensued little induction time value at 4°C and however slightly enhanced CH<sub>4</sub> hydrate nucleation observed at 1°C. Increasing the TMAOH concentration above 1 wt% reduced the induction time inhibition impact on CH<sub>4</sub> hydrates (see **Figure 6**). Furthermore, the induction data of 1 wt% TMAOH at 1°C condition is further compared with PVP data in **Figure 6(a)**. Similar to CO<sub>2</sub> hydrate, PVP is able to enhance the induction time of CH<sub>4</sub> more than TMAOH.

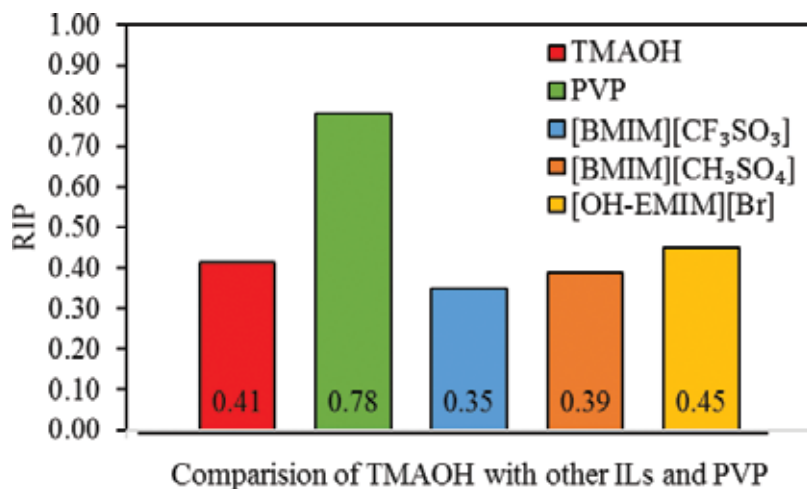
Additionally, obtained induction time results of 1 wt% TMAOH concentration of CH<sub>4</sub> hydrates at 1°C are also compared with recently published imidazolium-based IL data of Nashed et al. [44] in the form of RIP and perceived in **Figure 7**. Moreover, RIP data of studied AILs could easily be compatible with the previous study [44] as shown in **Figure 7**. TMAOH possess better RIP values compared to most earlier studied imidazolium-based ILs reported by Nashed et al. [44] (see **Figure 7**).

The initial rates of CH<sub>4</sub> hydrate formation with and without TMAOH mass concentrations (0.5, 1 and 2 wt%) at 1 and 4°C are illustrated in **Figures 8(a)** and **(b)**, respectively. At 4°C condition, the formation rates of TMAOH found for concentration are driven; as the quantity of TMAOH increases, the rate of CH<sub>4</sub> hydrate formation decreases. The similar behaviour was observed in CO<sub>2</sub> hydrate systems as well (**Figure 4(a)**). However, unlike CO<sub>2</sub> hydrates (see **Figure 4**), at 1°C the formation rates of CH<sub>4</sub> hydrates are found in non-linear trend (see **Figure 8(a)**) which demonstrates that the inhibition impact of TMAOH is not only concentration dependent but also significantly dependent on the type of hydrate formerly present. The presence of low driving force (subcooling = 7°C) at 4°C enhanced the inhibition of the rate of hydrate formation than at 1°C, which holds the higher driving force (subcooling = 10°C) resulting in catastrophic crystal growth as discussed in the preceding study [45].

Furthermore, the formation rate of 1 wt% TMAOH is also compared with PVP data in **Figure 8(a)**. The formation rate data revealed that TMAOH is able to reduce the formation rate moderately than PVP as also evident in the above results of CO<sub>2</sub> hydrates in an earlier section (see **Figure 4(a)**).

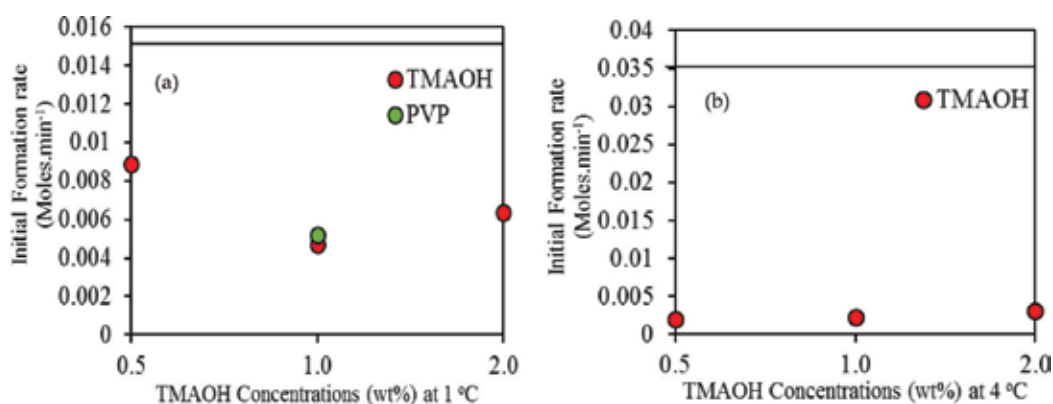


**Figure 6.** Induction time of CH<sub>4</sub> hydrate in the presence of water (straight line) and TMAOH at different temperatures (a) 1 and (b) 4°C.



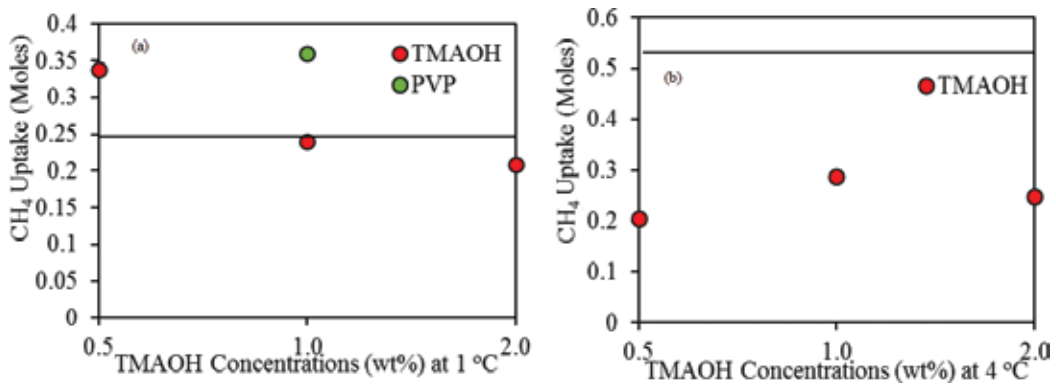
**Figure 7.** Influence of 1 wt% TMAOH on relative inhibition power (RIP) of CH<sub>4</sub> hydrates at 1°C, the solid line (0.00 RIP) represents pure water, and results are compared with commercial inhibitor (PVP) and ILs.

**Figure 9** presents the CH<sub>4</sub> mole consumed into hydrate with and without TMAOH. The presence of TMAOH poorly inhibited the CH<sub>4</sub> consumption into hydrate formation at both studied experimental temperatures. Especially at 1°C, all tested TMAOH concentrations significantly enhanced CH<sub>4</sub> hydrate formation, thus showing hydrate promotional impact. However, the moles of CH<sub>4</sub> consumed into the hydrate at 4°C are similar to the water sample; this may be due to the low driving force existing at that temperature (4°C). Therefore, the presence of TMAOH in CH<sub>4</sub> hydrate can inhibit the hydrate induction time and formation rate but will cause hydrate plug upon formation with time due to its CH<sub>4</sub> mole consumption promotion effect. Previous studies have shown that some conventional KHIs such as PVP have similar behaviour [46]. They form large hydrate plugs upon hydrate formation (i.e. after hydrate nucleation).



**Figure 8.** Rate of CH<sub>4</sub> hydrate formation in the presence of water (straight line) and TMAOH at different temperatures (a) 1 and (b) 4°C.



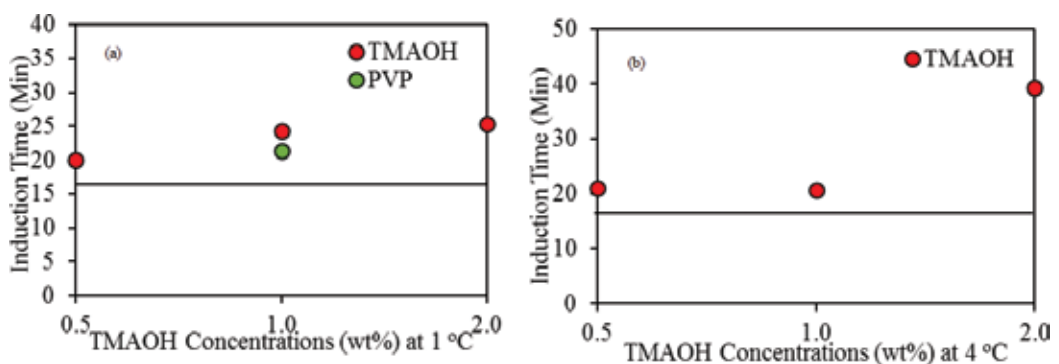


**Figure 9.** Moles of CH<sub>4</sub> consumption in the presence of water (straight line) and TMAOH at different temperatures (a) 1 and (b) 4°C.

### 3.3. Effect of TMAOH on the kinetics of binary mixed gas hydrates (50–50 mole% CO<sub>2</sub> + CH<sub>4</sub>)

The kinetic formation of mixed gas 50–50 CO<sub>2</sub> + CH<sub>4</sub> hydrates in the presence of various quantities of aqueous TMAOH solutions is discussed in this section. The hydrate induction time values for the mix gas hydrate systems are perceived in **Figure 10**. Results revealed that as TMAOH concentration increases the mixed gas hydrate induction time is further delayed, thus showing a significant inhibition impact for the mixed gas hydrates.

At the lowest concentration (0.5 wt%), TMAOH delayed the base sample induction time by about 1.2 times at both 1 and 4°C, while at 2 wt% about 1.5 and 2.3 times at 1 and 4°C, respectively. Additionally, the KHI impact (induction time) of 1 wt% TMAOH aqueous solution of the mixed gas is also compared with PVP data in **Figure 10(a)**. The comparisons of data are interestingly piercing that TMAOH can delay hydrate nucleation time further than commercial KHI inhibitor PVP. The potential of the improved delay time observed is perhaps due to the larger subcooling (11°C) conditions of studied mixed gas system compared to pure water



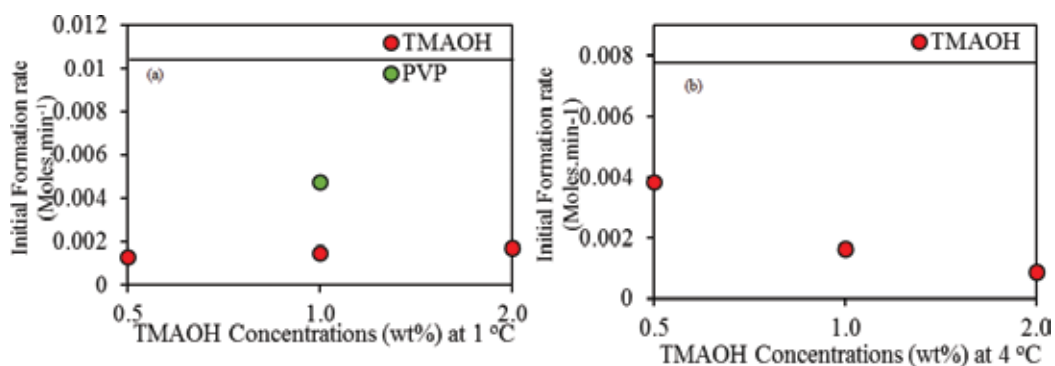
**Figure 10.** Induction time of binary mixed gas hydrate in the presence of water (straight line) and TMAOH at different temperatures (a) 1 and (b) 4°C.

systems ( $\text{CO}_2 = 7.32^\circ\text{C}$ ;  $\text{CH}_4 = 10^\circ\text{C}$ ). This observation also highlighted the limitation of PVP (commercial inhibitor) efficacy over harsh deep-water condition which loses its strength at higher subcooling conditions [38, 47].

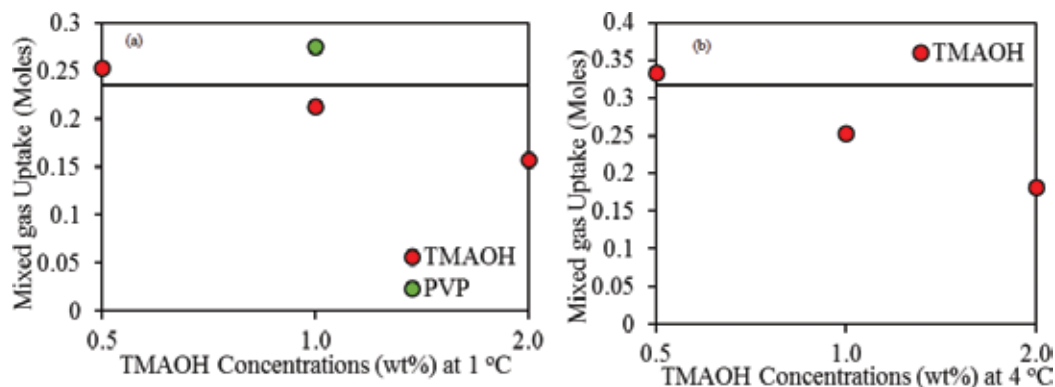
**Figure 11** refers the initial formation rate of 50–50  $\text{CO}_2 + \text{CH}_4$  mixed gas hydrates. Results revealed that initial rate of hydrate formation for mixed gas hydrates reduced with increasing TMAOH mass concentrations for both 1 and  $4^\circ\text{C}$ . The presence of 1 wt% TMAOH shows the optimal hydrate rate diminution. The hydrate formation rate is found to be reduced about five times at 1 wt% TMAOH for all subcooling compared with the mixed gas hydrate (pure water sample). Furthermore, the result of 1 wt% TMAOH is further compared with PVP in **Figure 11(a)** at a similar concentration. Like the pure gases hydrates, TMAOH can further reduce the initial formation rate compared to the PVP-based system.

In **Figure 12**, it is observed that the presence of TMAOH significantly reduces the amount of mixed gas consumption in both experimental (subcooling) conditions, unlike the case of pure  $\text{CH}_4$  hydrates. The inhibition of mixed gas consumed into hydrate is practically observed at all concentrations. However, the much significant inhibition impact is obtained at 2 wt% aqueous TMAOH solution. At 2 wt%, the amount of mixed gas consumed into hydrate is reduced about 1.7 times compared to the pure water system. This notable inhibition together with the THI impact [3] shows the potentials of applying TMAOH as a novel dual functional inhibitor for practical field operation, especially in high  $\text{CO}_2$  content reservoir productions of fluid transportation and procession.

A gas chromatography (GC) is used to explore the mixed gas composition after hydrates are entirely formed in all the binary mixed gas experiments. The data are used to calculate the amount of gas remaining in the gas phase after hydrate formation. However, the GC readings are also useful to understand the percentage of each gas entrapped in the hydrate phase in the presence and absence of TMAOH. The inhibition selectivity of TMAOH for the binary mixed gas composition may be suggested. The measured GC readings are tabularized in **Table 2**. The data revealed that  $\text{CO}_2$  compositions in the binary mixed gas are diminished after complete hydrate formation compared to original compositions (50–50%  $\text{CO}_2 + \text{CH}_4$ ) for all experiments.



**Figure 11.** Initial apparent rate of binary mixed gas hydrate formation in the presence of water (straight line) and TMAOH at different temperatures (a) 1 and (b)  $4^\circ\text{C}$ .



**Figure 12.** Moles of binary mixed gas consumption in the presence of water (straight line) and TMAOH at different temperatures (a) 1 and (b) 4°C.

Confirming that CO<sub>2</sub> hydrates are more formed in mixed gas hydrates compared to CH<sub>4</sub> hydrate, which is due to experimental pressure, provides more driving force to CO<sub>2</sub> than CH<sub>4</sub> hydrates as CO<sub>2</sub> is more prone to hydrate formation compared to CH<sub>4</sub> gas.

### 3.4. Kinetic mechanism of TMAOH

The kinetic inhibition influence of TMAOH observed for all studied gas systems in this work presents TMAOH as a potential KHI. TMAOH is speculated to demonstrate a kinetic inhibitory mechanisms effect via (1) coulombic forces of interactions and (2) hydrogen bonding affinity, which probably results in its kinetic hydrate inhibition influence. Firstly, TMAOH is an ionic liquid which can form hydrogen bonding with water molecules and thus disturb the hydrogen-bonded structure of water molecules owing to the presence of its anion and cation ions [4, 12, 15, 48]. TMAOH ionizes in aqueous solution as TMA<sup>+</sup> cation and OH<sup>-</sup> anions which

Sample	Concentration (wt%)	Experimental temperature (°C)	CH <sub>4</sub>	CO <sub>2</sub>
Pure water	0.00	4	53.26	46.74
Pure water	0.00	1	54.1	45.9
TMAOH	0.50	4	53.1	46.9
	1.00	4	55.38	44.62
	2.00	4	54.1	45.9
TMAOH	0.50	1	53	47
	1.00	1	55.8	44.17
	2.00	1	54	46
PVP	1.00	1	55.3	44.7

**Table 2.** Gas chromatography (GC) data for the average composition of binary mixed gas hydrates after complete hydrate formation.

interacts with the dipoles of the aqueous molecules with strong coulombic forces in additions to its hydrogen bonding ability [49]. This combined effect easily overcomes the hydrogen bond structure or the van der Waals forces which causes clustering of water molecules in hydrate formation nucleation and growth [3, 4, 12]. As the water structures are distorted, it promotes the hindrance/delay in hydrate nuclei clustering and gas consumption into hydrate. Additionally, TMAOH possesses four methyl cations [ $\text{CH}_3^+$ ] which is the least hydrophobic alkyl radical among other alkyl groups, which makes tetramethylammonium [ $\text{TMA}^+$ ] cation relatively more hydrophilic [3, 50–52]. Similarly, hydroxyl [ $\text{OH}^-$ ] anion is well known for its strong hydrogen bonding affinity for water molecules [3, 4, 32]. Therefore, TMAOH could adsorb on the gas-water interface, and retarded hydrate nucleation and crystal growth (through hydrogen bonding by the amide group and anion) and sterically block the hydrate formation [15, 53–56].

It is already proven from previous studies [1, 13, 35, 57, 58] that hydrate formation depends on the presence of a guest molecule. Therefore, the inhibition impact of TMAOH also differs according to the type of gas systems. For instance,  $\text{CO}_2$  hydrates showed lesser induction time in comparison with  $\text{CH}_4$  hydrates and 50–50  $\text{CO}_2$ - $\text{CH}_4$  mix gas hydrates in this study. The overall better KHI performance of TMAOH is found with 50–50  $\text{CO}_2$ - $\text{CH}_4$  mix gas hydrates for both experimental temperature conditions (1 and 4°C) for induction time, hydrate formation rate alongside moles of gas consumed. Additionally, although the kinetic inhibition is concentration dependent, as aqueous TMAOH concentration increases, the KHI performance enhances for most of the studied systems. However, for optimum performance evaluation, one% (1 wt%) TMAOH seems to be more efficient as not much differently observed (above results) between 1 and 2 wt% concentrations. It is also evident for all studied system that at higher experimental temperature condition 4°C TMAOH performs better in comparison to lower-temperature condition (1°C). It can be concluded that TMAOH successfully worked as a KHI inhibitor for all the studied system; earlier [3], TMAOH has already been proven as an efficient THI as well for  $\text{CH}_4$  and  $\text{CO}_2$  gas hydrates. Therefore, TMAOH possibly will work as dual-functional hydrate inhibitor and therefore could efficiently be contemplated for flow assurance strategies.

## 4. Conclusions

In the present work, ammonium-based ionic liquid, TMAOH, is tested as a potential kinetic inhibitor for pure  $\text{CO}_2$ ,  $\text{CH}_4$  and binary mixed (50–50)  $\text{CO}_2$  +  $\text{CH}_4$  hydrate systems at different mass concentrations (0.5, 1.0 and 2.0 wt%). The effect of subcooling was also investigated at two different experimental temperatures of 1 and 4°C at moderate pressures for all the studied TMAOH systems. Experimental results revealed that TMAOH kinetically inhibits hydrate formation by delaying hydrate nucleation through the enhancement of hydrate induction time and TMAOH also lessens the initial apparent rate of hydrate formation and accordingly decreased the mole consumptions for almost all studied systems. Influence of subcooling was also observed as the subcooling increased the hydrate formation due to the presence of excessive driving force. The effect of TMAOH concentration and the type of guest molecules under study are found to affect the TMAOH hydrate inhibition impact significantly. Furthermore, the experimental results of TMAOH were further compared with PVP at 1 wt% concentration at 1°C conditions. The induction time of PVP seems to be higher than TMAOH for both pure

gases; however, for binary mixed gas, the induction time of TMAOH is found to be higher than PVP due to enhanced subcooling conditions. The initial formation rate and mole consumption are found to be enhanced with TMAOH compared to the commercial counterpart. The TMAOH inhibitory mechanisms are driven by their coulombic forces of interactions and hydrogen bonding affinity for water molecules in hydrate formation environment. Therefore, the findings of this study highlighted the kinetic impact of TMAOH, which should be beneficial for gas hydrate-based technological applications such as storage and gas transportation, flow assurance and energy productions.

## Acknowledgements

PETRONAS Research Sdn Bhd (PRSB) financially supports this work under the Grant No. 053C1-024.

## Nomenclature

ILs	ionic liquids
LDHI	low-dosage hydrate inhibitor
KHI	kinetic hydrate inhibitors
PVP	polyvinyl pyrrolidinium
RIP	relative inhibition performance
TMAOH	tetramethylammonium hydroxide

## Author details

Muhammad Saad Khan<sup>1,2</sup>, Bavoh B. Cornelius<sup>1,2</sup>, Bhajan Lal<sup>1,2\*</sup> and Mohamad Azmi Bustam<sup>1,2</sup>

\*Address all correspondence to: [bhajan.lal@utp.edu.my](mailto:bhajan.lal@utp.edu.my)

1 Chemical Engineering Department, Universiti Teknologi of PETRONAS, Bandar Seri Iskandar, Perak, Malaysia

2 CO<sub>2</sub> Research Centre (CO2RES), Bandar Seri Iskandar, Perak, Malaysia

## References

- [1] Koh CA. Towards a fundamental understanding of natural gas hydrates. *Chemical Society Reviews*. 2002;**31**(3):157-167

- [2] Sloan ED, Koh CA. Clathrate Hydrates of Natural Gases. Fuel. New York: CRC Press Taylor & Francis; 2007. 3158p
- [3] Khan MS, Partoon B, Bavoh CB, Lal B, Mellon NB. Influence of tetramethylammonium hydroxide on methane and carbon dioxide gas hydrate phase equilibrium conditions. *Fluid Phase Equilibria*. 2017;**440**(May 2017):1-8
- [4] Khan MS, Lal B, Bavoh CB, Keong LK, Bustam A. Influence of ammonium based compounds for gas hydrate mitigation : A short review. *Indian Journal of Science and Technology*. 2017;**10**(5):1-6
- [5] Nashed O, Sabil KM, Lal B, Ismail L, Jaafar AJ. Study of 1-(2-hydroxyethyle) 3-methylimidazolium halide as thermodynamic inhibitors. *Applied Mechanics and Materials*. 2014;**625**:337-340
- [6] Roosta H, Dashti A, Mazloumi SH, Varaminian F. Inhibition properties of new amino acids for prevention of hydrate formation in carbon dioxide-water system: Experimental and modeling investigations. *Journal of Molecular Liquids*. Elsevier B.V. 2016;**215**:656-663
- [7] Shen X, Shi L, Long Z, Zhou X, Liang D. Experimental study on the kinetic effect of N-butyl-N-methylpyrrolidinium bromide on CO<sub>2</sub> hydrate. *Journal of Molecular Liquids* [Internet]. Elsevier B.V. 2016;**223**:672-677
- [8] Sloan ED, Koh CA. Clathrate Hydrates of Natural Gases. 3rd ed. New York: CRC Press Taylor & Francis; 2008. 758p
- [9] Nasir Q, Lau KK, Lal B, Sabil KM. Hydrate dissociation condition measurement of CO<sub>2</sub> - rich mixed gas in the presence of methanol/ethylene glycol and mixed methanol/ethylene glycol + electrolyte aqueous solution. *Journal of Chemical & Engineering Data*. 2014;**59**(11):3920-3926
- [10] Khodaverdiloo KR, Rad SA, Naeiji P, Peyvandi K, Varaminian F. Synergistic effects of nonylphenol ethoxylates and polyethylene glycols on performance of gas hydrate kinetic inhibitor. *Journal of Molecular Liquids*. Elsevier B.V. 2016;**216**:268-274
- [11] Daraboina N, Linga P. Experimental investigation of the effect of poly-N-vinyl pyrrolidone (PVP) on methane/propane clathrates using a new contact mode. *Chemical Engineering Science*. 2013;**93**:387-394
- [12] Khan MS, Bavoh CB, Partoon B, Lal B, Bustam MA, Shariff AM. Thermodynamic effect of ammonium based ionic liquids on CO<sub>2</sub> hydrates phase boundary. *Journal of Molecular Liquids*. Elsevier B.V. 2017;**238**(July):533-539
- [13] Sloan ED Jr. Fundamental principles and applications of natural gas hydrates. *Nature* 2003;**426**(6964):353-363
- [14] Qureshi MF, Atilhan M, Altamash T, Tariq M, Khraisheh M, Aparicio S, et al. Gas hydrate prevention and flow assurance by using mixtures of ionic liquids and Synergent compounds: Combined kinetics and thermodynamic approach. *Energy & Fuels*. 2016;**30**(4):3541-3548
- [15] Tariq M, Rooney D, Othman E, Aparicio S, Atilhan M, Khraisheh M. Gas hydrate inhibition: A review of the role of ionic liquids. *Industrial and Engineering Chemistry Research*. 2014;**53**(46):17855-17868

- [16] Rasoolzadeh A, Javanmardi J, Eslamimanesh A, Mohammadi AH. Experimental study and modeling of methane hydrate formation induction time in the presence of ionic liquids. *Journal of Molecular Liquids*. Elsevier B.V. 2016;**221**:149-155
- [17] Zare M, Haghtalab A, Ahmadi AN, Nazari K, Mehdizadeh A. Effect of imidazolium based ionic liquids and ethylene glycol monoethyl ether solutions on the kinetic of methane hydrate formation. *Journal of Molecular Liquids*. 2015;**204**(4):236-242
- [18] Shi L, Yi L, Shen X, Wu W, Liang D. The effect of tetrabutylphosphonium bromide on the formation process of CO<sub>2</sub> hydrates. *Journal of Molecular Liquids—Elsevier B.V.* 2017; **229**:98-105
- [19] Mohammadi A, Manteghian M, Mohammadi AH, Jahangiri A. Induction time, storage capacity, and rate of methane hydrate formation in the presence of SDS and silver nanoparticles. *Chemical Engineering Communications*. 2017;**204**(12):1420-1427
- [20] Karaaslan U, Parlaktuna M. Kinetic inhibition of methane hydrate by polymers. *American Chemical Society Division of Fuel Chemistry*. 2002;**47**(1):355-358
- [21] Xiao C, Adidharma H. Dual function inhibitors for methane hydrate. *Chemical Engineering Science*. 2009;**64**(7):1522-1527
- [22] Kim K, Kang S-P. Investigation of pyrrolidinium- and morpholinium-based ionic liquids into kinetic hydrate inhibitors on structure i methane hydrate. 7th International Conference on Gas Hydrates (ICGH) 2011. Edinburgh, Scotland; 2011. pp. 17-21
- [23] Nazari K, Ahmadi AN, Moradi MR, Sahraei V, Taghikhani V, Ghobti CA. A thermodynamic study of methane hydrate formation in the presence of [BMIM][BF<sub>4</sub>] and [BMIM][MS] ionic liquids. In: *Proceedings of the 7th International Conference on Gas Hydrates (ICGH 2011)*; 2011 Jul 17. pp. 17-21
- [24] Norland AK, Kelland MA. Crystal growth inhibition of tetrahydrofuran hydrate with bis- and polyquaternary ammonium salts. *Chemical Engineering Science—Journal—Elsevier*. 2012;**69**(1):483-491
- [25] Lee W, Shin J, Cha J, Kim K, Kang S. Inhibition effect of ionic liquids and their mixtures with poly(N-vinylcaprolactam) on methane hydrate formation. *Journal of Industrial and Engineering Chemistry*. The Korean Society of Industrial and Engineering Chemistry. 2016;**30**:3541-3548
- [26] Roosta H, Khosharay S, Varaminian F. Experimental study of methane hydrate formation kinetics with or without additives and modeling based on chemical affinity. *Energy Conversion and Management*. Elsevier Ltd. 2013;**76**:499-505
- [27] Zanoata ML, Dicharry C, Graciaa A. Hydrate plug prevention by quaternary ammonium salts. *Energy and Fuels*. 2005;**19**(11):584-590
- [28] Storr MT, Taylor PC, Monfort JP, Rodger PM. Kinetic inhibitor of hydrate crystallization. *Journal of the American Chemical Society*. 2004;**126**(5):1569-1576
- [29] Perrin A, Musa OM, Steed JW. The chemistry of low dosage clathrate hydrate inhibitors. *Chemical Society Reviews*. 2013;**42**(5):1996-2015

- [30] Kelland MA. History of the development of low dosage hydrate inhibitors. *Energy & Fuels*. 2006;**20**(3):825-847
- [31] Yasuda T, Kinoshita H, Miran MS, Tsuzuki S, Watanabe M. Comparative study on physicochemical properties of protic ionic liquids based on allylammonium and propylammonium cations. *Journal of Chemical & Engineering Data*. 2013;**58**(10):2724-2732
- [32] Khan MS, Lal B, Partoon B, Keong LK, Bustam MA, Mellon NB. Experimental evaluation of a novel thermodynamic inhibitor for CH<sub>4</sub> and CO<sub>2</sub> hydrates. *Procedia Engineering*. 2016;**148**(2016):932-940
- [33] Khan MS, Bavoh CB, Partoon B, Nashed O, Lal B, Mellon NB. Impacts of ammonium based ionic liquids alkyl chain on thermodynamic hydrate inhibition for carbon dioxide rich binary gas. *Journal of Molecular Liquids*. 2018 Apr 10
- [34] Nashed O, Dadebayev D, Khan MS, Bavoh CB, Lal B, Shariff AM. Experimental and modelling studies on thermodynamic methane hydrate inhibition in the presence of ionic liquids. *Journal of Molecular Liquids Elsevier B.V.* 2018;**249**:886-891
- [35] Kashchiev D, Firoozabadi A. Induction time in crystallization of gas hydrates. *Journal of Crystal Growth*. 2003;**250**(3-4):499-515
- [36] Fazlali A, Keshavarz-Moraveji M, Farjami M, Mohammadi AH. Experimental study of the effect of kinetic inhibitor on methane hydrate formation. In: Taylor JC, editor. *Advances in Chemistry Research*. NY, USA: Nova Science Publishers, Inc; 2016. pp. 133-148
- [37] Partoon B, Nurmala S, Malik A, Azemi MH, Sabil KM. Experimental investigations on the potential of SDS as low-dosage promoter for carbon dioxide hydrate formation. *Asia-Pacific Journal of Chemical Engineering*. 2013;**8**:916-921
- [38] Bavoh CB, Lal B, Keong LK, binti JM, binti IM. Synergic kinetic inhibition effect of EMIM-Cl + PVP on CO<sub>2</sub> hydrate formation. *Procedia Engineering*. 2016;**148**:1232
- [39] Kumar A, Bhattacharjee G, Kulkarni BD, Kumar R. Role of surfactants in promoting gas hydrate formation. *Industrial and Engineering Chemistry Research*. 2015;**54**(49):12217-12232
- [40] Akhfash M, Boxall JA, Aman ZM, Johns ML, May EF. Hydrate formation and particle distributions in gas-water systems. *Chemical Engineering Science*. Elsevier. 2013;**104**:177-188
- [41] Babae S, Hashemi H, Mohammadi AH, Naidoo P, Ramjugernath D. Kinetic and thermodynamic behaviour of CF<sub>4</sub> clathrate hydrates. *The Journal of Chemical Thermodynamics*. Elsevier Ltd. 2015;**81**:52-59
- [42] Koh CA, Westacott RE, Zhang W, Hirachand K, Creek JL, Soper AK. Mechanisms of gas hydrate formation and inhibition. *Fluid Phase Equilibria*. 2002;**194-197**:143-151
- [43] Chun LK, Jaafar A. Ionic liquid as low dosage hydrate inhibitor for flow assurance in pipeline. *Asian Journal of Scientific Research*. 2013;**6**(2):374-380
- [44] Nashed O, Sabil KM, Ismail L, Japper-Jaafar A, Lal B. Mean induction time and isothermal kinetic analysis of methane hydrate formation in water and imidazolium based ionic liquid solutions. *The Journal of Chemical Thermodynamics*. 2018 Feb 1;**117**:147-154



- [45] Parent JS, Bishnoi P. Investigations into the nucleation behaviour of methane gas hydrates. *Chemical Engineering Communications*. 1996;**144**(1):51-64
- [46] Sa J-H, Kwak G-H, Han K, Ahn D, Lee K-H. Gas hydrate inhibition by perturbation of liquid water structure. *Scientific Reports*. Nature Publishing Group. 2015;**5**:11526
- [47] Bavoh CB, Nashed O, Saad Khan M, Partoon B, Lal B, Sharif AM. The impact of amino acids on methane hydrate phase boundary and formation kinetics. *The Journal of Chemical Thermodynamics*. 2018;**117**:48-53
- [48] Tariq M, Connor E, Thompson J, Khraisheh M, Atilhan M, Rooney D. Doubly dual nature of ammonium-based ionic liquids for methane hydrates probed by rocking-rig assembly. *RSC Advances*. 2016;**6**(28):23827-23836
- [49] Saw VK, Das BB, Ahmad I, Mandal a, Laik S. Influence of electrolytes on methane hydrate formation and dissociation. *Energy Sources, Part A Recover Utilization, and Environmental Effects*. 2014;**36**(15):1659-1669
- [50] Filley TR, Minard RD, Hatcher PG. Tetramethylammonium hydroxide (TMAH) thermochemolysis: Proposed mechanisms based upon the application of <sup>13</sup>C-labeled TMAH to a synthetic model lignin dimer. *Organic Geochemistry*. 1999;**30**(7):607-621
- [51] Kavitha T, Attri P, Venkatesu P, Devi RSR, Hofman T. Influence of alkyl chain length and temperature on thermophysical properties of ammonium-based ionic liquids with molecular solvent. *The Journal of Physical Chemistry. B*. 2012;**116**(15):4561-4574
- [52] Govinda V, Attri P, Venkatesu P, Venkateswarlu P. Evaluation of thermophysical properties of ionic liquids with polar solvent: A comparable study of two families of ionic liquids with various ions. *The Journal of Physical Chemistry. B*. 2013;**117**(41):12535-12548
- [53] Abay HK, Svartaas TM. On the kinetics of methane hydrate formation: A time-dependent kinetic rate model. In: *Proceedings of the 7th International Conference on Gas Hydrates*. Edinburgh, Scotland, United Kingdom: 2011
- [54] Makogon YF. *Hydrates of Natural Gas*. Tulsa, Oklahoma: Penn Well Books; 1981. 125p
- [55] Servio P, Mahajan D. Kinetic reproducibility of methane production from methane hydrates. *Preprints of Papers—American Chemical Society, Division of Fuel Chemistry*. 2003;**48**(1987):881-882
- [56] Hong SY, Il LJ, Kim JH, Lee JD. Kinetic studies on methane hydrate formation in the presence of kinetic inhibitor via in situ Raman spectroscopy. *Energy & Fuels*. 2012;**26**:7045-7050
- [57] Koh CA, Sloan ED, Sum AK, Wu DT. Fundamentals and applications of gas hydrates. *Annual Review of Chemical and Biomolecular Engineering*. 2011;**2**:237-257
- [58] Daraboina N, Ripmeester J, Walker VK, Englezos P. Natural gas hydrate formation and decomposition in the presence of kinetic inhibitors. 3. Structural and compositional changes. *Energy & Fuels*. 2011;**25**:4398-4404





*Edited by Mohammed Muzibur Rahman*

*Recent Advances in Ionic Liquids* contains research on the preparation, characterization, and potential applications of stable ionic liquids (ILs). ILs are a class of low- and stable-melting point, ionic compounds that have a variety of properties allowing many of them to be sustainable green solvents. It is promising novel research from top to bottom and has received a lot of interest over the last few decades. It covers the advanced topics of physical, catalytic, chemical, polymeric, and potential applications of ILs. This book features interesting reports on cutting-edge science and technology related to the preparation, characterization, polymerization, and potential applications of ILs. This potentially unique work offers various approaches on the R&D implementation of ILs or related ionic catalysts and their conjugates.

With this in mind, the authors present R&D on the preparation, properties, potential applications, and utility of ILs. The chapters describe important applications in a wide variety of contexts, including polymerization, devices, electrochemistry, and biotechnology. Both the theoretical and practical, it can be passed from the stable as well as molten salt to the ionic liquid and vice versa. Experimental and theoretical techniques for examining these studies are elaborated based on the methods for preparation, utilization, applications, and analysis. This book epitomizes the transfer of these techniques and methods between the differing temperature regimes, and is a major contribution to the future of both fields. The book presents an overview of current ILs fundamentals: preparation, polymerization, substantial applications, and enhancement of research worldwide. The techniques of ILs preparation, total characterization, and possible applications related with ILs as well as modified or conjugated material research are investigated. *It is hoped that it will be an important book for research organizations, governmental research centers, and academic libraries engaged in recent R&D of ILs.*

Published in London, UK

© 2018 IntechOpen  
© Paul-Daniel Florea / iStock

**IntechOpen**

